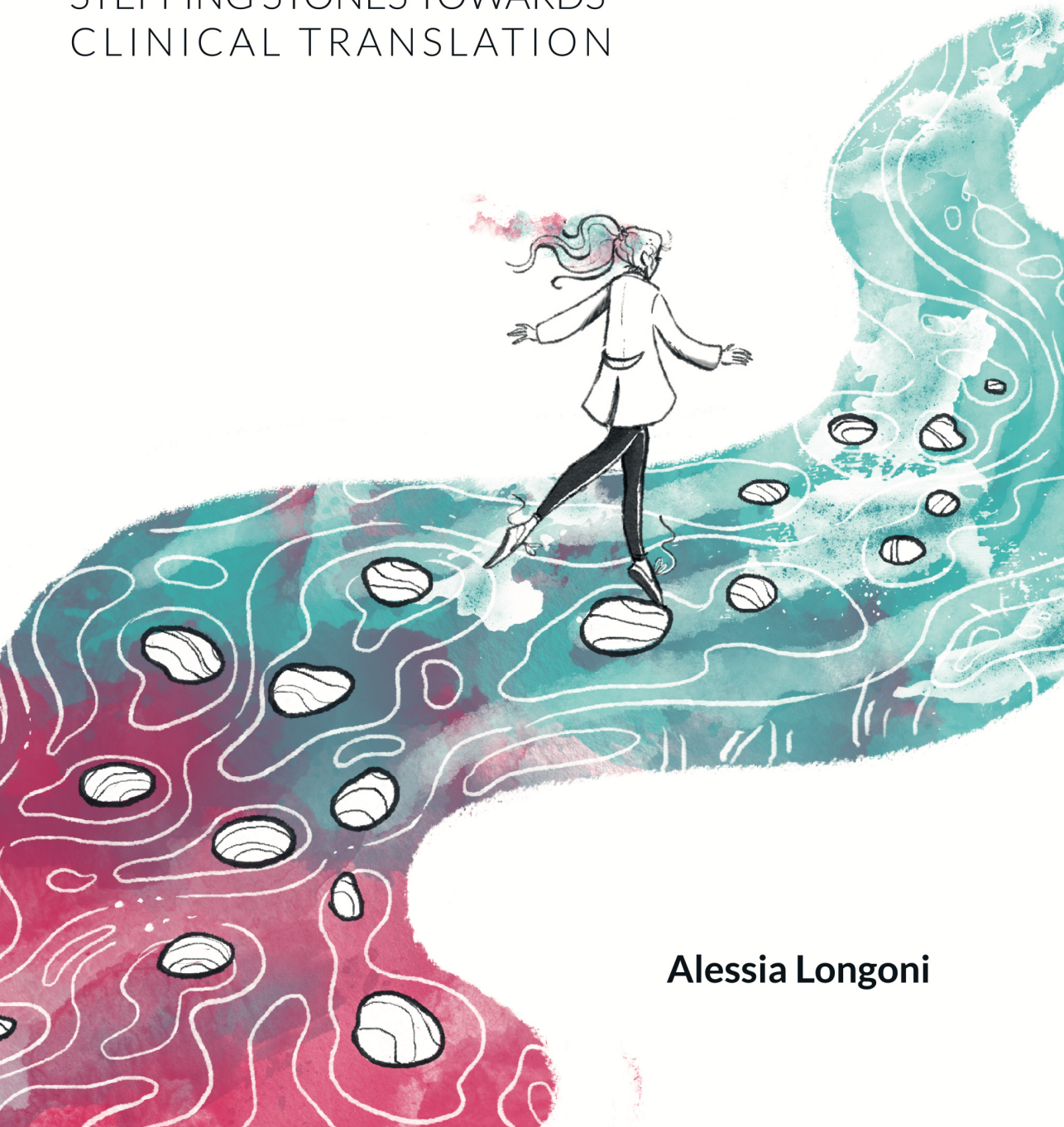


ENDOCHONDRAL BONE REGENERATION:

STEPPING STONES TOWARDS
CLINICAL TRANSLATION



Alessia Longoni

Endochondral bone regeneration: Stepping stones towards clinical translation

Alessia Longoni

Cover design: Alessia Moretti
Layout: Renate Siebes | Proefschrift.nu
Printed by: Proefschriftmaken.nl
ISBN: 978-90-393-7319-4

Copyright © Alessia Longoni, the Netherlands, 2020.

All rights reserved. No part of this thesis may be reproduced, distributed, stored in a retrieval system of any nature or transmitted in any form of by any means, without the written consent of the author or, when appropriate, the publisher of the respective publications.

Financial support for the printing of the thesis was kindly provided by the Dutch society for Biomaterials and Tissue Engineering (NBTE) and the 'Utrechtse Stichting tot Bevordering der Mondziekten, Kaak- en Aangezichtschirurgie'.

Endochondral bone regeneration: Stepping stones towards clinical translation

**Endochondrale botregeneratie:
Stappen voorwaarts richting klinische translatie**

(met een samenvatting in het Nederlands)

**Rigenerazione dell'osso tramite processo endocondrale:
Passi verso la traslazione clinica**

(con riassunto in Italiano)

Proefschrift

ter verkrijging van de graad van doctor aan de
Universiteit Utrecht op gezag van de rector magnificus,
prof.dr. H.R.B.M. Kummeling, ingevolge het besluit van het
college voor promoties in het openbaar te verdedigen
op vrijdag 25 september 2020 des ochtends te 11.00 uur

door

Alessia Longoni

geboren op 9 december 1990
te Como, Italië

Promotor:

Prof. dr. A.J.W.P. Rosenberg

Copromotoren:

Dr. ir. D. Gawlitta

Dr. L. Utomo

*“Happiness can be found even in the darkest of times,
if one only remembers to turn on the light.”*

Albus Dumbledore

Contents

Chapter 1	General introduction, thesis aim and outline	9
PART I Optimizing the cartilaginous template for endochondral bone regeneration		
<hr/>		
Chapter 2	The chondrogenic differentiation potential of dental pulp stem cells	25
Chapter 3	Intact vitreous humor as a potential extracellular matrix hydrogel for cartilage tissue engineering applications	47
Chapter 4	Vitreous humor as instructive biomaterial to support mesenchymal stem cell hypertrophy and endochondral ossification. <i>Preliminary data</i>	79
PART II Employing allogeneic mesenchymal stem cells for endochondral bone regeneration		
<hr/>		
Chapter 5	The impact of immune response on endochondral bone regeneration	99
Chapter 6	Endochondral bone regeneration by non-autologous mesenchymal stem cells	123
Chapter 7	Impressive acceleration of bone regeneration by a devital soft callus mimetic	149
Chapter 8	Summary and general discussion	177
	Summaries	191
	Nederlandse samenvatting	193
	Riassunto in Italiano	196
	References	201
	Acknowledgements	229
	List of publications	237
	Curriculum vitae	241



General introduction,
thesis aim and outline

1



PHYSIOLOGICAL BONE REPAIR AND CURRENT THERAPEUTIC OPTIONS



Bone physiology

Bone is a specialized connective tissue that provides mechanical support to soft tissue, protects vital organs and, by offering levers for muscles, aids locomotion. In addition, it represents a primary site for hematopoiesis and a reservoir for minerals and growth factors [1]. Bone can fulfill its structural function thanks to the particular features of its extracellular matrix (ECM). Specifically, hydroxyapatite crystals, which represent the inorganic part of the ECM, are responsible for bone strength, stiffness, and resistance to compressive forces [2]. On the other end, collagen type I, the major component of the organic phase of the bone's ECM, provides resistance to tensile forces [2]. In addition, the presence of other non-collagenous proteins, like osteocalcin and osteopontin, directly influence matrix mineralization [3].

Contrary to its static appearance, bone is a highly dynamic tissue, as its remodeling is necessary in order to maintain skeletal stability and mineral homeostasis, and to adapt to mechanical stress [3, 4]. Specifically, it is constantly remodeled through the concert action of three different cell types: osteoclasts, osteoblasts, and osteocytes [3]. Osteoclasts, giant multinucleated cells that derive from the hematopoietic lineage, are responsible for bone resorption. In order to achieve this goal, they interact with the bone ECM to create a bone-resorbing compartment known as sealing zone [5]. In this area, the inorganic components are removed by the acidification of the environment, whereas proteolytic enzymes are responsible for the degradation of the organic part [5]. After resorption, new bone formation is mediated by the osteoblasts, cuboidal cells that originate from mesenchymal stem cells (MSCs). Initially, osteoblasts deposit a soft ECM called osteoid, which is predominantly composed of collagen type I. The osteoid is subsequently mineralized to form the final bone ECM [3]. During ECM deposition, about 15% of the osteoblasts are entrapped in the new matrix and become osteocytes [3]. Osteocytes play a pivotal role in regulating bone remodeling. In particular, through the secretion of factors, like sclerostin, they signal to the residual osteoblasts to become quiescent [6]. In addition, they act as a sensor, promoting bone formation and remodeling according to the changes in mechanical load [7].

Fracture healing

Bone possesses a remarkable healing capability as, after a fracture, a fully functional and integrated new tissue can be formed without scar formation [8]. Successful physiological healing is a multistage process characterized by a series of well-orchestrated events, each

one characterized by specific players [9, 10]. In particular, three overlapping phases can be identified: inflammation, repair, and remodeling [9].

After a fracture, the integrity of the surrounding vessels and soft tissue is compromised. This induces an inflammatory state, characterized by vasodilatation and exudation of plasma and white blood cells, which can last up to a week [9, 11]. At this stage, the fibrinogen within the fracture gap is converted into fibrin, creating a temporary scaffold known as the fracture hematoma. The hematoma environment is characterized by a low pH [9], hypoxia [12], and high concentrations of pro- and anti-inflammatory cytokines [9, 11, 13-15]. Immune cells including neutrophils, macrophages and, afterwards, lymphocytes are recruited at the damaged site from the peripheral blood and the surrounding tissues [9, 11, 16, 17]. Here, they play a dual role. Firstly, they prevent the spread of pathogens and clear the wound from necrotic cell debris [16]. Secondly, they directly contribute to the inflammatory response by secreting pro-inflammatory cytokines, promoting additional immune cell infiltration and skewing macrophages towards a pro-inflammatory phenotype [11, 16]. At the same time, the hematoma's hypoxic state promotes the release of pro-angiogenic factors, inducing endothelial cell migration from pre-existing periosteal vessels and ultimately neo-angiogenesis within the bone gap [18-20]. Eventually, the concert action of immune cells, resident cells and the released cytokines promotes the recruitment of fibroblasts and MSCs at the fracture site and the remodeling of the hematoma into granulation tissue [9, 21]. This marks the transition towards the repair phase, which can last between 1-2 weeks.

During the repair stage, depending on the mechanical stability and the anatomical location of the fracture, two distinct processes are involved in new bone formation. In fractures characterized by high mechanical stability [13, 22] and at the periphery of the fracture site, intramembranous ossification occurs. Here, MSCs differentiate into osteoblasts and mediate the direct deposition of a mineralized bone matrix [9, 22]. On the contrary, in mechanically unstable fractures and at the central region of the fracture site, endochondral ossification is the predominant mechanism [9, 22]. During endochondral ossification, MSCs differentiate towards the chondrogenic lineage and, together with the infiltrated and resident fibroblasts, secrete a cartilaginous soft callus that stabilizes the bone defect [10]. This cartilaginous template is initially characterized by a matrix rich in collagen type II and proteoglycans [10, 23]. However, the chondrocytes present in the soft callus progressively acquire a hypertrophic phenotype, following a process similar to the one that characterizes long bone development in the active growth plate [23]. Specifically, the transition to hypertrophy is marked by a switch in gene expression, as they start expressing osteogenic genes including alkaline phosphatase (ALP), runt-related transcription factor 2 (RUNX-2), and collagen type I [24, 25]. In addition, hypertrophic chondrocytes considerably

increase in size [26, 27] and start to secrete collagen type X, pro-angiogenic factors, and metalloproteinases (MMPs). All together, these changes mediate cartilage calcification, matrix remodeling, and blood vessel invasion of the soft callus [10]. Osteoblasts and osteoclasts infiltrate the fracture site via the newly formed vasculature, leading to the deposition of woven bone [10, 22]. This is known as hard callus and it provides additional mechanical stability in the fracture.

The final stage of fracture healing is characterized by the remodeling of the hard callus. The coupled action of osteoclasts and osteoblasts replaces woven bone by lamellar bone. This process usually can initiate as early as 3-4 weeks after the fracture occurs, but it may take years to be completed [21].

When fracture healing fails: clinical problems and available treatments

Due to the great regenerative capacity of bone, the majority of fractures reach resolution through complete healing. Nevertheless, incomplete healing is observed in 10% of all fractures, usually because the size of the defect exceeds the intrinsic healing capability of bone [13]. Defining standard dimensions of such non-healing bone defects is challenging, as they depend on the anatomic location, the state of the soft tissue (*e.g.* injury of the periosteum or the surrounding muscles), patient's age, and the presence of other pre-existing clinical conditions (*e.g.* chronic diseases) [28]. Nevertheless, in general, defects with a length greater than 2 cm and larger than 50% of the bone circumference are likely to have a poor regenerative outcome [28, 29]. In the craniomaxillofacial area, such defects could be the result of cancer resection (*e.g.* squamous cell carcinoma with bone invasion, or osteosarcoma), after radiation therapy and osteoradionecrosis, trauma, infection, or congenital abnormalities (*e.g.* cleft lip and/or palate) [8, 30]. In addition to these large bone defects, non-healing lesions might also stem from relatively small traumatic insults of the dentoalveolar ridge or as a consequence of tooth extraction. These conditions progressively worsen over time due to the lack of physiological loading [30].

It has been estimated that worldwide over 2.2 million bone-grafting procedures are performed every year [31]. Currently, the gold standard for several maxillofacial, orthopedic and neurosurgery procedures is an autologous bone graft, whereby the patient's own bone is harvested from a secondary location (*e.g.* fibula, iliac crest or rib). Despite the effectiveness of this procedure, it is also associated with several drawbacks including an 8-39% risk of complications such as infection, nerve injury, donor site instability and donor site morbidity, with a possibility of developing chronic pain in up to 8% of the cases [32, 33]. In addition, tissue availability is limited and it is often challenging to achieve the required graft shape. Alternatively, bone grafts could be obtained from a human donor (allogeneic



transplantation), usually from cadaveric material. The use of fresh-frozen or freeze-dried allografts circumvents some of the aforementioned drawbacks, such as the donor site morbidity. Nevertheless, this grafting procedure brings the risks of immune rejection and disease transmission [31, 34]. Furthermore, due to the harsh sterilization techniques, osteoinductive properties of allografts are often compromised. As a consequence, the regeneration induced is subpar compared to bone restoration from autologous bone grafts [34]. In order to improve the osteoinductivity of the allografts, acid-treatments have been optimized to remove the bone's mineral fraction. This increases the bioavailability of growth factors like bone morphogenetic proteins (BMPs), which are entrapped in the ECM [35]. However, the osteoinductive features of demineralized bone matrix (DBM) are largely influenced by donor-specific factors, including gender and age and the processing method [35].

Due to these limitations, the use of synthetic bone grafts is becoming an increasingly popular option [31]. Currently, a great number of biomaterials that mimic the inorganic phase of bone is available. Among those, the most explored ones are combinations of hydroxyapatite, tricalcium phosphate, dicalcium phosphate or bioactive glasses [31]. Due to their different characteristics, the appropriate bone substitute should be selected based on the intended application (*e.g.* mechanical strength or filling) [32, 33]. Nevertheless, one of the main limitations of most of these biomaterials is that they are only osteoconductive and not osteoinductive. This means that they guide bone growth along their surface, without actively stimulating new bone formation [36]. In addition, their resorption rate is challenging to tailor and a foreign body reaction is occasionally observed as a consequence of their implantation [31, 37, 38]. Thus, the use of these bone substitutes as a stand-alone treatment is limited and currently they are mainly used as autologous graft extenders [33, 39, 40]. The drawbacks of autologous and allogeneic bone transplantation together with the lack of satisfactory bone substitutes represent the major driving force behind the search for alternatives.

MIMICKING FRACTURE HEALING: STRATEGIES FOR ENDOCHONDRAL BONE REGENERATION

Tissue engineering strategies for bone regeneration

The goal of bone tissue engineering (TE) is to develop effective regenerative strategies by combining relevant cell types with biomaterials and bioactive stimuli [41, 42]. The bone regenerative potential of a great number of different cell types, including MSCs derived

from different tissues (*e.g.* bone marrow [42, 43], adipose tissue [44, 45], dental pulp [46], placenta or umbilical cord [47]), embryonic stem cells [48] and induced pluripotent stem cells [49] has been investigated over the years. Similarly, the capability to support cell growth and differentiation has been explored for several biomaterials, including natural (*e.g.* collagen and fibrin) and synthetic polymers (*e.g.* poly(ϵ -caprolactone)) [42]. Finally, different types of stimuli can be used to enhance bone regeneration. The most studied ones are factors that promote osteogenesis (*e.g.* bone morphogenetic proteins 2 and 7) [50, 51], vasculogenesis (*e.g.* vascular endothelial growth factor) [52] and immunomodulation [53].

The most commonly employed strategy for bone regeneration is to mimic the intramembranous repair process. Traditionally, this approach relies on the use of cells with osteogenic potential, such as osteogenically differentiated MSCs, to directly produce a bone analogue prior to implantation [25, 54, 55]. However, so far, this type of approach has shown greater potential *in vitro* compared to *in vivo*, probably due to insufficient vascularization of the constructs upon implantation [56-58]. In particular, the lack of a vascular network hinders the nutrient and oxygen exchange, resulting in necrosis of the central part of the implant and impaired regeneration [58]. Several strategies have been developed in order to overcome this challenge, including the pre-vascularization of the osteogenic constructs *in vitro* [59, 60] or the local delivery of pro-angiogenic factors [52]. Nevertheless, the ideal solution has yet to be found [56].

A promising alternative strategy exploits the chondrogenic potential of stem cells to mimic the endochondral ossification process occurring during fracture healing [25, 56, 61]. Specifically, a cartilaginous soft callus is engineered *in vitro* and implanted at the bone defect site [25, 56]. Similarly to natural fracture repair, the implanted cartilage will acquire a hypertrophic phenotype, will be invaded by blood vessels, host osteoblasts and osteoclasts, and eventually be converted into new bone tissue [22, 25, 56, 62]. The suitability of various cell types to produce a cartilage template that triggers bone formation *in vivo* has been investigated. In particular, the feasibility of employing embryonic stem cells [63, 64], adipose-derived stem cells [65, 66], periosteum-derived cells [67] and bone marrow-derived MSCs [68-72] has been confirmed. Among these cell types, bone marrow-derived MSCs represent the most explored one, probably due to the well-established protocol for their chondrogenic differentiation [73] and their natural tendency to acquire a hypertrophic phenotype [74]. The advantages of exploiting this strategy for bone regeneration are multiple. Firstly, compared to MSC-derived osteogenic cells, chondrocytes can better survive in environments subjected to low nutrient availability and low oxygen tension [25, 75]. This could promote their survival upon implantation, as it has been shown that these cells could persist for several weeks at the defect site and actively contribute to new bone



formation [62, 76]. In addition, hypertrophic chondrocytes display an increased secretion of MMPs and pro-angiogenic factors, including vascular endothelial growth factor (VEGF) [77], transferrin [25] and angiopoietin 1 and 2 [56], which induces matrix remodeling and promotes blood vessel invasion. This means that, the vascularization of the engineered cartilage *in vivo* occurs in a self-governed manner that does not require any external stimuli [78]. Therefore, it eliminates the need for an integrated vascular network already *in vitro*, greatly simplifying the culturing process [57]. Thanks to these properties, when directly compared to osteogenically differentiated implants, the chondrogenically differentiated ones displayed superior bone regeneration [61, 76, 79]. Considering this evidence, it is possible to conclude that endochondral bone regeneration (EBR) is an attractive strategy for the regeneration of critical-size bone defects.

Endochondral bone regeneration: what comes after the proof of concept?

The proof of concept of recapitulating the natural endochondral healing process for regenerative purposes has been widely established in the last 15 years [56, 62, 68-71, 76, 80, 81]. MSCs have been used alone [69, 74, 81] or in combination with several biomaterials [68, 70, 80, 82] to develop a cartilaginous template that, upon implantation, would trigger new bone formation both ectopically [71, 74] and orthotopically [68-70, 82]. Together, this evidence supports the robustness and efficiency of EBR-based approaches. Nevertheless, several challenges still need to be faced in order to promote the clinical translation of EBR-based strategies. In particular, numerous aspects that pertain to the *in vitro* development of the engineered cartilage need to be standardized in order to obtain a predictable therapeutic effect upon implantation. For example, no consensus has been reached on the optimal length and protocol used to induce chondrogenic differentiation prior to implantation [56, 83, 84]. In more detail, *in vitro* differentiation can span from as little as 1 week [81] to 7 weeks [74] and could entail chondrogenic differentiation alone or include subsequent hypertrophic induction [56, 76, 83]. In addition, the optimal 3D culture system (*e.g.* scaffold free pellets, hydrogel or scaffold-based systems) and the ideal characteristics of the biomaterials used to support MSC chondrogenesis are still under investigation [56, 85, 86].

Another major bottleneck for standardization of EBR-based therapeutic solutions is the variability and unpredictability of the chondrogenic potential of MSCs isolated from different patients [87]. Several intrinsic factors, including the patient's age and sex, influence MSC variability in terms of chondrogenic potential [88]. Furthermore, extrinsic factors, including the technique used to harvest a patient's bone marrow can play a role in affecting the efficiency of MSC differentiation [87]. A consequence of this fluctuation



in MSC differentiation potential is that EBR-based treatments with autologous MSCs are not possible for all patients [69, 89, 90]. In addition, the need for *in vitro* expansion, an intermediate sub-culturing step necessary to achieve a number of cells that is sufficient to engineer the cartilage template, is known to negatively impact the stem cell characteristics of MSCs and their differentiation potential [91, 92]. This implies that, even if the MSCs present adequate chondrogenic capacity at low passages, it might still be reduced or lost during the expansion phase. Thus, to promote the clinical translation of EBR-based approaches, it is a priority to identify strategies to overcome this issue.

The use of non-autologous MSCs to fabricate the cartilaginous template could represent a promising solution to the donor-to-donor variability problem [93-95]. In more detail, xenogeneic - from a donor of a different species - or allogeneic - from an unrelated donor of the same species - MSCs could be isolated, chosen for their high chondrogenic potential and expanded in advance, establishing a collection of stored, pre-selected cells. This would not only eliminate the dependency on a patient's own MSCs but also reduce the time required to produce the graft substitute and avoid the need for two interventions for the patient. Therefore, the use of pre-screened, highly chondrogenic, allogeneic or xenogeneic MSCs could improve the predictability and the quality of the cartilaginous template developed *in vitro*, potentially enhancing *in vivo* bone formation. In spite of these advantages, a major concern is represented by the potential immunogenicity of non-autologous MSC-derived chondrocytes, as it could prevent the complete remodeling and integration of the cartilaginous construct [96-98]. It is known that culture-expanded, non-differentiated MSCs exhibit immunomodulatory properties and could be safely used in allogeneic settings [99-101]. Nevertheless, contrasting evidence has been reported upon the retention of such properties *in vitro* after chondrogenic differentiation [94, 98, 102]. Furthermore, since all experiments involving EBR were performed in an immunocompromised [62, 69, 77, 80, 103] or autologous setting [70, 76, 82], the immune response against MSC-derived chondrocytes *in vivo* is largely unknown. Thus, the feasibility of using non-autologous cells to induce EBR in the presence of a fully functional immune system has yet to be determined.

To increase the immune-compatibility and to enhance the clinical translatability of EBR-based approaches, native or engineered non-autologous cartilage could be decellularized [103, 104] or devitalized [78, 95, 105]. In both decellularized or devitalized tissues, the death of the resident cells is induced, enabling the creation of an off-the-shelf product for both strategies [78]. The main difference between the two methods is that, while in decellularization protocols the cellular debris is removed, this is not the case during devitalization [106]. The rationale behind the use of such non-vital cartilaginous tissues is that all the instructive elements necessary to trigger bone formation are secreted by

the cells and retained within the ECM. Therefore, to maximize the new bone formation upon *in vivo* implantation, it is crucial to find a balance between the removal of all the immunogenic elements derived from the non-autologous cells (e.g. DNA, mitochondria, and membrane debris) and the preservation of bioactive components (e.g. growth factors like VEGF and BMP-2) [78, 105, 107, 108]. However, this is particularly challenging for cartilage because, due to its avascular and dense nature, extensive physical, chemical and enzymatic treatments are required in order to remove the cellular debris. This ultimately leads to the partial loss of ECM bioactive components, limiting the regenerative potential of the obtained tissues [105, 109-113]. As a consequence, so far, decellularized and devitalized cartilaginous tissues have failed to match the regenerative capability of constructs containing living cells [104, 105, 114]. Thus, further research is required for this approach to become a viable alternative to the transplantation of autologous, living engineered cartilage.

RESEARCH AIM AND THESIS OUTLINE

The overall aim of this thesis is to improve the clinical translation of endochondral bone regeneration (EBR)-based strategies to treat critical-sized bone defects. To achieve this goal, two strategies are followed. For this reason, the work presented in this thesis is divided in two sections:

- Part I: optimizing the cartilaginous template for endochondral bone regeneration
- Part II: employing allogeneic mesenchymal stem cells for endochondral bone regeneration

Part I

The aim of the first part of the thesis is to investigate biomaterial-based and cell-based strategies to engineer a cartilaginous template with predictable features in vitro. Specifically, the research questions of this section are:

Is it possible to improve the cartilaginous template developed *in vitro* by:

- employing dental pulp stem cells as an alternative cell source (**chapter 2**)?
- employing vitreous humor as the supporting material (**chapter 3 and 4**)?

To overcome the limitations associated with the use of bone marrow-derived MSCs, in **chapter 2**, the feasibility of using dental pulp stem cells (DPSCs) as an alternative cell source to produce the cartilaginous template is explored. DPSC potential to differentiate towards the chondrogenic lineage has been previously reported [115, 116], even though not

thoroughly investigated. Hence, in this chapter, a systematic approach is used to evaluate DPSC chondrogenic potential and their capability of acquiring a hypertrophic phenotype. Since DPSCs were found to be more suitable for fibrocartilage TE, the next chapters focus on the use of MSCs for EBR.

In **chapters 3 and 4**, the possibility of improving the chondrogenic differentiation of MSCs by exploiting the characteristics of vitreous humor (VH) as supportive material is evaluated. In **chapter 3**, the tissue isolation method, the retention of the ECM components, VH cytocompatibility, and its capability to support MSC chondrogenic differentiation *in vitro* are all investigated. In **chapter 4**, the capability of VH to enhance chondrogenic differentiation and hypertrophic induction *in vitro* is evaluated for multiple MSC donors. In addition, the resulting engineered cartilaginous templates for EBR are examined in a subcutaneous rat model.

Part II

The aim of the second part of this thesis is to improve the clinical translatability of EBR-based approaches by exploring the possibility of using allogeneic MSCs. Specifically, the research questions of this section are:

Can allogeneic MSCs:

- represent a viable alternative to autologous cells for EBR (**chapter 5 and 6**)?
- be used to engineer a cartilage-based off-the-shelf product (**chapter 7**)?

The use of allogeneic MSCs would increase the clinical translatability of EBR-based strategies, as patients would not need to rely on the unpredictable potential of their own stem cells anymore. Nevertheless, the potential immunogenicity of allogeneic MSC-derived chondrocytes could hamper the regenerative process. Thus, in **chapter 5**, the feasibility of using allogeneic MSCs is investigated on a theoretical level. Specifically, the available literature is investigated to establish whether chondrogenic differentiation would negatively affect MSC immunoevasive and immunomodulatory properties and, consequently, compromise the conversion of the allogeneic cartilage into bone. Since contrasting evidence is reported, in **chapter 6**, the effectiveness of using non-autologous, chondrogenically differentiated MSCs to regenerate an orthotopic defect in the presence of a fully functional immune system is evaluated. Thereafter, aiming at developing an off-the-shelf product, in **chapter 7**, the feasibility of using allogeneic, devitalized engineered cartilage as a stand-alone treatment for regeneration of critical size bone defects is explored.



Finally, **chapter 8** summarizes all findings and provides a general overview of how the work presented in this thesis integrates with and contributes to the development of the field. Furthermore, additional aspects relevant for clinical translation of TE constructs for endochondral bone regeneration will be considered.



Part I

*Optimizing the cartilaginous template for
endochondral bone regeneration*







The chondrogenic differentiation potential of dental pulp stem cells

2

A. Longoni
L. Utomo
I.E.M. van Hooijdonk
G.K.P. Bittermann
V.C. Vetter
E.C. Kruijt Spanjer
J. Ross
A.J.W.P. Rosenberg
D. Gawlitta

European Cells and Materials, 2020, 39:121-135



ABSTRACT

Dental pulp stem cells (DPSCs) are particularly promising for tissue engineering (TE) due to the ease of their isolation procedure, great expansion potential and capability to differentiate towards several cell types of the mesodermal, ectodermal and endodermal lineages. Although several studies hint that DPSCs exhibit potential for cartilage tissue formation, the chondrogenic potential of DPSCs has only been marginally explored. Thus, the aim of the present study was to closely investigate the chondrogenic differentiation capacity of DPSCs for TE applications. More specifically, the potential of DPSCs for engineering hyaline and fibrous cartilage was determined.

DPSCs obtained from 7 human molars were expanded and chondrogenically differentiated in a 3D pellet culture model. After 21 d of differentiation with chondrogenic stimuli, DPSCs displayed glycosaminoglycan, aggrecan and limited collagen type II deposition. Cells presented an elongated morphology and produced a collagen-rich extracellular matrix, with a predominance of collagen type I in most of the samples, a characteristic of fibrous cartilage tissue. Variations in the administration periods of several chondro-inductive growth factors, including transforming growth factor beta 3, bone morphogenetic protein-2, -6, -7 and insulin-like growth factor-1, did not increase glycosaminoglycan or collagen type II deposition, typical markers of hyaline cartilage tissue. Furthermore, DPSCs could not be stimulated to go into hypertrophic chondrogenesis.

These results indicated that under a large variety of chondro-inductive culture conditions, DPSCs could form fibrocartilaginous tissues but not hyaline cartilage. Thus, DPSCs represent a valuable cell source for the regeneration of fibrocartilage in joints.

INTRODUCTION

Since their first reported isolation [117], dental pulp-derived stem cells (DPSCs) have emerged as a particularly promising cell type for tissue engineering (TE) for several reasons [118, 119]. One of these reasons is the accessibility of the surgical site, as DPSCs can be isolated from routinely extracted third molars and potentially stored for further use, without additional donor site morbidity [119-121]. After the extraction, DPSCs can then be obtained from the pulp through enzymatic digestion or direct plating of minced pulp tissue [116]. Previous work demonstrated that these cells display a higher proliferation rate and higher colony forming efficiency *in vitro* than other types of multipotent stem cells for both, human [117, 122, 123] and rats [124]. Additionally, due to their neural crest origin, DPSCs have the potential to differentiate towards cell types belonging to the mesodermal, ectodermal, and endodermal lineages, such as osteoblasts [115, 125], odontoblasts [117], adipocytes [115, 125], chondrocytes [115, 125], myoblasts [115], neurons [115], and hepatocytes [119, 126]. In particular, their osteogenic and odontoblastic differentiation potential for intramembranous bone TE and dentistry applications is the most extensively studied [46, 117, 118, 126-128]. In contrast, the chondrogenic potential of DPSCs for TE applications remains underexplored as most studies investigating DPSCs have only addressed their chondrogenesis as part of their multilineage differentiation potential for human [115, 116, 125, 129, 130], murine [131] and porcine cells [132]. Nevertheless, investigating DPSC chondrogenic potential might be appealing, as the dental pulp and its stem cells originate from the cranial neural crest stem cells (NCSCs), which are also involved in the development of the temporomandibular (TMJ) joint disc [133] and Meckel's cartilage - the supportive, transient hyaline cartilage tissue present during embryonic development of the mammalian mandible [133]. Thus, DPSCs might represent a promising cell source for cartilage TE. In particular, it is interesting to explore the suitability of DPSCs for the regeneration of hyaline cartilage and fibrocartilage. These two types of cartilage have different characteristics. Hyaline cartilage is typically found on the articulating surfaces of synovial joints such as knees and elbows, in the connection between ribs and sternum and in the respiratory system. It is composed of small numbers of chondrocytes dispersed in a matrix rich in glycosaminoglycans (GAGs) and collagen type II [134]. On the other hand, fibrocartilage is found in the TMJ, the intervertebral discs and the menisci. It is composed of a heterogeneous cell population, with most cells presenting a fibroblastic phenotype and the remainder being chondrocytes-like cells, which express chondrocyte markers but lack the typical hyaline pericellular matrix [135]. The smaller amount of GAGs and the predominance of collagen type I characterize the fibrocartilage matrix [135].

By applying differentiation protocols developed for bone marrow-derived mesenchymal stem cells (MSCs), a variable chondrogenic potential of DPSCs is observed. In particular,



depending on the donor and the culture conditions, DPSCs either fail to differentiate into chondrocytes [136, 137] or are able to express typical chondrogenic differentiation markers such as aggrecan [125, 138] and collagen type II [115, 129], as well as to secrete GAGs *in vitro* [115, 125, 138, 139]. Discrepancies in the applied culture methods could partially explain these differences as, in a few studies, chondrogenesis was induced in a monolayer culture system [124, 140, 141]. Despite this, the *in vitro* model presents limitations when compared to 3D culture methods (e.g. pellet culture) [142, 143]. Nevertheless, during chondrogenesis, DPSCs present a different gene expression profile than MSCs [137]. Thus, similar to other types of MSC-like populations such as adipose-derived stem cells [144], DPSCs might respond differently to chondrogenic stimuli. Therefore, differentiation protocols developed for MSCs might need to be further optimized to reveal the full chondrogenic potential of DPSCs.

It is uncertain whether differentiated DPSCs have the capability, as MSCs, to acquire a hypertrophic phenotype. This is particularly relevant when aiming at cartilage regeneration. If chondrocytes acquire a hypertrophic phenotype, they start secreting pro-angiogenic factors and metalloproteinases that promote blood vessel invasion and matrix remodeling upon *in vivo* implantation. Consequently, the cartilaginous TE construct could be eventually remodeled into bone, by following the endochondral ossification pathway [25, 145].

A more systematic approach is required for exploring the chondrogenic potential of DPSCs. Thus, the aim of the present study was to closely investigate the chondrogenic differentiation potential of human DPSCs to evaluate the feasibility of their use for hyaline cartilage and fibrocartilage TE applications. To do so, the differentiation potential of DPSCs was characterized from 7 third molars. Furthermore, the differentiation protocol was tailored by comparing the effect of several chondro-inductive growth factors (GFs). Finally, the potential of DPSCs to pursue hypertrophic chondrogenic differentiation was investigated.

MATERIALS AND METHODS

Isolation and expansion of human DPSCs

DPSCs were obtained from the dental pulp of 7 extracted third molars from 5 patients of the University Medical Centrum Utrecht after acquiring their written informed consent (UMCU biobank, protocol no. 15-149) (Table 1). Directly after extraction, the molars were sterilized in 70% ethanol and stored temporarily in sterile phosphate buffered saline (PBS) containing 100 units/mL penicillin with 100 µg/mL streptomycin (pen/strep; Invitrogen). Subsequently, a slit was created in the enamel along the buccal and lingual grooves using

a sterile dental aerator drill with diamond burr. Next, the teeth were sterilized in 10% povidone-iodine (Fresenius-Kabi, Bad Homburg vor der Höhe, Germany) for 5 min and, subsequently, bifurcated with a dental elevator. Then, the dental pulp was removed from the pulp chamber, cut into pieces of approximately 1 mm³ and incubated for 3 h at 37°C and 5% CO₂ in 3 mg/mL collagenase type II (Worthington). A single cell suspension was obtained from the digests using a 70 µm cell strainer. Cells were plated and cultured at 37°C and 5% CO₂ in expansion medium consisting of Minimum Essential Medium α (αMEM; Gibco) supplemented with 10% heat-inactivated fetal bovine serum (FBS; HyClone), 0.2 mM L-ascorbic acid-2-phosphate (Sigma-Aldrich), 1% pen/strep and 1 ng/mL basic fibroblast growth factor (R&D Systems). Medium was gently refreshed after 24 h to remove debris, and every 3 – 4 d thereafter. DPSCs were cultured until 80% confluency and passaged at a density of 1,500 cells/cm². Human MSCs used as control were isolated and characterized as previously described [89].

Table 1. DPSC donor demographics and molar origin

Donor	Age	Sex	Molar origin	Element number
A	21	Female	Maxilla	–
B	25	Female	Mandible	–
C	20	Male	Maxilla	–
D	20	Female	Maxilla	18
			Maxilla	28
			Mandible	38
E	21	Female	Mandible	38

– indicates unknown element number.

Marker expression profile

At passage 4, DPSCs were characterized for their surface and internal marker expression by flow cytometry using a FACS Canto II system (BD Biosciences). The presence of the MSC markers CD73 (PE-conjugated), CD90 (FITC-conjugated), CD105 (APC-conjugated) and CD271 (FITC-conjugated) along with the absence of the hematopoietic stem cell markers CD34 (APC-conjugated) and CD45 (PE-conjugated), the monocyte marker CD14 (FITC-conjugated) and the B cell marker CD79α (PE-conjugated) were determined. All antibodies were purchased from Abcam. Additionally, the level of internally expressed neural crest marker nestin (PE-conjugated; R&D Systems) was examined in fixed and permeabilized cells. DPSCs were stained for 15 min at room temperature, shielded from direct light. Dilutions of the antibodies were used according to the manufacturer's instructions. Isotype-matched



controls (Abcam) and unstained cells were included as negative controls for the gating strategy. For nestin, an additional control consisting of unstained, fixed and permeabilized cells was included. Data were analyzed using FlowJo (version 10, Ashland, OR, USA). Gating of single, viable cells for the groups that were stained for the extracellular CD markers was based on the forward and sideward scatter dot plots of the unstained cell controls. Since the number of recorded events per sample varied, the flow cytometry data are presented normalized to the peak height (number of events), resulting in relative percentages. A minimum of 10,000 events were recorded for each flow cytometry measurement.

Colony count and proliferation assay

To assess the colony forming potential, primary isolated DPSC colonies containing more than 25 cells were counted under a microscope (DMi1; Leica) in duplicate. Data are presented as the mean of the two individual counts.

At passage 3, DPSCs were seeded at 1,500 cells/cm² and cultured in expansion medium for 7 d at 37°C in 5% CO₂. Afterwards, cells were harvested and counted in triplicate on at least three time points (ranging from 1 to 7 d after seeding). In order to determine the time points in between which the cells displayed exponential growth, the logarithmic average cell yield values were plotted against time. In this graph, the lag phase, log phase and stationary phase of cell growth were identified. The log phase (*i.e.* the linear region of this graph) was selected to calculate the population doubling time (PDT) by applying the equation:

$$PDT = \frac{(Ty - Ti) * \log(2)}{\log\left(\frac{Y}{I}\right)}$$

where Ty = incubation time at end of log phase (h); Ti = incubation time at the start of log phase (h); Y = cell number at the end of the log phase; I = cell number at the start of the log phase.

Three-lineage differentiation potential

For osteogenic differentiation, DPSCs were cultured at passage 3 in monolayers in osteogenic differentiation medium [α MEM supplemented with 10% heat-inactivated FBS, 0.2 mM L-ascorbic acid-2-phosphate, 1% pen/strep, 10 mM β -glycerophosphate (Sigma-Aldrich) and 10 nM dexamethasone (Sigma-Aldrich)] that was refreshed twice per week. After 7 d, cells were fixed with 4% formaldehyde, permeabilized with 0.2% Triton-X in Tris-buffered saline and stained for alkaline phosphatase (ALP) activity using the Fuchsin + Substrate - Chromogen System (Dako) according to the manufacturer's instructions.

Mineralization was assessed at day 14 by staining the fixed monolayers with 2% alizarin red S (pH 4; Sigma-Aldrich) for 2 min. Images were acquired using a DMI1 microscope (Leica).

For adipogenic differentiation, DPSCs were cultured in monolayers in adipogenic differentiation medium [α MEM supplemented with 10% heat-inactivated FBS, 1% pen/strep, 1 μ M dexamethasone, 0.5 mM 3-isobutyl-1-methylxanthine (Sigma-Aldrich), 0.2 mM indomethacin (Sigma-Aldrich) and 1.72 μ M insulin (Sigma-Aldrich)] that was changed twice a week. After 21 d, cells were fixed in 10% formalin, washed with 60% isopropanol and stained with oil red O (Sigma-Aldrich) for 20 min. Images were acquired using a DMI1 microscope.

For chondrogenic differentiation, DPSCs were centrifuged into pellets (200,000 cells/pellet) in polypropylene tubes (Greiner) and cultured in 500 μ L chondrogenic differentiation medium (CDM) consisting of high-glucose DMEM (Thermo Fisher Scientific) supplemented with 1% ITS + Premix (Corning), 0.1 μ M dexamethasone, 0.2 mM L-ascorbic acid-2-phosphate, 1% pen/strep as previously described [89]. 10 ng/mL TGF- β 1 (PeproTech) was freshly added to the CDM. The medium was refreshed daily during the first 4 d after pellet formation, thereafter twice a week. After 21 d of culture, the pellets were fixed in 10% formalin, dehydrated, cleared in xylene and embedded in paraffin wax. 5 μ m-thick sections (cut using a Microm HM340E microtome; Thermo Fisher Scientific) were deparaffinized with xylene and rehydrated. To assess GAG production, sections were stained with 0.04% toluidine blue solution (Sigma-Aldrich) in 0.1 M sodium acetate (pH 4; Sigma-Aldrich) and counterstained with 0.2% fast green (Sigma-Aldrich). To evaluate collagen deposition, sections were stained with alcian blue (pH 2.5; Sigma-Aldrich) and picrosirius red (Klinipath, Duiven, the Netherlands). Images were acquired using an Olympus BX51 microscope and Olympus DP70 camera.

Gene expression analysis

DPSCs [$n = 3$, donor A, D(28) and E] were expanded and harvested at passage 4 to form pellets as described above. After 21 d of chondrogenic induction, pellets were mechanically crushed, using pestle and mortar, in TRIzol reagent (Thermo Fisher Scientific) and mRNA was isolated from the aqueous phase obtained, according to the manufacturer's instructions. DNA contaminations were removed by a DNase treatment (Turbo DNase; Thermo Fisher Scientific), according to the manufacturer's instructions. mRNA was quantified using a NanoDrop ND- 1000 spectrophotometer (Thermo Fisher Scientific) at 260/280 nm. cDNA was synthesized using the iScript cDNA Synthesis Kit (Bio-Rad) according to the manufacturer's instructions. Gene expression analysis of SRY-Box 9 (*SOX9*), cartilage oligomeric matrix protein (*COMP*), aggrecan (*ACAN*), collagen type I (*COL1A1*), collagen



type II (*COL2A1*) and collagen type X (*COL10A1*) was done on a Bio-Rad CFX96 Real-Time PCR Detection System (Bio-Rad) using FastStart SYBR Green Master mix (Sigma-Aldrich). Glyceraldehyde 3-phosphate (*GAPDH*) was used as a housekeeping gene and the relative expression was determined by the $2^{-\Delta CT}$ method. Values above cycle 40 were considered undetectable. Primers used are listed in Table 2.

Table 2. List of primers used

Gene	Primer forward (5'-3')	Primer reverse (5'-3')
SOX9	CAACGCCGAGCTCAGCA	TCCACGAAGGGCCGC
COMP	CCCCAATGAAAAGGACAACCTGC	GTCCTTTTGGTCGTCGTTCTTC
ACAN	ATGTTCCCTGCAATTACCACCT	TTGATCTCATACCGTCCTTCTTC
COL1A1	AAGAGGAAGGCCAAGTCGAG	GTTTCCACACGTCTCGGTC
COL2A1	GCCTCAAGGATTTCAAGGCAAT	GCTTTTCCAGTTTTCCAGCTT
COL10A1	CAAGGCACCATCTCCAGGAA	AAAGGGTATTTGTGGCAGCATATT
GAPDH	ATGGGGAAGGTGAAGGTCG	TAAAGCAGCCCTGGTGACC

Tailoring the DPSC chondrogenic differentiation protocol for hyaline cartilage

DPSCs [$n = 3$, donor A, D(28) and E] were expanded and harvested at passage 4 to form pellets (500,000 cells/pellet) in round-bottom, Corning® Costar® Ultra-Low Attachment 96-well plates. Different GFs associated with chondrogenesis were evaluated for their potential to stimulate GAG and collagen deposition when supplemented to the CDM, either singularly or in combinations. The screened GFs and their respective concentrations were: 10 ng/mL TGF- β 3 (PeproTech), 100 ng/mL BMP-2 (InductOS, Wyeth/Pfizer, New York, NY, USA), 100 ng/mL BMP-6 (PeproTech), 100 ng/mL BMP-7 (PeproTech) and 100 ng/mL IGF-1 (PeproTech). Pellets of each donor were divided into three groups. In the first group, pellets received only one single GF during the whole culture period (*i.e.* TGF- β 3, BMP-2, BMP-6, BMP-7 or IGF-1). In the second group, pellets received a Pellets of each donor were divided into three groups. In the first group, pellets received only one single GF during the whole culture period (*i.e.* TGF β -3, BMP-2, BMP-6, BMP-7 or IGF-1). In the second group, pellets received a continuous combination of TGF β -3 and one of the BMP isotypes or IGF-1 (*i.e.* TGF β -3 + BMP-2, TGF β -3 + BMP-6, TGF β -3 + BMP-7, TGF β -3 + IGF-1). The third group of pellets was stimulated with a cyclic alternating pattern of TGF β -3 and one of the BMP isotypes or IGF-1 (*i.e.* TGF β -3 and BMP-2, TGF β -3 and BMP-6, TGF β -3 and BMP-7, TGF β -3 and IGF-1). A schematic representation of the different medium changes is available in Figure 1. Pellets cultured in CDM without any additional GF were included as negative controls. After 28 d, 2 pellets per group were processed for histological analysis as described in the previous paragraph. 3 other pellets were digested overnight at 60°C in papain digestion

buffer [250 µg/mL papain, 0.2 M NaH₂PO₄, 0.1 EDTA and 0.01 M DL-cysteine hydrochloride (all Sigma-Aldrich)]. The total amount of GAGs was determined using the 1,9-dimethylmethylene blue (DMMB pH 3.0; Sigma-Aldrich) assay [146]. Chondroitin sulphate C (Sigma-Aldrich) was used as standard and the absorbance was measured. The sulphated GAG content was expressed as the ratio between the 525 and 595 absorbance values. To normalize the GAG content, DNA was quantified using a Quant-iT Picogreen dsDNA assay (Thermo Fisher Scientific) according to the manufacturer's instructions.

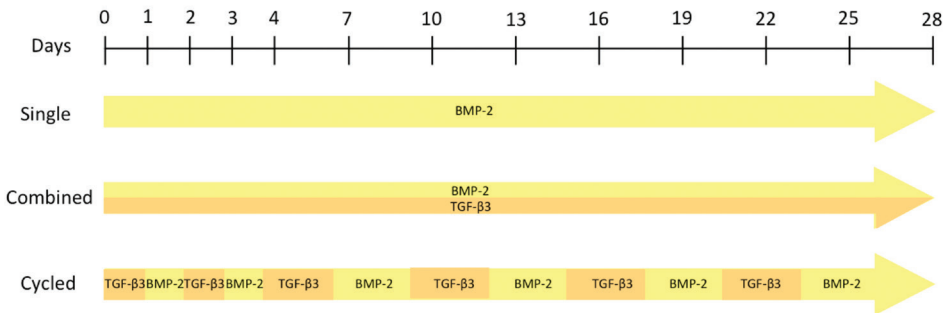


Figure 1. Schematic representation of the three different patterns of medium change. BMP-2 is used as an example to explain the patterns. The same patterns were applied for BMP-2, BMP-6, BMP-7 and IGF-1, all in combination with TGF-β3. After 28 d of culture, samples were harvested and processed for analysis.

Hypertrophy induction

To assess whether chondrogenically stimulated DPSCs were capable of responding to hypertrophic induction, pellets were formed at passage 4, as described above [$n = 3$, donor A, D(28) and E]. Since none of the tested (pattern of) GFs outperformed the others in terms of GAG deposition, chondrogenic differentiation was carried out by supplementing the medium with TGF-β3. After 28 d, the medium was changed to hypertrophic induction medium consisting of high-glucose DMEM supplemented with 1% ITS + Premix, 1 nM dexamethasone, 0.2 mM L-ascorbic acid-2-phosphate, 1% pen/strep, 10 mM β-glycerophosphate and 1 nM triiodothyronine (Sigma-Aldrich) for 7 additional days. At day 35, pellets were fixed and processed for histology as described above. In addition to toluidine blue staining, collagen type X immunostaining and von Kossa staining for mineralization were performed to assess hypertrophic matrix formation. von Kossa staining was done by incubating the sections for 1 h with 1% silver nitrate (Sigma-Aldrich) directly under a light bulb (Philips Master TL5 HO 54W 830, 1 m distance). Subsequently, the samples were washed with 5% sodium thiosulphate (Alta Aesar, Haverhill, MA, USA) and counterstained with haematoxylin.



Immunohistochemistry

To define the collagen types present in the matrix, immunohistochemical staining with primary antibodies directed against aggrecan (Novus Biologicals, Centennial, USA), collagen type I (Abcam), collagen type II (DSHB University of Iowa, USA), and collagen type X (Quartett, Berlin, Germany) was performed. All sections were deparaffinized and rehydrated as described above. For aggrecan and collagen type I stainings, antigens were retrieved by boiling the samples for 15 min at 95°C in 10 nM citrate buffer. For collagen type II detection, antigens were retrieved by treating the sections at 37°C with 1 mg/mL pronase (Sigma-Aldrich) and 10 mg/mL hyaluronidase (Sigma-Aldrich) for 30 min each. Finally, for collagen type X staining, antigens were retrieved by sequential incubation for 2 h with 1 mg/mL pepsin (Sigma-Aldrich) at pH 2.0 and for 30 min 10 mg/mL hyaluronidase, both at 37°C. The endogenous peroxidase activity was blocked by treating the sections for 10 min with 0.3% H₂O₂ solution. Furthermore, to prevent aspecific binding, the samples were incubated with 5% bovine serum albumin (BSA; Roche) in PBS for 30 min. Primary antibodies were diluted in 5% BSA/PBS (1:150 aggrecan, 3 µg/mL collagen type I, 0.6 µg/mL collagen type II, 10 µg/mL collagen type X) and incubated overnight at 4°C. Mouse isotypes (Dako) were used as negative controls at concentrations or dilutions matched with those of the primary antibodies. Samples were incubated for 30 min at room temperature with EnVision+ System- HRP labeled secondary antibody (Dako). Antigen detection was performed by incubation with 3,3'-diaminobenzidine tetrahydrochloride hydrate for no longer than 10 min. Sections were counterstained with 1:1 Mayer's haematoxylin in deionized water (Merck), dehydrated and mounted with permanent mounting medium (Depex; Merck).

Statistical analysis

The GAG/DNA-ratios are presented as means of at least three biological replicates and their standard deviations. A randomized block design with Bonferroni *post-hoc* analysis was applied to the GAG/DNA ratios, absolute DNA values and absolute GAG content, in order to evaluate statistical differences between groups. An unpaired *t*-test with Welch's correction was performed in order to evaluate the differences in gene expression between DPSCs and MSCs. SPSS (version 24, IBM) was used for all statistical analyses. Statistical significance was defined as $p < 0.05$.

RESULTS

DPSC isolation and characterization

7 cultures were successfully established from the dental pulp tissue derived from 5 healthy human donors (Table 1). Cells adhering to the tissue-culture plastic were visible within a maximum of 9 d after plating the tissue digests and grew out into distinct colonies. The numbers of colonies formed and the proliferation rates varied between DPSCs isolated from different donors (Figure 2b,c). After the first passage, all DPSCs displayed an elongated, fibroblastic morphology (Figure 2a).

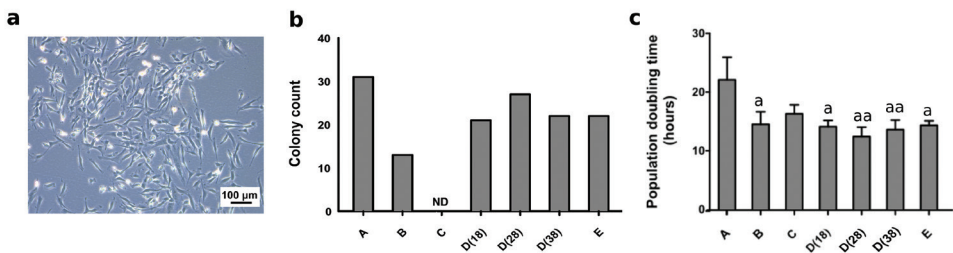


Figure 2. DPSCs characterization after isolation. **(a)** Representative images of DPSCs fibroblastic morphology and **(b)** number of colonies (mean of two individual countings of the same DPSC culture) formed by primary DPSCs. **(c)** Proliferation potential of all DPSC cultures expressed as PDT determined at passage 3. Statistical differences are shown as a $p \leq 0.01$, aa $p \leq 0.001$. ND: not determined because individual colonies could not be distinguished

Most DPSC cultures expressed cell surface markers (> 90% positive) associated with mesenchymal stem cells, including CD105, CD90 and CD73 and no expression (< 1.0% positive) of the hematopoietic stem cell markers CD34 and CD45, monocyte marker CD14 and B cell marker CD79α (Figure 3). Additionally, most of the DPSCs were positive for the neural crest marker nestin. Finally, CD271 was only expressed in a small subpopulation of each DPSC culture (1.4-9.6%). After characterization, DPSCs from donor C were excluded from further experiments as a relatively large cell population was positive for CD45 (35.3%), suggesting the presence of a hematopoietic subpopulation.

In contrast to the limited donor variation observed with respect to proliferation potential (Figure 2), the DPSCs exhibited heterogeneous differentiation capacity (Figure 4,5). Overall, all osteogenically stimulated DPSC cultures displayed ALP activity, an early osteogenesis marker, to various extents and mineralization nodules, a late osteogenesis marker. More variation was observed when DPSCs were differentiated towards the adipogenic lineage as the presence of intracellular lipid vesicles was observed in 5 out of 7 DPSC cultures.



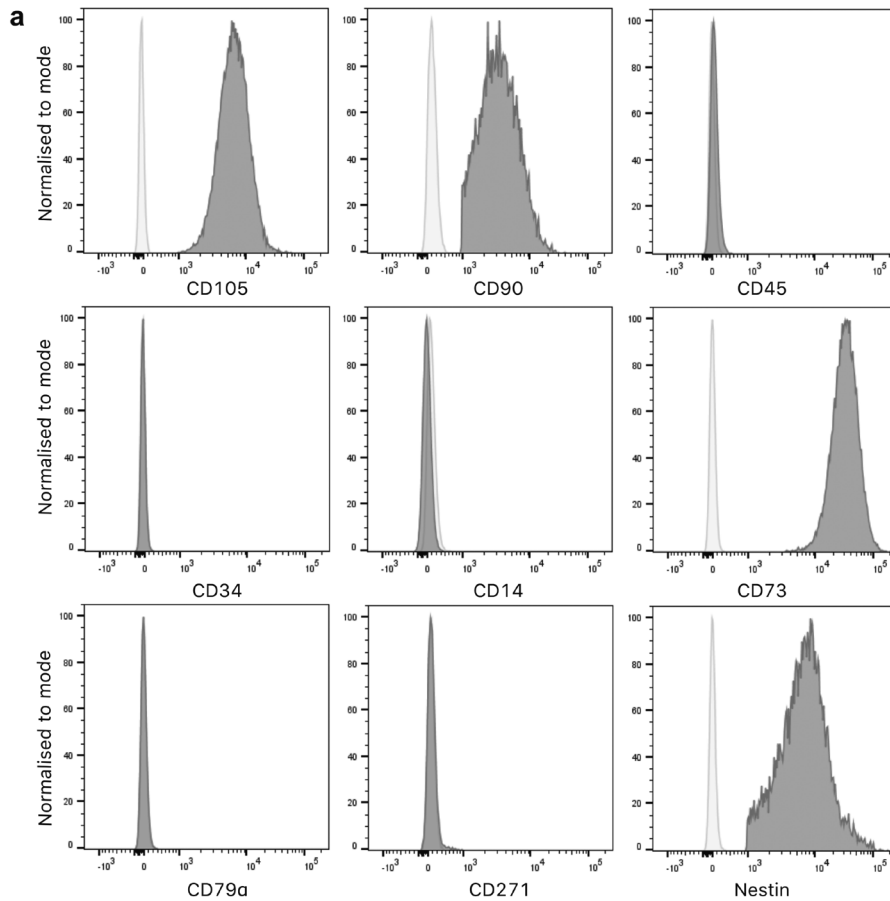


Figure 3. Expression of stem cell surface markers per DPSC culture. **(a)** An example of the graphs obtained from donor E (dark grey) and the relative isotype controls (light grey). **(b)** Percentage of positive cells for mesenchymal, hematopoietic and neural crest cell markers are depicted for DPSCs derived from the different donors.

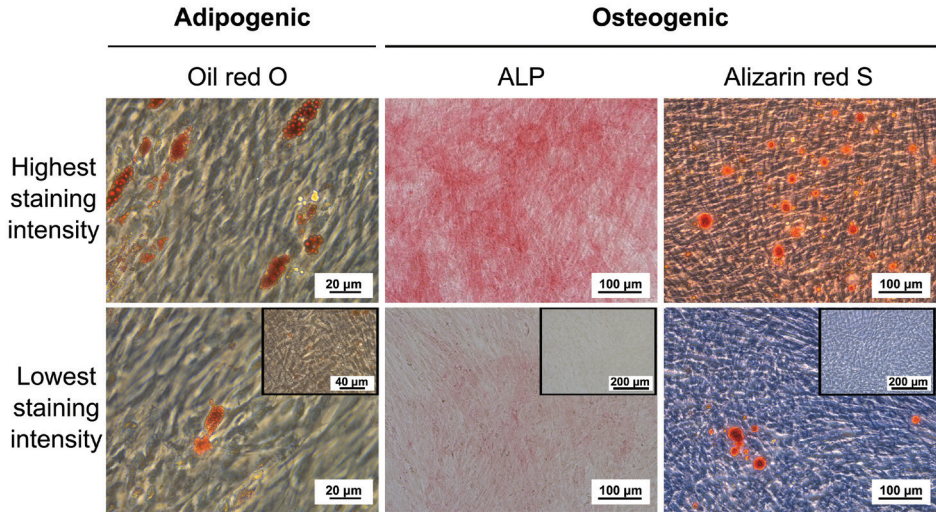


Figure 4. Microscopical evaluation of the differentiation potential of DPSCs towards the adipogenic and osteogenic lineages. Variations in lipid vacuole formation (orange/red vesicles), ALP activity (red staining) and mineralized nodule (bright red nodules) formation were observed between the DPSCs derived from different donors and within cultures derived from the same donor. Inserts represent the negative undifferentiated controls.

GAGs and aggrecan were present in all DPSC pellets after chondrogenic induction, although inter- and intra-donor variation was observed (Figure 5). Furthermore, for most DPSC pellets, collagen type I was most distinctly present in the ECM when compared to collagen type II (Figure 5). Gene expression analysis of the DPSCs confirmed the presence of chondrogenic markers including SOX9, COMP and ACAN in the pellet cultures derived from 3 donors. Consistent with the immunohistochemistry results, COL1A1 expression was upregulated in all cases. In contrast, COL2A1 expression was undetectable after 21 d of differentiation (Figure 6). In addition, the DPSCs adopted a flattened morphology, indicative of fibrocartilage formation, rather than a round morphology in lacunae (Figure 6), a characteristic of hyaline cartilage tissue.

Assessing DPSC potential for hyaline cartilage differentiation

To evaluate whether DPSCs also possessed the capacity to differentiate into the hyaline chondrogenic lineage *in vitro*, additional formulations and various patterns of exposure to chondro-inductive media were evaluated.

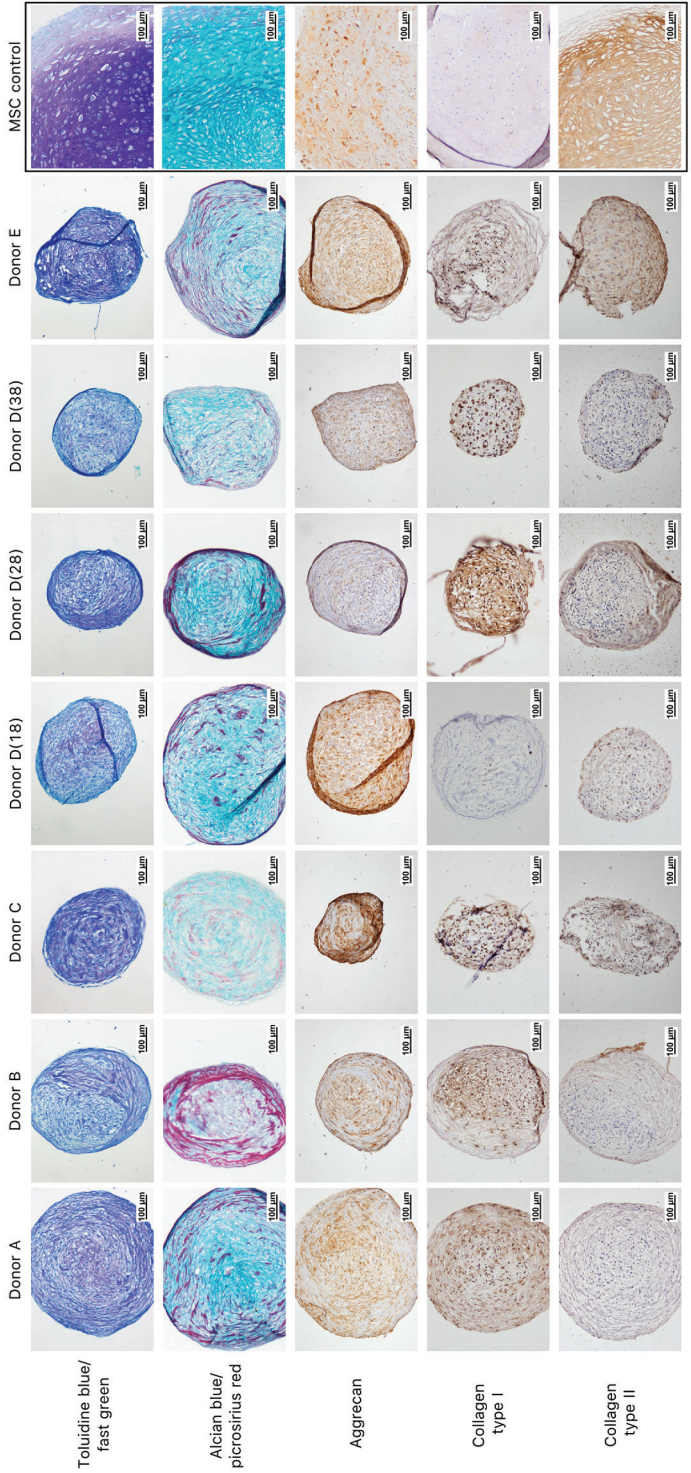


Figure 5. Overview of the chondrogenic differentiation potential of DPSCs from different molars and donors. DPSCs from all donors displayed chondrogenic differentiation, highlighted by GAG (toluidine blue and alcian blue staining) and aggrecan deposition. The presence of collagen was determined by picrosirius red staining and specific immunohistochemistry for collagen types I and II. Bone-marrow-derived MSCs cultured with the same differentiation protocol were included as a positive control for chondrogenic differentiation.

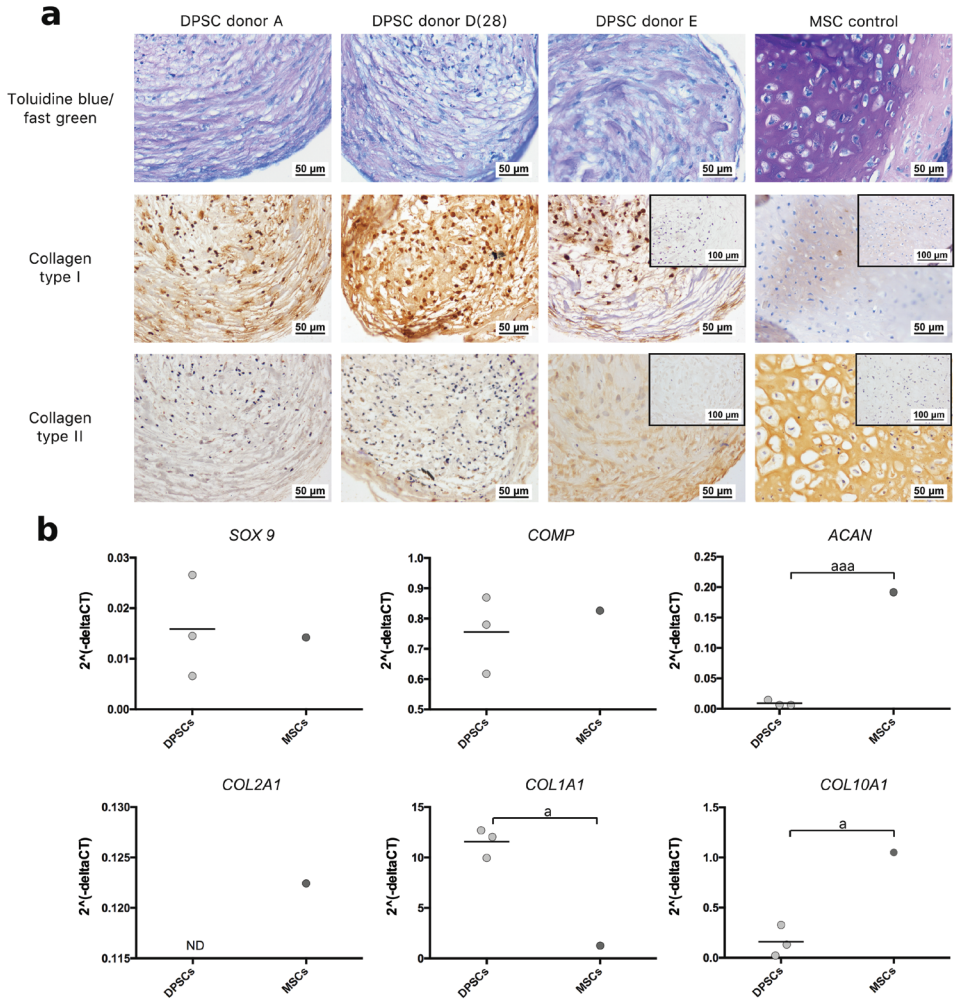


Figure 6. Evaluation of cell morphology and expression of chondrogenic markers for 3 DPSC donors. **(a)** A higher magnification of the toluidine-blue-stained sections highlighted the absence of the typical chondrocyte lacunae. Furthermore, the presence of collagen type I and II was highlighted when compared to the isotypes control depicted in the inserts. **(b)** Gene expression analysis confirmed the presence of chondrogenic markers after 21 d. MSC pellets cultured with the same differentiation protocol were included as a positive chondrogenic control. Dots represent the expression of the individual donors. ND: not detectable. Statistical differences are shown as a $p \leq 0.05$, aa $p \leq 0.001$.

Overall, the toluidine blue staining highlighted the GAG deposition for the different GFs and patterns of exposure (Figure 7a). No statistically significant differences were found in the GAG/DNA-ratios of the pellets that were cultured with the evaluated factors applied singularly or in an alternating pattern with TGF- β 3 (Figure 7b,c). Interestingly, the GAG/DNA-ratio of pellets exposed only to CDM was comparable to those receiving GFs in a singular

or cycled fashion (Figure 7b,c). Furthermore, pellets that received a BMP isotype combined with TGF- β 3 (Figure 7d) displayed the lowest GAG/DNA-ratio. Immunohistochemical evaluation highlighted that none of the conditions promoted extensive collagen type II deposition, while collagen type I remained an abundant component of the ECM in all conditions (Figure 8). In addition, cells remained flat and were not enclosed in lacunae.

DPSCs did not differentiate into the hypertrophic chondrogenic phenotype

Although differentiation into the hyaline cartilage lineage appeared limited, whether DPSCs were at all capable of continuing differentiation along this lineage into the hypertrophic chondrogenic phenotype was explored. Toluidine blue staining confirmed GAG production. However, no mineral deposition or collagen type X was present in the ECM of the pellets that were either exposed to chondrogenic medium only or to hypertrophic medium (Figure 9).

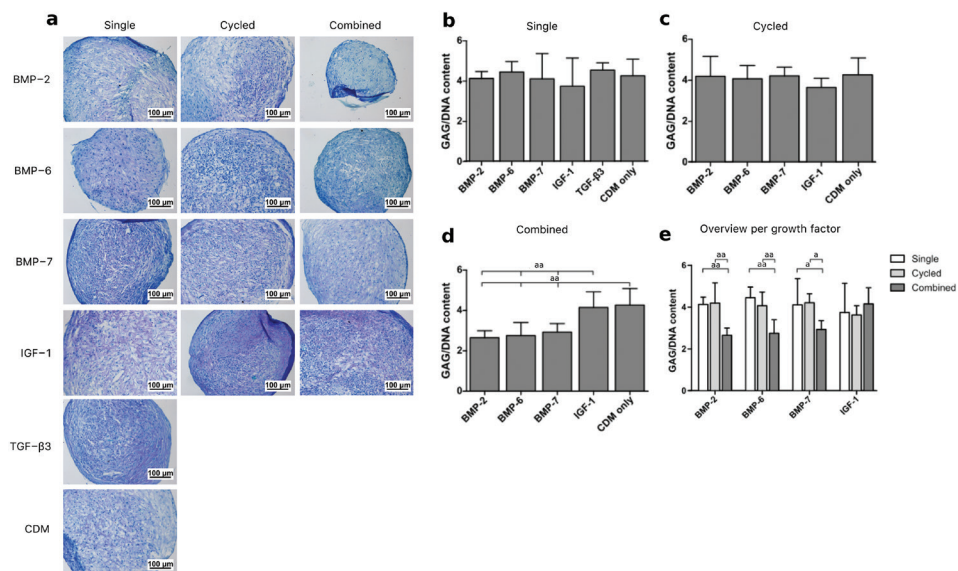


Figure 7. Effect of the different GFs and their administration patterns on GAG deposition. **(a)** Toluidine blue staining highlighted GAG deposition for all conditions. GAG/DNA ratios when GFs were applied **(b)** singularly, **(c)** in an alternating cyclic pattern or **(d)** combined. **(e)** Combined overview. In the cycled group, GFs were alternated with TGF- β 3 whereas, in the combined group, they were supplemented together with TGF- β 3. No GFs were added in the CDM group. Statistical differences are shown as ^a $p \leq 0.01$, ^{aa} $p \leq 0.001$.

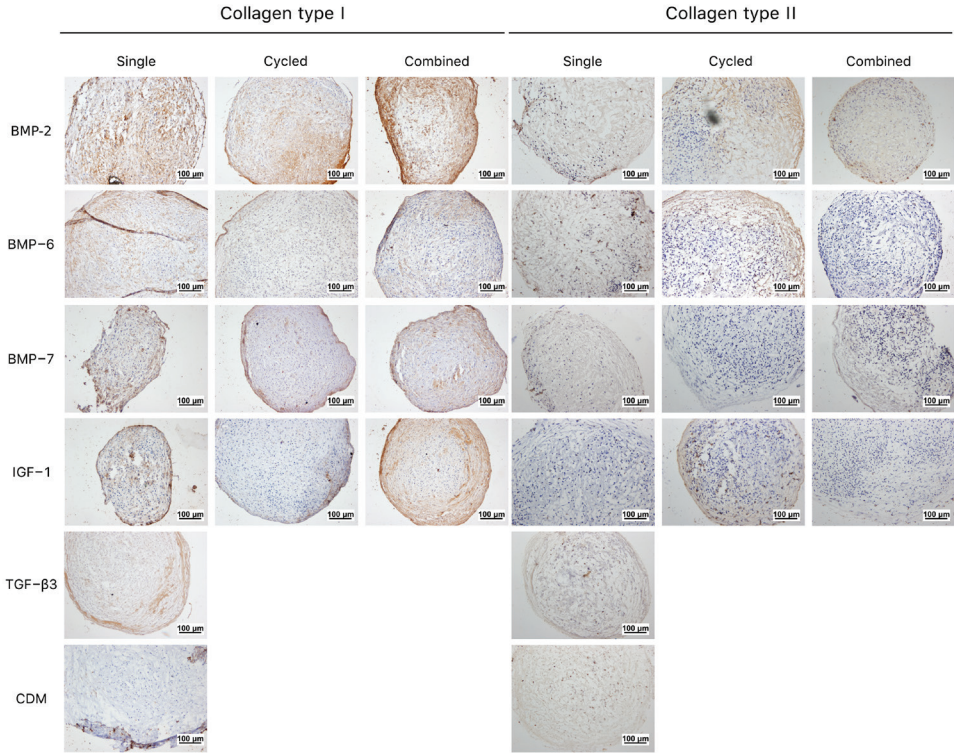


Figure 8. Effect of the different GFs and their administration patterns on collagen deposition. Immunohistochemical analysis highlighted the presence (brown) of collagen type I (left) and collagen type II (right) after 4 weeks of culture.

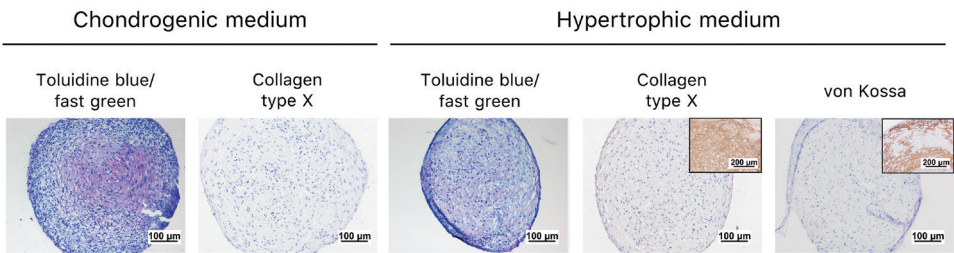


Figure 9. Hypertrophic marker presence in DPSCs after chondrogenic and hypertrophic induction for 35 d. Positive controls of differentiated BMSCs are depicted in the inserts.



DISCUSSION

Stem cells derived from the cranial neural crest, which during development are involved in the formation of Meckel's cartilage and the TMJ disc, can still be found after birth in the dental pulp [133]. Thus, the use of DPSCs was explored in the context of cartilage TE for maxillofacial applications. In particular, the present study extensively analyzed the DPSC capacity to form hyaline and fibrous cartilage *in vitro* by applying various differentiation regimes.

DPSC pellets derived from all 7 third molars extracted produced an ECM consisting of GAGs, aggrecan, collagen types I and II, which was consistent with other reports [115, 129, 131, 132]. This, together with the expression of *SOX9* and *COMP*, confirmed the competence of these cells to differentiate toward the chondrogenic lineage. However, histological analysis identified collagen type I as the predominant collagen type of the ECM in most of the cultures. Consistently, expression of *COL1A1* was also upregulated. Additionally, DPSCs displayed an elongated morphology typical of the fibroblast-like cells residing in the TMJ disc [135]. In contrast, GAG and collagen type II deposition was limited compared to the MSC cultures used as control condition. Interestingly, no *COL2A1* expression was detected. This apparent discrepancy between PCR quantification and histological results could be due to several factors, including post-transcriptional regulatory mechanism and difference in speed between the transcription and translation process and in half-life between mRNA and protein (2.6 to 7 hours for mRNA versus 46 hours for proteins) [147, 148]. Similarly, other studies reported collagen type I expression [137, 138] in DPSCs pellets and inferior (hyaline) chondrogenic potential when compared to other adult stem cell sources [124, 129, 137, 149]. As far as it can be ascertained, only one study explored the potential of using DPSCs embedded in a chitosan/alginate scaffold for the regeneration of the TMJ disc [150]. Consistent with the present study results, Bousnaki *et al.* observed an upregulation of collagen type I gene expression, together with expression of *SOX9*, aggrecan and *COMP* during chondrogenic differentiation [150]. These evidences indicated that, although it has been proposed that DPSCs could be applied for hyaline cartilage regeneration [126, 151], the *in vitro* deposited ECM had robust characteristics of fibrous cartilage tissue.

Several strategies have been reported in the literature to elicit the limited hyaline chondrogenic differentiation capacity of DPSCs, including transduction with an adeno-associated viral vector to induce TGF- β 3 expression [152], co-culturing with chondrocytes [153] and the use of nanopatterned hydrogels as a support material [139]. These strategies result in enhanced GAG [152, 153], collagen type II [139, 152, 153] and aggrecan [152] deposition. In the present study, the possibility of enhancing DPSC chondrogenesis was

evaluated by tailoring the composition of the differentiation medium. This is particularly appealing from a clinical translational perspective, as changing the supplied GFs represents a simpler and more straightforward option to implement. Thus, we evaluated if GAGs and collagen type II deposition could be enhanced by supplementing BMP-2, BMP-6, BMP-7 or IGF-1, alone or in combination with TGF- β 3. These (combinations of) GFs were selected because they are classically used in MSCs chondrogenic differentiation protocols [154]. Furthermore, BMP-2 and BMP-7 are particularly interesting candidates, not only because of their common use to stimulate MSC chondrogenesis, but also because they are expressed in early developing Meckel's cartilage [155] and the TMJ condyle [156]. Finally, since the administration of different GFs in an alternating, cyclic pattern can effectively enhance MSC chondrogenesis [157], its effect on DPSC differentiation was assessed. Results showed that culturing DPSC pellets with CDM alone already resulted in limited GAG deposition, which was not enhanced by any of the GFs or patterns evaluated. Remarkably, the combination of BMP-2, BMP-6, or BMP-7 with TGF- β 3 resulted in significantly lower GAG/DNA-ratios than when the DPSCs were cultured with either of these factors alone. This suggested that the continuous combination of one of the BMP isoforms with TGF- β 3 did not have a synergistic effect on DPSC chondrogenesis as observed for example for MSCs and adipose-derived stem cells [158, 159]. Furthermore, collagen type I remained an abundant component in the ECM in all conditions and the cells maintained an elongated morphology after differentiation, a phenomenon that is typical for fibro-chondrocytes [135]. These results further confirmed the DPSC predisposition to produce a fibrocartilaginous matrix under a large variety of chondro-inductive culture conditions.

Finally, the capability of chondrogenically differentiated DPSCs to acquire a hypertrophic phenotype was investigated. Inferior expression of collagen type X as compared to the MSC control was already observed upon chondrogenic induction. In addition, the absence of mineralization and collagen type X protein deposition after stimulation with both chondrogenic and hypertrophic media indicated that, unlike bone marrow-derived MSCs [74], DPSCs did not seem to have the potential to undergo hypertrophy under the differentiation conditions used in the study.

In conclusion, even if DPSCs are defined as MSC-like cells, they respond differently to the classical chondrogenic stimulation protocol for MSCs. The reasons for this behavior could be multiple. Interestingly, already without any GF stimulation, the expression of chondro-related genes is dissimilar between MSCs and DPSCs. These differences dramatically increase upon chondrogenic stimulation in a micromass model system [137]. Comparably, other studies have previously reported a different extent of GAG and collagen type II production by MSCs isolated from different tissues [149] or within different regions of the



same tissue [160] upon stimulation with the same chondrogenic medium. Even though the reason behind this heterogeneity in chondrogenic differentiation response is not clear, it can be hypothesized that it correlates with the presence of different GFs in the natural microenvironment [160], a different epigenetic profile or a different cell origin.

CONCLUSIONS

Our results indicated that, despite existing indications that DPSCs could be used for engineering hyaline cartilage [151] and hypertrophic chondrogenic tissues [120], these cells would be more suitable for engineering of fibrocartilaginous tissues, including the disc and condylar cartilage, for TMJ regeneration.

ACKNOWLEDGEMENTS

This study was part of project no. AOCMF-17-17G, supported by the AO Foundation, Davos, Switzerland. Part of the study was also supported by the BOOA research grant of the NVMKA. The antibody against collagen type II (II-II6B3), developed by T.F. Linsenmayer, was obtained from the DSHB developed under the auspices of the NICHD and maintained by The University of Iowa, Department of Biology, Iowa City, IA 52242.





Intact vitreous humor as a potential extracellular matrix hydrogel for cartilage tissue engineering applications

G.C.J. Lindberg
A. Longoni
K.S. Lim
A.J.W.P. Rosenberg
G.J. Hooper
D. Gawlitta
T.B.F. Woodfield

Acta Biomaterialia, 2019, 85:117-130

3



ABSTRACT

Decellularization of tissues, utilizing their biochemical cues, poses exciting tissue engineering (TE) opportunities. However, removing DNA from cartilage (dCart) requires harsh treatments due to its dense structure, causing loss of bioactivity and limiting its application as a cartilaginous extra cellular matrix (ECM). In this study, we demonstrate for the first time the successful application of vitreous humor (VH), a highly hydrated tissue closely resembling the glycosaminoglycan (GAG) and collagen composition of cartilage, as an ECM hydrogel to support chondrogenic differentiation.

Equine VH was extracted followed by biochemical quantifications, histological examinations, cytotoxicity (human mesenchymal stromal cells, hMSCs and human articular chondrocytes, hACs) and U937 cell proliferation studies. VH was further seeded with hACs or MSCs and cultured for 3-weeks to study chondrogenesis compared to scaffold-free micro-tissue pellet cultures and collagen-I hydrogels. Viability, metabolic activity, GAG and DNA content, chondrogenic gene expression (aggrecan, collagen I/II mRNA) and mechanical properties were quantified and matrix deposition was visualized using immunohistochemistry (Safranin-O, Collagen I/II).

VH was successfully extracted, exhibiting negligible amounts of DNA ($0.4\pm 0.4\mu\text{g}/\text{mg}$ dry-weight) and notable preservation of ECM components. VH displayed neither cytotoxic responses nor proliferation of macrophage-like U937 cells, instead enhancing both hMSC and hAC proliferation. Interestingly, encapsulated cells self-assembled the VH-hydrogel into spheroids, resulting in uniform distribution of both GAGs and collagen type II with increased compressive mechanical properties, rendering VH a permissive native ECM source to fabricate cartilaginous hydrogels for potential TE applications.

INTRODUCTION

The generally accepted tissue engineering and regenerative medicine (TERM) paradigm calls for the placement and cultivation of cells in a 3-dimensional (3D) environmental niche that mimics the complexity of the native extracellular matrix (ECM), thereby recreating and propagating the necessary cell-cell and cell-ECM interactions to elicit tissue formation and repair [161-165]. Decellularizing organs or tissues and utilizing their inherent sophisticated biological composition as naturally-derived biomaterials therefore has been extensively investigated as a tissue engineering (TE) strategy [162, 164-167]. Solubilization and chemical modifications of these decellularised tissues, enabling the formation of ECM-hydrogels, has further expanded their applicability and poses as a very exciting opportunity to guide the cellular development. This rationale is currently exploited for regeneration of several tissues, including heart valves, trachea, small intestinal submucosa, muscle, kidney, tendon and cartilage [106, 112, 164, 166, 168-170]. However, the effectiveness of the initial decellularization processes varies from organ to organ. In particular, more efficient decellularization has been observed in tissues with a less dense ECM architecture, and in those in which milder perfusion-based methods can be applied, *e.g.* vascular tissues including skin, bladder, liver, heart, lungs, and kidneys [106, 171]. Consequently, native cartilage tissue poses as a unique challenge to decellularize due to its dense ECM – consisting of a tight network of collagen type-II fibres and highly negatively-charged proteoglycan chains – and its avascular nature, ultimately limiting the success of many decellularization methods applied [106, 112, 168, 169, 172-174].

While several new protocols have recently been developed to more effectively remove resident chondrocytes from the native cartilage tissue [80, 103, 161, 164, 174, 175], the harshness of the required physical and chemical treatments compromises the integrity and microstructure of the cartilage ECM, leading to loss of bioactivity [105, 106, 112, 163, 168, 169, 172, 175-180]. Alternatively, near native glycosaminoglycan (GAG) preservation has been reported with milder decellularization protocols, but is instead plagued by significant retention of undesirable cellular material, including nucleic acids [175, 178]. Although cartilage is often suggested to be an immunologically privileged tissue – due to its limited vascular, lymphatic and neural supply – the successful removal of DNA contaminants from the native tissue matrix is still a key requirement [106, 167, 172, 181-183]. In particular, it has been described that incomplete removal of cell remnants and the presence of DNA fragments promotes macrophage polarization towards the inflammatory phenotype (M1), whereas a more effective removal of cellular debris is associated with a predominance of anti-inflammatory macrophages (M2) [183, 184]. Therefore, DNA removal is of pivotal interest, since a high M2/M1 ratio correlates with the host acceptance of bioengineered



implants and improved regeneration outcomes [162]. As cartilage tissue currently requires harsh processing techniques that concomitantly hinders the bioactivity of the material, there is a need to explore alternative tissue sources. Out of the connective tissues in our body, the vitreous humor (VH) is a soft tissue candidate whose makeup resembles the natural composition of the cartilage matrix (as detailed in Table 1), and yet despite this has received very little attention as a potential naturally-derived biomaterial, particularly for cartilage regeneration.

Table 1. Biochemical composition of articular cartilage and vitreous humor (VH) as reported in literature [176, 185-191] with respect to: water and cell content as described as percentage (%) of the total tissue composition; collagen type and composition as percentage of total collagen content (if previously reported); and examples of specific GAGs found in both cartilage and VH

	Component	Cartilage	VH
As % of total tissue	Water	66-79%	98-99.7%
	Cells	2%	No
As % of collagen content	Collagen II	90-95%	60-75%
	Collagen IX	Yes	25%
	Collagen V/XI	Yes	10-25%
	Collagen VI	Yes	Yes
	Collagen IV	Yes	Yes
	Opticin	Yes	Yes
	Fibrillin	Yes	Yes
	Hyaluronic acid	Yes	Yes
	Chondroitin sulfate	Yes	Yes
	Heparan sulfate	Yes	Yes

Vitreous humor, along with the aqueous humor (AH), ora serrata, cornea and ciliary muscle, are major tissues of the eye, as illustrated in Figure 1. Essentially, VH is an avascular tissue, predominantly consisting of GAGs, such as hyaluronic acid and chondroitin sulfate, and collagen types II and IX. VH is furthermore acellular and contains non-structural proteins and vitamins, such as albumin, globulins and ascorbic acid [192]. Interestingly, it was early investigations into bovine VH in 1934 that resulted in the very discovery and identification of hyaluronic acid [193, 194], which has become a globally applied biomedical, pharmaceutical and cosmetic material, nowadays typically sourced from bacterial expression systems [195-197].

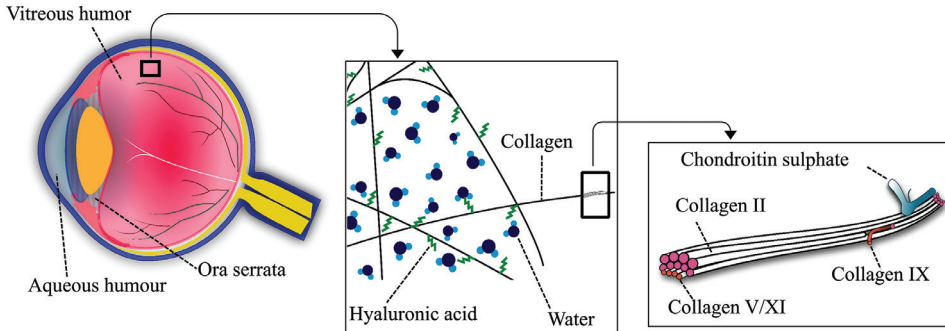


Figure 1. Anatomy of the eye as a cross section illustration. The vitreous humor is an acellular and avascular tissue that predominantly consists of collagen II fibres and hyaluronic acid.

Previous studies have described the ability of VH to inhibit growth of both gram-positive and -negative bacteria strains, thereby demonstrating inherent antibacterial properties as additional advantages of the tissue [198, 199]. Extracts of VH and/or AH has further been shown to inhibit endothelial cell growth and neovascularization [200] while it is claimed to support proliferation of renal cells [201], pericytes and fibroblasts [202]. In parallel with further mapping the physical, biomechanical and chemical properties of VH, the focus of current studies has predominantly been related to understanding the developmental stages and native role of VH and AH in ocular medicine such as intravitreal drug delivery [203-205], vitrectomy [206, 207], xeno- and allogenic-transplantation [208-210] as well as diagnostics of a wide array of eye diseases [211-214]. Given that VH cannot regenerate on its own, there is a growing interest to design substitute biomaterials, for example to fill the cavity after a vitrectomy [189, 215]. However, despite the large body of work investigating VH-tissue and its biomaterial substitutes, to the best of our knowledge, intact and un-modified VH hydrogels have not yet been investigated or applied as a cell instructive biomaterial for tissue engineering applications. Given the similarity in biochemical composition between native cartilage and native VH, as well as the inherent hydrogel structure of VH and wide adoption of VH-derived hyaluronic acid as a biomaterial, the aim of this study was to investigate if VH can be used as a native, un-modified, ECM hydrogel platform for supporting cartilage tissue formation *in vitro*. We adopted a systemic approach to compare frozen- and freshly-isolated VH tissues, evaluating if mild extraction conditions allowed for sufficient removal of DNA components while retaining high concentrations of protein and extracellular matrix components. Furthermore, we investigated the subsequent impact of isolated VH on influencing human mesenchymal stromal cell (hMSCs) and human articular chondrocyte (hACs) proliferation, pre-monocytic U937 (ATCC® CRL-1593.2™) cell maturation and chondrogenic differentiation capacity of hACs and hMSCs *in vitro*.

MATERIALS AND METHODS

Proteinase-K, gelatin (porcine skin, type A, gel strength 300), Trizma[®] base, ethylenediaminetetraacetic acid disodium salt dihydrate (Di-sodium-EDTA), 1,9-dimethyl-methylene blue zinc chloride double salt (DMMB), chondroitin-4-Sulfate, hyaluronidase, pronase, hydrogen peroxide (H₂O₂), 4% neutral buffered formalin, glycine, sodium chloride (NaCl), sodium hydroxide (NaOH), Ficoll[®]-paque, phosphate buffered saline (PBS), ITS+1, L-proline, L-ascorbic acid-2-phosphate sesquimagnesium salt (AsAp), dexamethasone, fast green, safranin-O, sodium pyruvate, 12-myristate 13-acetate (PMA), RNase free water, Chloroform, 2-Propanol (Isopropanol) were all purchased from Sigma-Aldrich, St Louis, MO. Trypsin-EDTA solution, DAB (3,3'-diaminobenzidine tetrahydrochloride), CyQuant[®] cell proliferation assay kit, Gibco[®] Dulbecco's Modified Eagle Medium (DMEM) hi-glucose glutaMAX[™] media (10569-010), bovine serum albumin (BSA), AlamarBlue[®], Gibco[®] 4-(2-hydroxyethyl)-1-piperazineethanesulfonic acid (HEPES), Gibco[®] non-essential amino acids (NEAA), penicillin-streptomycin (10,000 U/mL and 10,000 µg/mL), Gibco[®] fetal bovine serum (FBS), Gibco[®] Roswell Park Memorial Institute (RPMI) 1640 medium, Gibco[®] αMEM nucleosides glutaMAX[™] media (32571101), molecular probes calcein-AM and propidium iodide, fibroblast growth factor 2 (FGF2), Quant-iT[™] PicoGreen[®] dsDNA assay kit, Coomassie (Bradford) Protein Assay Kit and DNase-free RNase A, Ambion[®] DNA-free[™] DNase Treatment, SYBRGreen[™] master mix, TRizol[®], TaqMan[™] and Gibco[®] collagen type I (rat tail, 3mg/ml) were obtained from Thermo Fisher Scientific, Auckland, NZ. Transforming growth factor β-1 (TGFβ-1) and recombinant human fibroblastic growth factor basic (FGF-b) was purchased from R&D systems, Minneapolis, USA. Type II collagenase was purchased from Worthington biochemical corporation, Lakewood, USA. Di-sodium hydrogen phosphate (Na₂HPO₄), acetic acid (glacial, 100%), and Gill's haematoxylin were purchased from Merck Millipore, North Shore City, NZ. Tissue-Tek[®] O.C.T Compound Sakura[®] Fintek was purchased from VWR International, Radnor, USA. U937 cells were purchased from ATCC, Manassas, USA.

Vitreous humor harvest

Equine ocular tissue was obtained from local slaughterhouses and veterinary clinics (with permission), submerged in sterile PBS supplemented with penicillin (500 IU/mL) and streptomycin (500 µg/mL), and either freshly processed (< 24 h) or stored frozen (< 3 months, -20°C). Excess connective tissue and anterior segment of the oculus were removed using aseptic techniques followed by three ethanol washes (70%, 100%, 100%) prior to extraction. An incision was made from the center of the ocular body towards the optic nerve end and the VH was carefully extracted and separated from the lens and the ora

serrata. The two harvesting techniques (fresh or frozen), and subsequent centrifugation treatments were systematically investigated, as outlined in Table 2, to establish an optimal protocol for extraction of VH. Centrifugation is based on separation by size and density where low to medium speed is known to separate whole cells, nuclei and cytoskeletons. As the native VH tissue is a loose, highly hydrated amorphous network, we sought to evaluate if it would be compatible with centrifugation based separation of cellular components, given that other tissue types, especially cartilage, with its extremely dense ECM, are unsuitable with this type of mild decellularisation protocol. Isolated VH samples were weighed and stored at +2-8°C (< 1 month) until further downstream processing.

Table 2. Extraction conditions and nomenclature

Nomenclature	Harvesting technique	Centrifugation	Cycles
VH	Fresh	None	None
cVH	Fresh	3000 g, 30 min	1
fVH	Frozen	None	None
fcVH	Frozen	3000 g, 30 min	1

Biochemical analysis

Samples were weighed, lyophilized, and weighed again prior to digestion at 56°C in 1 mg/mL proteinase K, dissolved in 10 mM Tris-HCl and 1mM disodium EDTA solution. GAGs were quantified by allowing samples to react with DMMB solution according to previously described protocols [216, 217]. In brief, 50 µL of each sample and standard curve dilutions were transferred in triplicates to a 96-well microplate, to which 200 µL of DMMB solution (16 µg/mL, pH=3) was added and the absorbance was read at 520 nm (VERSAmix microplate reader, Molecular devices, Wokingham, UK). GAG content could then be calculated from a matching standard curve generated by reacting known amounts chondroitin sulfate. Total DNA was quantified using either the CyQUANT® Cell Proliferation Assay Kit, following a pre-treatment of each sample with DNase-free RNase A (135 Kunitz/mL) to eliminate the RNA components of the fluorescent signal, or the Quant-iT™ PicoGreen® dsDNA assay kit according to manufacturer's instructions. Total protein content was quantified using Pierce™ modified Lowry protein assay kit according to manufacturer's description. Amounts of GAG, DNA and protein are reported as absolute values per intact ocular sample and furthermore normalized to dry weight.



Histological and immunohistological analysis

Samples were fixed in 4% formaldehyde overnight at room temperature (RT), dehydrated through a graded ethanol series, cleared in xylene, embedded in paraffin and left overnight before cut into 5 μm thick sections. The sections were deparaffinized in xylene, rehydrated through serial dilutions of ethanol followed by staining using histological and immunohistological staining protocols to visualize the retention of GAGs and collagens. Haematoxylin, Alcian blue, and Picrosirius red were applied to visualize cell nuclei, extracellular GAGs, and collagens, respectively. Collagen types II and IX were stained by immunohistochemistry based on previously described protocols [80, 218]. In brief, sections were blocked in 0.3% H_2O_2 and 5% BSA, antigens were retrieved by treatment with pronase (1 mg/mL) and hyaluronidase (10 mg/mL) followed by incubation with primary murine antibodies (1:100, clone II-II6B3, Developmental Studies Hybridoma Bank, 57 $\mu\text{g}/\text{mL}$; 1:100, clone D1-9, Developmental Studies Hybridoma Bank) and secondary antibodies conjugated with HRP (1:200, P0447 Dako, 1 mg/mL) and labeling was visualized with diaminobenzidine as a substrate. Sections were counterstained with haematoxylin and isotype controls were performed by using mouse isotype immunoglobulin G_1 (IgG_1) monoclonal antibody at concentrations similar to those used for the stainings. Sections were then washed, dehydrated, and mounted in depex. All sections were visualized using an Olympus BX51 microscope (Olympus DP70 camera, Olympus, Hamburg, Germany).

Cytotoxicity assay

Human bone marrow aspirates were obtained from the iliac crest of healthy patients undergoing surgery following informed consent (New Zealand Health and Disability Ethics Committees, URA/08/08/049/AM06). The mononuclear fraction was isolated by centrifuging on Ficoll-Paque. In brief, the bone marrow samples were diluted in PBS (1-4x) and filtered through a cell strainer (100 μm). 15 mL of Ficoll-paque was aliquoted into a 50 mL falcon tube, to which 35 mL of the diluted cell suspension was carefully added followed by centrifugation (400 g, 30 min, 20°C, no break). The mononuclear cell layer was carefully aspirated from the interface and washed with PBS followed by centrifugation (400 g, 15 min, and 20°C). The pellet was resuspended in MSC expansion medium (Gibco® αMEM nucleosides glutaMAX™ supplemented with 10% (v/v) FBS, 100 U/mL penicillin, 0.1 mg/mL streptomycin and 1 ng/mL FGF-b) and expanded (300,000 cells/ cm^2 first passage) into ~80% confluent monolayers. Unattached cells were washed away and adherent cells were expanded (3,000 cells/ cm^2) in MSC expansion medium, incubated at 37°C in a humidified air incubator (5% CO_2 /95% air) and multi-lineage potential was confirmed by a tri-lineage differentiation assay in the presence or absence of adipogenic, osteogenic, and chondrogenic differentiation media as previously described [73]. After 3 weeks culture

in vitro, cells were fixed and stained for adipogenic (Oil Red O), osteogenic (Alizarin Red), and chondrogenic (Safranin-O) differentiation markers (Figure S5). In addition, hACs were harvested from macroscopically healthy regions of the articular cartilage from human patients undergoing anterior cruciate ligament (ACL) reconstruction (New Zealand Health and Disability Ethics Committees, URB/07/04/014/AM02). The tissue was digested in chondrogenic base medium (Gibco® DMEM high glucose glutaMAX™ supplemented with 0.4 mM L-proline, 10 mM HEPES, 0.1 mM NEAA, 100 U/mL penicillin, 0.1 mg/mL streptomycin, 0.1 mM AsAp and 10% (v/v) FBS) with 0.15% type II collagenase at 37°C in a humidified air incubator (5% CO₂/95% air) for 16-20h. The solution was filtered through a cell strainer (100 μm) and isolated chondrocytes were expanded (3,000 cells/cm²) into high-density monolayers for two passages cultured in chondrogenic base medium. Both hMSCs and hACs were expanded for two passages before plating in 48-well cell culture plates (10,000 cells/well), incubated at 37°C in a humidified air incubator (5% CO₂/95% air). After 48 h culture, the medium was removed and replaced with either 500 μL PBS, chondrogenic base medium or chondrogenic base medium supplemented with either gelatin (5 mg, 1 wt%), VH (1 μL, 10 μL, 50 μL) or Ethanol (0%, 4%, 5%, 7.5%) and incubated for another 48 h. AlamarBlue® was used to quantify the metabolic activity per well, indicative of the total cell number, as per manufacturer's description and in accordance with the ISO10993 standard. Briefly, the reduction of AlamarBlue® in the solution was determined per well by reading fluorescence at wavelengths of 545 nm excitation and 590 nm emission using a spectrophotometer (Thermo Scientific Varioskan Flash). Chondrogenic base medium, without ethanol, gelatin or VH supplements, was used as baseline to calculate % growth inhibition according to:

$$\text{Inhibition (\%)} = 100 \times \left(1 - \left(\frac{A_{\text{sample}}}{A_{\text{base}}} \right) \right) \quad (\text{Eq 1})$$

Where A_{sample} is the metabolic activity measured for each sample and control sample well and A_{base} is the metabolic activity measured for cells cultured in normal chondrogenic base medium. Inhibition of hMSCs was then presented as a function of VH amount, gelatin or ethanol directly added to living cells in relation to the baseline (A_{base}).

U937 cell culture

The immortalized cell line U937 (ATCC® CRL-1593.2™) was used between passages 8-18, in accordance with American Type Culture Collection (ATCC) guidelines. Cells were maintained in base medium (RPMI-1640 supplemented with 1mM sodium pyruvate, 1% (v/v) penicillin-streptomycin, and 10% (v/v) FBS) at 37 °C under 5% CO₂. Cells were seeded in 96-well cell culture plates at 25,000 cells/well. To investigate the adherent U937 cell response to the



VH material, the cells were exposed to 250 μ L cell culture medium supplemented with VH matrix components (1 μ L, 10 μ L and 50 μ L) and cultured for 72 h. Cell exposed to VH were compared to cells cultured with only base medium (negative control) and cells cultured in the presence of 100 ng/mL 12-myristate 13-acetate (PMA; positive control) to initiate and maintain the cells in a fully adherent and differentiated state, as previously described [219-221]. Cells were imaged following 1h and 72h incubation using Olympus CKX41 microscope (Japan). Each well was then washed twice with PBS, to remove non-adherent U937 cells, and left hydrated for further imaging. Cells were counted at three random locations (10x lens magnification, field of view 0.7 mm) of each well per time point using Image J (version 6.1 Fiji, National Institutes of Health). The change in cell number and cell attachment was calculated according to:

$$\text{Change in cell number (fold change)} = \frac{\text{cells}_{72h}}{\text{cells}_{1h}} \quad (\text{Eq 2})$$

$$\text{Cell attachment (\%)} = 100 \times \frac{\text{cells}_{72h \text{ wash}}}{\text{cells}_{72h}} \quad (\text{Eq 3})$$

Where cells_{1h} and cells_{72h} is the number of cells after 1 h and 72 h culture, respectively, and $\text{cells}_{72h \text{ wash}}$ is the number of cells attached after 72 h culture and post two PBS washes.

Cell encapsulation

Collagen type I hydrogels (0.1 wt%) were prepared according to manufacturer's instructions. Cells were seeded in 50 μ L VH or collagen type I hydrogels by pipetting them on top of the hydrogels followed by gently mixing with a spatula to homogeneously distribute the cells throughout the highly hydrated and amorphous biomaterials. The cell-laden hydrogels were cultured in 96-flat bottom polypropylene cell culture well plates, at a concentration of either 250,000 or 750,000 cells/well and cultured for 3 weeks in chondrogenic differentiation media (Gibco® DMEM high glucose glutaMAX™ supplemented with 0.4 mM L-proline, 10 mM HEPES, 0.1 mM NEAA, 100 U/mL penicillin, 0.1 mg/mL streptomycin, 0.2 mM AsAp, 1 x ITS+1 premix, 1.25 mg/mL BSA, 10 nM dexamethasone and 10 ng/mL TGF β -1). Chondrocytes were further cultivated as high-density \varnothing 1 mm micro-tissues, using a previously described high-throughput fabrication method [216]. In brief, cells suspended in chondrogenic base media were seeded in v-bottom 96-well plates at a concentration of 250,000 cells/well. Plates were then centrifuged at 200 g for 4 min, to force cellular aggregation, and cultured at 37°C in a humidified air incubator (5% CO₂/95% air) overnight. The next day, the condensed cell spheroids were allowed to de-attach from the bottom by gently pipetting the media up and down. The cell spheroids were cultured for 3 weeks in chondrogenic differentiation media, refreshed twice a week.

Size and shape of cell-laden constructs

Digital images of micro-tissues, VH and collagen type I spheroids were obtained using an Olympus CKX41 microscope (Japan) connected to an Olympus OM-D E-M10 camera (Japan). Size was estimated as the mean diameter measured from three different angles (0°, 45°, 90°) per sample using Image J software (version 6.1 Fiji, National Institutes of Health). Circularity was further measured by firstly applying the built-in threshold function of Image J, establishing the area of the sample, and the shape was subsequently calculated using the Image J built-in circularity calculation:

$$\text{Circularity} = 4\pi \times \frac{\text{area}}{\text{perimeter}^2} \quad (\text{Eq 4})$$

Where a value of 1.0 indicates a perfect circle and 0 an infinitely elongated polygon.

Metabolic activity in chondrocyte-laden VH hydrogels

AlamarBlue® was used to quantify the metabolic activity of cells encapsulated in VH and collagen type I hydrogels (spheroids) and biomaterial free micro-tissues. Briefly, each well was incubated with 330 µL AlamarBlue solution for 1.5 h. The reduction of AlamarBlue® in the solution was determined by reading absorbance at wavelengths of 570 nm and 600 nm using a spectrophotometer (Thermo Scientific Varioskan Flash) followed by data processing according to manufacturer's instructions.

Biochemical analysis of cell-laden constructs

Cells were collected after 1 day and 3 weeks of culture in chondrogenic differentiation medium, washed in PBS, weighed, lyophilized and weighed again prior to digestion at 56°C in 1 mg/mL proteinase K, dissolved in 10 mM Tris-HCl and 1mM disodium EDTA solution. The GAG content was quantified by allowing samples to react with DMMB solution, as previously described [216]. Total DNA content was quantified using the CyQUANT® Cell Proliferation Assay Kit according to manufacturer's instructions following a pre-treatment of each sample with DNase-free RNase A to eliminate RNA components from the fluorescent signal [216].

Histology and immunohistochemistry of cell-laden constructs

Cell-laden constructs were collected after 3 weeks of culture, washed with PBS, followed by fixation in 4% formaldehyde for 1 h at RT and washed in PBS supplemented with 0.3 M glycine to quench free aldehyde groups. Samples were then embedded in optimal cutting temperature compound (O.C.T) and cryo-sectioned into 30 µm thick sections. Haematoxylin, fast green, and Safranin-O staining was applied to visualize cell nuclei, collagens and



extracellular GAGs. Collagen types I and II were stained by immunohistochemistry as previously described [217]. In brief, samples were incubated in 0.2% hyaluronidase for 30 min at RT and washed with PBS to reveal antigen epitopes. Constructs were blocked with 2% bovine serum albumin (BSA) in PBS for 30 min at RT. Primary antibodies for collagen type I (1:200) and collagen type II (1:200) were diluted in blocking buffer and applied for 3 h at RT. Samples were washed 3 times in blocking buffer for 10 min each followed by incubation with a goat-anti-mouse (Alexa Fluor® 488) and donkey-anti-rabbit (Alexa Fluor® 594) secondary antibodies, diluted in blocking buffer (1:400), in the dark for 1 h at RT. Constructs were washed a further 3 times with blocking buffer before incubation with blocking buffer containing 4',6-Diamidino-2-Phenylindole, Dihydrochloride (DAPI, 1:1000 dilution) in the dark for 10 min at RT. Lastly, all constructs were washed 3 times in PBS, left hydrated and visualized using the Zeiss Axioimager Z1 microscope.

Gene expression

hMSC-laden VH and collagen type I hydrogels and micro-tissue samples were collected after 3 weeks, homogenized in 10mg/mL proteinase K solution at 55°C for 30 min, incubated with 1mL TRIzol reagent for 5min at RT followed by RNA isolation in accordance with the manufacturer's guidelines. In brief, samples were vigorously mixed with 200 µL chloroform, incubated at RT for 3 min followed by 15 min centrifugation at 12,000 g. The aqueous phase containing the RNA was transferred to tubes containing 500 µL isopropanol, inverted and incubated at RT for 20 min followed by centrifugation for 10 min at 12,000 g. The RNA pellet was washed twice in ice cold 70% ethanol and re-suspended in RNase free water. Ambion® DNA-free™ DNase Treatment was further used to remove any contaminating DNA according to manufacturer's instructions. Total RNA yield was determined spectrophotometrically (Thermo Scientific, NanoDrop 8000) and the integrity was validated electrophoretically (Agilent Technologies, 2200 TapeStation). 300 ng total RNA per sample was reverse transcribed into complementary DNA (cDNA) using TaqMan™ first strand synthesis. Polymerase chain reaction (PCR) was then performed using an iCycler quantitative real-time PCR (qRT-PCR) machine (Roche, LightCycler® 480 II), SYBRGreen™ and primers (Sigma Aldrich, KiCqStart® SYBR® Green Primers), used as published previously [216]. The specific genes of interest were collagen type IA1 (GenBank accession no NM_000088), collagen type IIA1 (GenBank accession no NM_001844) and aggrecan (GenBank accession no NM_001135). Glyceraldehyde-3-phosphate dehydrogenase (GAPDH, Sigma Aldrich, GenBank accession no NM_002046) was selected as housekeeping gene. Each sample was run in duplicate and the threshold cycle and primer efficiency were analyzed, where the geometric mean of the reference genes (GAPDH and MSC micro-tissues) was used to calculate the normalized mRNA expression of each target gene.

Mechanical testing

The load bearing nature of functional cartilage tissue means that appropriate characterization of mechanical properties of tissue engineered constructs represents one of the most important factors in addressing the clinical need [196]. Mechanical compression testing of MSC-laden constructs was performed using a mechanical testing machine (MTS criterion 42) equipped with a 5N load cell. For compression tests, samples were tested at a constant cross head displacement rate of 0.01 mm sec⁻¹. To characterize the compressive modulus of spherical samples, the change in contact area between the sphere and the indenter was taken into account in accordance with current literature [222]. Hertz [223] described the relationship between the applied force and the displacement of a compressed sphere between two flat surfaces for up to 10% strain according to equation 5:

$$F = \frac{4r^{1/2}}{3} \times \frac{E}{1 - \nu^2} \times \left(\frac{H}{2}\right)^{3/2} \quad (\text{Eq 5})$$

F is the applied force (N), r the initial radius (m), E is the compressive modulus, ν the Poisson ratio (dimensionless) and H the displacement (m). In this study, a Poisson ratio of 0.47 was chosen for all samples given that native cartilage lies between 0.44-0.49 [224]. The compressive modulus was given by the least-square regression of equation 5 in the linear elastic range (strain: 0-10%).

Statistical analysis

All GAG, DNA and protein extraction and isolation studies were prepared from at least two biological donors to study variability between samples. Cell studies were prepared in triplicates and were repeated three times with biological duplicates to study variability between samples ($n = 9$). Differences between groups were assessed by one-way ANOVA with *post-hoc* Tukey analysis (GraphPad Prism 7). All values are reported as the mean and standard error of the mean. Differences between data were considered significant when $p < 0.05$ for all tests.

RESULTS

Tissue extraction, DNA removal and matrix retention

Native VH was successfully extracted from both fresh- and frozen ocular tissues with a preserved hydrogel network structure, as seen in Figure 2A-C. Tissue harvested from freshly isolated VH samples allowed the collection of considerably larger samples (224.7 ± 58.1 mg dry weight) as compared to the frozen conditions (54.6 ± 15.7 mg dry weight), as seen



in Figure 3A. In addition, the frozen samples displayed more viscous and interconnected characteristics as compared to the freshly collected VH, illustrated in Figure 2B-C.

The PicoGreen™, DMMB and Coomassie blue assays were subsequently used to quantify the DNA, GAG and protein content present in the VH samples. As seen in Figure 3B, small amounts of DNA were detected in both VH ($62 \pm 48 \mu\text{g}$) and fVH ($59 \pm 29 \mu\text{g}$) samples. DNA normalized to the dry weight demonstrated that both fVH and fcVH contained significantly ($p \leq 0.045$) greater DNA per dry weight as compared to both the freshly isolated samples, VH and cVH, as observed in Figure 3C. Applying a post-processing de-nucleation step (centrifugation) allowed the removal of up to 70-75% of the detected DNA ($p \leq 0.013$), after which no significant difference ($p \geq 1.00$) could be observed between fresh ($19 \pm 8 \mu\text{g}$) and frozen samples ($16 \pm 4 \mu\text{g}$). As demonstrated in Figure 3D-E, no difference in GAG retention ($p \geq 0.28$) between any of the four protocols was recorded while fresh isolation of samples resulted in superior protein retention compared to frozen samples. Normalized to the dry weight, both frozen and centrifuged samples demonstrated significantly higher GAG and protein accumulation compared to other extraction techniques. This is in line with the macroscopic observations that frozen samples display more viscous and interconnected characteristics with low dry weight yield as compared to the freshly collected VH.

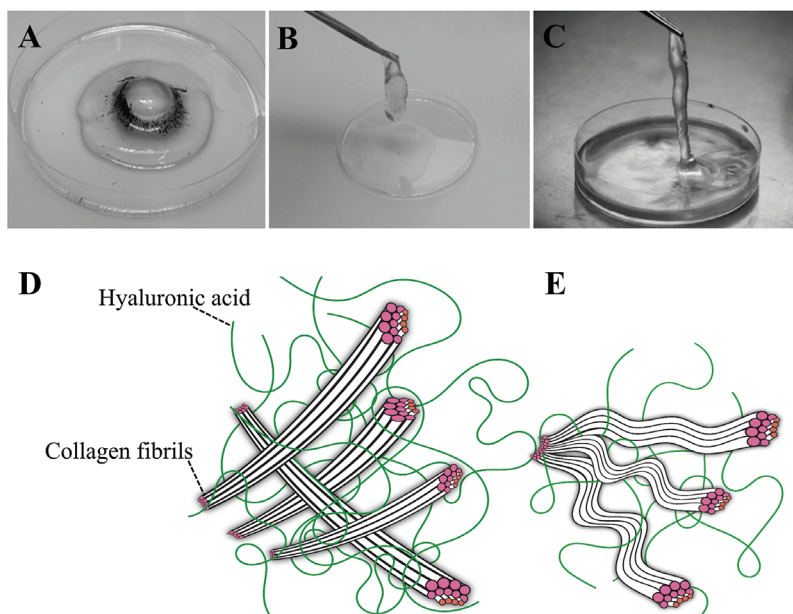


Figure 2. VH extracted from frozen (A-B) and freshly (C) collected VH samples. Petri dishes are of standard 90 mm in diameter. Schematic of the bridging between collagen fibres in a ladder-like structure in native VH (D), stabilizing and organizing the structure in a healthy eye. The collagen structures may however collapse due to aging or physical disruption of the long- and short-range spacing via ECM bonds and charges (E).

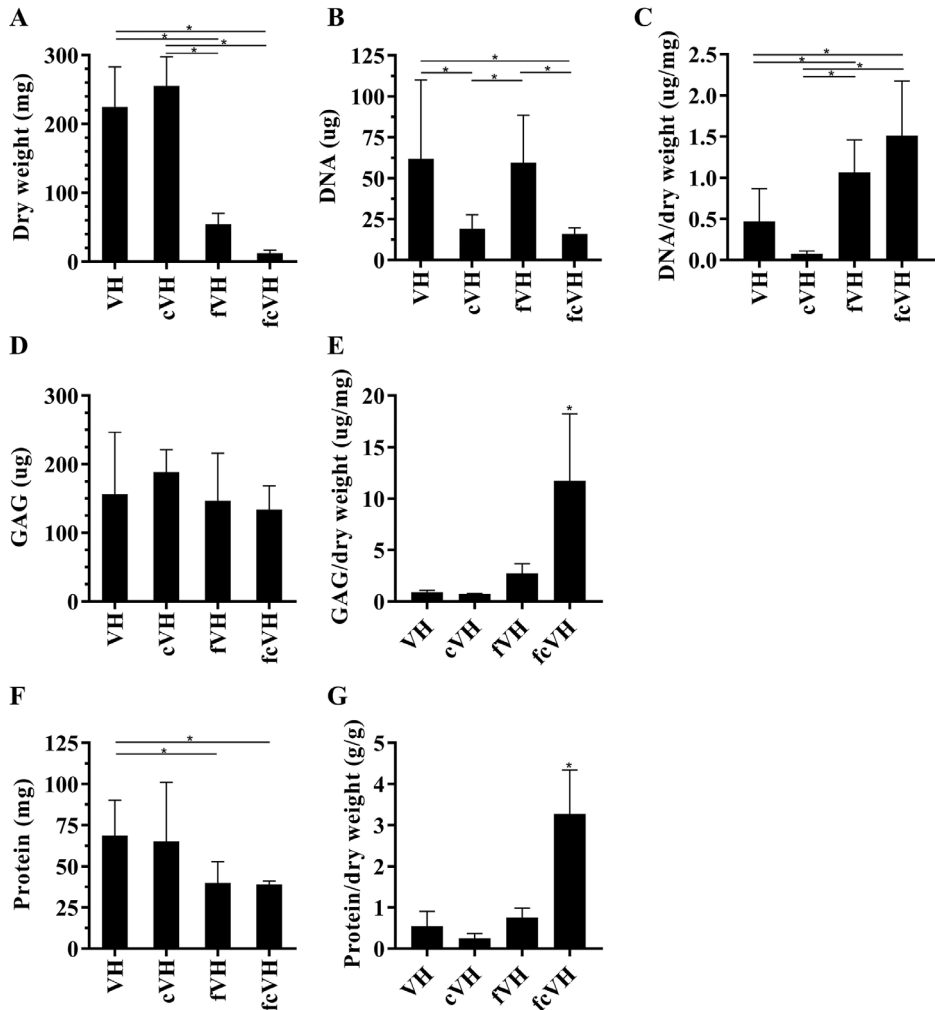


Figure 3. Quantification of dry weight (A), DNA (B-C), GAGs (D, E) and proteins (F, G) isolated using fresh (VH) and frozen (fVH) harvesting techniques, without or with the addition of a centrifugation post-processing step (cVH, fcVH). Error bars represent the mean \pm SE of 9 samples. * indicates significant difference ($p < 0.05$).

Histology and immunohistology

The VH tissue structure and composition was visualized by alcian blue and picosirius red or collagen type II and IX stained histological sections. In all conditions, VH appeared as a loose, acellular tissue, as observed in Figure 4, where the presence of heterogeneous matrix areas could be observed. In particular, a clear separation of the collagen-rich and GAG-rich areas could be noted in all the alcian blue and picosirius red stained sections. Consistent with these macroscopic observations, collagen type II also exhibited an inhomogeneous

distribution, especially in the non-centrifuged samples. The presence of collagen IX was furthermore confirmed in all samples while collagen type IX appeared to be both more uniformly distributed and abundantly present.

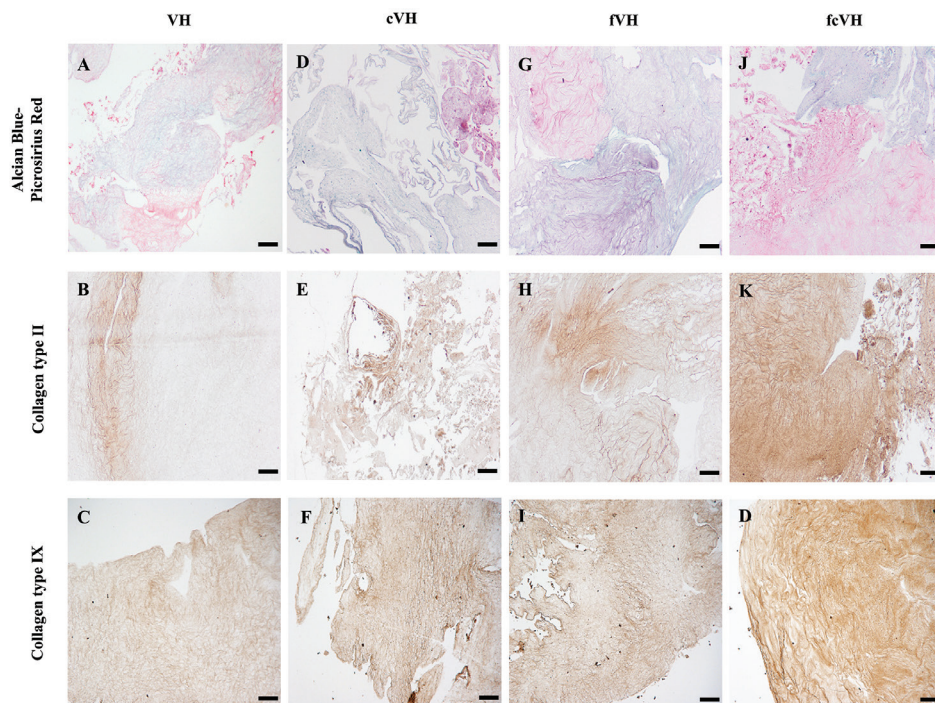


Figure 4. Collagen and GAG distribution in vitreous humor samples. Alcian blue and picrosirius red staining highlights the presence of GAG rich areas (blue) and collagen fibres (pink). Collagen type II was more patched, whereas collagen type IX was evenly distributed throughout the samples. No cell nuclei were detected by the haematoxylin counterstaining, commonly used to satisfy the intent of decellularization. Scale bars = 50 μ m.

Cytotoxicity

VH isolated from freshly harvested samples, without post-processing (centrifugation), was evaluated for its ability to influence cell proliferation. Cell growth inhibition of both hAC and hMSCs – a clinically relevant cell source – was evaluated as a function of VH supplements directly added to living cells as well as compared to media supplemented with a series of ethanol dilutions or gelatin controls, in accordance with the ISO10993 standard. Media without ethanol, gelatin or VH supplements was used as baseline to calculate percent-growth inhibition, as per Equation 1. Media supplemented with PBS was furthermore included as an internal negative control (data not shown). As observed in Figure 5, results clearly demonstrated that none of the VH volumes added to either hMSCs or hACs had

an inhibitory effect ($p \leq 0.0001$). Instead VH consistently, and significantly, promoted cell proliferation (negative cell growth inhibition % values).

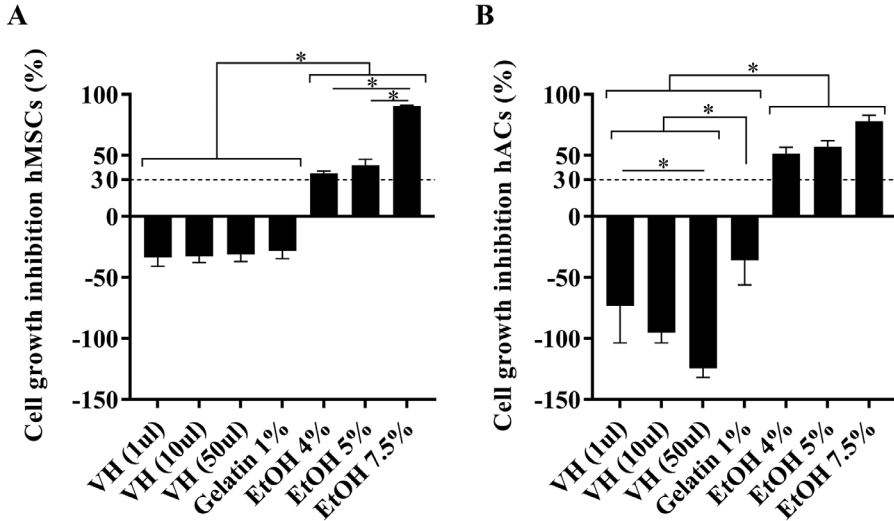


Figure 5. hMSCs (A) and hACs (B) survival and proliferative capacity, measure with the AlamarBlue® assay, after exposure to a range of VH volumes (1 μ L, 10 μ L, and 50 μ L), gelatin and ethanol controls relative to the chondrogenic media base line. Error bars represent the mean \pm SE of 6 samples (2 repeats). * indicates significant difference ($p < 0.05$).

U937 cell adhesion and proliferation

U937 cells, a pro-monocytic human cell line, were cultured in the presence of VH hydrogels (1 μ L, 10 μ L and 50 μ L). The change in cell number and cell attachment were quantified to assess the indirect inflammatory potential of VH in comparison to media with or without PMA as positive and negative controls, respectively. It was observed that PMA activated the U937 cells by limiting the increase in cell number, as compared to the base medium control ($p = 0.011$), as seen in Figures 6 and S2. In contrast, no significant difference could be observed between any of the VH additions and the negative medium control group ($p \geq 0.06$). This was further validated by quantifying the number of adherent cells, where a majority of the cells exposed to PMA ($84 \pm 38\%$) had attached to the culture plate. U937 cells only exposed to medium displayed a very low cellular attachment ($< 6\%$), indistinguishable from all the VH conditions ($p \geq 0.93$), while being significantly lower as compared to PMA ($p \leq 0.01$).

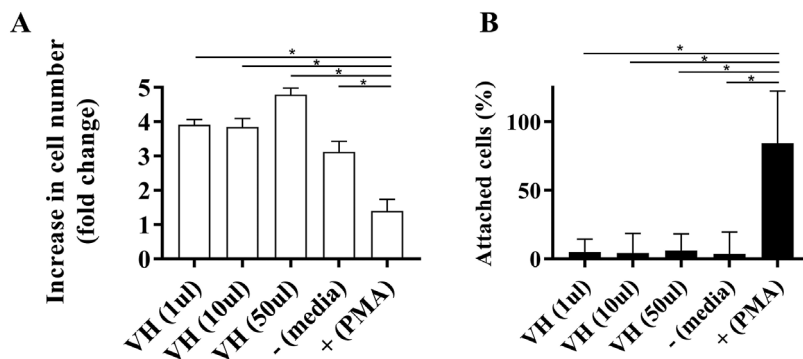


Figure 6. Inflammatory response of U937 cells, quantified as cell proliferation after 72 h **(A)** and cell attachment after 72 h and 2 PBS washes **(B)**, after exposure to media, PMA and a range of VH volumes (1 μ L, 10 μ L, and 50 μ L). Error bars represent the mean \pm SE of 9 samples (3 repeats). * indicates significant difference ($p < 0.05$).

Size, shape and metabolic activity of cell-laden VH hydrogels

hACs and hMSCs were encapsulated in VH hydrogels and cultured for 3 weeks to evaluate cell viability and metabolic activity as a function of time and two different cell seeding densities. It was observed that the cells seeded in the soft VH and collagen type I control samples rapidly adhered to the hydrogel material after 1 hour, as seen in Figure S3A. The seeded cells subsequently commenced to contract and remodel the matrix, and, interestingly, over the three week time period self-assembled into dense spheroids similar to a standard micro-tissue pellet culture [216]. Results demonstrated that hydrogel spheroid size was affected by both the addition of VH and cell density, with 750,000 hACs in 50 μ L VH hydrogels yielding the largest hydrogel spheroid ($\varnothing 1.86 \pm 0.29$ mm, $p \leq 0.0001$), as seen in Figure S3B. After 3 weeks of culture in chondrogenic differentiation media, all constructs were spheroidal in shape, with no significant difference in circularity ($p \geq 0.06$) observed between any of the conditions, as detailed in Figure S3C. Metabolic activity was further quantified using an AlamarBlue[®] assay, confirming that the micro-tissues, VH hydrogels and collagen type I hydrogels were able to provide both the hACs and MSCs with a permissive microenvironment that supported cell function over time, as seen in Figure S3D.

Cell proliferation and ECM production in cell-laden VH Hydrogels

A DMMB spectrophotometric assay was used to quantify GAG content while histological and immunohistological techniques were applied to visualize the extracellular matrix formation of hACs or hMSCs cultured in VH hydrogels for 3 weeks in chondrogenic differentiation media. Furthermore, DNA was quantified using the CyQuant[®] assay to indicate cell proliferation and used to normalize the GAG production to obtain a qualitative measurement of differentiation.

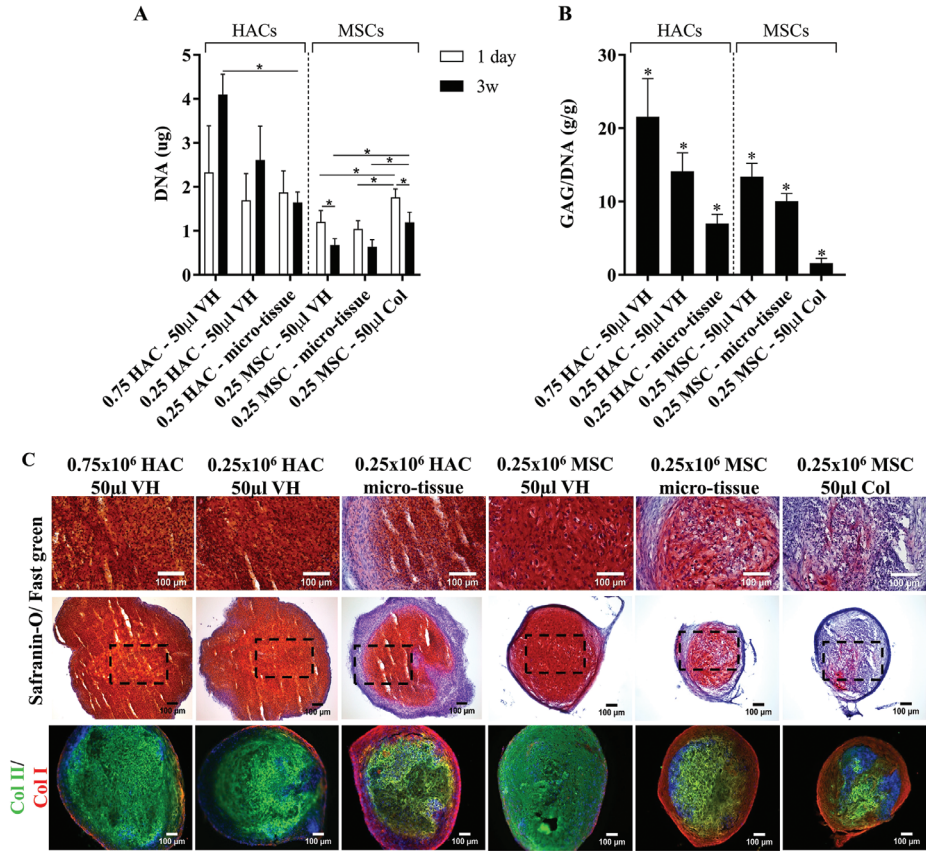


Figure 7. Quantification of DNA (**A**) and GAG/DNA (**B**) content and visualization safranin-O/fast green, and collagen type II (green)/collagen type I (red) stained cryosections (**C**) of micro-tissues (0.25×10^6 /sample) and cell-laden collagen type I and VH hydrogels ($0.25 \times 10^6 - 50 \mu\text{L}$, $0.75 \times 10^6 - 50 \mu\text{L}$) after 3 weeks in culture. Error bars represent the mean \pm SE of 6 samples. * indicates significant difference ($p < 0.05$).

Neither the HAC micro-tissues ($p \geq 1$) nor the hAC cell-laden VH spheroids ($p \geq 0.07$) displayed cellular proliferation after 21 days, as seen in Figure 7A. A reduction in DNA content was detected in the hMSC laden VH and collagen type I hydrogels. This phenomenon may be attributed to the self-assembly process as not all seeded cells will be able to attach and take part in the remodeling of the amorphous hydrogel material into spheroids. Both the HAC and hMSC seeded VH hydrogels further displayed a significant increase in GAG/DNA content after 3 weeks, with significantly greater differentiation compared to the microtissue controls ($p \leq 0.0170$) as well as standard collagen type I cultures ($p \leq 0.0001$). The higher HAC seeding density in VH was shown to further increase GAG/DNA compared to a lower cell concentration ($p \leq 0.04$), as seen in Figure 7B.

The distribution of ECM components was evaluated using histological techniques. Sections stained with Safranin-O, collagen type I and II after 21 days culture revealed very homogeneous tissue formation in all of the VH hydrogel spheroid conditions, as seen in Figure 7C. However, an outer region of fibroblastic-like cells was observed in the microtissue cultures of both hACs and hMSCs, trademarked by elongated morphologies, low GAG and high collagen type I accumulation [225]. hMSCs cultured in collagen type I hydrogels demonstrated limited overall deposition of GAGs as well as collagen type II.

Gene expression and mechanical properties in hMSC-laden VH hydrogels

MSC-laden collagen type I hydrogels, VH and MSC micro-tissues were cultured for 3 weeks and analyzed using polymerase chain reaction to quantify the presence of cartilage specific genes. Upregulated gene expression of aggrecan and collagen type II, and downregulation of collagen type I are herein widely used markers to identify chondrogenic cell development. As seen in Figure 8, aggrecan gene expression was significantly downregulated in collagen type I hydrogels ($p < 0.0038$) compared to both VH and control micro-tissues, indicating limited chondrogenic tissue formation. Results further demonstrated that hMSCs encapsulated in VH hydrogels had significantly ($p < 0.0129$) higher collagen type II expression compared to the standard collagen type I hydrogel cultures. It was also observed that hMSC micro-tissue cultures had significantly higher expression of collagen type I compared to cells encapsulated in both VH and collagen type I hydrogels ($p < 0.0136$).

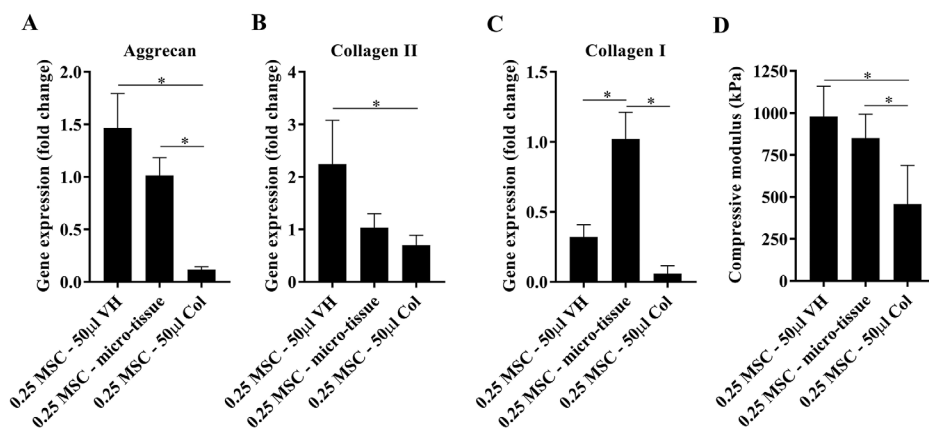


Figure 8. Gene expression by hMSCs in micro-tissues, collagen type I and VH and hydrogels cultured in chondrogenic differentiation media for 3 weeks (A-C). GADHP was used as housekeeping gene and values are presented as relative values to MSC micro-tissues. Compressive modulus of MSC-laden VH and collagen type I hydrogels and micro-tissues after 3 weeks culture in chondrogenic differentiation media (D). * indicates significant difference ($p < 0.05$).

In addition, the compressive modulus of MSC-laden VH and collagen hydrogels and micro-tissues incubated for 3 weeks in chondrogenic differentiation media was evaluated via unconfined compression testing. A significant ($p < 0.0199$) increase in compressive modulus was observed for both MSC micro-tissues and VH hydrogels cultures compared to collagen type I hydrogels. All samples were too soft and amorphous to measure after 1 day of culture, whereas up to approximately 1 MPa compressive stiffness detected after 3 weeks of culture corresponded directly with biochemical and histological observations that MSCs encapsulated in VH hydrogels secreted high quality cartilage tissue.

DISCUSSION

The discovery that native tissues could be decellularised, solubilized and subsequently manipulated to polymerize in situ to form hydrogels poses as a very exciting tissue engineering opportunity to recapitulate the native role of the ECM to regulate the cellular development. The potency of decellularised materials for tissue regeneration is however highly reliant on the successful removal of DNA components and the preservation of inherent biochemical cues post processing [167, 174, 226]. The current outcome is thus dependent on the targeted organ tissue and its native organization and structure for decellularization. Fabricating bioactive substrates of cartilage extra cellular matrices remains a considerable challenge due to native cartilage's dense and avascular characteristics. This study therefore investigated alternative strategies to isolate cartilaginous matrix components and found that highly permissive and bioactive ECM-hydrogels could be fabricated from freshly isolated and intact native VH tissue. This is the first report of using native VH tissues for cartilage tissue engineering applications, which in their natural composition highly resemble the cartilage extracellular matrix but lack its dense structure. This is in contrast to many existing decellularised biomaterials which are modified significantly to form ECM hydrogels, and is independent of the large body of work investigating the application of VH exclusively to benefit diagnosis and treatment of ocular diseases [203-214].

In this study, four different methods to extract VH were compared by systematically evaluating DNA removal, retention of ECM components, cytocompatibility and chondrogenic differentiation. The extent of DNA present in VH samples was selected as a key factor for evaluating downstream compatibility for tissue engineering applications, mainly as it is a sensitive and quantitative marker for cellular material [167]. The results demonstrated the successful extraction of VH with the DNA retention (0.02-2.97 μg DNA/mg dry weight) being significantly lower as compared to decellularised cartilage matrices (23.4 ± 33.3 μg DNA/mg dry weight) previously formulated for cartilage tissue engineering applications [170].



It should, however, be noted that the research community is currently facing challenges in defining a standardized approach to normalize DNA content in decellularised tissues, with at least 11 different strategies currently applied [103, 112, 161, 170, 227, 228]. It is, as such, problematic to identify a gold standard or safe minimum, non-antigenic, DNA content limit to comply with and should thus be closely evaluated and monitored.

In addition to the removal of DNA components, it is further important to characterize the preservation of endogenous factors in order to establish an optimal protocol of isolation and extraction. Results demonstrated no difference in GAG retention while it was possible to obtain both larger samples volumes and higher retention of proteins in freshly sourced VH samples compared to frozen. The significant difference in protein retention may be partially attributed to the difference in dry weight recorded or possibly due to protease activity. This may be due to the physical aggregation of collagen following hydrogen bond dissolution and destabilization of collagen helixes during the freezing-thawing process, possibly leading to loss of water, phase separation or release of non-gelatinous factors [110, 189, 228-231].

Changes in VH structure and composition was subsequently analyzed by comparing histological sections of freshly extracted VH to frozen VH samples, in addition to the effect of the centrifugation step. Specifically alcian blue and picosirius red stainings highlighted the presence of heterogeneous matrix areas, results that are consistent with previous reports in which VH is described as a highly hydrated, heterogeneous and acellular tissue [186-188, 230, 231]. In native VH, GAGs are entangled between the collagen fibrils, forming a vast meshwork of fragile honeycomb structures with an intrinsic inhomogeneous nature [187, 188]. The difference in distribution between collagen types II and IX observed may further be associated with the different role of these molecules within the VH [188]. Collagen type II molecules form the major bulk of the heterotypic collagen fibrils (75%), whereas it has been suggested that collagen type IX plays a role in linking the fibrils, organizing them in a contiguous network [188, 190]. More specifically, collagen type IX, estimated to be 25% of the total collagen content in VH, is found covalently linked to the surface of the heterotypic and thin collagen fibrils (mixtures of collagen types II, IX and V/XI) in a regular periodicity [187, 232]. As such, it seems logical that collagen type IX may be more evenly distributed, although collagen type II is suggested to be the most abundant collagen type [187, 232].

The presence of collagen types II and IX further highlights the similarity in extracellular matrix composition between native cartilage and VH. However, despite these proven similarities, there are also distinct differences in the biochemical compositions previously reported that should be considered [186, 190, 233-235]. The capacity of VH hydrogels to

transduce biochemical signals is subsequently important to investigate thoroughly. Taking the combined data into consideration, freshly harvested samples emerged as the most optimal protocol for isolating VH, with lowest DNA content per dry weight, high GAG and significantly greater protein retention. It was also observed that freshly isolated VH samples proved a more attractive and clinically relevant VH candidate due to ease of sterile extraction as it has low interconnectivity with the surrounding tissues while it further yields significantly larger volume of sample. As no significant difference was observed between VH and cVH samples with respect to DNA per dry weight, total GAG and protein content, freshly isolated VH was thus selected as the simplest and most user friendly protocol for downstream biocompatibility evaluation.

In this study, cultures of both hMSC's and HACs revealed that even small amounts (1 μL) of VH had a significant positive effect on cellular growth *in vitro*, comparable to or better than the 1 wt% gelatin controls commonly used for cell culture applications, and that no introduced matrix alterations from the isolation process act as cytotoxic agents [236].

In order to also assess potential harmful effects of any cellular debris in the hydrogels, pro-monocytic human U937 cells, known to yield a pro-inflammatory response to harmful biochemical molecules *in vitro* [219-221], were further cultured in the presence of VH hydrogels. U937 cells cultured in the presence of large volume (50 μL) of VH demonstrated a proliferative growth curve, were non-adherent and exhibited small and rounded morphologies similar to previous reports of non-activated U937 cells [219-221]. These results underlined that VH is neither causes cytotoxic responses nor proliferation of macrophage-like U937 cells and can safely be used in combinations with human cells *in vitro*.

To investigate the chondrogenic capacity of VH hydrogels, hACS and hMSCs were subsequently encapsulated in VH hydrogels and cultivated in parallel to established 3D cultures of standard micro-tissues [216] and collagen type I hydrogels. The results were consistent with previous research, in which chondrocytes encapsulated in porous collagen-based materials have been shown to express α -smooth muscle actin, which lead to construct contraction and consequent alteration of its shape into spheroidal constructs [237-241]. The individual metabolic trends for both the self-assembled VH and collagen type I hydrogel spheroids and biomaterial free micro-tissue controls indicated a maintained metabolic activity long-term and no distinct apoptotic behavior for any of the conditions. The lack of cellular proliferation was further supported by quantified DNA data, consistent with previous research typically reporting low proliferative capacity in differentiating chondrocytes [216, 242].

Other key characteristics of functional cartilage tissue formation is the synthesis and deposition of GAGs and collagen type II, replicating those levels of healthy articular



cartilage [225]. In this study, the significant increase in GAG content observed in the higher hAC seeding density condition may be attributed to increased N-cadherin activity and/or connexin 43 as compared to the lower seeding density [243, 244]. The importance of these gap junction-mediated intracellular communications has been previously highlighted. However, it has been demonstrated that culturing chondrocytes or MCSs as traditional micro-tissues brought no advantage compared with chondrocytes embedded in alginate hydrogel cultures, in terms of chondrogenic markers and GAG synthesis [243]. This further emphasizes the importance of our findings, as the VH hydrogels used in this study provided a biomaterial which yielded greater GAG/DNA of both hMSCs and hACs compared to standard micro-tissues and collagen type I hydrogels after 21 days in culture. The quantitative data was furthermore supported by histological images, as seen in Figure 8C, demonstrating large homogenous areas of sulfated GAG deposition in VH hydrogels. Immunohistological images further indicated favorable collagen II/I ratios in VH hydrogels, a similar trend as was observed in the gene expression analysis. Collagen type I secretion is typically considered as detrimental in hyaline cartilage tissue engineering and a high ratio between collagen types II and I deposition reflects the chondrogenic phenotype [245-247]. The transition of cells from a fibroblastic and de-differentiated nature with elongated morphologies to a chondrogenic phenotype with spherical morphologies is typically accompanied by the replacement of collagen type I by collagen II, and vice versa [248]. It is well-established that collagen type II fibres play a role in providing sufficient mechanical strength in the native cartilage tissue. The significant increase in compressive modulus observed in VH hydrogels compared to collagen type I hydrogels may further be attributed to other secreted and/or inherent factors such as hyaluronic acid (HA), among other glycosaminoglycans. In healthy cartilage, aggrecan for example interacts with HA to generate an increase in negative charges to alter the swelling properties and provide resistance to compression [235]. The VH may, as such, facilitate cell-ECM interactions, as either a catalytic stimulant or via conformational changes [249]. These results thereby underline that VH can be applied as a matrix component to successfully guide extracellular matrix formation, with significant accumulation of both collagen type II and aggrecan. This contributed to a tissue engineered construct whose mechanical properties improved over time with tissue maturation (approximately 1MPa compressive stiffness). It should be noted however that the compressive mechanical properties of VH cultures measured in this study are still lower than the dynamic stiffness of mature human articular cartilage (approximately 4.5MPa) [250, 251]. Combining these innovative VH spheroid cultures with 3D printed thermoplastics and 3D-bioassembly approaches could thus be a powerful tool to meet the mechanical design criteria for replacing native cartilage [252].

While the exact mechanism behind the difference in cellular responses observed between self-assembled VH spheroids, collagen type I hydrogels and the micro-tissue controls remains unknown, it could be attributed to the inherent biochemical cues present in the VH hydrogel. The observed differences in tissue formation may also be due to the difference in micro-environmental 3D niche. Native VH is characterized as a lightly crosslinked amorphous network of macromolecules [253, 254] while the micro-tissues generates a densely packed construct within the first few days of culture, possibly displaying very different nutrient, oxygen and waste material diffusion profiles.

It was also noted that cell-free VH hydrogels display very low inherent GAG content compared to cell-laden samples cultured for 3 weeks, as seen in Figure S4, indicating that the sulfated GAGs stained positive with safranin-O in the cell-laden VH hydrogels are ECM components secreted by the encapsulated cells. Collagen type I and II primary antibodies both, however, have equine and human positive species reactivity, which complicates the determination of the origin of immunofluorescent visualized collagens in the cell-laden constructs. Nonetheless, tissue engineered constructs containing a homogeneous distribution of collagen type II is desirable in regenerative medicine of cartilage in order to replicate native tissue composition and mechanical properties.

In conclusion, these results highlight that VH hydrogels can be favorably applied with multiple cell types at both high and low seeding densities to support chondrogenic differentiation and tissue remodeling with uniform distribution of both GAGs and collagen type II, yielding cartilage tissue constructs with and high compressive modulus. The successful isolation and application of intact and unmodified VH-derived hydrogels could potentially help in understanding complex cell-material interactions and further guide the development of suitable ECM components that support homogenous cartilage tissue formation. Future studies should focus on identifying the biological and physical mechanisms behind the chondrogenesis observed while further investigating the compatibility of VH hydrogels with emerging hydrogel and/or bioink platforms for sophisticated spatial-temporal designs developed [252, 255, 256]. To further gain clinical relevance, we envision the scale-up of the VH material platform to be as a bioactive supplement in synthetic- or naturally-derived 3D hydrogels or bioinks for 3D bioprinting. Furthermore, the cell-laden VH spheres may be applied as tissue modules together with newly developed automated 3D-bioassembly strategies - a powerful bottom-up TE strategy for direct 3D-bioassembly of micro-scale tissues into complex, anatomically-shaped, and mechanically strong 3D scaffolds [252]. It is also necessary to assess VH performance *in vivo* to confirm the none-inflammatory and -cytotoxic responses observed *in vitro*, while further comparing the cellular performance to existing decellularised cartilage matrices.



ACKNOWLEDGEMENTS

This study was supported by the Royal Society of New Zealand Rutherford Discovery Fellowship (RDF-UOO1204; TW) and the European Union FP7-IRSES Mobility Grant 'skelGEN' (under grant agreement n° 318553). KL would like to acknowledge funding support from the Health Research Council of New Zealand Emerging Researcher First Grant (HRC 15/483). The authors are grateful to J. van Dassel, Utrecht University, for generously providing equine ocular samples. The primary antibody against collagen type II (II-II6B3), developed by T. F. Linsenmayer, was obtained from the DSHB developed under the auspices of the NICHD and maintained by The University of Iowa, Department of Biology, Iowa City, IA 52242.

SUPPLEMENTARY DATA

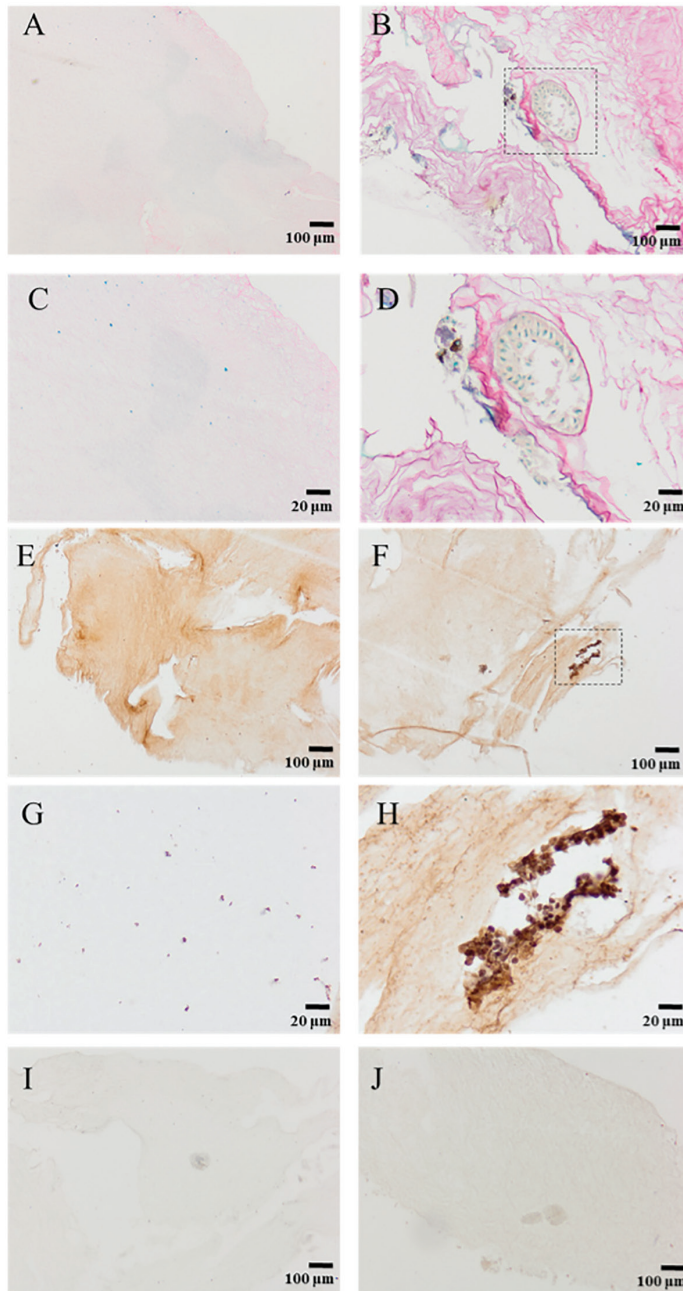


Figure S1. VH paraffin embedded tissue sections stained with alcian blue/picosirius red (**A-D**) and DAB/haematoxylin (**E-J**). Regions with dye precipitation (**A, C, E, G**) and cellular contaminants (**B, D, F, H**) were detected. Sections incubated with mouse isotype IgG1 was used as negative controls to determine non-specific binding of collagen type II (**G**) collagen IX (**H**) primary antibodies.



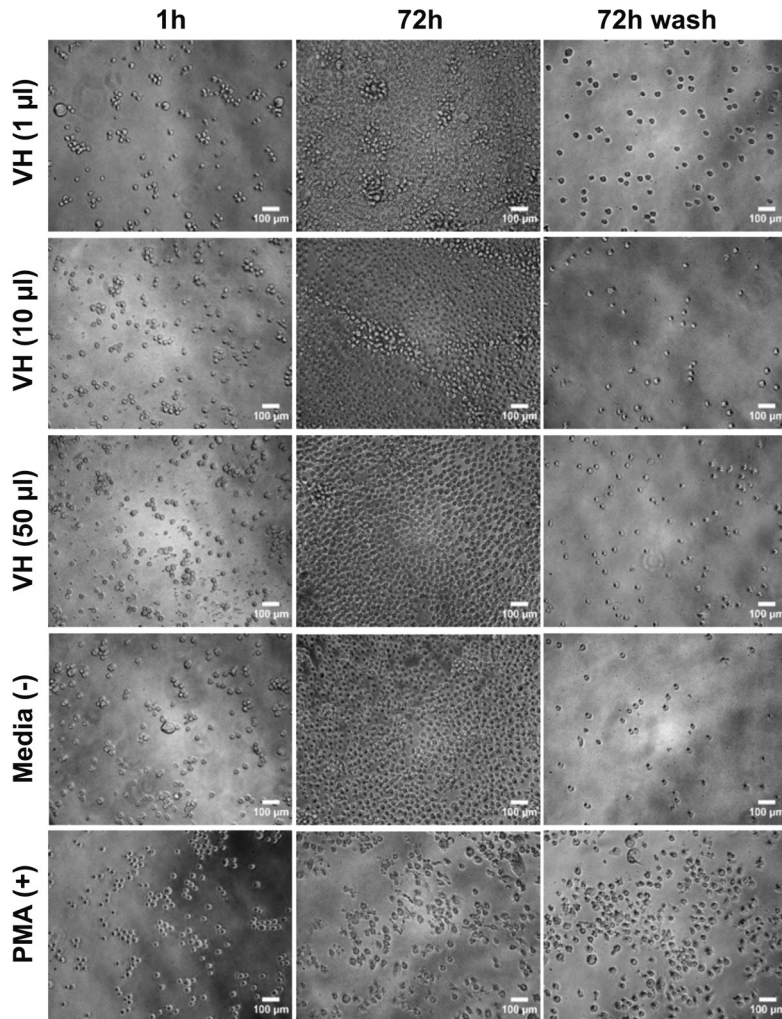


Figure S2. Inflammatory response of U937 cells visualized after exposure to medium, PMA and a range of VH volumes (1 μ L, 10 μ L, and 50 μ L). U937 activities are regulated differently in response PMA (positive control) and media (negative control), 1 μ L VH, 10 μ L VH and 50 μ L VH.

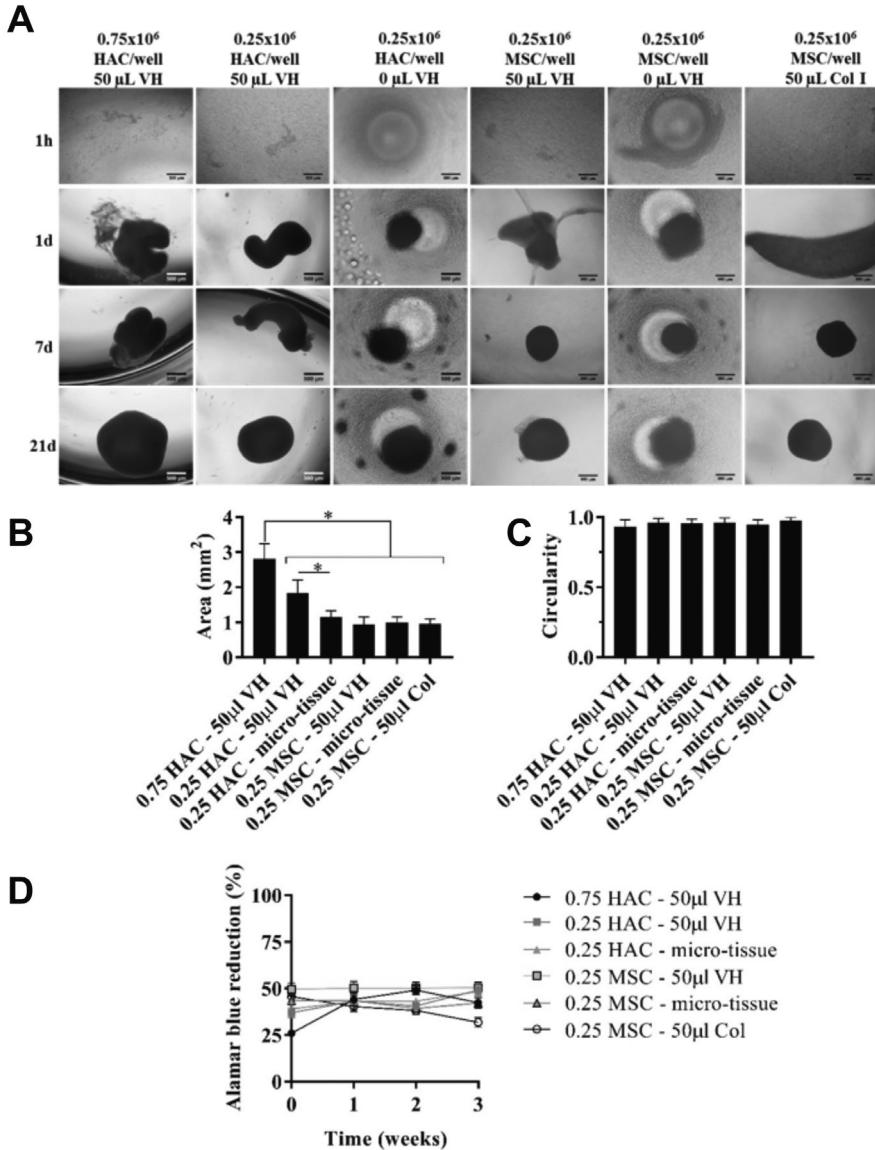


Figure S3. hACs and hMSCs cultured as micro-tissues (0.25×10^6 cells/well) compared to cells seeded in $50 \mu\text{L}$ collagen type I and VH hydrogels at two different densities (0.25×10^6 cells or 0.75×10^6 cells per well) (A). Cell-laden collagen type I and VH constructs display a significant change in architecture over time, remodeling the matrix into self-assembled spheroids, revealing homogeneous tissue formation in all of the VH hydrogels. The area (B) and circularity (C) of the samples was quantified after 3 weeks in culture, and metabolic activity (D) was recorded once a week, plotted as a function of time. * indicates significant difference ($p < 0.05$).

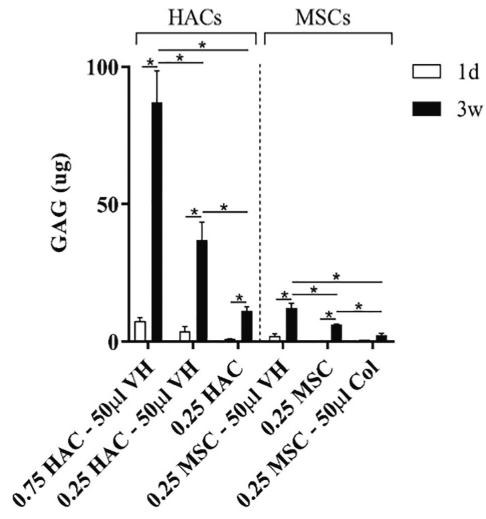


Figure S4. Quantification total GAG (B) content of HAC and MSC micro-tissues compared to cells seeded in VH hydrogels and collagen type I hydrogels. Both the HAC and MSC seeded VH hydrogels displayed a significant increase in GAG content after 3 weeks, with greater GAG accumulation compared to the micro-tissue controls as well as standard collagen type I cultures of MSCs. Error bars represent the mean \pm SE of 6 samples. * indicates significant difference ($p < 0.05$).

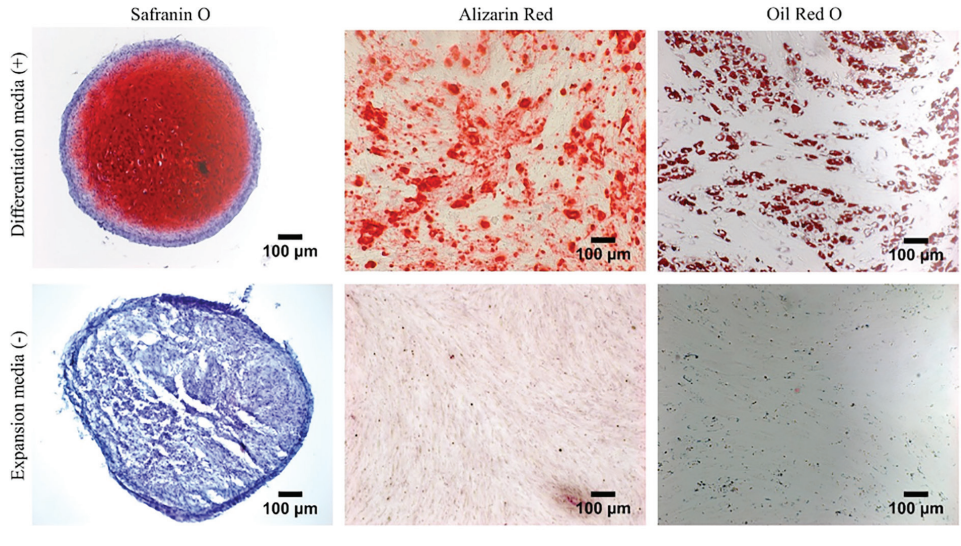


Figure S5. Multi-lineage potential of hMSCs was confirmed by a tri-lineage differentiation (adipogenic, osteogenic, and chondrogenic) assay. After 3 weeks in vitro, samples were stained for adipogenic (Oil Red O), osteogenic (Alizarin Red), and chondrogenic (Safranin O) differentiation markers.



Vitreous humor as instructive
biomaterial to support
mesenchymal stem cell
hypertrophy and
endochondral ossification

Preliminary data

A. Longoni
I. Pennings
G.C.J. Lindberg
T.B.F. Woodfield
A.J.W.P. Rosenberg
K.S. Lim
D. Gawlitta

In preparation

4



ABSTRACT

Regenerative strategies that aim at inducing new bone formation following the endochondral pathway entail the engineering of a hypertrophic cartilaginous intermediary *in vitro*, which is subsequently remodeled upon *in vivo* implantation. To develop a cartilage construct that promotes prime bone formation, current efforts focus on identifying biomaterials that optimally support mesenchymal stem cell (MSC) chondrogenesis and hypertrophy. Our previous work presented vitreous humor (VH) as a cell-instructive material that enhanced MSC chondrogenic differentiation. In this study, we investigated the suitability of VH in supporting the progression of MSC-derived chondrocytes into a hypertrophic state *in vitro* and the capability of supporting endochondral bone regeneration (EBR) *in vivo*.

To achieve this goal, MSCs embedded in VH hydrogels were stimulated to achieve an early hypertrophic phenotype (chondrogenic medium only) or a late hypertrophic phenotype (chondrogenic + hypertrophic medium). The presence of chondrogenic (glycosaminoglycan and collagen type II) and hypertrophic (collagen type X and mineralization) markers was evaluated after 31 days of culturing *in vitro*. Afterwards, the capability of these cell-laden VH hydrogels to trigger new bone formation *in vivo* was evaluated in a subcutaneous, immunodeficient rat model.

VH supported a reproducible differentiation, as chondrogenic and hypertrophic markers were present in all samples from 3 different donors. Once implanted, chondrogenically differentiated and hypertrophic stimulated MSC-laden VH hydrogels induced comparable neo-bone formation. However, a larger portion of non-remodeled cartilage was observed in the hypertrophic group. In addition, smaller bone marrow cavities were observed compared to the chondrogenic group, although with a more pronounced hematopoietic component.

In conclusion, these preliminary results indicate that VH hydrogels effectively support MSC chondrogenesis and hypertrophy *in vitro*. Furthermore, irrespective of the culture conditions used prior to implantation, new bone formation was observed *in vivo*. Taken together, this evidence indicates that VH is an ideal biomaterial for EBR-based regenerative approaches.

INTRODUCTION

Over the last few years, regenerative medicine strategies focused on mimicking the native characteristics of tissues and their developmental pathways [62, 71, 257-259]. In line with this, studying the endochondral ossification process, which happens naturally during long bone development and fracture healing, has gained increased attention for application in bone tissue engineering [83, 260]. Strategies based on endochondral bone regeneration (EBR) aim at mimicking this endochondral ossification process, in which a cartilaginous template that originates from condensed mesenchymal stem cells (MSCs) progressively acquires a hypertrophic phenotype, calcifies and is remodeled into new bone tissue [62, 71, 260]. The feasibility of triggering new bone formation by exploiting MSC chondrogenic potential and their intrinsic capability of acquiring a hypertrophic phenotype to create a cartilaginous template *in vitro* has been well established [56, 62, 68-70, 76]. Nevertheless, comparing studies where different EBR-based strategies were used, or even comparing different samples within the same study, a considerable variation in the amount of orthotopic or ectopic bone formation has been observed [65, 69, 81, 261]. One of the factors that has emerged as a crucial prerequisite for successful bone formation, is adequate induction of chondrogenic differentiation before *in vivo* implantation [61, 62]. For instance, it has been observed that the subcutaneous implantation of MSC-based constructs characterized by limited glycosaminoglycan (GAG) content, led to their complete resorption without inducing new bone formation [62, 81]. In contrast, constructs with sufficient display of chondrogenic and hypertrophy hallmarks resulted in endochondral bone regeneration *in vivo* [62, 69, 84, 262].

This evidence suggests that the *in vivo* outcome may be connected with the *in vitro* differentiation. Therefore, to obtain prime bone formation *in vivo*, it is of importance to ensure appropriate chondrogenic induction and to reach an optimal differentiation state prior to implantation [62, 262, 263]. An interesting method to promote MSC chondrogenesis is to exploit the different properties of the biomaterials used as a 3D culture platform [86, 264]. Among the different biomaterials that have been investigated, decellularized natural or engineered cartilage tissue has emerged as a promising candidate to support and enhance MSC chondrogenic differentiation. The incorporation of decellularized cartilage particles to 3D cultures [80, 109, 112] or their use as a scaffold [265, 266] induced an increase in MSC expression of chondrogenic genes including collagen type II, Sox 9 and aggrecan [109, 112]. In addition, enhanced deposition of GAGs and collagen type II was also reported [109]. These beneficial effects are connected to the retention of bioactive molecules in the extracellular matrix (ECM) after the decellularization process [112, 166]. Nevertheless, the presence of active chondro-inductive molecules and their concentration



in the ECM-based scaffolds varies greatly depending on the origin of the decellularized tissue [266] and on the method used for decellularization [267]. In particular, due to the intrinsic avascular and dense nature of cartilage ECM, the decellularization process requires a combination of physical, chemical and enzymatic treatments that often compromises its integrity and affects its biochemical composition [106, 267]. Furthermore, the potential retention of chemical reagents such as detergents could undermine the biocompatibility of the decellularized cartilage, ultimately hampering its recellularization both *in vitro* and *in vivo* [268].

The length and complexity of the decellularization protocols, which increase the risk of contamination and the washing out of essential bioactive components, represent shortcomings of employing cartilage-based biomaterials. In search for alternative solutions, vitreous humor (VH) has recently been proposed as a cell-instructive substrate to promote MSC chondrogenesis [269]. VH is a clear, gelatinous mass that comprises a large portion of the eyeball, filling the space in between the lens and the retina. VH represents an interesting alternative to decellularized cartilage-based biomaterials because of its similar biochemical composition to native cartilage [188, 269]. This suggests that it might contain similar bioactive stimuli. In addition, similar to decellularized cartilage, the use of VH-based hydrogels as culture platforms has shown to enhance MSC chondrogenesis when compared to other type of traditional culture systems (collagen control scaffold and classic pellet culture) [269]. Finally, it presents the advantage of being already virtually acellular and of a hydrogel-like consistency. Thus, differently from other types of natural biomaterials, native VH can be directly employed without any post-isolation processing or after only a mild centrifugation step [269]. Therefore, exploiting the VH characteristics to engineer an adequate cartilaginous template *in vitro* for EBR-based approaches seems a logical choice. Nevertheless, whether the bioactive cues present in the VH matrix support the progression of MSCs towards a hypertrophic phenotype -a fundamental step in EBR- has yet to be determined. In particular, it has been reported that, due to the presence of anti-angiogenic molecules like thrombospondin-1, native VH inhibits endothelial cell growth and neovascularization [270, 271]. This could hamper EBR *in vivo*, as the invasion of the cartilaginous template by blood vessels represents a crucial step for its remodeling into new bone tissue [25].

Therefore, the goal of this chapter was to gather preliminary information regarding the suitability of VH to support the progression of MSC-derived chondrocytes towards a hypertrophic phenotype *in vitro* and the capability of supporting EBR *in vivo*. To do so, we first evaluated the reproducibility of producing an MSC-derived cartilaginous template by using VH isolated from several equine donors. Secondly, the capability of VH to support

progression of MSCs towards a hypertrophic state was investigated *in vitro*. Finally, the feasibility of achieving EBR in a subcutaneous model was evaluated. In more detail, to identify the optimal differentiation state required prior to the implantation, new bone formation induced by MSC-laden VH hydrogels that were either chondrogenically differentiated (early hypertrophy) or hypertrophically induced (late hypertrophy) was compared.

MATERIALS AND METHODS

Study design

Batch-to-batch variability was assessed by evaluating the capability of VH isolated from 5 different equine donors to support chondrogenesis of MSCs derived from one human donor. Afterwards, the capability of VH to support MSC progression towards a hypertrophic phenotype was investigated using three different MSC donors. Two different culture regimens were used by differentiating the samples in either chondrogenic medium (31 days), or chondrogenic medium followed by hypertrophic medium (21+10 days). As collagen is commonly used to support MSC chondrogenic differentiation, cell-laden collagen type I hydrogels were included as control (Figure S1 and S2), along with cell-free VH hydrogel controls. Finally, chondrogenically differentiated and hypertrophically stimulated cell-laden VH hydrogels, derived from one MSC donor, were implanted in an immunodeficient subcutaneous rat model.

Vitreous humor isolation

Equine eyes were obtained from local slaughterhouses and freshly processed (<12 h) as previously described [269]. Briefly, the surrounding connective and muscular tissues were carefully removed. Before extraction under aseptic conditions, the ocular tissue was rinsed in 70% ethanol (3 consecutive washes). To access the VH, an incision from the center of the ocular body towards the optic nerve end was performed. Finally, the VH was carefully separated from the lens and the ora serrata and stored at +2–8°C. All samples were used within one week from isolation.

Isolation of bone marrow-derived human MSCs

Human MSCs were isolated from bone marrow aspirates of three patients (donor 1: 30-year old, female; donor 2: 73-year old, male; donor 3: 20-year old, female) after obtaining the written informed consent (under biobank release protocol TCBio-08-001-K, University Medical Center Utrecht). After the centrifugation with ficoll-paque (GE Healthcare, Little Chalfont, UK) to separate the mononuclear fraction, cells were further selected based



on plastic adherence as previously described [89]. Adherent cells were cultured at 37°C under humidified conditions and 5% carbon dioxide (CO₂) in MSC expansion medium, which was composed of α -MEM (22561, Invitrogen, Carlsbad, USA) supplemented with 10% heat-inactivated fetal bovine serum (S14068S1810, Biowest, Nuaille - France), 0.2 mM L-ascorbic acid 2-phosphate (A8960, Sigma-Aldrich, St. Louis, USA), 100U/mL penicillin with 100 mg/mL streptomycin (15140, Invitrogen) and 1 ng/mL basic fibroblast growth factor (233-FB; R&D Systems, Minneapolis, USA). The medium was refreshed three times per week and at 80% confluency MSCs were passaged. MSCs from donor 3 were used to study the batch-to-batch variability and *in vivo* bone formation.

MSC encapsulation and differentiation in VH Hydrogels

At passage 4, 2.5×10^5 MSCs derived from 3 different donors were encapsulated in VH hydrogel (354249, Corning, New York, USA). Briefly, MSCs were seeded in 50 μ L VH by pipetting them on top of the hydrogel and by gently mixing with a spatula to homogeneously distribute the cells throughout the biomaterial as previously described [269]. Cell-laden hydrogels were cultured in 96-well flat bottom polypropylene cell culture plates in serum-free chondrogenic medium consisting of high glucose DMEM (31966, Invitrogen) with 1% Insulin-Transferrin-Selenium (ITS)+ premix (354352; Corning), 10^{-7} M dexamethasone (D8893; Sigma-Aldrich), 0.2 mM L-ascorbic acid 2-phosphate (A8960, Sigma-Aldrich), 100 U/mL penicillin and, 100 mg/mL streptomycin (15140, Invitrogen) and 10 ng/mL TGF- β 1 (Peprotech, New Jersey, USA). Medium was refreshed daily for the first 4 days and afterwards three times per week. After 21 days of chondrogenic differentiation, half of the constructs were maintained in chondrogenic medium (VH chondro group) for 10 additional days, whereas the other half was subjected to hypertrophic medium (VH hyper group), consisting of DMEM (31966, Invitrogen), 1% ITS + premix, 100 U/mL penicillin with 100 mg/mL streptomycin, 0.2 mM L-ascorbic acid-2-phosphate, 1 nM dexamethasone, 10 mM β -glycerophosphate (G9891; Sigma-Aldrich), 1 nM triiodothyronine (2877; Sigma-Aldrich). The total differentiation period for both groups was 31 days, after which the samples were processed for histological analysis.

Subcutaneous implantation

MSCs derived from one donor were embedded in VH and chondrogenically differentiated or hypertrophically induced for 31 days as described above. VH controls without MSCs were entirely degraded after 31 days of cultures. Therefore they were not implanted *in vivo*.

Animal experiments were performed with the approval of the animal ethical committee of the University Medical Center Utrecht (approval number: AVD1150020172465) in

accordance with the ARRIVE guidelines [272]. To ensure the randomization of the samples over multiple experimental animals, the samples of this study were combined with those of another experiment (manuscript submitted). A total of 14 nude rats (CrI:NIH-Foxn1^{nu} Charles River) were included in the study and randomly housed in sterile filter-top cages in triplets at the animal facility of the Utrecht University. There, animals received standard food pellets and water *ad libitum*, under climate-controlled conditions (21°C; 12 h light/12 h darkness). At the age of 12 weeks, after at least 7 days of acclimatization, subcutaneous pockets were created as previously described [103]. Briefly, 5 mm dorsal incisions followed by blunt dissection were performed under general anesthesia (1-3.5% isoflurane in oxygen, AST Farma, Oudewater, the Netherlands). In each pocket, 4 cell-laden VH hydrogels belonging to the chondrogenic or the hypertrophic group were implanted. In total, 6 pockets ($n=6$) per group were created. Each animal received a maximum of 6 subcutaneous pockets. After implantation, the skin was closed transcutaneously with Vicryl Rapide 4-0 sutures (VR 2297; Ethicon). A single dose of antibiotics (Duplocillin LA, 22.000 IE/kg, MSD Animal Health, Boxmeer, the Netherlands) was injected intramuscularly. Subcutaneous injection of pain medication (carprofen, 0.05 mg/kg body weight) was administered pre-operatively and once a day for the following three days. Rats were euthanized 8 weeks after surgery by exsanguination while under deep anesthesia (5% isoflurane in oxygen). Subcutaneous implants were retrieved and processed for further analysis.

MicroCT scanning and fluorochrome administration

Mineralization of the implants was assessed by microCT at 0, 2, 4, 6 and 8 weeks after surgery. While under general anesthesia (1-3.5% isoflurane in oxygen), the rats were positioned on a custom-made support in prone position. Scanning was performed using a microCT imaging system (Quantum FX, PerkinElmer, Waltham, MA, USA). Three minutes of scan time was required per implant for an isotropic voxel size of 42 μm^3 resolution (voltage 90 kV, current 180 mA, field of view = 21 mm). A volume of interest (VOI) corresponding to the mineralized implant was selected per sample. Images were segmented using a global threshold and mineralized volume was measured in mm^3 using the image processing software plugin BoneJ [273] (Image-J 2.0.0; Java, Redwood Shores, CA, USA). 3D reconstructions of the femur defect were based on the microCT data and created using ParaView (ParaView, Kitware Inc, USA).

To evaluate the onset of bone formation, fluorescent calcium-binding fluorochromes that are incorporated at sites of active mineralization were administered subcutaneously while the animals were under general anesthesia for the microCT scanning. Three fluorochromes were injected. After 2 weeks, 100 mg/kg xylene orange tetrasodium salt (XO, red) (33825,



Sigma-Aldrich, 20 g/L in NaHCO₃ 1%) was administered. At 4 weeks, 10 mg/kg calcein green (C0875, Sigma-Aldrich; 3 g/L in NaHCO₃ 2%) was injected. Finally, after 6 weeks, tetracycline hydrochloride (yellow) 20 mg/kg (T3383, Sigma-Aldrich; 2 g/L in 50% demi/PBS) was used.

Histological and immunohistochemical analysis

After 31 days of culture *in vitro*, samples ($n=3$ for each donor) were fixed in 10% neutral buffered formalin solution. For the subcutaneous explants, after fixation in 10% neutral buffered formalin solution for 3 days, an additional decalcification step of 3 weeks in a 10% EDTA-phosphate buffered saline solution (pH 7.4) was included. Afterwards, all samples were dehydrated in increasing ethanol concentrations (70-100%), cleared in xylene and embedded in paraffin. Finally, they were sliced into 5 μm thick sections (Microm HM340E; Thermo Fischer Scientific). Before staining, all tissue sections were deparaffinized with xylene and progressively rehydrated through decreasing ethanol solutions (100-70%).

For the *in vitro* cultures, triple staining consisting of Weigert's haematoxylin (640490; Klinipath BV), fast green (FN1066522; Merck), and Safranin-O (FN1164048213; Merck) was used to identify cell nuclei, collagen fibers, and glycosaminoglycans (GAGs), respectively. Von Kossa staining was performed in order to detect matrix mineralization. Samples were incubated with 1% silver nitrate (209139, Sigma-Aldrich) for 1 hour, directly under a light bulb (Philips Master TL5HO 54W 830, 1m distance). After rinsing with 5% sodium thiosulphate (A17629, Alta Aesar, Haverhill, USA) sections were counterstained with haematoxylin.

For the subcutaneous explants, new bone formation was evaluated qualitatively using H&E staining. In addition, the persistence of the implanted cartilaginous template was confirmed by alcian blue/picrosirius red. TRAP staining was performed to visualize the osteoclasts. Briefly, hydrated sections were incubated for 20 minutes in 0.2 M acetate buffer at room temperature. Afterwards, sections were incubated in 0.2 M acetate buffer supplemented with 0.5 mg/mL naphthol AS-MX phosphate (855, Sigma) and 1.1 mg/mL fast red TR salt (F8764, Sigma) for 4 hours at 37°C. Mayer's haematoxylin was used as nuclear counterstaining and mounted in ecomount (Biomedical care, Pacheco, CA, USA).

Immunostaining for collagen type II (antibody at 0.6 $\mu\text{g}/\text{mL}$, II-II6B3, Developmental Studies Hybridoma Bank) and collagen type X (antibody at 10 $\mu\text{g}/\text{mL}$, 1-CO097-05, Quartett, Germany) were performed as previously described [89]. Briefly, endogenous peroxidase activity was blocked by incubating samples for 15 minutes with 0.3% H₂O₂. Sequential incubation with 1 mg/mL pronase (Sigma-Aldrich) and 10 mg/mL hyaluronidase (Sigma-Aldrich) at 37°C for 30 minutes each was used as antigen retrieval for collagen

type II. For collagen type X staining, antigens were retrieved by exposing the samples to 1 mg/mL pepsin (Sigma-Aldrich) at pH 2.0 for 2 hours and afterwards to 10 mg/mL hyaluronidase for 30 minutes, both at 37°C. After blocking with 5% BSA/PBS for 30 minutes at room temperature, samples were incubated with the primary antibody overnight at 4°C. After 30 minutes incubation with the secondary antibody (VWRKDPVM110HRP, BrightVision poly HRP-anti-mouse IgG, VWR, Radnor, USA), the labels were visualized by 3,3'-diaminobenzidine oxidation. To visualize the nuclei, sections were then counterstained with haematoxylin. Mouse isotypes (X0931, Dako, Santa Clara, USA) were used as negative controls. The isotype concentrations were matched with the ones of the primary antibodies.

For all the staining beside the TRAP one, samples were dehydrated and mounted with depex mounting medium. Images were acquired with an Olympus BX51 microscope (Olympus DP73 camera, Olympus, Hamburg, Germany).

Histological analysis on MMA sections

After fixation, non-decalcified samples ($n=2$ per group) were dehydrated through a graded ethanol series and embedded in methylmethacrylate (MMA) solution (S7351990702, Merck) with Plastoid®-N (74432, Sigma-Aldrich Chemie GmbH, Steinheim, Germany) and benzoyl peroxide (Sigma-Aldrich, St Louis, MO, USA) (0.8 mL MMA, 0.2 mL Plastoid®-N and 28 mg benzoyl peroxide). Cross-sectional slides (20-30 μm) were made using a saw microtome (Leica SP1600; Leica Biosystems Nussloch GmbH, Nussloch, Germany). Sections were stained with 1% methylene blue solution and 0.3% basic fuchsin solution. Slides were alternated between the fuchsin staining and remaining unstained to visualize the fluorochrome labels. Fluorochromes were visualized using a confocal microscope (Leica SP8X confocal).

Histomorphometric analysis

Histomorphometric analysis was performed combining H&E (paraffin sections) and methylene blue/basic fuchsin (MMA sections) staining. Briefly, a panoramic image of the entire sample was created by merging images (4x/0.04 FN26.5 objective) in Adobe Photoshop C6. For each image, the total area of the cartilaginous implant and newly formed bone was calculated. Three different areas were manually selected: bone, hypertrophic cartilage and bone marrow. The number of pixels for each area was manually quantified via the function "recording measurement" and expressed as percentage of the total area for each sample. Osteoclasts detected with the TRAP staining in the paraffin sections were manually counted using the cell counter plugin from Image-J.



Statistics

A two-way ANOVA, followed by a Bonferroni *post-hoc* analysis, was performed to evaluate differences in mineralization volumes over time. A two-tailed Mann-Whitney test was performed to compare the results of the histomorphometric analysis (GraphPad Prism 6, San Diego, CA, USA). A *p*-value of less than 0.05 was considered statistically significant.

RESULTS

Histological analysis indicates limited VH batch-to-batch variation

VH isolated from 5 different equine eyes consistently supported MSC chondrogenic differentiation (Figure 1). Abundant deposition of GAGs and collagen type II was observed in all samples after 31 days of chondrogenic differentiation.

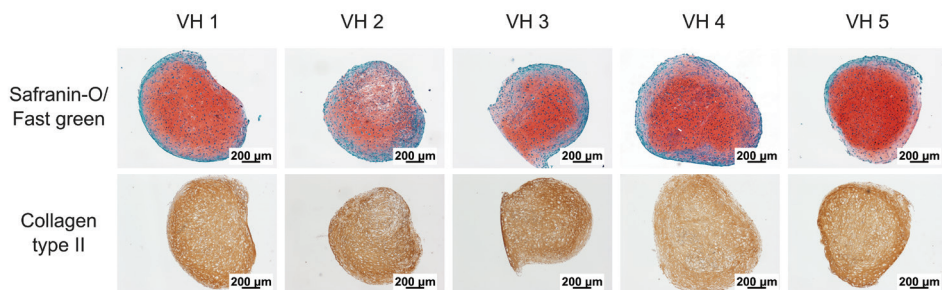


Figure 1. Chondrogenically differentiated MSCs embedded in VH isolated from ocular tissues of different equine donors. All batches of VH supported deposition of GAGs (Safranin-O/Fast Green stain; red) and collagen type II (brown) by the embedded human MSCs of one donor and cultured for 31 days.

VH supports MSC hypertrophy *in vitro*

After 31 days of chondrogenic differentiation (Figure 2A), hallmarks of chondrogenic differentiation (GAGs and collagen type II) and hypertrophy (collagen type X) were observed for all MSC-seeded VH samples from 3 donors. In addition, the typical chondrocyte lacunae could be observed. When hypertrophic stimulation was induced (Figure 2B) in the last 10 days of culture, a reduction in GAG content occurred for all MSC donors. Consistent results in terms of collagen type X deposition and matrix mineralization were observed for all the MSC donors. In contrast, the MSCs seeded in collagen control hydrogels displayed heterogeneous results, as no chondrogenic or hypertrophic markers could be detected in donor 3 (Figure S1). The differences observed in terms of differentiation and ECM deposition were also partially reflected in the final dimension of the constructs (Figure S2). For instance, for donor 2 an increase in size was obtained when VH was used as culture platform.

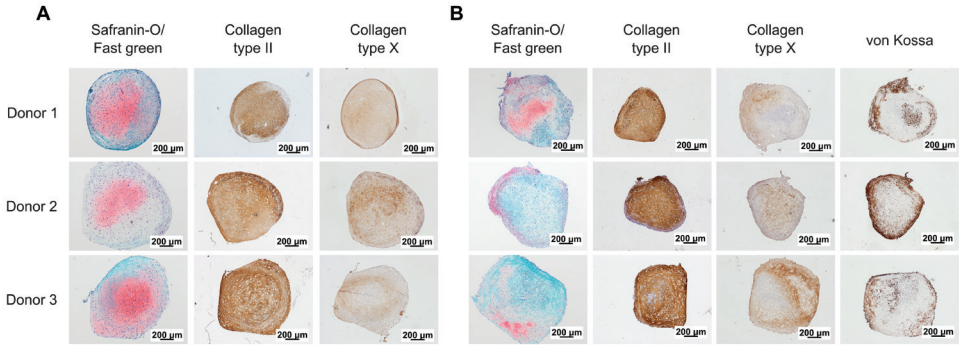


Figure 2. Overview of the cell-laden VH hydrogels after 31 days of culture. **(A)** Chondrogenic differentiation was confirmed by safranin-O/fast green staining, which highlights the presence of GAGs (red), and by collagen type II immunostaining (brown). Collagen type X (brown), a hallmark of hypertrophy was also stained. **(B)** After hypertrophy induction, mineralization of the ECM was also observed for all the MSCs donor.

MSC-laden VH hydrogels induce neo-bone formation *in vivo*

After 6.5 weeks one of the experimental animals was prematurely euthanized due to the reaching of human endpoint. As the causes of the increased animal discomfort were unknown, this data was excluded from further analysis.

The mineralized volumes (microCT) observed for the VH chondrogenic ($1.92 \pm 1.14 \text{ mm}^3$) and hypertrophic ($0.9 \pm 0.59 \text{ mm}^3$) group were not significantly different (Figure 3A) 8 weeks post-implantation. Nevertheless, a different temporal mineralization pattern was observed for the two groups (Figure 3A). For the VH chondrogenic group, the maximum mineralized tissue volume was observed after 4 weeks ($3.44 \pm 1.28 \text{ mm}^3$). Afterwards, a decreasing trend was observed, possibly due to remodeling and formation of a bone marrow cavity. Such a trend was not present in the VH hypertrophic group, where the mineralized volume remained stable after 4 weeks. Consistently, fluorochrome incorporation (Figure 3B) indicated an earlier onset of active bone formation at 2 weeks in the chondrogenic group. In contrast, no bone formation seemed to occur in the hypertrophic group, as indicated by the absence of XO incorporation (red color). Afterwards, at 4 and 6 weeks, comparable new bone formation was observed in both groups (green and yellow color, respectively).

Interestingly, even if the same total mineralized volume was observed after 8 weeks, cell-laden hydrogels belonging to the chondrogenic group tended to form a single bone ossicle (Figure 3C). In particular, in all implants (5/5) from the chondrogenic group, 3 to 4 MSC-laden VH hydrogels had fused. In the hypertrophic group, only 2 out of 5 samples displayed a similar fusion rate (Figure S3). In addition, from cross-sectional microCT images, the center of the implants of the chondrogenic group appeared hollow, probably due to



the presence of bone marrow. This was less evident for the hypertrophic group, where only multiple marrow cavities of smaller dimension were observed.

Histological analysis confirmed new bone formation in both groups (Figure 4). Significantly more non-remodeled cartilage was observed in the hypertrophic group compared to the chondrogenic one. An inverse trend was observed for bone marrow content, as it was significantly higher in the chondrogenic group. Finally, in both groups, the presence of osteoclasts suggests that the new bone formation or bone remodeling was still ongoing at 8 weeks. Even if not statistically significant, a higher number of osteoclasts was observed in all samples belonging to the hypertrophic group.

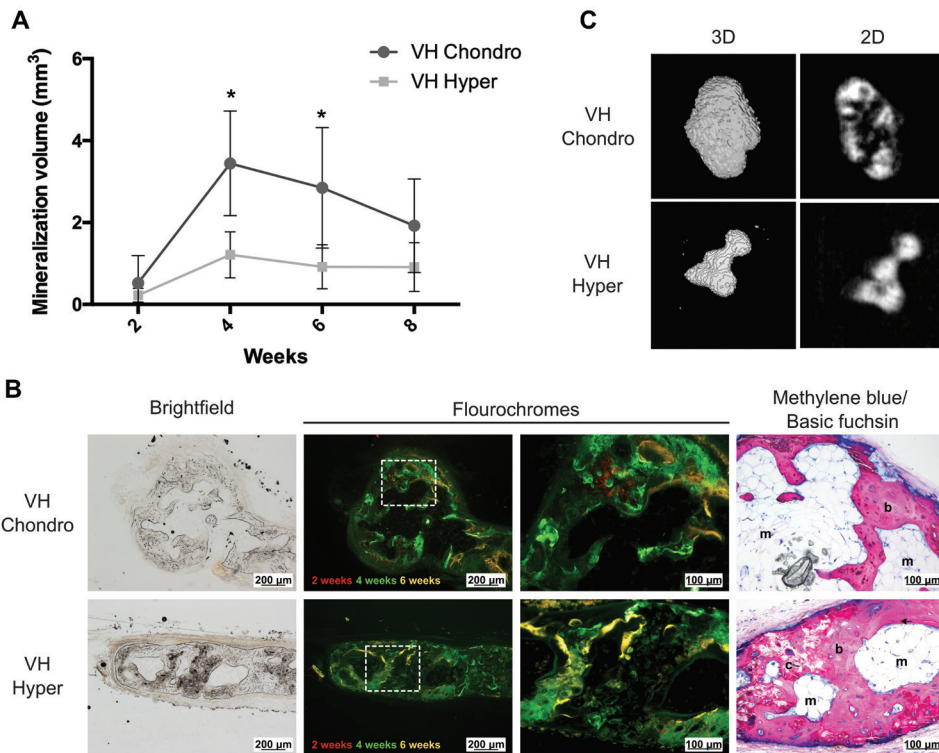


Figure 3. New bone formation *in vivo*. **(A)** Mineralization volume over time based on microCT after subcutaneous implantation of VH Chondro and VH Hyper samples. **(B)** Brightfield overview of the MMA embedded samples. Fluorochromes incorporation, which indicates the onset of mineralization after 2 (red), 4 (green) and 6 (yellow) weeks, was investigated in the same location. The white rectangles highlight the magnified areas. Methylene blue/basic fuchsin confirmed new bone formation. **(C)** 3D reconstructions and 2D sections in the center of the newly formed bone highlighted the presence of a large marrow cavity in the VH Chondro group. Smaller marrow cavities were observed for the VH Hyper group. m: bone marrow; c: cartilage, b: bone; **(A)** data points represent the mean mineralization (\pm standard deviation); * $p < 0.05$.

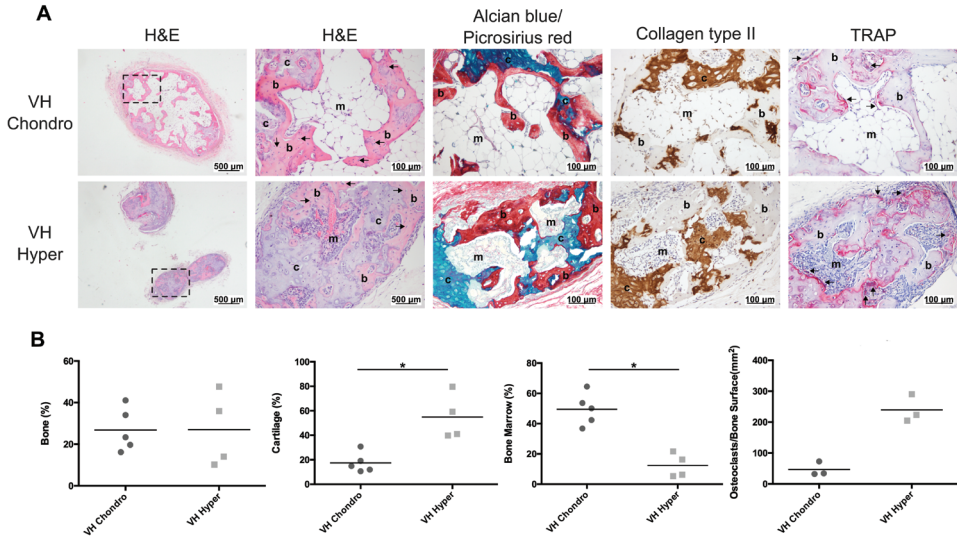


Figure 4. (Immuno)stainings and histomorphometric analysis 8 weeks post-implantation. **(A)** H&E staining indicates that new bone formation occurred in both VH Chondro and VH Hyper groups. Osteocytes are indicated with black arrows in the H&E-stained sections. Non-remodeled cartilage persisted in both groups (brown staining in collagen type II-stained sections). Active remodeling was confirmed by the presence of osteoclasts with the TRAP staining (red staining, the black arrows indicate the osteoclasts). **(B)** Bone, cartilage and bone marrow contents were assessed via histomorphometric analysis and expressed as a percentage of the total area. TRAP positive osteoclasts were also quantified. m: bone marrow; c: cartilage, b: bone; black rectangles highlight the magnified area; **(B)** data points represent the different experimental animals; ** $p < 0.01$.

DISCUSSION

To successfully achieve new bone formation, chondrogenic differentiation before *in vivo* implantation is a crucial step in EBR-based approaches. It has been established that the properties of the biomaterials used for the 3D culture of MSCs can influence their chondrogenesis [90, 264, 274]. Nevertheless, the identification of the ideal features that the biomaterial should possess in order to optimally support and enhance MSC chondrogenesis and their progression towards hypertrophy is still an ongoing process [56, 85]. Employing decellularized cartilage to fabricate scaffolds and hydrogels has taught us that the preservation of the native bioactive molecules and the sites for cell-ECM interaction plays a crucial role in affecting cellular fate [106]. Due to its similarity in composition to native cartilage and its rather limited post-isolation processing, VH represents an appealing natural biomaterial to support and guide MSC chondrogenesis. In this study we demonstrated that, under adequate differentiation conditions, VH also supported MSC hypertrophy *in vitro* and new bone formation *in vivo*. Thus, it represents a valuable tool for EBR-based strategies for bone tissue engineering.



In vitro, heterogeneous results were achieved when MSCs were embedded in collagen type I control hydrogels in terms of GAGs, collagen type II and X deposition and matrix mineralization. While this could be associated to the inherent inter-donor variability of the chondrogenic potential of MSCs [88-90], this variation was not observed in MSC-laden VH hydrogels. Although quantitative analyses and the inclusion of additional MSC donors that do not differentiate in traditional culture systems are required, these findings suggest that VH could possess some chondro-inductive properties that enhance the chondrogenic differentiation for MSCs isolated from different donors. An interesting next step is to identify the bioactive components responsible for this beneficial effect. Possible candidates are hyaluronic acid, chondroitin sulphate and heparan sulphate, as they are commonly present in the VH [269] and have proven to positively affect MSC chondrogenic differentiation [274-276]. Additional ECM components that might play a role in promoting MSC chondrogenesis are proteoglycans such as decorin and biglycan [277]. More specifically, thanks to specific binding sites, these proteoglycans are able to sequester growth factors like TGF- β – a fundamental inducer of MSC chondrogenic differentiation – and enhance its biological effect [277, 278].

Controversial evidence exists in literature regarding what is considered the “optimal differentiation stage” that has to be achieved *in vitro* in order to fully exploit the bone regenerative potential of the engineered cartilaginous template *in vivo* [62, 69, 76, 81, 84]. On the one hand, it has been observed that insufficient presence of hypertrophic markers, like collagen type X, resulted in hampered [262] or delayed [62] bone formation. On the other hand, the development of a too dense matrix *in vitro* could also result in incomplete remodeling of the calcified cartilage and, as a consequence, reduced bone formation [81]. Thus, in this study, two stages of MSC differentiation were compared: early hypertrophy (chondrogenic medium) and late hypertrophy (chondrogenic and hypertrophic medium). In both cases, new bone formation was observed upon *in vivo* implantation. This suggests that any potential anti-angiogenic properties of VH [270, 271] did not hamper its vascularization and the remodeling of the cartilage, most likely due to the secretion of pro-angiogenic factors by the MSC-derived hypertrophic chondrocytes [25].

Interestingly, even if the same amount of bone formation was observed 8 weeks post-implantation, the VH chondrogenic and hypertrophic groups displayed different characteristics. Notably, in the VH chondrogenic group, matrix mineralization occurred predominantly within the first 2-4 weeks. Furthermore, after 8 weeks, only a limited amount of non-remodeled cartilage (17% of the total area) and an increased marrow volume (49% of the total area) was observed. In the VH hypertrophic group, mineralization and matrix remodeling appeared to proceed slower and evenly throughout the 2-8 weeks. This might

have resulted in a slower remodeling of the cartilage (59% of the total area) and, as a consequence, to limited bone marrow presence (11% of the total area). Nevertheless, the bone marrow appeared to have a more pronounced hematopoietic component in this group. This might be a more desirable characteristic, as it has been shown that the increased presence of adipocytes negatively influences hematopoiesis [279] and granulopoiesis [280]. In addition, the presence of an increased fatty component is associated with a decrease in plasma levels of insulin-like growth factor 1, a growth factor implicated in skeletal maintenance, and stromal-derived factor 1, a chemoattractant for stem cells [281].

A potential downside of the use of hypertrophic induced MSC-derived constructs is the limited fusion of the constructs observed in this group. The slower remodeling and the lower fusion rate could be due to a decrease in metalloproteinase, which has been observed when the mineralization of the cartilaginous template occurred [77]. Thus, based on these data, one could suggest that chondrogenic differentiation of the MSCs in the VH hydrogel could promote faster bone formation and better integration with the pre-existing bone defect edges compared to the hypertrophic induced MSC-VH constructs. Nevertheless this has to be established in an orthotopic setting.

In conclusion, these preliminary results indicate that VH hydrogels could be used as an instructive biomaterial to support adequate chondrogenic differentiation of MSCs for EBR- based approaches. In addition, irrespective of the culture conditions used to produce the cartilaginous template *in vitro*, new bone formation was observed *in vivo*. Future studies should focus on the identification of the bioactive components responsible for the beneficial effects observed. Also, it would be interesting to elucidate why different bone forming processes occurred for the two medium conditions. Finally, in order to develop an off-the-shelf product, it would be valuable to investigate whether VH intrinsic properties are sufficient to trigger EBR in an ectopic or orthotopic location in a stable cell-free variant.

ACKNOWLEDGMENTS

The antibody against collagen type II (II-II6B3), developed by T.F. Linsenmayer, was obtained from the DSHB developed under the auspices of the NICHD and maintained by The University of Iowa, Department of Biology, Iowa City, IA52242. The authors would like to thank Paolo Grassi for the precious help with histomorphometric analysis and professor Harrie Weinans for the support with the microCT data acquisition and analysis.



SUPPLEMENTARY DATA

Supplementary materials and methods: MSC encapsulation in collagen type I hydrogels

As collagen is a commonly used biomaterial to support MSC chondrogenic differentiation and EBR [56, 264], cell-laden collagen type I hydrogels served as controls. Collagen controls were created in parallel with the VH ones, by encapsulating MSCs into 50 μ L collagen type I gel (1 mg/mL) after pH neutralization, according to manufacturer instructions. Gelation was carried out for 30 minutes at 37°C under humidified conditions and 5% carbon dioxide (CO_2). Collagen controls were differentiated and analyzed in an identical fashion compared to the VH samples. As the VH-based group outperformed the collagen controls *in vitro* and the latter displayed limited chondrogenesis, only the chondrogenically differentiated or hypertrophically induced MSC-laden VH constructs were implanted *in vivo*.

Supplementary figures

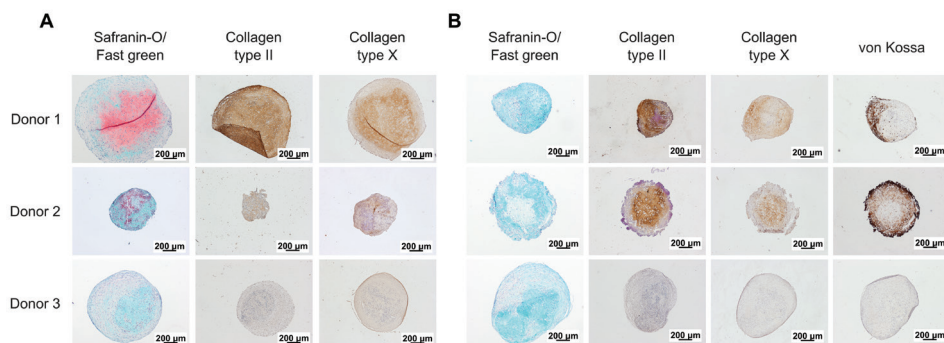


Figure S1. Overview of the cell-laden collagen hydrogels after 31 days of culture. **(A)** After chondrogenic differentiation the presence of GAG was confirmed by safranin-O/fast green staining in 2/3 MSCs donors (red). Similarly, collagen type II and X deposition (brown) was not observed for donor 3. **(B)** After hypertrophy induction, mineralization of the ECM was observed for donor 1 and 2.

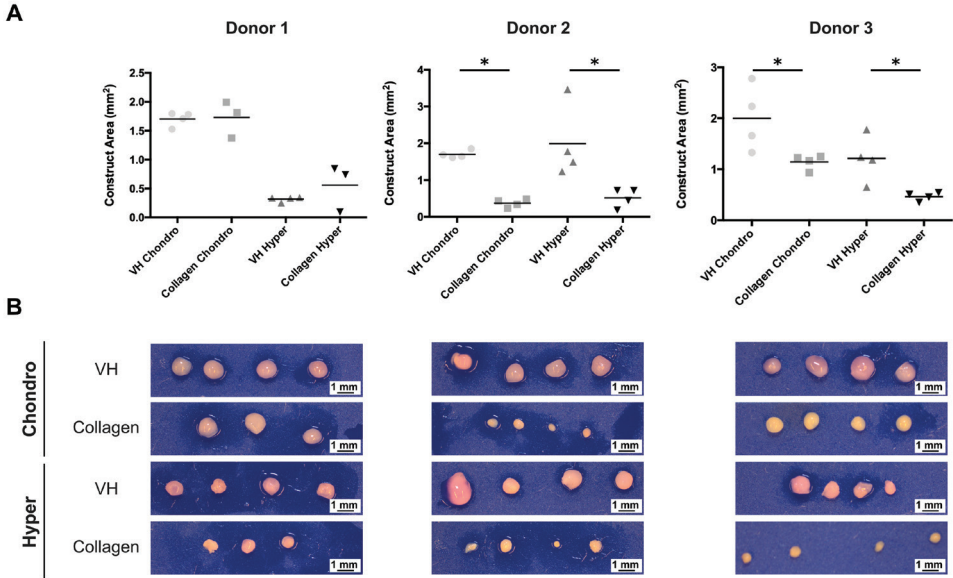


Figure S2. Overview of the constructs dimension after 31 days of *in vitro* culture. **(A)** Quantification of the constructs area was performed using the “recording measurement” function of Photoshop. **(B)** Overview of the variation in constructs dimension was presented per donor. * $p < 0.05$.



Figure S3. 3D reconstruction of the subcutaneous implants 8 weeks post-implantation. Construct fusion seems to occur with higher frequency in the chondrogenic group compared to the hypertrophic one.



Part II

Employing allogeneic mesenchymal stem cells for endochondral bone regeneration







The impact of immune response on endochondral bone regeneration

A. Longoni
L. Knežević
K. Schepers
H. Weinans
A.J.W.P. Rosenberg
D. Gawlitta

npj Regenerative Medicine, 2018, 3:22

5



ABSTRACT

Tissue engineered cartilage substitutes, which induce the process of endochondral ossification, represent a regenerative strategy for bone defect healing. Such constructs typically consist of multipotent mesenchymal stromal cells (MSCs) forming a cartilage template *in vitro*, which can be implanted to stimulate bone formation *in vivo*. The use of MSCs of allogeneic origin could potentially improve the clinical utility of the tissue engineered cartilage constructs in three ways. First, ready-to-use construct availability can speed up the treatment process. Second, MSCs derived and expanded from a single donor could be applied to treat several patients and thus the costs of the medical interventions would decrease. Finally, it would allow more control over the quality of the MSC chondrogenic differentiation. However, even though the envisaged clinical use of allogeneic cell sources for bone regeneration is advantageous, their immunogenicity poses a significant obstacle to their clinical application.

The aim of this review is to increase the awareness of the role played by immune cells during endochondral ossification, and in particular during regenerative strategies when the immune response is altered by the presence of implanted biomaterials and/or cells. More specifically, we focus on how this balance between immune response and bone regeneration is affected by the implantation of a cartilaginous tissue engineered construct of allogeneic origin.

INTRODUCTION

Bone healing is a remarkable process that can deliver fully functional and integrated new tissue, without scar formation [8]. Due to this regenerative capacity, the majority of bone fractures, which are the most common large organ injuries, reach resolution through complete healing. Nevertheless, 10% of all fractures do not completely heal, resulting in failed bridging of the bone defect, called a non-union [13]. In addition, certain bone degenerative disorders, as well as osteosarcomas, can result in loss of bone tissue that cannot be repaired through the natural healing process [8]. Bone grafting has been the treatment of choice in such cases, primarily autologous, and occasionally allogeneic. However, both options have well-known disadvantages: the first one includes morbidity of the surgical site from where the graft is removed, while the latter bears the risks of immune rejection and disease transmission [31]. Besides, the scarcity of graft material represents another driving force behind the search for alternatives [31].

Tissue engineered bone constructs represent an attractive alternative. Traditionally, they rely on osteogenic cells seeded in 3D scaffolds to enhance the natural healing capacity of the recipient [56]. The most commonly employed regenerative strategy is to mimic the intramembranous repair process, where a bone matrix is directly synthesized *in vitro* and subsequently implanted *in vivo* [56, 260]. So far, these cell-seeded constructs have shown greater potential *in vitro* compared to *in vivo*, probably due to insufficient vascularization of the constructs upon implantation [56, 57]. A promising alternative strategy exploits the chondrogenic potential of cells to mimic the endochondral ossification process. Similarly to the long bone natural development, during the tissue regeneration therapies, an implanted cartilaginous template will acquire a hypertrophic chondrogenic phenotype; will be invaded by blood vessels, host osteoblasts and osteoclasts, and will eventually be converted into bone tissue [22, 56, 62, 260]. The endochondral strategy encompasses several advantages over other cell-based approaches. For example, chondrocytes can survive in low-nutrient environments [75, 260] and are thus an attractive cell source for implantation. Also, this eliminates the need for an integrated vascular network, simplifying the culturing process [57]. Further, the proposed terminal nature of the hypertrophic chondrocyte differentiation [13, 23] suggests an eventual deletion of the majority of the implanted cells [76]. These features together with the robustness and efficiency of this approach [62, 69-71, 76, 80] make endochondral bone regeneration (EBR) an appealing strategy for clinical translation.

However, some considerations pertain to the clinical translatability of the approach. Currently, bone marrow-derived multipotent mesenchymal stromal cells (MSCs) are the most frequently used cell source for EBR research [56]. Although adipose-derived stem



cells may be an alternative cell source for EBR [79, 95], only few reports exist to date. Thus, in this review we focus on bone marrow derived MSCs. MSCs are not only capable of differentiating toward the chondrogenic lineage [73], but they also spontaneously progress into a hypertrophic phenotype [74], which is a particularly favorable characteristic for the endochondral application. However, the development of bone substitutes using MSCs requires expansion and *in vitro* differentiation to produce an implantable cartilaginous template. The (1) unpredictable lengthiness of the pre-operative laboratory work, which includes MSC isolation, expansion, characterization and differentiation; together with (2) the difficulties in synchronizing the process with the surgical schedule; and most importantly, (3) the heterogeneity in differentiation potential between MSCs isolated from different donors [69, 282], pose an obstacle for the use of autologous MSCs and the second point also for allogeneic MSCs. Furthermore, the harvest of autologous cells represents an additional discomfort for the patient and a logistical challenge, as it involves an invasive intervention for the patient prior to the regular operation for bone reconstructive purposes. Finally, high costs are associated with growing and differentiating the MSCs under Good Manufacturing Practice conditions when performing such a procedure in a personalized fashion [283].

Allogeneic cell sources represent an attractive alternative, offering the possibility of developing a “ready-to-use” product [284]. In particular, allogeneic MSCs could be isolated, expanded and characterized for their hypertrophic chondrogenic potential in advance, reducing the time required to produce the graft substitute, avoiding complex logistics and the need of two interventions for the patient. In addition, this approach would benefit patients whose own MSCs have a lower chondrogenic potential, such as the elderly [88, 285]. Lastly, MSCs harvested from one donor could be used to treat multiple patients, which would reduce the costs of treatment considerably. Obviously, the use of non-autologous cell sources in EBR could potentially simplify the implementation into the clinical practice. However, the main problem posed by the use of non-autologous cells is their immunogenicity. Transplanted cells could be recognized and cleared by the host immune system, preventing the integration and the remodeling of allogeneic tissue engineered constructs [96, 286]. Furthermore, it is known that an extensive crosstalk exists between bone cells and cells of the innate and adaptive immune systems during bone development and fracture healing [287]. For instance, there is consistent evidence in literature of new bone formation enhancement achieved by promoting the initial acute inflammatory response with localized pro-inflammatory stimuli [288-291]. However, altering the homeostasis between immune and bone cells by, for example, inducing a chronic inflammatory condition due to the presence of allogeneic cells, might negatively affect the balance between bone formation and resorption [53]. This could lead to the

failure of the EBR process. Apart from studies focusing on bone regeneration following implantation of allogeneic osteogenically differentiated MSCs [96, 292, 293], the *in vivo* regenerative potential of non-autologous MSCs has been studied mainly on non-differentiated MSCs [294-297] or in immunocompromised animal models [56, 62, 80]. Thus, the role of the immune system in EBR, especially when allogeneic, chondrogenically differentiated MSCs will be used, is largely unknown.

The scope of this review is to highlight the immunological aspects that can affect the outcome of EBR strategies. To this end, a general analysis of the role of the immune system in endochondral fracture healing and in response to implanted cells and/or biomaterials is provided. Then endochondral bone regeneration is detailed before we propose a speculative analysis of the feasibility of using allogeneic, chondrogenically differentiated MSCs for EBR. Further, understanding the fate of the allogeneic chondrocytes after implantation will help elucidating if the exposure to allogeneic epitopes is only a transient or long-lasting challenge for the host immune system.

THE ROLE OF THE IMMUNE SYSTEM IN BONE HOMEOSTASIS AND HEALING

Two distinct bone forming processes are responsible for fracture healing, namely intramembranous and endochondral ossification. Intramembranous ossification, which involves the direct differentiation of MSCs into osteoblastic cells, is mainly found in bone healing of fractures characterized by high mechanical stability due to the presence of, for example, rigid fixation [13, 22]. On the other hand, the healing of larger defects with mechanical instability due to macro and micromotion between the bone edges (*e.g.* fractures treated in a cast or with traction) occurs predominantly through endochondral ossification [22]. In this section the cascade of events occurring during endochondral ossification will be reviewed together with the approaches used to mimic this process for regenerative purposes. Furthermore, the cells and factors from the innate and adaptive immune systems relevant in EBR will be presented. This will provide the basis to understand the cellular and molecular interactions of immune cells and cells involved in bone regeneration.

Endochondral bone formation in fracture healing

After trauma, two areas are primarily involved in bone repair: at the periphery of the fracture site the periosteum elevation mediates direct bone deposition, whereas in the



central region of the defect, a cartilaginous soft callus is formed in order to stabilize it [22]. The structure of the fracture callus has often been compared to the one of the growth plate, present during long bone development. Both structures present an organized cartilaginous template composed of similar structural proteins (*e.g.* collagen types I, II and X) and signaling molecules (*e.g.* Indian hedgehog, bone morphogenetic proteins) [18, 22]. Also, the resident chondrocytes are arranged in a zonal fashion [25]. In a first zone, chondrocytes are embedded in an avascular matrix, rich in collagen type II and proteoglycans. In the adjacent areas, chondrocytes proliferate and organize themselves into columnar structures, where they acquire a hypertrophic phenotype [25, 56]. Few changes mark the chondrocyte transition towards hypertrophy. Firstly, they start synthesizing collagen type X, metalloproteinases (*e.g.* MMP-2, MMP-9 and MMP-13) and pro-angiogenic factors, including transferrin and vascular endothelial growth factor (VEGF) [25, 56]. Furthermore, chondrocytes undergo morphological changes, considerably increasing their size [25, 298]. Finally, this stage is characterized by a downregulation of genes involved in chondrogenesis followed by an upregulation of those involved in osteogenesis, including runt-related transcription factor 2, alkaline phosphatase and osteonectin, which will eventually lead to the mineralization of the cartilaginous matrix [24, 25]. The remodeling of the cartilaginous matrix, promoted by the presence of the degrading enzymes, metalloproteinases, in combination with the secretion of pro-angiogenic factors, facilitate blood vessel invasion and the infiltration of osteoprogenitor cells and osteoclasts [23, 56]. As a consequence, the mineralized cartilage matrix is replaced by woven bone to form a more stable hard callus [10]. Finally, the woven bone is remodeled by the concerted actions of osteoblasts and osteoclasts, and the original cortical and/or trabecular bone architecture is restored [10, 18].

EBR strategies

The feasibility of recapitulating the above described natural healing process for regenerative purposes has been widely explored in the last decades [56, 62, 68-71, 76, 80, 81]. Several studies demonstrated that *in vitro* engineered cartilage templates obtained from MSCs alone [69, 74, 81], or in combination with different biomaterials [68, 70, 80, 82], could be successfully converted into new bone tissue upon implantation, both ectopically [71, 74] and orthotopically [68-70, 82]. However, so far no consensus has been reached regarding the optimal length of the period for chondrogenic differentiation prior to implantation [56, 83]. It could span from as little as 1 week [81] to 7 weeks [74]. Also, no agreement exists regarding the optimal differentiation status (chondrogenic or hypertrophic chondrogenic) before implantation [56, 83]. These issues were explored in a recent publication by Yang *et al.* [84], where the effect of different chondrogenic priming periods preceding

implantation on endochondral bone formation was explored. In particular, when rat MSCs were chondrogenically differentiated for 2,3 or 4 weeks, differences in glycosaminoglycans (GAGs) content and extracellular matrix distribution were found prior to the *in vivo* implantation. Nevertheless, this did not lead to differences in bone volume after 8 weeks of subcutaneous implantation [84]. This was explained by the fact that the markers, which are typical of the hypertrophic stage (VEGF and collagen type X), were already present in the constructs after 2 weeks. This indicates that, as soon as expression of factors related to the hypertrophic stage is reached, further differentiation *in vitro* may not be required to maximize the extent of new bone formation.

After implantation, one of the most interesting aspects to consider is the contribution of the donor (implanted) cells to the new bone formation. After 4 to 16 weeks, the newly formed bone tissue presents an appearance similar to native bone, with a cortical outline and an inner bone marrow-like structure [70, 71, 76]. Scotti *et al.* [71] determined the contribution of xenogeneic, chondrogenically differentiated MSCs to endochondral bone formation in a subcutaneous, immunodeficient mouse model by staining the explants for specific human *Alu* repeats. Interestingly, after 12 weeks, donor-derived cells were present in the more inner, trabecular-like bone structures. On the contrary, the outer, cortical-like bone was completely remodeled and populated by donor-derived cells [71]. Comparable results were obtained by Farrell *et al.* [76] and by Bahney *et al.* [299] after the subcutaneous implantation of rat and human chondrogenically differentiated MSCs in a co-isogenic rat and immunodeficient mouse model, respectively. In particular, the presence of donor-derived osteocytes was confirmed after 6 [299] and 8 weeks [76] of implantation, demonstrating the active contribution of the tissue engineered cartilaginous template to the endochondral ossification process. On a final note, implanted MSCs could be involved in recruiting host cells at the remodeling site, promoting neovascularization and new bone formation [56]. Long-term persistence of implanted cells in the bone tissue has not been investigated to date. It is to be expected that depending on the size of the implanted construct, the natural process of bone remodeling will eventually replace the implanted cells with host cells.

Key players of the immune system in bone healing

When bone is fractured, it usually results in damage of the surrounding tissues and vasculature, thereby inducing a state of inflammation and the formation of a hematoma [9]. The hematoma environment is characterized by a low pH [9], hypoxia [12], high concentrations of both pro- and anti-inflammatory cytokines [9, 11, 13, 14] and both innate and adaptive immune cells invading from the peripheral blood and the surrounding tissues



[9, 11]. The first cells to act in the fracture zone are neutrophils [300] that prevent the spread of pathogens and attract macrophages to the injured site [11]. Following neutrophil infiltration, tissue resident macrophages, together with the infiltrating macrophages, release pro-inflammatory cytokines, and promote mesenchymal stem cell migration to the hematoma [10, 13, 300]. Here, endogenous mesenchymal stem cells are directly involved in the fracture healing process. In particular, they can differentiate towards both, the chondrogenic lineage to participate in the synthesis of the cartilaginous matrix of the soft callus; and the osteogenic lineage to promote intramembranous ossification at the fracture edges [56]. In response to the inflammatory environment, the infiltrating macrophages acquire a pro-inflammatory phenotype (M1), secreting pro-inflammatory cytokines, including interleukin-6 (IL-6), tumour necrosis factor- α (TNF- α) and interferon- γ (IFN- γ) [16]. This eventually leads to amplification of the pro-inflammatory response and to the activation of the adaptive immune response, in particular of T lymphocytes [16]. Their role in fracture healing can be both detrimental as well as beneficial, depending on the T cell subsets recruited [301, 302]. For example, terminally differentiated CD8+ T cells were found to secrete pro-inflammatory signals such as TNF- α and IFN- γ in the fracture hematoma. These signals are known to negatively affect MSC osteogenic differentiation *in vitro* [301]. Accordingly, depleting CD8+ T cells from an osteotomy gap improved bone regeneration [301]. Furthermore, Toben *et al.* [303] reported faster bone regeneration, lower levels of TNF- α and higher levels of anti-inflammatory cytokines like IL-10, in RAG-1^{-/-} mice model, which lacks an adaptive immune system [303]. However, when depleting all activated T cells by injecting an anti-CD25 antibody during the inflammatory phase, no improved fracture healing was reported [304]. This was attributed to the fact that anti-CD25 antibody also depletes regulatory T cells (Tregs), which can promote bone formation through the downregulation of TNF- α and IFN- γ and the secretion of IL-4, a chemoattractant for osteoblast [11, 304].

Even if the initial inflammatory response is a crucial step and initiates the cascade, the resolution of the hematoma and its conversion to granulation tissue is essential for the healing of the fracture. In the subsequent proliferative phase, macrophages, which are known to be an extremely plastic population, acquire mostly an anti-inflammatory and angiogenic phenotype (M2) in response to a change in the surrounding cellular and cytokine milieu [16]. In particular, M2 macrophages start to secrete VEGF to enhance vascularization in the fracture area [305] and immunomodulatory cytokines including IL-10 and transforming growth factor β (TGF- β) [16]. TGF- β plays a vital role in chondrogenic differentiation of mesenchymal stem cells for the formation of the soft, cartilaginous callus [16]. Thereafter, the acquisition of the hypertrophic phenotype is essential for the

subsequent mineralization of the callus and its conversion into bone by the joint actions of osteoblasts and osteoclasts [13]. The newly deposited bone, known as hard callus, is typically irregular. Its remodeling into cortical and/or trabecular bone represents the last stage of the fracture repair [10].

Crosstalk between immune cells and bone remodeling

Besides their role in removing dead tissue remnants and in reducing the spread of infection, cells from the adaptive and innate immune systems also affect bone homeostasis [287, 306]. The most obvious immune cells that affect bone homeostasis are the osteoclasts that, like dendritic cells (DC) and macrophages, derive from a myeloid precursor [287]. Osteoclasts are responsible for the catabolic phase of bone remodeling, which means that they play an active role in bone resorption. Their activity is tightly coupled with the anabolic phase of bone remodeling, where osteoblasts are responsible for new bone deposition [287]. Key molecules responsible for the connection between osteoclasts and osteoblasts are the receptor activator of nuclear factor κ B (RANK), receptor activator of nuclear factor κ B ligand (RANKL) and osteoprotegerin (OPG). Their interaction is known as the RANK/RANKL/OPG axis [287, 307, 308]. Specifically, RANKL is a transmembrane protein synthesized by the osteoblasts that is involved in osteoclast maturation and activation. Its action is mediated by the binding to its receptor RANK, present on the pre-osteoclast surface [309]. The balance between bone resorption and deposition is tightly regulated by the presence of OPG, a decoy receptor also secreted by the osteoblasts [308]. The production of RANKL by several immune cells including monocytes, neutrophils, DC and B and T lymphocytes, highlights their role in the regulation of osteoclast and osteoblast activity [308]. Besides RANKL production by multiple immune cells, several more examples can show the tight connection between immune cells and bone homeostasis. For instance, activated T cells can both positively and negatively influence bone homeostasis by secreting osteoclastogenic cytokines, depending on the T cell subpopulation involved [307]. T helper 17 (Th17) cells, for example, represent the T lymphocyte subpopulation renowned for the involvement in bone resorption. They secrete IL-17 that, besides being a potent stimulator of RANKL expression, induces the synthesis of matrix-degrading enzymes [308, 310]. On the other hand, T helper 1 (Th1) and 2 (Th2) primarily inhibit osteoclasts maturation through the secretion of IFN- γ and IL-4, respectively [311]. Similarly, regulatory T cells (Tregs) are known to express anti-inflammatory cytokines like IL-4, IL-10 and TGF- β , which suppress osteoclastogenesis [308]. Besides T lymphocytes, other immune cells are known to be able to influence bone homeostasis. B cells and bone marrow plasma cells, are known to be involved in modulating the balance between bone resorption and deposition, as they represent a major source of OPG [307, 312]. In addition to adaptive immune cells, innate immune



cells, including macrophages and neutrophils, can influence bone formation secreting pro or anti-inflammatory cytokines [313]. In particular, pro-inflammatory cytokines like TNF- α , IL-6, and IL-1 β promote RANKL secretion, increase osteoclast differentiation and resorption capacity, while inhibiting osteoblast differentiation and activity [287]. On the other hand, anti-inflammatory cytokines including IL-4 and IL-10 increase bone formation by inducing osteoblast proliferation and inhibiting osteoclastogenesis [308]. Thus, it is clear that immune cells play a role in bone remodeling and the outcome depend on the balance between factors that promote or inhibit osteoclasts maturation and catabolic activity and factors that attract and promote osteoblasts differentiation and bone formation.

TISSUE ENGINEERING: BALANCING THE IMMUNE RESPONSE AND BONE FORMATION

Tissue engineered bone substitutes can have various compositions. In general, they can contain biomaterials and/or cells and proteins. The cell source can be either autologous or non-autologous, which includes xenogeneic or allogeneic sources. Frequently, cells used for bone regeneration in preclinical studies are chondrogenically or osteogenically differentiated or undifferentiated MSCs, whether or not incorporated in a scaffold material as a carrier. Such scaffolds are most commonly made of nature-derived materials, such as collagen and fibrin or synthetic polymers, such as poly(e-caprolactone) [314]. Following implantation, the presence of a biomaterial and/or non-autologous cells often can intensify the inflammatory response and eventually affect the outcome of the fracture healing process [315]. Here, the effects of implantation of biomaterials and allogeneic cells on the immune response and bone formation will be discussed (Figure 1).

Immune response to biomaterials

Due to the surgical procedure required for the implantation of the biomaterial, the integrity of the tissue inevitably becomes compromised. In particular, the cell death by necrosis can lead to the release of danger signals known as alarmins (*e.g.* heat shock proteins, high-mobility-group box proteins and ATP), which can recruit to the implantation site DCs and macrophages [316]. As a consequence, even if the biomaterial is defined as biocompatible, the implantation itself can trigger an immune response that affects the fracture healing process [316]. After the implantation, the first step in the cascade of inflammatory events is the activation of the coagulation cascade and the complement system [316]. The activation of factor XII, the initiator of the intrinsic coagulation cascade, is promoted by its direct contact with the surface of biomaterials [317] and by platelet adhesion to the surface and activation [318].

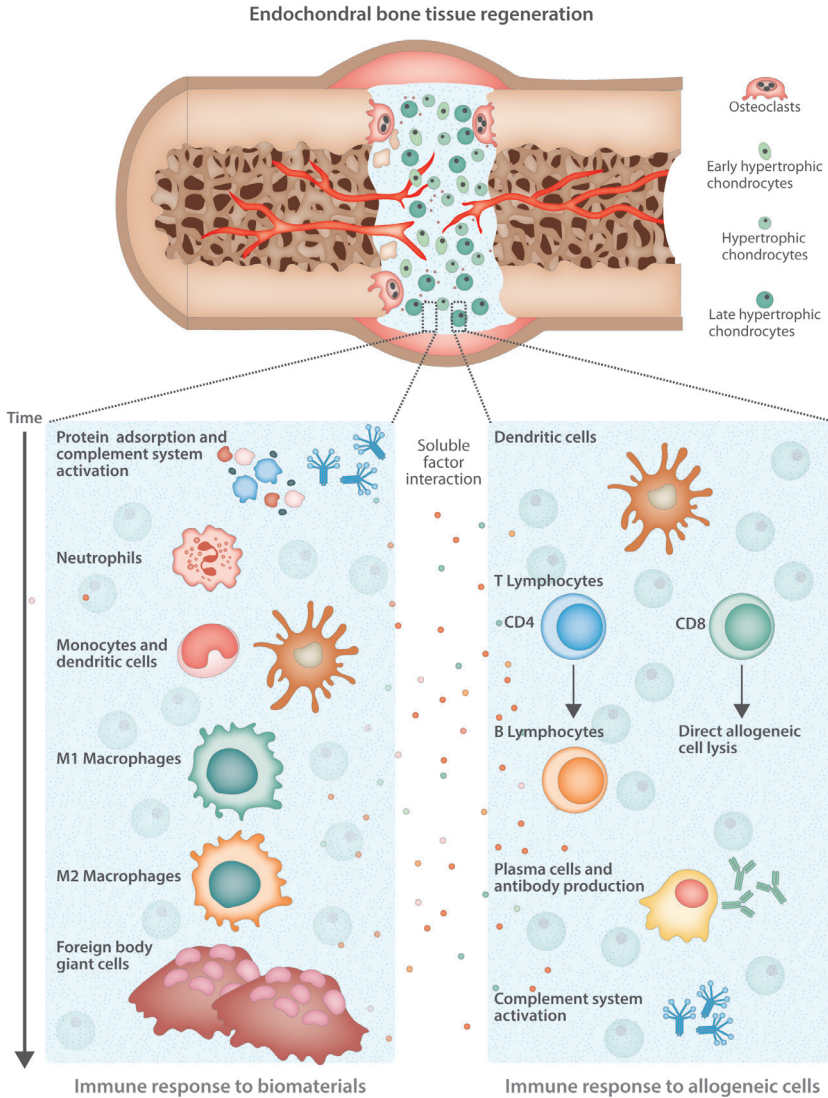


Figure 1. Schematic overview of the cell types involved in the endochondral ossification process induced by an allogeneic tissue engineered construct and the immune response elicited. After implantation, the phenotype of MSC derived chondrocytes progresses until the late hypertrophic stage, a stage that is characterized by increased secretion of pro-angiogenic factors and MMPs to promote matrix remodeling and new bone formation. However, the implantation of a biomaterial, together with the presence of allogeneic cells, at the same time induces the recruitment of host immune cells. In particular, the immune response against the carrier biomaterial (left panel) is mainly characterized by the presence of cells from the innate branch of the immune system while the presence of allogeneic cells triggers mostly an adaptive response (right panel). Nonetheless, the recruited cells can influence each other through the engagement of common players (e.g. dendritic cells and the complement system) and through the secretion of soluble factors such as cytokines that can promote the induction of a pro-inflammatory or anti-inflammatory environment. The final outcome of the bone regeneration process is determined by the balance between the promotion of endochondral ossification and the exacerbation of the immune response by the allogeneic construct.



Downstream, thrombin activation catalyzes fibrinogen cleavage, to form the primary fibrous mesh around the biomaterial [316]. The complement system is also activated, mostly via the classical and the alternative pathway [319]. Together with fibrinogen [320], fibrin and the anaphylatoxins of the complement cascade, other proteins adsorb to the biomaterial surface. Among those, fibronectin and vitronectin have a pivotal role in the regulation of the inflammatory response to the implanted biomaterial [316]. The proteins adsorbed to the surface form a provisional matrix, which influences the subsequent immune cell adhesion and activation [321, 322]. Furthermore, the newly formed matrix is a rich source of chemokines, cytokines and growth factors involved in attracting immune cells [323]. Thus, immune cells migration to the implantation site, adhesion and activation on biomaterials mainly occurs through the interaction of adhesion receptors, like integrins with the adsorbed proteins.

Similarly to the fracture healing process, the first cells recruited to the implant site are neutrophils [323, 324]. The interaction with the adsorbed matrix proteins promotes their phagocytic activity, the release of granules loaded with proteases and the production of reactive oxygen intermediates (ROIs) [325]. Together, these destructive agents may damage the implant [326] and promote the recruitment of monocytes and macrophages [323]. The infiltration of macrophages and lymphocyte to the implantation site mark the transition from acute to chronic inflammation [327]. M1 is the macrophage phenotype that is predominantly present during the first stages of inflammation, as these macrophages are directly involved in pathogen killing, secretion of pro-inflammatory cytokines, and Th1 cell recruitment. The uptake of wound debris and apoptotic neutrophils by macrophages can stimulate the production of immunomodulatory molecules, including TGF- β , IL-10 and prostaglandin E2. Together with IL-4 and IL-13 that are secreted by granulocytes, mast cells and Th2 cells, these immunomodulatory molecules trigger M2 polarization of the macrophages. Depending on the specific M2 macrophage subtype that is being generated, they could be involved in immunomodulation or in tissue repair [328]. In general, M2 macrophages support wound healing by secreting growth factors like TGF- β , basic fibroblast growth factor (bFGF), platelet-derived growth factor (PDGF) and VEGF, which are involved fibroblast recruitment, proliferation, extracellular matrix (ECM) synthesis and blood vessel invasion [316, 323]. However, if macrophages fail to phagocytose the biomaterial due to the high material-to-cell size ratio, they fuse together to form foreign body giant cells (FBGCs). If also FBGCs fail in phagocytosing the foreign material, they become frustrated multinucleated macrophages. This means that they increase their degradative capacity, organizing podosomal structures to seal the interface with the biomaterial surface and start to secrete ROIs and degradative enzymes [316, 329]. Interestingly, FBGCs are also thought

to be responsible for the secretion of anti-inflammatory cytokines and pro-fibrotic growth factors (*e.g.* TGF- β and PDGF) [316]. However, continuous action of FBGCs is associated with prolonged fibroblast activation and impaired matrix deposition. In particular, within two to four weeks, the foreign material is encapsulated within an almost avascular, fibrotic tissue capsule, which might lead to the loss of implant function [330].

The crosstalk between the innate immune response and T lymphocytes is mainly mediated by antigen presenting cells (APCs), in particular by DCs [331]. According to the type of pathogen recognition receptors (PRRs) involved in the interaction with the biomaterial, different DC maturation stages are stimulated. Immature and semi-matured DCs, for example, stimulate tolerance and limit the inflammatory response whereas fully mature DCs promote the development of an immune response [316]. The presence of T lymphocytes during the inflammatory phase of the foreign body response directed against an implanted biomaterial has been confirmed in several *in vivo* studies. The specific T cell subpopulations present in this phase can steer macrophage polarization and fusion [328]. On the contrary, little is known about lymphocytes B role during immune response against synthetic materials. However, their role becomes crucial when nature-derived biomaterials, such as decellularised tissues, are implanted. In particular, when a biomaterial is derived from non-human primates (*e.g.* pigs), two different types of antibodies can be produced. The most abundant ones are antibodies against a carbohydrate antigen called “ α -gal epitope”, which is present on glycolipids, glycoproteins and proteoglycans of the ECM. The second type of antibodies, defined as anti-non gal antibodies, is instead produced against different immunogenic peptides of the ECM [332].

Immune response to allogeneic cells

Compared to the immune response to biomaterials, the one directed against allogeneic cells is characterized by a more pronounced adaptive component [315]. The major histocompatibility complex (MHC) molecules, cell-surface glycoproteins known in humans as the human leukocyte antigen (HLA) molecules, represent the principal target of the allogeneic immune response against grafted cells [333]. Two different classes of MHC, MHC class I and class II, are responsible for the antigen presentation to the T lymphocytes. To present the allogeneic cell antigens to the immune cells, both MHC molecules bind small peptide fragments and display them on the cell surface. Together, the complex of a loaded peptide and a MHC molecule can be recognized by the T cell receptor (TCR). The capability of the TCR to recognize a unique combination of features of both, the loaded peptide and the MHC presenting molecules is known as MHC restriction [334]. MHC class I and II are characterized by a different structure and distribution among the cells. This affects the



type of effector T cells they can interact with. In general, MHC class I, which is present in all nucleated cells, is loaded with intracellular peptides and it is recognized by CD8⁺ cells. MHC class II is instead loaded with extracellular peptides. It is present on APCs, including macrophages, DC and B lymphocytes and it is recognized by CD4⁺ T lymphocytes [335]. However, APCs can also present on their MHC class I extracellular antigens acquired via phagocytosis and endocytosis, in order to activate CD8⁺ lymphocytes, by a mechanism called cross-presentation or cross-priming [336]. Considering the complexity and the high polymorphism of the MHC loci, the region of MHC interaction with the TCR and the peptide binding site can differ from one individual to another. As a consequence, when donor cells are implanted, they can be directly recognized by the host immune system because of the differences in peptides presented on the donor MHC and the distinct features of donor MHC molecules [334]. It has been estimated that a high proportion of 1% to 10% of all mature host T cells will respond to stimulation by cells from another, unrelated member of the same species [337]. Besides the direct recognition of the foreign cells by T lymphocytes, MHCs from donor cells can be taken up by the host APCs, processed to obtain allopeptides and can be indirectly presented on the APC surface to recipient T cells [333, 338, 339]. Further, donor MHC class I and II molecules can be transferred to the host's APCs via direct cell-to-cell contact or via the release and uptake of exosomes [340]. As a consequence, it is possible to find host APCs presenting both, allogeneic antigens retrieved by phagocytosis on their MHC class II and also donor MHC class I surface expression derived from the concurrent vesicle trafficking [338]. These different pathways of allo-recognition are non-mutually exclusive and they all trigger host adaptive immune reactions [339]. Together this means that, in case of cell transplantation between non-identical or MHC-mismatched individuals, the likelihood of MHC associated rejection is high [333, 341]. However, many factors, including the type of implanted cells, the site of the body where they are introduced and the immunological status of the recipient, can influence the nature and magnitude of the T cell response induced. Furthermore, the ratio of CD4⁺ and CD8⁺ T lymphocytes that are activated during the response against the allogeneic antigens can change according to the players involved in the recognition process (*e.g.* direct recognition of the allogeneic MHC-peptide complex from T cells or indirect activation via indirect presentation by the APC of the host) [342]. Activated CD8⁺ T cells secrete pro-inflammatory cytokines, including IFN- γ , that promote the skewing of CD4⁺ T cells toward the pro-inflammatory Th1 cells. Furthermore, both CD8⁺ and Th1 lymphocytes are responsible for the direct lysis of donor cells [333]. On the other hand, Th2 lymphocytes secrete interleukins IL-4, IL-5, IL-9, IL 10 and IL-13, involved in the recruitment and activation of eosinophils [333]. After activation, eosinophils are known to release granules containing enzymes responsible for tissue damage and graft rejection [333]. In

addition to the above mentioned consequences of Th1 and Th2 polarization, CD4+ cells can also establish interactions with B lymphocytes, which can produce anti-MHC class I and II antibodies [333]. The antibodies produced against the allogeneic antigens will coat the grafted cells, promoting their killing in several ways, including their direct lysis due to the activation of the complement cascade and the natural killer (NK) cells. Besides producing alloantibodies, B cells are also involved in the activation and modulation of T cells, since they are directly involved in antigen presentation. Further, they are involved in modulating the immune response, secreting cytokines like IL-10 and TGB- β [343].

As previously mentioned, cells from the adaptive immunity are the principal mediator of the allogeneic response. However, recent studies have attributed more importance to the innate branch of the immune system. In particular, since macrophages and neutrophils are the first cells recruited to the site of cell implantation, they can influence lymphocyte activation and polarization through cytokine secretion, promoting eventual rejection or tolerance of the implanted cells [344]. Furthermore, NK cells are directly involved in allogeneic MHC recognition and in transplanted cells depletion [344].

IMMUNE REACTION AGAINST ALLOGENEIC, CHONDROGENICALLY DIFFERENTIATED MSCS

When implanting cell-seeded constructs for EBR, it is essential that the cells survive in the defect site long enough to initiate the conversion of cartilage into bone. The hematoma microenvironment, as well as the persistent actions of immune cells might act to destroy the grafted MSC-derived chondrocytes prior to the beginning of bone formation.

Culture-expanded MSCs have been shown to exhibit immunomodulatory properties [99-101]. They express intermediate to low levels of MHC class I molecules, low levels of co-stimulatory CD40, CD80 and CD86 and very low to no expression of MHC class II, which enables them to evade the immune surveillance by the CD4+ T cells [100, 102]. MSCs have also been shown to inhibit T cell proliferation through indoleamine 2,3- dioxygenase (IDO) and cyclooxygenase-2 (COX-2) mediated depletion of tryptophan and production of prostaglandin E2 (PGE2), respectively [345, 346].

In addition, MSCs can shift the Th cell phenotype from pro-inflammatory Th1 and Th17 cells to the regulatory Treg phenotype, either by directly influencing their polarization by secreting TGF- β or by inhibiting the proliferation of the inflammatory subsets [99, 346, 347]. Besides influencing T cells, MSCs can also play a role in modulating other immune cell types. For example, MSCs can also inhibit DC maturation, resulting in decreased expression



of MHC class II and co-stimulatory molecules on DCs surface [348, 349]. Furthermore, they can inhibit B lymphocytes and NK cells activation and expansion through the secretion of TGF- β . Finally, by producing IDO and PGE2, MSCs induce the macrophage skewing toward the anti-inflammatory M2 phenotype [350]. These mechanisms make undifferentiated MSCs an attractive source in non-autologous transplantation. In particular, recent clinical studies have confirmed the safety of implanting allogeneic MSCs and their beneficial effect in diseases, such as graft versus host disease and Crohn's disease [351-353].

However, regenerative constructs that aim to induce EBR are typically seeded with chondrogenically differentiated MSCs. Only a limited number of studies have studied the change in immunomodulatory properties upon chondrogenic differentiation of MSCs so far [93, 94, 97, 98, 102, 354-357]. In 2003, Le Blanc *et al.* [102] analyzed the changes in HLA I and II expression when MSCs were differentiated toward the chondrogenic lineage [102]. Similarly to undifferentiated MSCs, chondrogenically differentiated MSCs expressed intermediate levels of HLA class I and no HLA class II molecules. After stimulating chondrogenically differentiated MSCs with IFN- γ , a low expression of HLA class II was detected, like in undifferentiated MSCs. Further, they showed that chondrogenically differentiated MSCs do not stimulate allogeneic lymphocytes proliferation in co-culture experiments, suggesting the preservation of their capability to not elicit an immune response [102]. Interestingly, chondrogenically differentiated MSCs also maintain their ability to actively suppress lymphocytes allo-response, indicating that they possess immunosuppressive properties similar to those of undifferentiated MSCs [102]. Further data supporting the immunomodulatory effect of chondrogenically differentiated MSCs are reported in an *in vitro* study performed by Zheng *et al.* [355]. Similarly to Le Blanc *et al.* [102], they showed that both undifferentiated and chondrogenically differentiated MSCs can inhibit proliferation and activation of allogeneic T cells [355]. Additionally, both chondrogenically differentiated and undifferentiated MSCs were equally effective in inhibiting IFN- γ and TNF- α secretion when co-cultured with allogeneic CD4+ and CD8+ T cells, while upregulating the levels of IL-10 [355]. In line with these results, Du *et al.* [356] showed that even in a pro-inflammatory environment, MSC-derived chondrocytes displayed immunosuppressive effects on allogeneic T cell proliferation and natural killer cell-mediated cytotoxicity *in vitro* [356]. Despite the incomplete understanding of the mechanisms with which chondrogenically differentiated MSCs retain their immunoregulatory properties, it has been proposed that TGF- β 1 and HLA-G could play a role herein [355, 356]. It was also suggested that, similar to undifferentiated MSCs [358], the presence of allogeneic, chondrogenically MSCs-derived chondrocytes do not induce DC maturation *in vitro* [359]. In particular, no upregulation of maturation markers, such as CD80, CD86 and HLA-DR,

was observed on DCs during co-culture of chondrogenically differentiated MSCs and immature or LPS-matured DCs. Further, though the DCs infiltrated the chondrogenically differentiated MSC pellets, the presence of chondrogenically differentiated MSCs did not induced an increase in antigen uptake over time [359]. Taking the aforementioned into account, we could speculate that, even in an *in vivo* setting, the implantation of allogeneic, chondrogenically differentiated MSCs will not trigger an allogeneic T cell response. Furthermore, even if a T cell response would be triggered, an active suppression is expected. The formation of a tolerogenic environment would allow the remodeling of the cartilaginous construct into new bone tissue, following the endochondral pathway.

However, results that contrast the above observations have been reported in literature. A recent study by Kiernan *et al.* [94] demonstrated that chondrogenically differentiated MSCs were not able to actively alter the proliferation of allogeneic CD4+ and CD8+ T cells *in vitro*. Further, histological analysis revealed that after co-culturing peripheral blood mononuclear cells with chondrogenically differentiated MSCs *in vitro*, T cells (as identified using anti-CD3 antibodies) infiltrated the chondrogenic matrix. Although in this study these infiltrating lymphocytes did not appear active, as they showed low expression levels of genes coding for T activation proteins, including CD25 and CD69, and pro-inflammatory cytokines like TNF- α [94], Chen *et al.* [354] reported the ability of chondrogenically differentiated MSCs to stimulate lymphocyte proliferation, cytotoxicity and DC maturation *in vitro*. The authors suggested that the upregulation of the co-stimulatory molecules CD80 and CD86 on the chondrogenically differentiated MSCs could be involved in this response, since blocking their expression reduced DCs maturation and restored levels of T lymphocytes proliferation similar to the ones of the undifferentiated MSCs [354]. Even though this study [354] was performed in a xenogeneic setting, as rat MSCs were presented to human dendritic cells, the loss of immunosuppressive properties in MSC-derived chondrocytes was confirmed in an allogeneic setting, both *in vitro* and *in vivo* [98]. In particular, undifferentiated or chondrogenically differentiated MSCs were implanted subcutaneously alone or in combination with an alginate gel in a fully MHC-mismatched allogeneic rat model. Higher number of CD3+ lymphocytes and CD68+ macrophages infiltrated the alginate carrier when chondrogenically differentiated MSCs were encapsulated. Further, T cells reactive to allogeneic antigens were found in the draining lymph node of both, the rat group in which differentiated MSCs were implanted as well as in the one that received undifferentiated MSCs. After the encapsulation of the allogeneic cells into an alginate carrier, a protective effect was observed for the undifferentiated MSCs group, as no antidonor T-cell response was observed in the local lymph node. However, such positive influence was not observed in the chondrogenically differentiated group. Finally, it must be noted that, despite its



protective role against T cells, the encapsulation in alginate enhanced the production of donor-specific IgG₂ antibodies [98]. Similar results were obtained by Butnariu-Epharat *et al.* [360] in an orthotopic implantation model in goats. In more detail, when allogeneic, chondrogenically differentiated MSCs were embedded in a hyaluronic acid-based gel to resurface the articular knee cartilage, a mild immunologic rejection characterized by blood cell infiltrates was observed. These findings offer valuable insight in the differences in immune reaction to differentiated and undifferentiated MSCs, as well as the role of an encapsulating biomaterial *in vivo*.

The contrasting *in vitro* results and the scarceness of *in vivo* studies do not provide a clear portrait of the immunological processes associated with allogeneic chondrogenic MSC implantation [93, 97]. The contradictory results could be partially explained by the differences in the ratios of chondrogenically differentiated MSCs and T cells, as it has been shown that *in vitro*, the suppressive action of the MSC-derived chondrocytes on T cell activation is dose dependent [94, 355, 356]. More specifically, Ryan *et al.* [98] observed an immune response to differentiated MSCs using a low MSC/T ratio (1:50 and 1:100) compared to the studies carried out by Kiernan *et al.* [94] and Zheng *et al.* [355] (1:5 and 1:1, 1:5 and 1:10, respectively). Further, the composition of the induction medium, as well as the culture and assay conditions might play a role in increasing the immunogenicity of chondrogenically differentiated MSCs [356, 357, 361]. For example, TGF- β , a key component of chondrogenic induction medium, is also involved in regulation of the expression of HLA-DR [362] and CD80 and CD86 [354]. This should be taken into account, especially when the changes in expression of these molecules is analyzed. Finally, it must be noted that most of the studies are focusing only on T lymphocytes response, whereas little is known about allogeneic, chondrogenically differentiated MSCs influence on DCs, macrophages, NK cells and B cells. Thus, so far it is not possible to define whether MSCs-derived chondrocytes will evoke an immune response upon implantation. Further, the possible interference of a potential allogeneic response with the endochondral process remains yet to be elucidated.

IMPLICATIONS OF IMMUNE REACTIONS FOR EBR

In the previous sections, the physiological healing process and its alteration due to the immune response induced by the implantation of a biomaterial and allogeneic, chondrogenically differentiated MSCs were discussed. Only few studies have studied the changes of immunological properties of allogeneic MSCs-derived chondrocytes *in vitro* or *in vivo*. However, a great number of studies have evaluated the immunogenicity of allogeneic chondrocytes for cartilage tissue engineering. Thus, in this section we will try to integrate

this information and speculate on what could be expected after the implantation of an engineered cartilage template in terms of its endochondral bone regenerative capacity.

In EBR, chondrocytes within the cartilage template acquire a hypertrophic phenotype and start to secrete proangiogenic factors and metalloproteinases to promote blood vessel invasion and matrix remodeling. As a result, host cells involved in bone remodeling are recruited to the implantation site and promote cartilage remodeling and new bone formation [56]. This process could potentially be hampered by an abnormal chronic inflammation induced by both the carrier biomaterial and the MSC-derived chondrocytes.

As described in the previous section, an increased immunogenicity of allogeneic, chondrogenically differentiated MSCs was observed *in vivo* [98, 360]. Although similar results were sometimes obtained when implanting allogeneic chondrocytes [182, 363, 364], an overwhelming number of *in vitro* and *in vivo* studies suggest that cartilage tissue possesses immunoprivileged properties, and no, or only a minor immune response is elicited in an allogeneic setting [182, 365-369]. This is thought to be due to the presence of a tight extracellular matrix that shields chondrocyte-associated antigens and protects the embedded cells from the immune surveillance [182]. Thus, the discrepancy between these results could be at least partially explained by heterogeneity in MSCs chondrogenic differentiation [182, 360]. The reduced ECM shielding due to the retention of a small, undifferentiated MSCs subpopulation might have hampered the immunoprivileged characteristics of cartilage, enhancing host immune reaction. Even though the main goal of the studies involving allogeneic chondrocytes was to obtain stable articular cartilage and not EBR, these results tend to support the idea that only a minor immune reaction against an engineered, allogeneic cartilaginous construct is to be expected. Therefore, even though evidence is diverging, we postulate that EBR will not be hampered in its first steps because of a reaction against the cartilage template and could proceed toward the remodeling phase. After the conversion from cartilage to bone, understanding the fate of the chondrocyte is crucial to define the time span within which the host is exposed to the allogeneic antigens. It has long been accepted that the endochondral processes encompassed chondrocyte terminal differentiation [370] including apoptosis [371-373]. As a result, allogeneic cells in EBR would eventually disappear from the implantation site and the allogeneic cells and antigens would only be exposed to the immune system for a limited amount of time. However, outcomes of recent studies in lineage tracing support the hypothesis that only a subset of the hypertrophic chondrocytes undergo apoptosis, while most transdifferentiate to osteoblasts and osteocytes [299, 371, 374, 375]. The mechanisms at the base of this transformation to osteogenic cells are not fully understood yet [371]. Nevertheless, the implications for EBR are evident. At least part of the regenerated bone would be donor-derived,



which means that the allogeneic cells and antigens could be exposed to the host immune system cells for a longer period [299]. Several studies describe the immunogenicity of allogeneic, osteogenically differentiated MSCs [93, 96, 97]. Overall, it seems that allogeneic MSC-derived osteoblasts induce a milder allogeneic immune reaction compared to the chondrogenically differentiated MSCs both *in vitro* [102, 354, 376-378] and *in vivo* [292, 293]. In particular, osteogenically differentiated MSCs seem to retain immunoevasive and immunomodulatory properties similar to the undifferentiated MSCs, since they not only fail to stimulate alloreactive lymphocytes responses, but they also actively suppress T cells proliferation *in vitro* [102]. Further, MSC-derived osteoblasts showed an inhibitory effect on DCs maturation even in a xenogeneic setting [354]. However, the implications of the presence of these allogeneic, osteogenic cells in the bone regenerative process are unknown.

The intricacy of the interactions between host immune cells, implanted cells and the carrier material, complicates a reliable prediction of their effect on the EBR process. The low immunogenicity of the cartilage matrix, together with the suppressive effect on T lymphocytes of MSC-derived chondrocytes support the feasibility of using allogeneic, chondrogenically differentiated MSCs for endochondral bone tissue engineering applications. However, these immunoevasive and immunomodulatory properties might change during the cartilaginous template remodeling, as the blood vessels invasion required for EBR could disrupt the protective ECM shield, exposing the allogeneic MSC-derived chondrocytes. Thus, to investigate the complex balance between EBR and immune response the use of a relevant preclinical animal model is required (as discussed in [93]).

CONCLUSIVE REMARKS AND FUTURE PERSPECTIVE

The implantation of an allogeneic MSC-containing engineered construct for EBR purposes will alter the inflammatory phase of the fracture healing process due to the presence of a biomaterial and the chondrogenically differentiated, allogeneic cells. Depending on the balance between pro- and anti-inflammatory cytokines and immune cell subsets, the survival of the construct and the regeneration process may be hampered or improved.

To reduce the chances of developing a strong immune response, selecting the appropriate carrier material is of pivotal interest. Firstly, the biomaterial should support MSCs chondrogenic differentiation and offer shielding from the immune system. In addition, the use of immunomodulating biomaterials represents a promising strategy to tailor the immune cell recruitment, enhancing bone healing and promoting the integration of the cell-seeded constructs. In particular, changing the surface chemistry will influence protein

adsorption on the biomaterial surface, dictating the type of immune cell that will interact with it. Alternatively, the incorporation of bioactive molecules can induce the creation of a more tolerogenic environment, which will prevent the implant rejection [316]. Specifically, the local delivery of immunosuppressants through their incorporation into the carrier material could represent a promising strategy [379, 380] as the temporary release of the drugs could buy enough time for the allogeneic cartilage template to remodel into new bone tissue, avoiding the complications associated with systemic immune suppression.

Considering the use of an allogeneic cell source, a (partially) HLA matched donor might help in reducing the immune reaction against the differentiated chondrocytes or osteocytes. For instance, a higher transplant success rate after 10 years from the surgery has been reported for kidney transplantation when HLA are fully, or at least partially matched between donor and patient [381]. It has been shown that the impact in graft loss depends mostly on the effects of three antigens, HLA-A, HLA-B and HLA-DR. In particular, the impact of an HLA-DR mismatch can be observed in the first 6 months after transplantation, whereas the HLA-B mismatch effect emerges in the first 2 years, and HLA-A mismatches have an adverse effect on long-term in renal graft survival [341, 382]. This may suggest that, for EBR applications it might be enough to have an HLA-DR and/or HLA-B match, since part of the allogeneic cells will be lost during the cartilage conversion into bone and the newly formed bone tissue will be remodeled and slowly replaced entirely by the host tissue. This means that, by the time HLA-A mismatch effects manifest themselves, the donor cells will not be present in the host anymore.

Finally, a logical next step in EBR research entails the development of a clinically relevant immunocompetent animal model to validate the regenerative potential of differentiated allogeneic MSCs. Kovach *et al.* [306] reported a discrepancy between immunogenicity of allogeneic MSCs when transplanted into mouse models, compared to larger animal models. In particular, the majority of the studies performed in mice demonstrated immunogenic properties of allografted MSCs, while in larger animals such as rabbits, dogs and sheep this was not the case. In addition, Kovach *et al.* noticed that the majority of the studies demonstrating the immunoprivileged status of MSCs were performed in a bone orthotopic setting (*e.g.* bone healing) [306]. This suggested that some factors in the inflammatory environment after a bone injury promote allogeneic MSCs survival and differentiation. Thus, the location of implantation should be carefully chosen when the interaction with the immune system is analyzed.

In conclusion, when aiming at developing tissue engineered constructs for bone regeneration, it is crucial to consider if and in which ways the implanted biomaterials and/or cells could



trigger an immune response. Different immune cells involved in the response can promote either bone formation or bone resorption, affecting the regenerative outcome. As an instrumental example, we evaluated the potential immunological effects when implanting allogeneic, chondrogenically differentiated MSCs for bone regeneration. Further steps need to be taken to evaluate whether they represent a realistic option to improve the clinical translation of endochondral bone regeneration. Balancing the immune responses with regenerative processes will be a next challenge in this promising field.

ACKNOWLEDGEMENTS

The authors thank the AO Research Fund of the AO Foundation for the financial support (project no. S-16-130G). Furthermore, the authors thank Matilde Bongio (Matilde Bongio Visual Science) for her help with image preparation.





Endochondral bone regeneration by non- autologous mesenchymal stem cells

A. Longoni
I. Pennings
M. Cuenca Lopera
M.H.P. van Rijn
V. Peperzak
A.J.W.P. Rosenberg
R. Levato
D. Gawlitta

Frontiers in Bioengineering and Biotechnology,
2020, 8:615

6



ABSTRACT

Mimicking endochondral bone formation is a promising strategy for bone regeneration. To become a successful therapy, the cell source is a crucial translational aspect. Typically, autologous cells are used. The use of non-autologous mesenchymal stromal cells (MSCs) represents an interesting alternative. Nevertheless, non-autologous, differentiated MSCs may trigger an undesired immune response, hampering bone regeneration. The aim of this study was to unravel the influence of the immune response on endochondral bone regeneration, when using xenogeneic (human) or allogeneic (Dark Agouti) MSCs. To this end, chondrogenically differentiated MSCs embedded in a collagen carrier were implanted in critical size femoral defects of immunocompetent Brown Norway rats. Control groups were included with syngeneic/autologous (Brown Norway) MSCs or a cell-free carrier.

The amount of neo-bone formation was proportional to the degree of host-donor relatedness, as no full bridging of the defect was observed in the xenogeneic group whereas 2/8 and 7/7 bridges occurred in the allogeneic and the syngeneic group, respectively. One week post-implantation, the xenogeneic grafts were invaded by pro-inflammatory macrophages, T lymphocytes, which persisted after 12 weeks, and anti-human antibodies were developed. The immune response towards the allogeneic graft was comparable to the one evoked by the syngeneic implants, aside from an increased production of alloantibodies, which might be responsible for the more heterogeneous bone formation.

Our results demonstrate for the first time the feasibility of using non-autologous MSC-derived chondrocytes to elicit endochondral bone regeneration *in vivo*. Nevertheless, the pronounced immune response and the limited bone formation observed in the xenogeneic group undermine the clinical relevance of this group. On the contrary, although further research on how to achieve robust bone formation with allogeneic cells is needed, they may represent an alternative to autologous transplantation.

INTRODUCTION

Endochondral bone formation represents a key process in bone development and fracture healing [18, 22]. In particular, the growth plate and the fracture callus are characterized by a highly organized cartilaginous structure where chondrocytes progressively acquire a hypertrophic phenotype [18]. Once hypertrophic, chondrocytes switch their expression profile, upregulate genes involved in osteogenesis and start secreting pro-angiogenic factors and metalloproteinases [25]. This promotes blood vessel invasion, the infiltration of osteoprogenitor cells and osteoclasts, and the final remodeling of the cartilaginous template into new bone [25].

Over the last decade, tissue engineering has successfully mimicked this process to regenerate bone defects *in vivo* [56]. Various types of cells, including multipotent mesenchymal stromal cells (MSCs) [68-72], embryonic stem cells [63] and adipose-derived stem cells [65] were used alone or in combination with biomaterials to develop a cartilaginous template that, upon implantation, would trigger new bone formation. Despite these promising results, the clinical translation of endochondral bone regeneration (EBR) is in an early stage for several reasons. One of the major challenges is represented by the variability of chondrogenic potential between MSC donors [69, 89] and its unpredictability [87]. In other words, the successful treatment of all patients with autologous MSCs is not feasible, as the differentiation potential of the isolated MSCs would vary from highly potent to completely incapable, in a patient-dependent manner. Furthermore, the personalized use of cells is associated with high costs when performed under Good Manufacturing Practice (GMP) [383, 384]. Here, we propose the use of non-autologous MSCs (*i.e.* allogeneic or xenogeneic) as a potential strategy to increase the clinical translatability of EBR, ideally in a single-step surgical procedure. Non-autologous cells could be screened and pre-selected for their high chondrogenic potential in advance, circumventing the issue of the donor-to-donor variability, and leading to an off-the-shelf product. In addition, if MSCs with high chondrogenic potential could be pooled and used to treat multiple patients, the high costs associated with isolating and differentiating these cells under GMP restrictions would decrease. Finally, the use of non-autologous MSCs will eliminate any discomfort for the patients related to taking a bone marrow biopsy.

It is evident that the use of allogeneic or xenogeneic cells represents a clinically and economically attractive option. However, the immunogenicity of non-autologous grafts poses a potential obstacle to the clinical implementation, as it could affect the integration and functionality of the grafted tissues [385]. Nevertheless, differently from other types of transplantation (*e.g.* heart, lungs or liver), in which the grafted organ represents the



final functional tissue; in EBR, the cartilage template produced *in vitro* solely serves as a transient substrate that is remodeled into new, mostly recipient-derived bone tissue [71, 76]. As a result, the host is only gradually and temporarily exposed to the non-autologous MSC-derived chondrocytes and matrix during the remodeling process. Thus, it can be hypothesized that, if the initial remodeling steps would not be hampered by the immune reaction to the engineered non-autologous cartilage, the graft could be replaced by new, partially autologous [71, 76] bone tissue. Only a limited number of *in vitro* studies have provided clues about the retention of the MSC immunomodulatory and immunoevasive properties after differentiation. It was shown that allogeneic MSC-derived chondrocytes retain their capability to actively suppress allogeneic T lymphocyte proliferation [102, 355], decrease the secretion of pro-inflammatory cytokines such as interferon gamma and tumor necrosis factor alpha [355] and inhibit the natural killer cell-mediated cytotoxicity [356]. Additionally, chondrogenically differentiated MSCs do not induce dendritic cell (DC) maturation nor increase in their antigen uptake or migration [386]. On the contrary, it has been reported that xenogeneic, MSC-derived chondrocytes trigger T lymphocyte proliferation, cytotoxicity and DC maturation, increasing antigen presentation and further activation of the adaptive immune response [354]. All together, these *in vitro* findings hint that the intensity of the host immune response to the non-autologous implants is different, depending on whether they are allogeneic or xenogeneic. Nevertheless, no study has explored how potential changes in immunological response could affect EBR *in vivo*. As a consequence, based on the available information, it is not possible to predict if in any of these two cases, the host immune response will prevent new bone formation *in vivo*. Therefore, the aim of this study was to evaluate the impact of the immune response evoked by non-autologous MSC-derived chondrocytes on the conversion from cartilage to bone during EBR. To do so, cartilaginous constructs derived from full major histocompatibility complex class I and II (in rats RT1 class I and II) mismatched (Dark Agouti rat) or xenogeneic (human) MSCs were implanted in a critical size femur defect of an immunocompetent rat (Brown Norway) to closely monitor both the elicited immune response and the new bone formation.

MATERIALS AND METHODS

Study design and overview

Four experimental groups were included in this study: two different types of a non-autologous cell source, namely allogeneic (Dark Agouti rat, full RT1 mismatch) and xenogeneic (human). These were pre-selected based on their high and similar

chondrogenic potential and compared to the syngeneic group (Brown Norway, autologous transplantation). Additionally, a control group consisting of the collagen carrier only was included. A critical size femoral defect introduced in Brown Norway immunocompetent rats was used as a model to observe the immune reaction and EBR induced by the different groups. Two end-points were analyzed, at one ($n=5$ per group) and twelve weeks ($n=8$ per group for the syngeneic, allogeneic and xenogeneic and $n=5$ for the collagen control group) post-implantation. Mineralization over time was monitored by micro-CT at 0, 4, 8 and 12 weeks after surgery. Systemic immune response was monitored by checking the blood for the presence of an inflammation marker (α -1-acid glycoprotein) and antibody production (IgG and IgM) at 0,1,2,4,8 and 12 weeks. After euthanasia at one or twelve weeks post-implantation, the local immune response was analyzed via immunohistological stainings. Markers belonging to the innate (macrophages: CD68, CD163, iNOS and CD206) and adaptive (T lymphocytes: CD3) immune response were investigated. Finally, bone formation and remodeling were investigated via histological analysis and histomorphometry (H&E, Safranin-O/Fast Green and TRAP staining) after twelve weeks.

Isolation and expansion of bone marrow-derived MSCs

Human MSCs were isolated from the bone marrow aspirate of a 20-year old female patient. The aspirate was obtained after informed consent, according to a protocol approved by the local Medical Ethics Committee (University Medical Center Utrecht). The mononuclear fraction was separated using Ficoll-paque (Sigma-Aldrich, Zwijndrecht, the Netherlands) and seeded on plastic to select for adherence, as previously described [89]. The adherent cells were cultured at 37°C under humidified conditions and 5% carbon dioxide (CO₂) in MSC expansion medium consisting of α -MEM (22561, Invitrogen), supplemented with 10% heat-inactivated fetal bovine serum (S14068S1810, Biowest), 0.2 mM L-ascorbic acid 2-phosphate (A8960, Sigma), 100U/mL penicillin with 100 mg/mL streptomycin (15140, Invitrogen) and 1 ng/mL basic fibroblast growth factor (233-FB; R&D Systems).

Rat MSCs were isolated from 4 weeks old female Dark Agouti and Brown Norway rats. Briefly, rats were euthanized through CO₂ asphyxiation and femur and tibia were collected. After removing the epiphysis, bone-marrow was obtained by flushing through the diaphysis with MSC expansion medium supplemented with 0.025% EDTA and cells were plated in a Petri dish. After 24 hours, the medium was switched to StemXVivo (CCM004, R&D Systems) and refreshed three times per week. MSCs were passaged at subconfluency until passage 4. MSC multilineage potential (Figure S1) was confirmed as reported previously [89].



Chondrogenic differentiation of MSC spheroids

At passage 4, human and rat MSCs were harvested for chondrogenic differentiation. Collagen spheroids were created by encapsulating MSCs (20×10^6 /mL) into 50 μ L collagen type I gel (4 mg/mL) (CB354249, Corning) according to the manufacturer's instruction. Gelation was allowed for 45 minutes at 37°C. The spheroids were cultured in chondrogenic differentiation medium consisting of high glucose DMEM (31966, Invitrogen) with 1% ITS + premix (354352; BD Biosciences), 10^{-7} M dexamethasone (D8893; Sigma), 0.2 mM L-ascorbic acid 2-phosphate (A8960, Sigma), 100 U/mL penicillin with 100 mg/mL streptomycin (15140, Invitrogen). Chondrogenic differentiation medium for human MSCs was supplemented with 10 ng/mL TGF β 1 (100-21, PeproTech), whereas for rat MSCs, also 100 ng/mL BMP-2 was added. Medium was refreshed every day for the first 4 days and thereafter three times per week. Chondrogenic differentiation was confirmed via histological analysis.

Construct preparation

Comparable spheroid sizes were obtained among the different groups after 28 days of differentiation. For each construct, eight chondrogenic spheroids were placed in a square cuboid custom-made mold (3.5 mm x 3.5 mm x 6 mm). Collagen (CB354249, Corning) gels (4 mg/mL) were casted into the mold around the eight spheroids and gelation was allowed for 45 minutes according to manufacturer's instruction. The constructs were prepared the day before implantation and incubated overnight in chondrogenic differentiation medium without TGF β 1 and BMP-2

Animal experiment and surgical procedure

The research protocol and procedures were approved by the animal ethical committee of the University Medical Center Utrecht (2465-2-01) and was in accordance with the national law on animal experiments. Forty-nine male Brown Norway rats (Envigo, the Netherlands) were housed in pairs in the animal facility of the University Medical Center Utrecht. Animals received standard food pellets and water *ad libitum*, under climate-controlled conditions (21°C; 12 h light/12 h darkness). At the age of 12 weeks, after at least 7 days of acclimatization, a 6 mm critical-size segmental bone defect was created under general anesthesia (1-3.5% isoflurane in oxygen, AST Farma, Oudewater, the Netherlands) as previously described [69]. Briefly, the right hind leg was shaved and disinfected. The right femur was exposed through a lateral skin incision and dissection of soft tissue. Three proximal and three distal screws were used to stabilize a 23 x 3 x 2 mm polyether ether ketone (PEEK) plate to the femur in the anterolateral plane. After the

bone's fixation to the PEEK plate, a 6 mm bone segment was removed using a saw guide and a wire saw (RISystem, Davos, Switzerland). The collagen constructs were press-fit in the defects and a single dose of antibiotic (Duplocillin LA, 22.000 IE/kg) was injected intramuscularly. Finally, the fascia and skin were sutured in layers using Vicryl Rapide 4-0 (VR 2297, Ethicon). Subcutaneous injection of pain medication (buprenorphine, 0.05 mg/kg bodyweight, AST Farma, Oudewater, the Netherlands) was given pre-operatively and twice a day for the following three days. Rats were euthanized after either 1 or 12 weeks with an overdose of barbiturates (phenobarbital; 200 mg/kg body weight, TEVA Pharma, Haarlem, the Netherlands). The femora were analyzed by histology and micro-computed tomography (microCT) scanning.

MicroCT scanning

To evaluate tissue mineralization at 0, 4, 8 and 12 weeks after surgery, the hind leg of the rat was fixed in a custom-made support under anesthesia (1-3.5% isoflurane in oxygen) and scanned with a microCT imaging system (Quantum FX; PerkinElmer, Waltham, MA, USA). Three minutes of scanning time was required per leg at an isotropic voxel size of 42 μm^3 resolution (voltage 90 kV, current 180 mA, field of view = 21 mm). All scans were oriented in the same fashion using the ImageJ plugin Reorient3 TP and the same volume of interest (VOI: 6.3 x 5 x 5 mm^3) was selected for all samples. VOIs were segmented with a global threshold and mineralized volumes were measured in mm^3 using the image processing software plugin BoneJ [273] (Image-J 2.0.0; Java, Redwood Shores, CA, USA). 3D reconstructions of the femur defect were based on the microCT data and created using ParaView (ParaView, Kitware Inc, USA).

Blood sampling and systemic immune response

Blood was sampled at 0, 1, 2, 4, 8 and 12 weeks from the tail vein using a catheter (BD angiocath, Becton Dickinson, Vianen, the Netherlands). Serum and plasma were collected in non-coated or EDTA coated MiniCollect tubes (450534 and 450532 Greiner Bio-one), respectively. Sample types were centrifuged for 15 min at 1500 g and the supernatant was stored at -80°C .

In the serum, the acute-phase protein α -1-acid glycoprotein (AGP), indicative for inflammation, was quantified using an ELISA kit (AGP-2, Life Diagnostic, Wes Chester, USA), according to the manufacturer's instructions. Total IgG content in the plasma was quantified using the IgG Rat Uncoated ELISA kit (88-50490-86, Invitrogen), according to the manufacturer's instructions.



Detection of anti-donor immunoglobulin in serum

To assess the production of alloreactive and xenoreactive IgM and IgG by the host, donor MSCs (either syngeneic, allogeneic or xenogeneic) were expanded until 80% of confluency and chondrogenically differentiated for 10 days [102, 354] in a 96 wells plate. The monolayers were fixed in 10% buffered formalin solution for 30 minutes and incubated in 5% BSA-PBS for 30 minutes at room temperature. Rat sera were heat-inactivated for 30 minutes at 56°C, diluted 1:100 in 5% BSA-PBS and incubated with the donor MSC monolayer correspondent to the type of graft they received *in vivo* for one hour at room temperature (adapted from Mathieux *et al.* [387]). After extensive washing with PBS, monolayers were incubated with a TRITC-conjugated antibody (8 µg/mL, goat-anti-rat IgM and IgG (H&L), 3010-03, SouthernBiotech) for one hour at room temperature. Finally, samples were washed and counterstained with DAPI for 10 minutes. Representative pictures of the anti-donor immunoglobulin produced 0, 2 and 4 weeks post implantation were taken for displaying purposes using a confocal microscope (Leica SP8X confocal). At 4 weeks, six pictures per sample (Olympus IX53) taken at random locations were used for the quantification. TRITC pixel quantification and nuclei count were performed using image-J after applying a global threshold. Data are presented as TRITC-positive pixels normalized to the number of nuclei per field of view. Controls for sample cross-reactivity are included in Figure S2.

T cell proliferation assay

To evaluate if the donor cells specifically triggered a T lymphocyte response, at 12 weeks the inguinal and popliteal lymph node were retrieved, crushed and T cells were stained with CellTrace Violet (C34571, Thermo Fisher) for 20 minutes at 37°C, according to the manufacturer's instruction. After washing, 2×10^5 stained T cells were resuspended in RPMI (11875093, Invitrogen) supplemented with 10% FBS 100 U/mL penicillin with 100 mg/mL streptomycin and added to the respective donor MSCs, which were beforehand expanded until 80% of confluency and chondrogenically differentiated for 10 days in a 96 wells plate. T cell-donor:MSC co-cultures were incubated for 4 days at 37°C under humidified conditions and 5% CO₂ (protocol adapted from Ryan *et al.* [98]). Afterward, cells were detached with trypsin and resuspended in FACS buffer consisting of PBS supplemented with 2% FBS. T cells were stained with CD3-PE conjugated antibody (0.4 µg/mL, 201411, BioLegend, San Diego, USA) for 30 minutes at 4°C and analyzed on an LSR-Fortessa flow cytometer (BD Bioscience, California, USA). Proliferation peaks were analyzed performing a deconvolution analysis with FlowJo and compared to lymphocytes that were not exposed to any other cell types (Nil) and T lymphocytes co-cultured with a third-party Sprague Dawley MSCs (Aspecific).

Histology and immunohistochemistry

At week 1 and 12, the right femora were retrieved for histological processing. All specimens were fixed in a 10% neutral buffered formalin solution for 1 week. After fixation, they were decalcified in a 10% EDTA-phosphate buffered saline solution (pH 7.4), dehydrated in graded ethanol solutions (70-100%) and cleared in xylene. The samples were subsequently embedded in paraffin and sliced into 5 μm thick sections (Microm HM340E). *In vitro* samples were fixed, dehydrated and sliced following a similar procedure. Before staining, samples were deparaffinized with xylene and gradually rehydrated through decreasing ethanol solutions (100-70%).

Overall appearance of sections and new bone formation was evaluated using H&E staining (Sigma). A triple staining of Weigert's haematoxylin (640490; Klinipath BV), fast green (FN1066522; Merck), and Safranin-O (FN1164048213; Merck) was applied to identify cell nuclei, collagenous fibers and GAGs. For the TRAP staining, hydrated sections were incubated for 20 minutes in 0.2 M acetate buffer at room temperature. To identify the osteoclasts, sections were incubated in 0.2 M acetate buffer supplemented with 0.5 mg/mL naphthol AS-MX phosphate (855, Sigma) and 1.1 mg/mL fast red TR salt (F8764, Sigma) for 4 hours at 37°C. Mayer's haematoxylin was used for nuclear counterstaining. Histomorphometric analysis was performed on samples stained with H&E. Briefly, an overview of the whole sample was made by merging images (1.25x/0.04 FN26.5 objective) into a panoramic image in Adobe Photoshop C6. For each image, a region of interest (ROI) of 5 x 2.5 mm² was selected in the center of the defect. The titanium screw holes present on each side of the defect were used as reference point in order to ensure an equivalent positioning of ROI in all samples. Three different areas were manually selected for each ROI: bone, hypertrophic cartilage and bone marrow. The amount of pixel for each area was quantified via the function "recording measurement" and normalized for the ROI area. Osteoclasts in the ROI were counted using the cell counter plugin from Image-J.

For collagen type II (II-II6B3), CD68 (ab31630, Abcam), CD206 (AF2535, R&D Systems), CD163 (ab182422, Abcam), CD3 (ab16669, Abcam) and iNOS (ab15323, Abcam) staining, endogenous peroxidase activity was blocked by incubating samples for 15 minutes with 0.5% H₂O₂, followed by aspecific protein blocking with 5% BSA-PBS for 45 minutes at room temperature. Details about the antigen retrieval, primary and secondary antibody used can be found in Table S1. The labels were visualized by DAB oxidation. Sections were then counterstained with haematoxylin, washed, dehydrated and mounted in depex. Rabbit and mouse isotypes (X0903 and X0931, Dako) were used as negative controls at concentrations matched with those of the primary antibodies. All sections were visualized using an Olympus BX51 microscope (Olympus DP73 camera, Olympus). Immune cells were



quantified in three different areas of the defect site: the collagen carrier, the infiltrating tissue and the spheroids (Figure S3). Three images per sample per area were taken and positive cells were counted using the cell counter plug-in from Image-J. The operator was blinded during the staining, acquisition and counting phases.

Statistics

The data are presented as means with standard deviations. For the analysis of the microCT results, AGP and IgG levels, a mixed linear model was used. The tests were adjusted for multiple comparisons by a Bonferroni's post hoc comparison test (IBM SPSS 22.0, New York, USA). For the analysis of the immune cells infiltrating the defects (IHC slides) after 1 week and the histomorphometric measures, a Kruskal-Wallis test was performed, followed by a Dunn's post-hoc test (GraphPad Prism 6, San Diego, CA, USA). For the analysis of the T cell proliferation a one-way ANOVA was performed, followed by a Dunnett's post-hoc test (GraphPad Prism 6). A p-value of less than 0.05 was considered statistically significant.

RESULTS

Macroscopic observations

At the time of surgery, the mean bodyweight of the rats was 258 ± 27 g and increased to 344 ± 28 g after 12 weeks. In total, three animals (1 xenogenic, 1 syngeneic and 1 collagen group) were euthanized before the experimental endpoint was reached due to failure of the PEEK plate and were therefore not included in the analyses. No external signs of adverse reactions (*i.e.* swelling or redness) to the implants were observed for any of the rats during the course of the experiment.

***In vitro* chondrogenic differentiation**

After 4 weeks, the collagen spheroids derived from human, Dark Agouti or Brown Norway MSCs displayed abundant glycosaminoglycan (GAG) and collagen type II deposition (Figure 1). Cells displayed the typical chondrocyte morphology, with a rounded shape and were embedded in lacunae.

New bone formation

After 12 weeks, new bone formation was observed close to the extremities of the osteotomy gap in all samples. 7/7 defects of the syngeneic control group and 2/8 of the allogeneic group were fully bridged whereas no full bridges were observed in the xenogenic or the

collagen groups (Figure 2 A and B). Furthermore, bone regeneration in the center of the defect was observed in all the samples in which MSCs were implanted, but not in the collagen control (Figure 2 A). In particular, mineralized volumes resembling the shape and size of the implanted spheroid structures were still evident, especially in the xenogeneic group (Figure 2 A). In these areas, human cells were found in the newly formed bone, suggesting the direct involvement of the cartilaginous templates in the regenerative process (Figure S4).

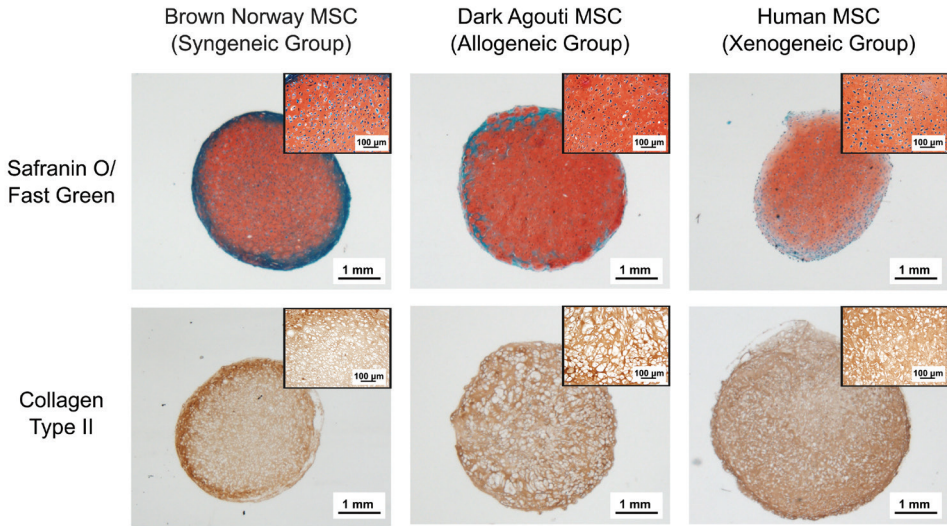


Figure 1. Chondrogenic differentiation of the different MSCs donors. Chondrogenic differentiation is confirmed by the presence of GAGs (red) and Collagen Type II (brown). Inserts contain higher magnification pictures of the collagen spheroids.

Based on microCT data, mineralization was highest in the syngeneic group ($92.6 \pm 13.7 \text{ mm}^3$), followed by $37.2 \pm 32.6 \text{ mm}^3$ for allogeneic, $16.4 \pm 5.9 \text{ mm}^3$ for xenogeneic, and $5.96 \pm 5.9 \text{ mm}^3$ for the collagen control (Figure 2 C). A similar trend was observed after histomorphometric analysis (Figure 2 D). Interestingly, hypertrophic cartilage was present also in the syngeneic group, indicating that remodeling is still ongoing at the proximal edge of the defect. On the contrary, in the allogeneic and xenogeneic group the hypertrophic cartilage was predominantly found in the non-remodeled parts of the spheroids. Consistent with the 3D reconstructions, the H&E staining highlighted the presence of bone islands at the edges of the spheroidal structures (Figure 3). Finally, in areas of active EBR, it was possible to discern osteoclasts, confirming that remodeling was ongoing after 12 weeks (Figure 2 D and 3 B).



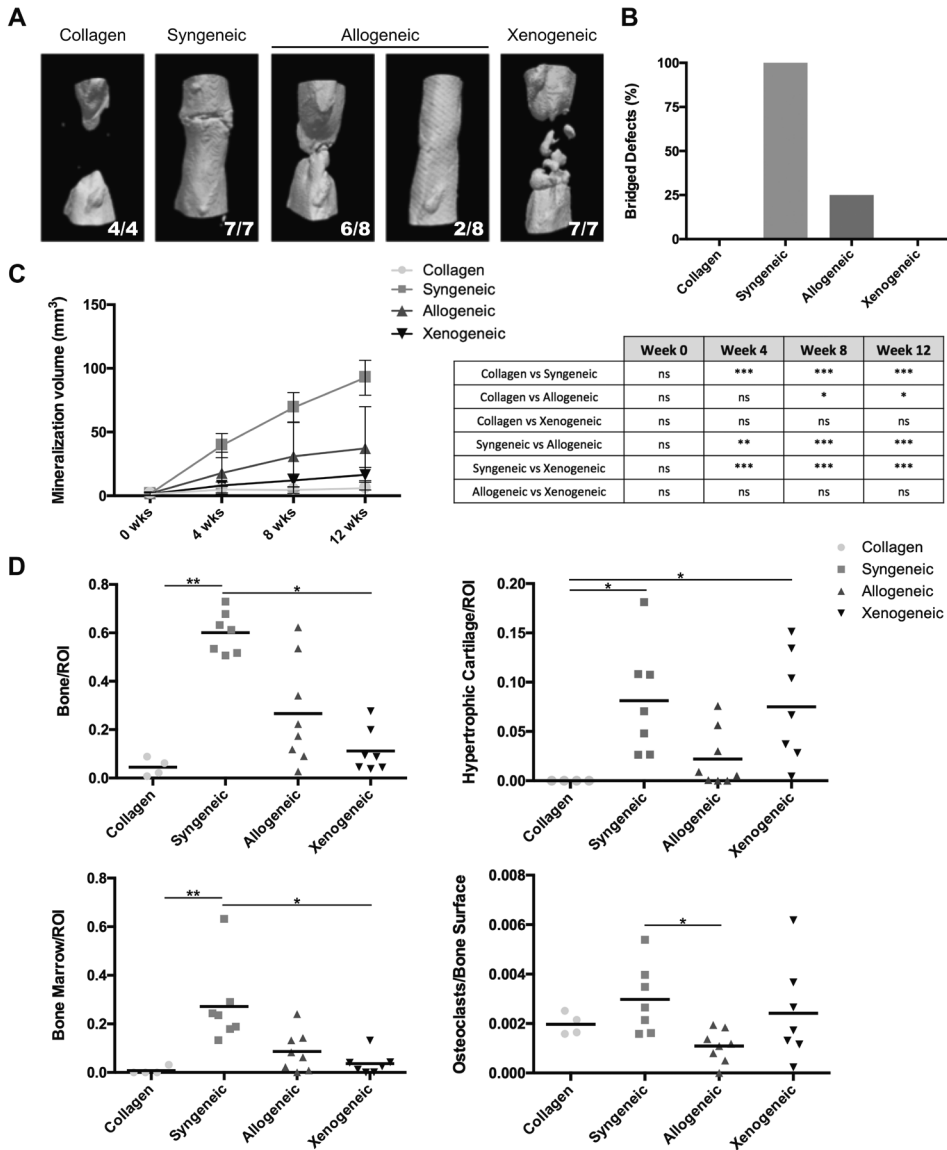


Figure 2. Evaluation of bone formation in the defect area. **(A)** The 3D microCT reconstructions of the defect areas after 12 weeks highlight the presence of mineralized areas with the shape of the implanted cartilaginous spheroids in the allogeneic and xenogeneic groups. **(B)** Heterogeneous results were observed in the allogeneic group, with 2/8 full bridging of the defect (25%) whereas 7/7 defects were bridged in the syngeneic group (100%). **(C)** Quantification of the mineralization over time confirmed that new bone formation was enhanced in the syngeneic group. **(D)** Results of the histomorphometric analysis performed 12 weeks post implantation presented a similar trend. * $p < 0.05$; ** $p < 0.01$.

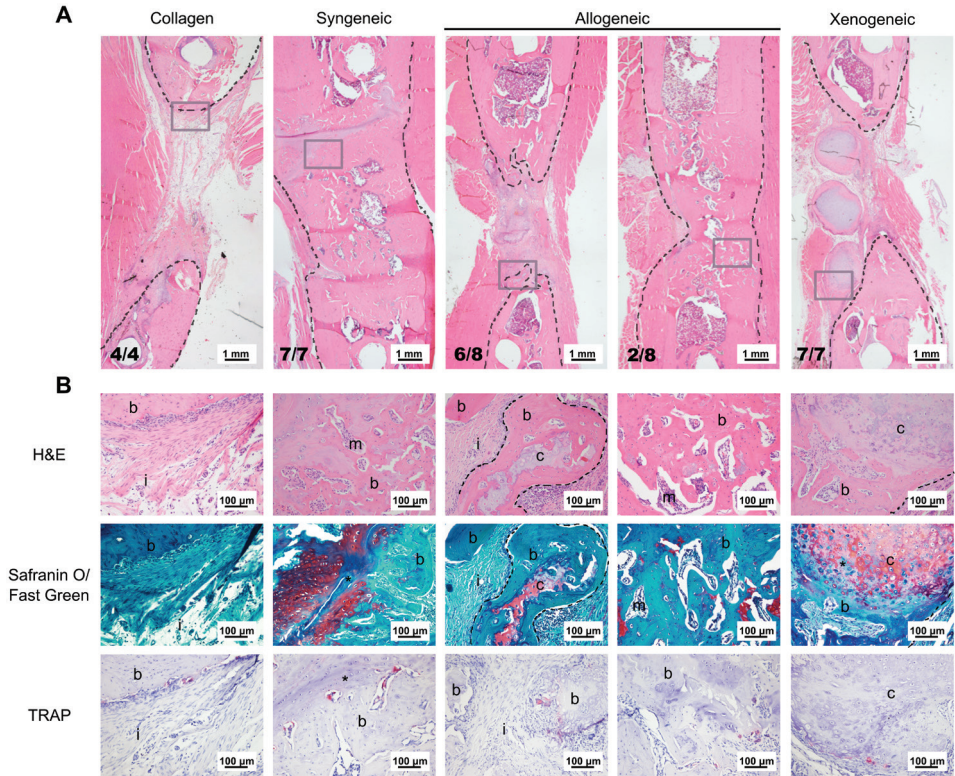


Figure 3. Representative images of the bone defect repair after 12 weeks. **(A)** Overview of the defect area stained with H&E. The black dotted lines indicate the bone edges whereas the grey boxes highlight the area depicted in the higher magnification in **(B)**. **(B)** H&E staining shows that the edges of the cartilaginous spheroids (limited by the dotted line) were converted into bone. Safranin O/fast green staining highlights active EBR in the syngeneic group and the presence of some non-remodeled cartilage (red) in the core of the spheroids of the allogeneic and xenogeneic groups. TRAP staining (bright pink) indicates the presence of active osteoclasts in all groups. i: tissue infiltration, b: bone, m: bone marrow, c: cartilaginous spheroids, * EBR.

Implant-induced early macrophage polarization and T-cell infiltration

One week after implantation, macrophages positive for CD68 were most abundant in the xenogeneic group, especially when considering the tissue infiltration in the implanted spheroids (Figure 4 and 5). Similarly, CD163+ macrophages were most abundant in the xenogeneic group in all the three analyzed areas (Figure 4 and 5). When analyzing the polarization of the macrophages, a significantly higher (p value 0.01) amount of pro-inflammatory iNOS+ cells was detected in the spheroids of the xenogeneic group whereas no differences in anti-inflammatory CD206+ macrophages were observed (Figure 5). Finally, CD3+ lymphocytes were higher for the xenogeneic group in all three analyzed areas; the collagen carrier, the infiltrating tissue and the spheroids (Figure 4 and 5). On the contrary,



no differences in T-cell infiltration or macrophage polarization were observed between the collagen, syngeneic and allogeneic groups.

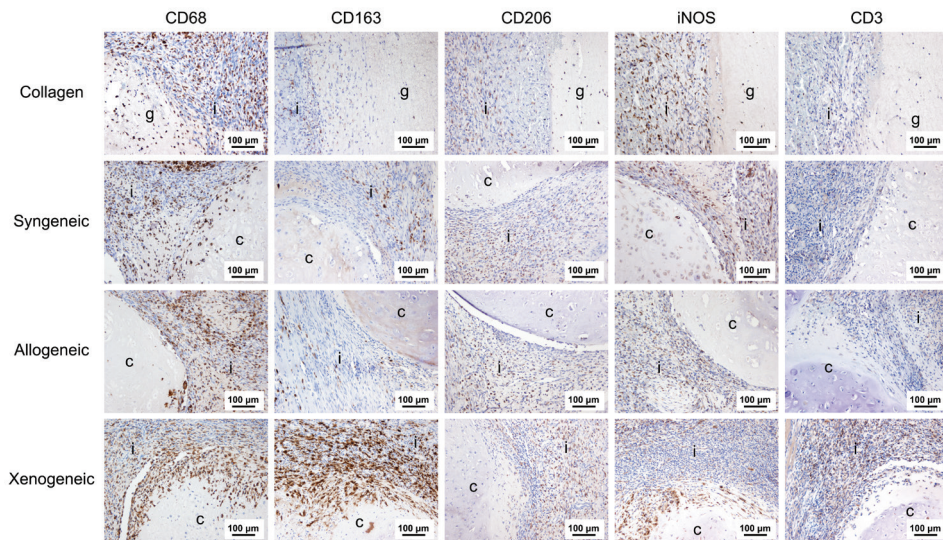


Figure 4. Local adaptive and innate immune response after 1 week from the implantation. CD68+ and CD163+ macrophages were particularly abundant in the xenogeneic group, especially in the spheroids infiltration. No differences were evident in CD206+ macrophages distribution whereas more iNOS + cells were infiltrating the cartilaginous spheroids. CD3+ lymphocytes were predominant in the osteotomy gap of the xenogeneic samples compared to the other groups. Brown color indicates the positive staining. i: tissue infiltration, c: cartilaginous spheroids, g: collagen gel.

Late T cell response

Only the chondrogenically differentiated donor MSCs from the xenogeneic group stimulated the proliferation of T-cells isolated from the draining lymph nodes adjacent to the implant during the *in vitro* co-culturing with donor cells (Figure 6 A). Accordingly, the xenogeneic group presented the highest level of T-lymphocyte infiltration *in vivo*, after 12 weeks from implantation (Figure 6 B). No T-cell proliferation was observed in the co-culture model for the allogeneic and the syngeneic group. Consistently, a limited amount of CD3+ lymphocytes was present in the defect after 12 weeks.

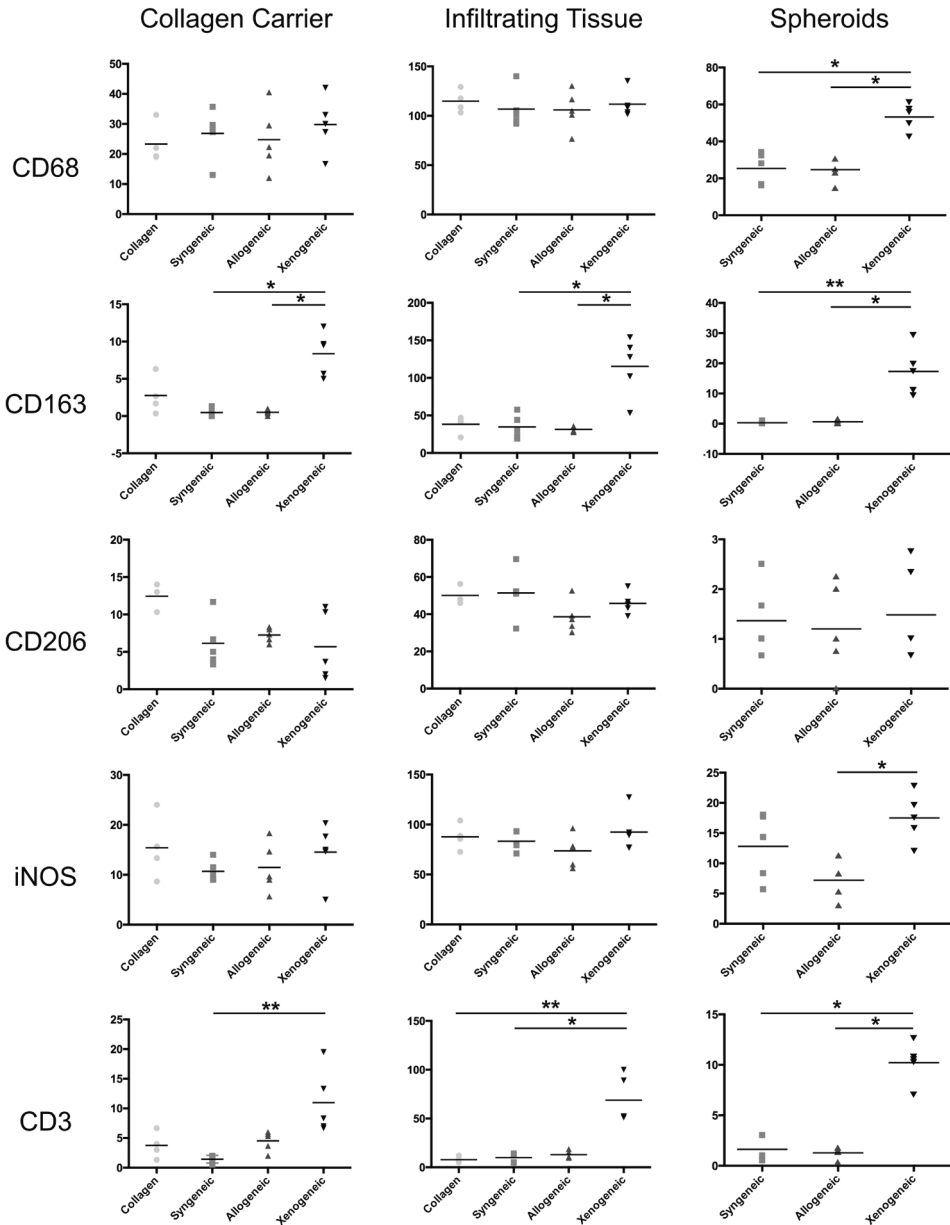


Figure 5. Quantification of the immune cell infiltration in the different defect areas (collagen remnant, infiltration and spheroids) after 1 week. The major differences were observed in the spheroids, where significantly more CD68+ and CD163+ macrophages, iNOS+ cells and CD3+ lymphocytes were found in the xenogeneic group. * $p<0.05$; ** $p<0.01$.



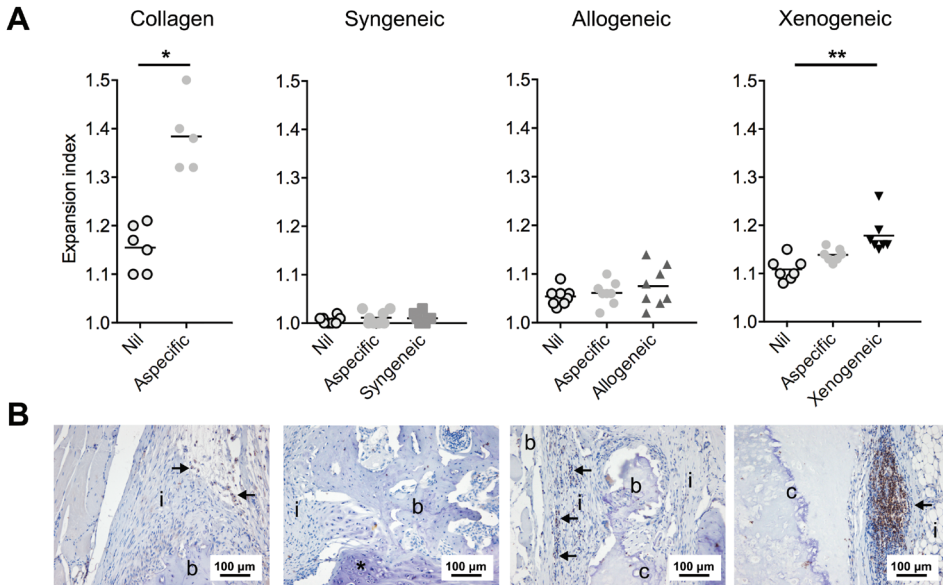


Figure 6. T lymphocyte reaction to the non-autologous implants after 12 weeks. **(A)** Proliferation of the T cells isolated from the draining lymph nodes was assessed in a co-culture model with the donor cells. Specific proliferation induced by the donor cells was observed only in the xenogeneic group. Nil: lymphocytes that were not exposed to any other cell type; Aspecific: lymphocytes co-cultured with third-party Sprague Dawley MSCs; * $p < 0.05$; ** $p < 0.01$. **(B)** CD3+ T Lymphocytes (indicated by the arrows) were still prominent in the local immune response against the xenogeneic implants. Fewer CD3+ cells were spotted in the collagen and allogeneic samples. Brown color indicates the positive staining; i: tissue infiltration, b: bone, c: cartilaginous construct, * EBR.

Systemic immune response and antibody production

An increase in serum concentration of AGP, an acute phase protein produced by the liver, was observed for all groups one week after the surgery (Figure S5) as a consequence of the tissue injury during surgery. However, the AGP level had returned to baseline values in all animals after two weeks. On the contrary, the total IgG concentration in the plasma continued to increase over the 12 weeks, without any statistically significant differences between groups at any of the analyzed time-points (Figure 7 A). However, when analyzing the binding of IgM and IgG to the implanted MSCs by immunocytochemistry, differences were observed (Figure 7 B and C). In particular, lower levels of anti-donor immunoglobulins were detected in the syngeneic group (mean of 213 ± 74 positive pixels/nuclei) compared to both, the xenogeneic (mean of $14,382 \pm 2,259$ positive pixels/nuclei) and the allogeneic groups (mean of $1,032 \pm 1,276$ positive pixels/nuclei).

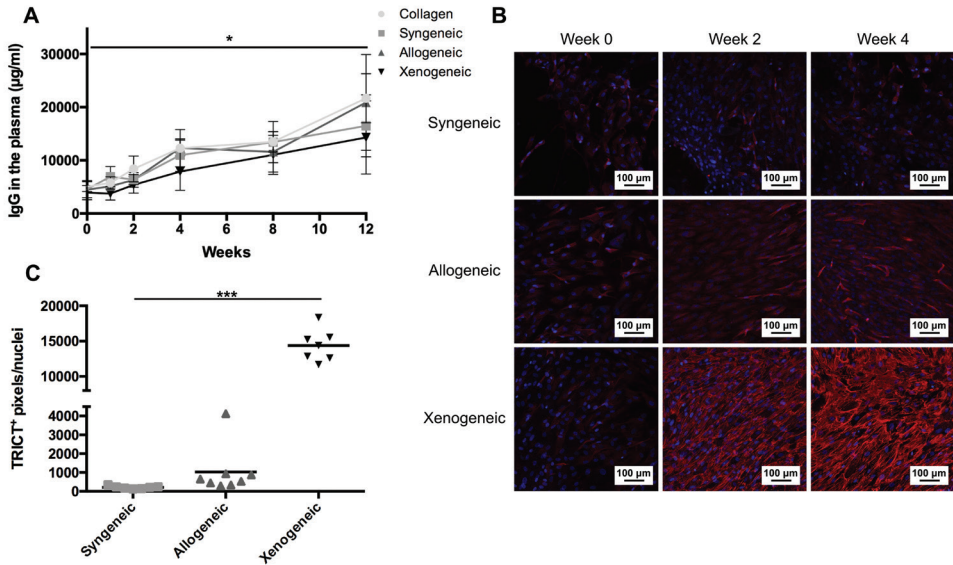


Figure 7. Humoral response to the non-autologous implants. **(A)** Systemic IgG quantification shows a significant increase over time for all samples, but no differences between groups at any time-points. **(B)** Specific anti-donor IgG and IgM (red staining) were observed in all groups, but in particular in the xenogeneic group. **(C)** Quantification of the fluorescent staining confirmed that significantly more antibodies are produced against the xenogeneic implant. Although not statistically significant, more antibodies are produced on average against the allogeneic implants compared to the syngeneic ones. * $p < 0.05$; ** $p < 0.01$; *** $p < 0.001$.

DISCUSSION

The use of non-autologous MSCs with high chondrogenic differentiation capability has the potential to open up new avenues for the clinical translation of cell-based methods for EBR. For such a therapy to be viable, it is crucial to unravel if, and to which extent, the host immune reaction against the foreign implants prevents new bone formation. Here, using immunocompetent animals as a model, we proved that the conversion of the xenogeneic or allogeneic cartilaginous substrates into new bone is feasible even in the presence of a functional immune system. However, the extent of tissue mineralization was found to increase as a function of how close the donor cells are related to the recipient. This suggests that the activation of the immune system played a role in hampering EBR.

Xenogeneic cartilaginous spheroids suffered from an immune rejection, which impaired bone healing. Interestingly, despite this rejection, bone formation was not entirely inhibited in this group. The strong immune response was mediated by multiple immune cell types, belonging to both the innate and adaptive branch of the immune system. In particular, CD68+ and CD163+ macrophages were significantly more present within and in the



proximity of the xenogeneic spheroids. This is in line with previous observations, where macrophages were found to be one of the driving forces responsible for the rejection of xenogeneic primary chondrocytes in an orthotopic minipig model [388]. The direct involvement of macrophages in xenotransplantation rejection is probably due to their intrinsic capability of identifying non-self cells, through the recognition of species-specific surface antigens such as CD47 [389, 390]. The expression of iNOS in the majority of the cells that infiltrated the xenogeneic spheroids further supports their involvement in the cartilaginous spheroid rejection, as iNOS is a marker that usually indicates macrophage polarization towards a pro-inflammatory phenotype. Furthermore, the presence of iNOS positive macrophages usually correlates with poor regenerative outcomes [184]. B and T lymphocytes were also involved in the rejection of the xenogeneic implants. In particular, CD3+ T lymphocytes infiltrated both the implanted construct and the surrounding tissue already within one week, and their presence persisted until the explantation at 12 weeks. This could have negatively affected the remodeling of the cartilaginous constructs, as T lymphocytes can promote the lysis of the grafted cells and stimulate the activation of other immune cells, including macrophages and B lymphocytes [391]. In addition, a correlation between the prolonged presence of effector T cells and delayed fracture repair was previously established [301, 306, 392]. We further confirmed that the xenogeneic antigens specifically activated host lymphocytes, as in the co-culture model chondrogenically differentiated human MSCs induced the proliferation of T cells isolated from the draining lymph node. Similarly, by exposing the rat serum to human MSC-derived chondrocytes, the presence of antibodies against the xenogeneic antigens was observed. These findings are in line with the activation pattern of the adaptive branch of the immune system during both acute and chronic transplant rejection [297, 387, 393].

In contrast to the xenogeneic group, only a limited immune response was observed in the allogeneic group. More specifically, 1 week post implantation no differences between the syngeneic and the allogeneic group were found in terms of CD68+ and CD163+ macrophage infiltration and M1 (iNOS)/M2 (CD206) polarization in the defect area and in the cartilaginous spheroids. Similarly, when comparing CD3+ T cell infiltration within the engineered constructs and in the surrounding tissues *in vivo*, no differences between the allogeneic and the syngeneic groups were observed at both 1 and 12 weeks post-implantation. Furthermore, no T cell proliferation was induced *in vitro* after co-culture with allogeneic MSCs. This outcome reinforces previous *in vitro* findings that suggest retention of immunoevasive or immunomodulatory properties in allogeneic chondrogenically differentiated MSCs [93, 94, 102]. To the best of our knowledge, only two other studies analyzed the immune response elicited by allogeneic MSCs-derived chondrocytes *in vivo*

albeit for cartilage TE applications [98, 360]. Here, chondrogenically differentiated MSCs were encapsulated in an alginate [98] or hyaluronic acid carrier [360] and implanted subcutaneously [98] or in an articular cartilage defect [360]. CD68+ macrophage and CD3+ lymphocyte infiltration [98] and fibrosis [360] were reported after 6 [98] and 12 [360] weeks, respectively. Based on our findings, such an exacerbated immune response was not stimulated upon implantation in a segmental bone defect. Furthermore, differently from these studies, which aimed at obtaining stable cartilage, the unique goal of our study was to exploit the allogeneic spheroids only as a temporary substrate to trigger EBR. Thus, at the 12 weeks mark, the allogeneic graft was partially or entirely remodeled into new, partially autologous bone tissue. As a consequence, it is possible that this gradual remodeling over time and the cartilage conversion to non-immunogenic host neo-tissue did not trigger any additional immune cell activation and migration. Nevertheless, in spite of an immune reaction comparable to the syngeneic control in terms of early inflammation, macrophage and T lymphocyte infiltration and activation, the extent of bone formation showed more variability across the animals within the allogeneic group. In particular, 2/8 animals displayed full regeneration, comparable to the one induced by the syngeneic constructs whereas in 6/8 rats only partial regeneration was observed. While the origin of this difference could be multifaceted, one important contribution could be the production of IgM and IgG by the B lymphocytes. A trend towards increased IgM and IgG production against the allogeneic implant was observed after 4 weeks. Production of alloreactive antibodies against different antigens, including the major histocompatibility complex (MHC) class I and class II molecules, the ABO blood-group antigens and other minor alloantigens, has been reported in several preclinical models [98, 394, 395], marking the pivotal role of B cells in allorejection. In our study, the presence of immunoglobulin might have induced the activation of the complement system [395, 396], interfering with the total remodeling of the construct in a host-dependent fashion. In particular, it is known that receptors for the complement anaphylatoxins (*e.g.* C5aR and C3aR) are expressed not only by immune cells, but also by cells involved in the fracture repair like osteoblasts, hypertrophic chondroblasts and osteoclasts [397, 398]. In addition, altering their expression pattern was shown to alter of the inflammatory phase of fracture healing and ultimately impaired bone repair [398, 399]. Thus, future studies in the field could unravel if transient suppression of the B cell response would allow a more homogeneous and predictable extent of bone formation from allogeneic engineered cartilage grafts. Furthermore, investigating the role played by other immune cells, including polymorphonuclear cells, natural killer cells and the complement system could shed the light on additional reasons behind the heterogeneous outcome observed in the allogeneic group.



Importantly, in our study we explored the feasibility of EBR in the context of a full RT1 class I and II allogeneic mismatch [400]. Nevertheless, even in such a challenging immune mismatch, successful bone regeneration comparable to the one induced by the syngeneic grafts was observed in 25% of the cases. These results present first hints towards a potential clinical translation, provided that a more homogeneous and predictable outcome could be achieved. An interesting option that could be explored is a partial donor-recipient MHC match. A partial RT 1 match might decrease the alloantibody production and promote a more reliable regenerative outcome, opening the way to a fully reproducible protocol for optimizing allogeneic EBR-based strategies.

On a final note, controversial evidence exists in literature regarding the direct contribution of MSCs to tissue regeneration. In particular, MSC secretome also exhibits regenerative capacity, as it promotes immune modulation, cell survival and reduces tissue fibrosis [401]. Nevertheless, it has been established in several studies that in EBR, the implanted cells directly contribute to new bone formation, as part of the non-autologous chondrocytes transdifferentiate towards osteoblasts or osteocytes, and persist in the implanted matrix [71, 76, 299, 374]. Thus, it must be considered that the newly formed tissue could contain donor cells and this might still affect bone homeostasis at a later stage, as an immune system reactivation could damage the newly formed bone. Although further analyses are required to exclude this possibility, our results suggest that the rejection of the newly deposited tissue is not a likely event. Our histological analyses do not show any sign of degradation of the newly formed bone after 12 weeks, underlining the safety and feasibility of using allogeneic cell sources for EBR.

CONCLUSIONS

The use of non-autologous MSCs for EBR offers great benefits from a translational clinical perspective, such as enabling a pre-selection of MSCs with high chondrogenic differentiation potential to guarantee a beneficial therapeutic outcome. Our results represent the first proof-of-concept of the feasibility of using non-autologous, chondrogenically differentiated MSCs to trigger EBR. A severe immune response did result in a low level of bone formation in the xenogeneic group, rendering it unsuitable for clinical translation applications. On the contrary, a milder immune response, mainly characterized by the production of specific anti-donor IgM and IgG was observed in the allogeneic group. While this might have affected the variability in terms of percentage of defect bridging between the different experimental animals, the successful bone formation observed in the allogeneic group provides encouraging evidence of its potential as an alternative to autologous

transplantation. Overall, these findings provide fundamental information for the design and translation of the next generation of EBR-based strategies.

ACKNOWLEDGEMENTS

The antibody against collagen type II (II-II6B3), developed by T.F. Linsenmayer, was obtained from the DSHB developed under the auspices of the NICHD and maintained by The University of Iowa, Department of Biology, Iowa City, IA52242. Furthermore, the help of Imke Jansen, Irina Mancini and Lizette Utomo was highly appreciated. Finally, the authors would like to thank Anja van der Sar and Nicky van Kronenburg for all the support during the animal experiment and professor Harrie Weinans for the support with the microCT data acquisition and analysis.



SUPPLEMENTARY DATA

Table S1. Specifics of the antigen retrieval method, and primary and secondary antibodies used for the immunohistochemical analyses

Primary antibody	Concentration	Antigen retrieval	Secondary antibody
Collagen type II	0.6 µg/ml, incubation O/N at 4°C	Sequential incubation with 1mg/ml pronase and 1mg/ml hyaluronidase at 37° for 30m	BrightVision poly HRP-anti-mouse IgG (VWRKDPVM110HRP)
CD68	4 µg/ml, incubation O/N at 4°C	Incubation with 0.1% pepsin at 37° for 30m	BrightVision poly HRP-anti-mouse IgG (VWRKDPVM110HRP)
CD206	3.3 µg/ml incubation O/N at 4°C	Boiling at 80° in 10mM citrate buffer pH 6 for 45m	Donkey anti-Goat IgG H&L (ab6886)
CD163	1.342 µg/ml incubation O/N at 4°C	Boiling at 95° in TRIS-EDTA buffer pH 9 for 20m	BrightVision poly HRP-anti-rabbit IgG (VWRKDPVR110HRP)
CD3	20 µg/ml incubation O/N at 4°C	Boiling at 95° in 10mM citrate buffer pH 6 for 20m	BrightVision poly HRP-anti-rabbit IgG (VWRKDPVR110HRP)
iNOS	0.52 µg/ml incubation O/N at 4°C	Boiling at 80° in 10mM citrate buffer pH 6 for 45m	BrightVision poly HRP-anti-rabbit IgG (VWRKDPVR110HRP)
Human mitochondria (ab92824)	1 µg/ml incubation O/N at 4°C	Boiling at 95° in TRIS-EDTA buffer pH 9 for 30m	BrightVision poly HRP-anti-mouse IgG (VWRKDPVM110HRP)

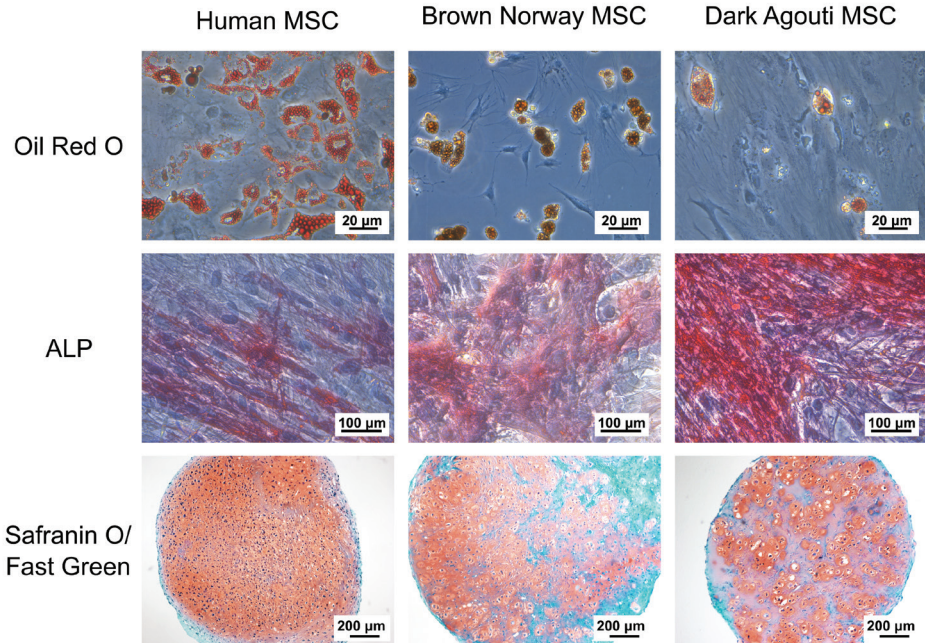


Figure S1. Three lineage differentiation of the isolated MSCs. The differentiation towards the adipogenic (oil red O), osteogenic (alkaline phosphatase, ALP) and chondrogenic (Safranin O/ Fast green) lineage confirm the multipotency of the isolated MSCs.

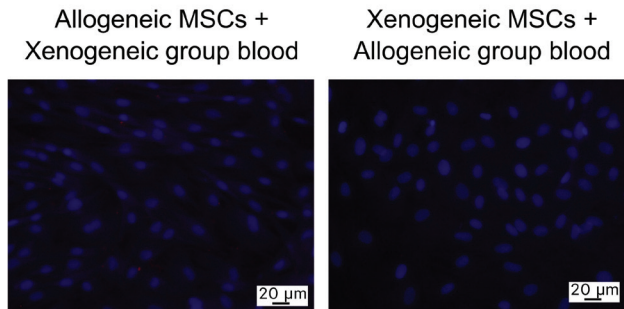


Figure S2. Representative images of the cross-controls for results shown in Figure 7. For each condition, three different serum samples, in which a positive signal was detected when exposed to their respective group, were incubated with the cells from a different group. No TRITC-positive staining was observed.



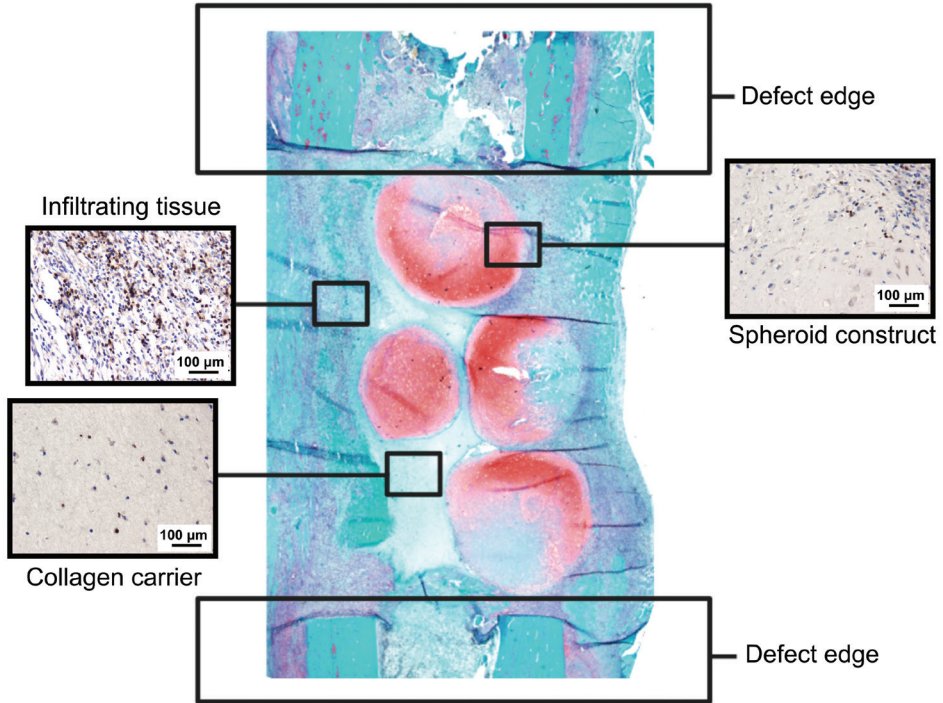


Figure S3. Overview of the defect (Safranin O/fast green staining) and the three areas selected for the immune cell quantification after 1 week. Examples of images used for the CD3+ lymphocyte quantification are shown.

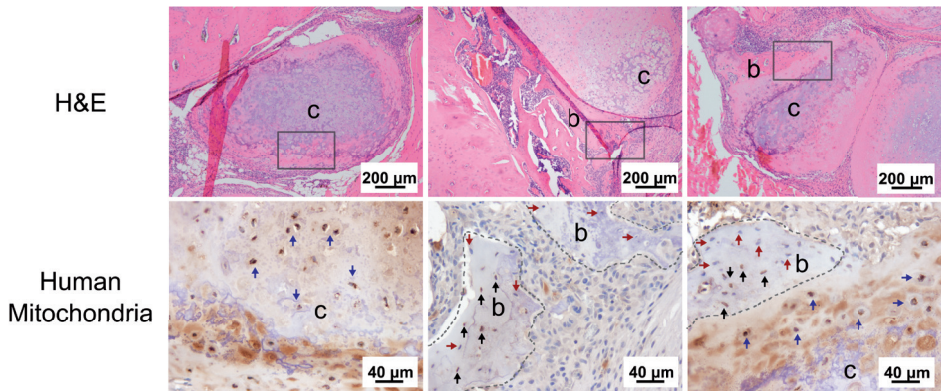


Figure S4. Anti-human mitochondria staining. Human cells were still found 12 weeks post-implantation within the cartilage spheroids in several samples of the xenogenic group (brown intra-cellular staining). In addition, human cells seem to directly contribute the tissue regeneration, as they were found in the mineralized cartilage (blue arrows) and in areas of the spheroids where cartilage had been converted into new bone (black arrows). The newly formed bone contains both human and rats cells (the latter are indicated by red arrows). b: bone, c: cartilage, dark grey box: area depicted in the anti-mitochondria staining, light grey dotted line: outline of bone tissue.

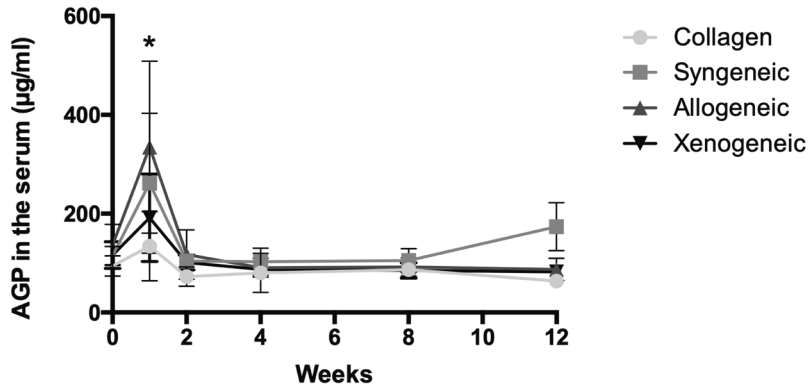


Figure S5. α -1-acid glycoprotein (AGP) quantification in the serum of the rats of the four groups. No differences were observed between groups over time, except for an increase of AGP concentration in all groups after 1 week, most probably due to the surgery. * $p < 0.05$.



Impressive acceleration of bone regeneration by a devital soft callus mimetic

A. Longoni
L. Utomo
A. Robinson
R. Levato
A.J.W.P. Rosenberg
D. Gawlitta

Under consideration for patenting

7



ABSTRACT

The idea of developing a devitalized cartilaginous template that could be exploited to induce bone regeneration was conceived almost a century ago. However, the development of effective strategies that induce cell death while preserving the bioactive components of the extracellular matrix (ECM), still represents a major challenge in the field. Furthermore, no consensus has been reached regarding the use of a chondrogenic or a hypertrophic engineered tissue to maximize new bone formation *in vivo*. Thus, the aim of this study was to investigate bone regeneration induced by devitalized soft callus mimetic spheroids after chondrogenic or hypertrophic stimulation. To fully challenge the clinical translatability of this approach, the constructs were implanted in immunologically mismatched allogeneic recipients. New bone formation was evaluated subcutaneously and in a critical size femur defect in an immunocompetent rat model. Living constructs were used as controls.

The devitalization procedure successfully induced cell death without affecting the ECM composition or bioactivity. Histological and biochemical analyses displayed no differences in protein, GAG, collagen type II, X, and calcium content or ALP activity between vital and devital groups. *In vivo*, larger amount of neo-bone formation was observed for the devital chondrogenic group both ectopically and orthotopically. In the femur defect, impressive bone regeneration was observed in the devital chondrogenic group, where full defect bridging was observed as early as 4 weeks after implantation. As a comparison, after 12 weeks complete defect healing was observed only in 3/8 samples of the devital hypertrophic group, 1/3 sample of the living chondrogenic group and in none of the constructs from the vital hypertrophic group.

Our results show, for the first time, that a dramatic increase in the rate of bone formation was induced by devitalized cartilage constructs. These findings could pave the way for the development of an allogeneic, “off-the-shelf” product for endochondral bone regeneration.

INTRODUCTION

Over the last years, an interest has grown in the use of decellularized and devitalized extracellular matrices as bioactive scaffolds for *in situ* tissue engineering (TE) [402-404]. Both decellularization and devitalization processes aim at preserving the bioactive components and biomechanical properties of the native extracellular matrix (ECM) [106]. Yet, the main difference between the two is that with decellularization protocols, cellular debris is removed whereas this is not the case for devitalization strategies [106]. The use of native or engineered decellularized and devitalized tissues as scaffolds for TE presents several advantages. The fundamental one is that the cells that are migrating into a decellularized or devitalized matrix, are surrounded by the ECM naturally present in the target tissue. Here, the retention of biochemical cues promote cell attachment, migration [405], differentiation [403, 405], and ultimately tissue repair [406, 407]. This offers a clear benefit from a regenerative perspective compared to using less instructive scaffolds. Besides their role in enhancing the regenerative capacity of tissues, ECM-based regenerative strategies are also attractive from a translational point of view. In particular, the absence of living cells would simplify regulations around the marketing and use of ECM-derived products [105, 108, 164, 408]. Furthermore, if all immunogenic components are removed, allogeneic tissues derived from non-immunologically matched donors could be potentially used [108]. Finally, the implementation of ECM-based products in clinical practice would be easier from a logistical point of view because, in contrast to engineered living tissues, decellularized and devitalized cartilaginous constructs can be mass-produced, easily stored and used when needed [106].

In line with this trend, decellularized or devitalized options have already been explored in the orthopedic field to promote fracture healing and bone regeneration [164, 407]. Several examples of decellularized ECM-based scaffolds that mimic the hard callus, the late stage repair tissue of a bone fracture, have been reported in literature [78]. One of the most well-known ones is the demineralized bone matrix, an osteoinductive and osteoconductive biomaterial obtained after the removal of minerals from allogeneic bone [35, 78]. On the contrary, a less explored area is the use of decellularized and devitalized tissues that mimic the soft, cartilaginous callus present in the early stages of fracture healing [78].

Evidence supporting the feasibility of using devitalized native cartilage for endochondral bone regeneration (EBR) has been available since 1920, when Asami and Dock [409] implanted boiled ear and xiphoid cartilage subcutaneously in a rabbit and observed new bone formation. Recent studies further confirmed the feasibility of using decellularized



or devitalized cartilaginous templates to trigger EBR ectopically [66, 95, 103-105] and orthotopically in rodents [95, 104, 114, 410]. Nevertheless, unsatisfactory results in terms of bone regeneration were observed when the decellularized or devitalized cartilaginous constructs were compared to the respective living control [104, 105, 114]. Furthermore, in some cases the addition of living progenitor cells to the decellularized cartilage-derived matrix before implantation was found to be necessary in order to observe new bone formation [95, 103]. All together, these results suggest that the applied decellularization or devitalization methods lead to suboptimal regeneration, potentially caused by loss of bioactivity of tissue components. This led to the hypothesis that milder devitalization methods are essential to preserve the structural and biochemical integrity of the tissue's ECM. A downside of this mild approach is that cellular debris and DNA are retained within the construct. This is believed to trigger an immune response that hampers the regenerative process induced by non-autologous ECM-based scaffolds [107, 108, 183]. Finally, contrasting evidence is present in literature regarding the optimal timing for devitalization (*e.g.* after chondrogenic differentiation or hypertrophic induction) in order to maximize the conversion of the cartilage template into new bone upon implantation *in vivo* [78, 83, 104].

Therefore, the aim of this study was to investigate the regenerative potential of devitalized soft callus-mimicking cartilaginous spheroids for bone TE application. To do so, the bone regeneration induced by devitalized ECM-based scaffolds produced after MSC chondrogenic or hypertrophic stimulation was compared to neo-bone formation induced by their living counterparts. In the context of the development of an off-the-shelf product, all cartilaginous constructs were produced from allogeneic MSCs and evaluated in a challenging and fully immunologically mismatched setting.

MATERIALS AND METHODS

Study design and overview

For *in vitro* characterization of the constructs, human MSCs were embedded in a collagen gel and chondrogenically differentiated or stimulated towards a hypertrophic state prior to devitalization. The devitalized ECM was characterized and compared with those of vital control samples.

For the *in vivo* studies, the same four groups (vital chondrogenic or hypertrophic; devital chondrogenic or hypertrophic) were used but now with constructs derived from rat MSCs. Allogeneic rat MSCs were processed into the constructs and implanted in a rat of a different strain, having a fully functional immune system. The constructs were

implanted subcutaneously ($n=6$ for each group) and in a critical size femur defect in rats. For the subcutaneous implantation, a carrier material only (collagen) was included. For the femur defect, $n=8$ was used for the experimental conditions (devital chondrogenic and hypertrophic) and $n=4$ was used for the control conditions (vital chondrogenic and hypertrophic). The overall experimental outline is depicted in Figure 1.

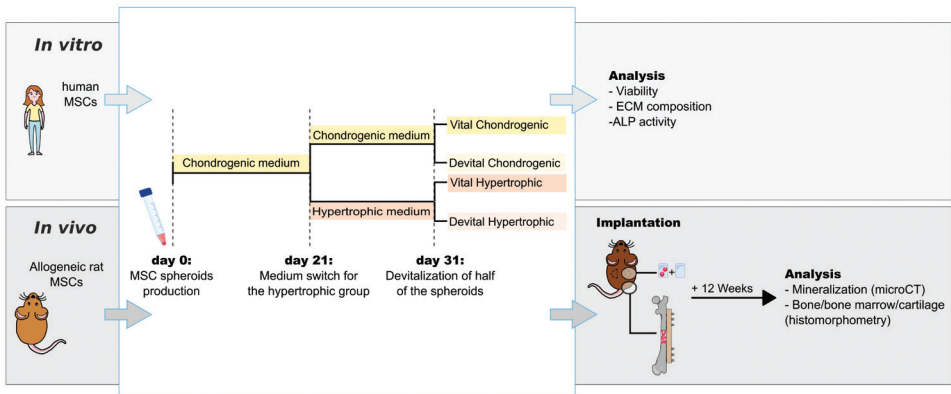


Figure 1. Experimental outline. For the *in vitro* characterization, human MSCs were embedded in collagen hydrogels and differentiated either in chondrogenic medium (31 days) or in chondrogenic + hypertrophic media (21+10 days). After 31 days, half of the constructs of each group were devitalized. The viability of the cells and retention of ECM components was evaluated. For *in vivo* implantation, rat MSCs were used and an identical differentiation protocol was followed. After 31 days spheroids were assembled in a multi-modular constructs and implanted either subcutaneously (2 spheroids per construct) or in a femur defect (8 spheroids per constructs). Carrier material control was included in the subcutaneous implantation. After 12 weeks, samples were explanted and the new bone formation was evaluated.

Isolation and expansion of human and rat bone marrow-derived MSCs

Human MSCs were isolated from bone marrow aspirates of three patients (donor 1: 20-year old, female; donor 2: 60-year old, female; donor 3: 20-year old, female) that were obtained after informed consent, in accordance to a protocol approved by the local Medical Ethics Committee (TCBio-08-001-K University Medical Center Utrecht). Ficoll-paque (GE Healthcare, Little Chalfont, UK) was used to separate the mononuclear fraction, which was further selected based on plastic adherence as previously described [89]. Adherent cells were cultured at 37°C under humidified conditions and 5% carbon dioxide (CO₂) in MSC expansion medium consisting of α -MEM (22561, Invitrogen, Carlsbad, USA) supplemented with 10% heat-inactivated fetal bovine serum (S14068S1810, Biowest, Nuaille - France), 0.2 mM L-ascorbic acid 2-phosphate (A8960, Sigma-Aldrich, St. Louis, USA), 100U/mL penicillin with 100 mg/mL streptomycin (15140, Invitrogen), and 1 ng/mL basic fibroblast growth factor (233-FB; R&D Systems, Minneapolis, USA).



Rat MSCs were isolated from 4-week old Dark Agouti rats (Envigo, Indianapolis, USA) with the approval of the Central Authority for Scientific Procedures on Animals (CCD, no. AVD1150020172465) and the animal ethical committee of the University Medical Center Utrecht. Briefly, the rats were euthanized through CO₂ asphyxiation. After removal of the epiphysis, bone-marrow was obtained by flushing through the diaphysis with MSC expansion medium supplemented with 0.025% ethylenediaminetetraacetic acid (EDTA). Cells were allowed to adhere in a Petri dish overnight. Afterwards, StemX Vivo medium (CCM004, R&D Systems) was used for sub-culturing. Both rat and human MSCs were passaged at 80% confluency until passage 4.

Chondrogenic differentiation of MSC spheroids

At passage 4, human or rat MSCs were chondrogenically differentiated. Briefly, collagen spheroids were created by encapsulating MSCs (20×10^6 /mL) in 50 μ L collagen type I gel droplets (4 mg/mL) (354249, Corning, New York, USA), according to manufacturer instructions. After gelation, the samples were cultured in serum-free chondrogenic medium consisting of high glucose DMEM (31966, Invitrogen) with 1% Insulin-Transferrin-Selenium (ITS) + premix (354352; Corning), 10^{-7} M dexamethasone (D8893; Sigma-Aldrich), 0.2 mM L-ascorbic acid 2-phosphate (A8960, Sigma-Aldrich), 100 U/mL penicillin and, 100 mg/mL streptomycin (15140, Invitrogen). To differentiate human MSCs, the medium was supplemented with 10 ng/mL TGF- β 1 (Peprotech, New Jersey, USA). For rat MSCs, also 100 ng/mL BMP-2 (InductOS, Wyeth/Pfizer, New York, USA) was added. Medium was refreshed daily for the first 4 days and afterwards three times per week. After 21 days of chondrogenic differentiation, half of the spheroids were subjected to hypertrophic medium, consisting of DMEM (31966, Invitrogen), 1% ITS + premix, 100 U/mL penicillin with 100 mg/mL streptomycin, 0.2 mM L-ascorbic acid-2-phosphate, 1 nM dexamethasone, 10 mM β -glycerophosphate (G9891; Sigma-Aldrich), 1 nM 3,3',5-triiodo-L-thyronine (T2877; Sigma-Aldrich). Differentiation in chondrogenic or hypertrophic medium proceeded for 10 additional days till day 31. As mentioned in the study design, human MSCs were used for the ECM characterization, whereas Dark Agouti rat MSCs were used for the *in vivo* experiments.

Devitalization procedure of the spheroids and viability analyses

After 31 days, samples were harvested and devitalized by lyophilization (Alpha 1-2 LD, Salm en Kipp, Breukelen, the Netherlands). Metabolic activity was assessed by bioreduction of resazurin sodium salt (R7017; Sigma-Aldrich). Briefly, the vital and devitalized chondrogenic and hypertrophic constructs were incubated for 18 hours at 37°C in the dark with 500 μ L

of 10% resazurin sodium salt in chondrogenic medium without TGF- β 1. Absorbance was measured on a spectrophotometer at 570nm and at 600nm for background correction (Versamax; Molecular Devices, Sunnyvale, USA). Data are presented as percentage, considering the metabolic activity of the vital chondrogenic and hypertrophic groups as 100%. The values obtained from empty collagen controls were subtracted.

To further confirm the absence of viable cells, constructs were digested using a 3 mg/mL collagenase type II (LS004177, Worthington; Lakewood, NJ, USA) in phosphate-buffered saline (PBS) digest solution for a minimum of 2 hours at 37°C. The extracted cells were stained with 0.5 μ g/mL Calcein-AM (Molecular Probes, Thermo Fisher Scientific, Massachusetts, USA) for 30 minutes at 37°C. Samples were excited at 495 nm and emission was registered at 515 nm (ASCENT Fluoroskan plate reader; Labsystem). For quantitative analysis, the signal was calibrated with known concentrations of MSCs to produce a standard curve.

Images were acquired using an Olympus IX53 inverted fluorescence microscope. Finally, the spheroid digests were re-plated in a 96-well plate and incubated with MSC expansion medium for 2 days to check for any remaining viable cell. Wells were washed with PBS, fixed in 10% neutral buffered formalin, and stained with methylene blue (341088-1G, Sigma-Aldrich) for 5 minutes. Images of the monolayers were taken with an Olympus IX53 inverted microscope. At least three constructs per condition for each donor were used.

Histological analysis of vital and devitalized human MSC-derived cartilage constructs

After fixation, samples were dehydrated in a series of increasing ethanol solutions (70-100%) and cleared in xylene. Subsequently, the samples were embedded in paraffin and sliced into 5 μ m thick sections (Microm HM340E; Thermo Fischer Scientific). Prior to staining, tissue sections were deparaffinized with xylene and gradually rehydrated through decreasing ethanol solutions (100-70%).

To identify cell nuclei, collagenous fibers, and glycosaminoglycans (GAGs), sections were triple stained with Weigert's haematoxylin (640490; Klinipath BV), fast green (FN1066522; Merck), and Safranin-O (FN1164048213; Merck).

To detect mineralization, von Kossa staining was performed by incubating the sections with 1% silver nitrate (209139, Sigma-Aldrich) directly under a light bulb (Philips Master TL5HO 54W 830, 1m distance), for 1 hour. The samples were subsequently washed with 5% sodium thiosulphate (A17629, Alta Aesar, Haverhill, USA) and counterstained with haematoxylin.



For collagen type II (0.6 µg/mL, II-II6B3, Developmental Studies Hybridoma Bank) and collagen type X (10 µg/mL, 1-CO097-05, Quartett, Germany) endogenous peroxidase activity was blocked by incubating samples for 15 minutes with 0.3% H₂O₂. For collagen type II staining, antigen retrieval was done by a sequential treatment of 1 mg/mL pronase (Sigma-Aldrich) and 10 mg/mL hyaluronidase (Sigma-Aldrich) for 30 minutes each at 37°C. For collagen type X staining, antigens were retrieved by sequential incubation with 1 mg/mL pepsin (Sigma-Aldrich) at pH 2.0 for 2 hours and 10 mg/mL hyaluronidase for 30 minutes, both at 37°C. Prior to primary antibody incubation, samples were blocked with 5% BSA/PBS for 30 minutes at room temperature. Samples were incubated with the primary antibody overnight at 4°C. After 30 minutes incubation with the secondary brightvision antibody (VWRKDPVM110HRP, BrightVision poly HRP-anti-mouse IgG, VWR, Radnor, USA), the labels were visualized by 3,3'-diaminobenzidine oxidation. Sections were then counterstained with haematoxylin, washed, dehydrated, and mounted with depex mounting medium. Mouse isotypes (X0931, Dako, Santa Clara, USA) were used as negative controls at the same concentration as the primary antibodies.

Images were taken with an Olympus BX51 microscope (Olympus DP73 camera, Olympus, Hamburg, Germany). Histology of empty collagen controls can be found in Figure S1.

Biochemical analysis

For total protein quantification, samples were digested with 0.5 mg/mL collagenase II for 5 hours at 37°C. Protein concentration was determined using the Pierce™ BCA protein assay kit (23225, Thermo Fisher Scientific) according to manufacturer's instructions. Known concentrations of bovine serum albumin were used to create a standard curve. Absorbance was measured at 562 nm.

Samples for GAGs and collagen analysis were digested overnight at 60°C in papain digestion buffer (250 µg/mL papain, 0.2 M NaH₂PO₄, 0.1 EDTA and 0.01 M DL-cysteine hydrochloride (all Sigma-Aldrich)). The total amount of GAGs was determined using the 1,9-dimethyl-methylene blue (DMMB pH 3.0; Sigma-Aldrich) assay [146]. Known concentration of shark chondroitin sulphate C (Sigma-Aldrich) was used as standard. Absorbance values were detected at 525 and 595 and expressed as a ratio.

To measure hydroxyproline content, 50 µL of the papain digests of all the samples were freeze-dried overnight. Afterwards, samples were hydrolyzed by sequential incubation with 0.4M NaOH at 108°C and 1.4M citric acid. Hydroxyproline contents were measured using a colorimetric method (extinction 570 nm), with chloramine-T and dimethylaminobenzaldehyde as reagents as previously described [411]. Hydroxyproline (Merck) was used as a standard.

Alkaline phosphatase (ALP) activity was measured by using the p-Nitrophenyl Phosphate (pNPP) substrate system (N2765; Sigma). Different concentrations of ALP with a known activity (U/mL) were used as standard curve. The constructs and the standard series were incubated with the pNPP substrate at 37°C for 8 minutes. Absorbance was measured at 405nm with 655nm as a reference wavelength.

The DNA content was quantified using a Quant-iT Picogreen dsDNA assay (P11496, Thermo Fisher Scientific) according to the manufacturer's instructions. Four constructs were used per condition for each donor in all analyses. Two MSC donors were used for the total protein quantification. Three MSC donors were used for the analysis of GAGs, collagen, ALP and DNA.

Evaluation of the ECM porosity and susceptibility to degradation

Fixed samples were dehydrated using a critical point dryer (CPD 030, Bal-Tec) for scanning electron microscopy ($n=1$ per group). After gold sputtering (JEOL, JFC-1300, JEOL Ltd, Tokyo, Japan), samples were imaged using a scanning electron microscope (SEM; JEOL JSM-5600, JEOL Ltd).

For the degradation study, samples ($n=3$ per group) were incubated with 10 U/mL collagenase II (Worthington) in plain DMEM at 37°C. Medium was collected and replaced after 1, 2, 4, 12, 18, 24, 36, 48, 60, 72, and 80 hours. The collected medium was processed as described above to measure hydroxyproline.

To indirectly measure the porosity of the constructs, samples ($n=3$ per group, 1 MSC donor) were immobilized at the bottom of a custom-made mold of 3% agarose gel. The top of the spheroid was exposed to Visipaque solution (iodixanol, GE Healthcare) and microCT images (Quantum FX; PerkinElmer, Waltham, USA) were taken at different timepoints (20 μm^3 resolution, voltage 90 kV, current 180 mA, field of view = 10 mm). For each spheroid, the diameter was measured and a ROI of 0.1 x 1.8 mm was selected at the center. The changes in average pixel intensity within the ROI due to the inward diffusion of the contrast agent was monitored over time using the image processing software Image-J (Java, Redwood Shores, USA).

Construct preparation for *in vivo* implantation

Chondrogenic differentiation and metabolic activity of the Dark Agouti MSCs was verified prior to *in vivo* implantation (Figure S2 and S3). For subcutaneous implantation, two chondrogenic spheroids per group (vital chondrogenic and hypertrophic; and devital chondrogenic and hypertrophic) were embedded in collagen (4 mg/mL) and cast in custom-made



square cuboid molds (3 mm x 3 mm x 2 mm). Gelation was allowed for 45 minutes at 37°C according to manufacturer instructions. Empty collagen controls ($n=6$) were included as controls. For the orthotopic defects, eight chondrogenic spheroids were encapsulated in collagen gels using a 3.5 mm x 3.5 mm x 6 mm custom-made mold, as described above. The constructs were prepared the day before implantation and incubated overnight in chondrogenic differentiation medium without TGF- β 1 and BMP-2.

Animal experiment and surgical procedures

The animal experiments were performed with the approval of the animal ethical committee of the University Medical Center Utrecht (2465-2-01) in accordance with the ARRIVE guidelines for animal experimentation [272]. Twenty-four male Brown Norway rats of 11 weeks old (Envigo) were randomly housed in pairs at the animal facility of the Utrecht University. Animals received standard food pellets and water *ad libitum*, under climate-controlled conditions (21°C; 12 h light/12 h darkness). After 7 days of acclimatization, subcutaneous pockets were created from 5 mm dorsal incisions and blunt dissection as previously described [103] under general anesthesia (1-3.5% isoflurane in oxygen, AST Farma, Oudewater, the Netherlands). In each pocket, one construct of either group (collagen control, vital chondrogenic, vital hypertrophic, devital chondrogenic, or devital hypertrophic) was implanted ($n=6$ per group). The skin was closed transcutaneously with Vicryl Rapide 4-0 sutures (VR 2297; Ethicon). Each animal received a maximum of 2 subcutaneous pockets. For the implantation of the construct in a femur defect, a 6 mm critical-size segmental bone defect was created as previously described [69] ($n=8$ for the devital chondrogenic and hypertrophic group and $n=4$ for the vital chondrogenic and hypertrophic controls). Briefly, the right hind leg was shaved and carefully disinfected. A lateral skin incision was made and soft tissue was dissected in order to expose the right femur. After the periosteum removal, three proximal and three distal screws were used to stabilize a 23 x 3 x 2 mm polyether ether ketone (PEEK) plate to the femur in the anterolateral plane. After fixation, a saw guide and a wire saw (RISystem, Davos, Switzerland) were used to remove a 6 mm cortical bone segment. The collagen constructs were press-fit into the defect and a single dose of antibiotic (Duplocillin LA, 22.000 IE/kg, MSD Animal Health, Boxmeer, the Netherlands) was locally injected intramuscularly. The fascia and skin were sutured in layers using resorbable Vicryl Rapide 4-0 sutures (Ethicon). Subcutaneous injection of pain medication (buprenorphine, 0.05 mg/kg bodyweight, AST Farma, Oudewater, the Netherlands) was given pre-operatively and twice a day for the following three days. When devital constructs were implanted in the orthotopic defect, the rats also received only devital constructs subcutaneously. Rats were euthanized 12 weeks after surgery with an overdose of barbiturates (phenobarbital; 200 mg/kg body weight, TEVA Pharma, Haarlem, the Netherlands). The femora and the

subcutaneous implants were retrieved and processed for histological analysis and micro-computed tomography (microCT) scanning.

MicroCT scanning

Mineralization in the orthotopic defect area was assessed at 0, 4, 8, and 12 weeks after surgery. While under general anesthesia, the hind leg of the rat was fixed to a custom-made support to allow scanning of the femur with a microCT imaging system (Quantum FX). Three minutes of scan time was required per leg for an isotropic voxel size of $42 \mu\text{m}^3$ resolution (voltage 90 kV, current 180 mA, field of view = 21 mm). All scans were oriented in the same fashion using the ImageJ plugin Reorient3 TP (Image-J 2.0.0; Java, Redwood Shores, CA, USA). A volume of interest (VOI) of $6.3 \times 5 \times 5 \text{ mm}^3$ was selected. After euthanasia, subcutaneous implants were also analyzed. Three minutes of scan time was required per subcutaneous implant for an isotropic voxel size of $20 \mu\text{m}^3$ resolution (voltage 90 kV, current 180 mA, field of view = 10 mm). After segmentation with a global threshold, the mineralized volumes (MV) for both the subcutaneous and femur implants were measured in mm^3 using the image processing software plugin BoneJ [273] (Image -J). 3D reconstructions of the femur defect were based on the microCT data and created using ParaView (ParaView 5.3.0, Kitware Inc, USA).

Histological analysis of the *in vivo* samples

All specimens were fixed in a 10% neutral buffered formalin solution for 1 week and thereafter decalcified for 6 weeks in a 10% EDTA-phosphate buffered saline solution (pH 7.4). After decalcification, samples were additionally fixed for two days, dehydrated in a Leica ASP300S tissue processor in graded ethanol solutions (70-100%), cleared in xylene, embedded in paraffin and sliced into $5 \mu\text{m}$ thick sections (Microm). Before staining, samples were deparaffinized with xylene and gradually rehydrated through decreasing ethanol solutions (100-70%). New bone formation was evaluated using H&E and Safranin-O/fast green staining following the same staining procedure described in the previous section.

Histomorphometric analysis was performed for both the subcutaneous and orthotopic samples after H&E staining. Briefly, an overview of the whole sample was made by merging images into a panoramic image in Adobe Photoshop C6. For the subcutaneous implants, bone formation throughout the entire construct area was quantified. For the orthotopic implants, a region of interest (ROI) of $5 \times 2.5 \text{ mm}^2$ was selected in the center of the defect. The titanium screw holes present on each side of the defect were used as reference point in order to ensure an equivalent positioning of ROI in all samples. Three different areas were manually selected for each ROI: bone, hypertrophic cartilage and bone marrow. The number of pixels for each area was quantified via the function “recording measurement”



and expressed as a percentage of the total construct area for the ectopic implants and of the ROI area in the orthotopic ones.

Statistics

A randomized block design with Bonferroni's *post-hoc* correction was applied for the *in vitro* data to accommodate donor variation, including viability and biochemical analysis (protein, GAG, hydroxyproline and DNA content and ALP activity). A linear mixed model followed by a Bonferroni's *post-hoc* correction was used to compare mineralization in the femur defect over time and to evaluate statistical differences in the Visipaque diffusion test (IBM SPSS 22.0, New York, USA). For the histomorphometric measures, a one-way ANOVA test was performed, followed by a Bonferroni *post-hoc* test (GraphPad Prism 6, San Diego, CA, USA). Differences were considered to be statistically significant for $p < 0.05$.

RESULTS

Effects of devitalization on human MSC-derived cartilage constructs *in vitro*

The metabolic activity of the chondrogenic and hypertrophic samples was significantly reduced following the devitalization treatment, to $4.9 \pm 2.6\%$ and $3.7 \pm 2.3\%$ of their vital counterparts, respectively (Figure 2A). After digestion of the spheroids, no calcein-positive (living) cells were detected in the devitalized groups (Figure 2B). On the contrary, viable cells were observed for both vital chondrogenic and hypertrophic groups. Furthermore, no cells were attached to the tissue culture plastic after the digested constructs were re-plated, while they were for the living controls (Figure 2C). Overall, no differences in viability between the chondrogenically differentiated samples and the samples stimulated into hypertrophy were observed, although a lower number of viable cells was observed for Donor 2 in the vital hypertrophic group. After devitalization, cellular debris was still present in the devitalized construct, as confirmed by the unchanged DNA content (Figure S4).

ECM components were preserved after devitalization, as evaluated by histological analysis. There was no evident reduction in GAGs, collagen type II, collagen type X, and calcium content in the constructs (Figure 3). These observations were supported by the quantitative assays, where no statistically significant differences were found in total protein content (Figure 4A), GAG (Figure 4B) or hydroxyproline content (Figure 4C) between the devitalized and vital samples. Moreover, ALP activity, which is more likely to be affected by the devitalization than protein content, was not reduced in the devital groups and was higher in the hypertrophic spheroids than in the chondrogenic ones (Figure 4D).

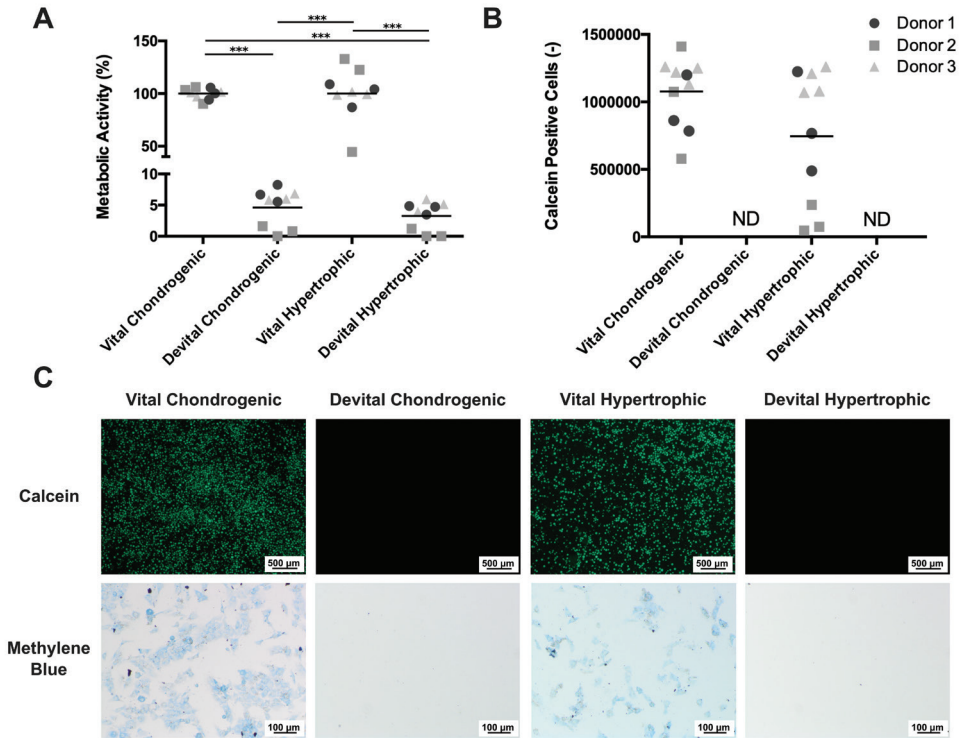


Figure 2. Cell viability after devitalization of engineered cartilage spheroids. **(A)** Metabolic activity before and after devitalization and **(B)** the number of living cells left as detected by calcein staining (green staining). **(C)** Calcein-positive cells extracted from the digested constructs were stained with methylene blue after replating and culturing for 2 days. * $p < 0.05$, ** $p < 0.01$, *** $p < 0.001$; ND: not detectable.

The surface roughness and porosity were evaluated by SEM analysis, highlighting the increased porosity at the surface of the chondrogenic devital samples, compared to the vital chondrogenic samples (Figure 5A). This difference was less evident in the hypertrophic group due to the minerals present on their surfaces. Furthermore, the increased porosity in devital chondrogenic samples was indirectly confirmed by their faster degradation rate compared to other groups (Figure 5B and Figure S5). In particular, all samples from the devitalized chondrogenic group were completely degraded after a maximum of 24 hours (degrading time 20 ± 3.5 h). This was 6.6 hours faster than their vital counterparts (degrading time 26.6 ± 4.6 h). For the hypertrophic group, the spheroids were not fully degraded after 80 hours, with no evident differences observed between the vital and devital groups. Consistently, the diffusion of iodixanol (Figure 5C), a neutrally charged contrast agent, into the ROI selected at the center of the spheroids, was highest in the devitalized chondrogenic group.



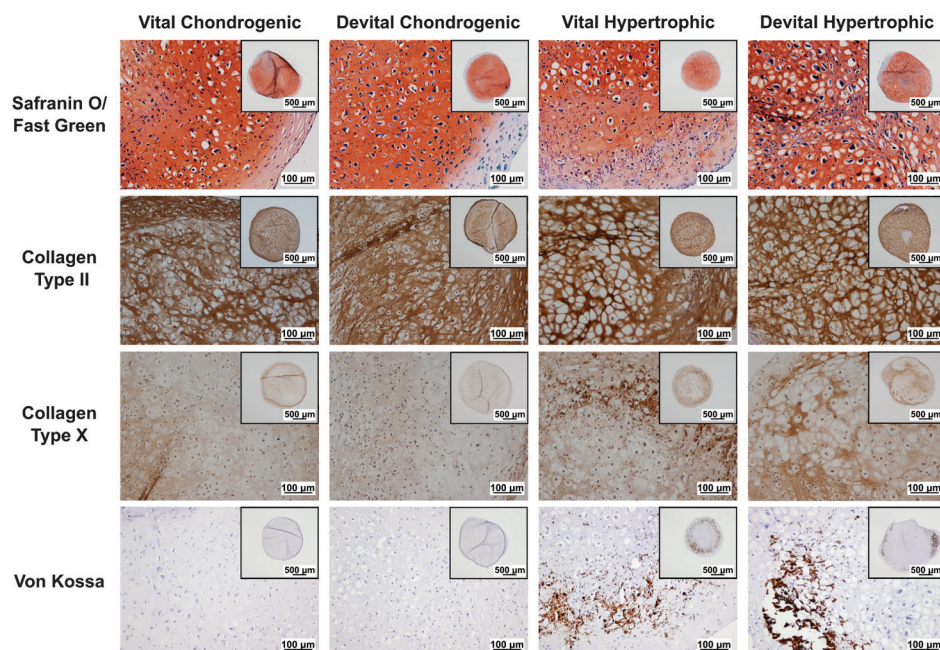


Figure 3. Qualitative evaluation of morphology and ECM preservation after devitalization. Sections of spheroids from the four experimental groups were stained for GAGs (red staining) in the top row, for collagen type II and X (brown staining) and for mineralization in the bottom row (dark brown). Inserts: appearance of the complete spheroids.

Post-surgery observations

Prior to surgery, the mean bodyweight of the rats was 288.75 ± 19 grams and increased throughout the entire period, reaching 358.4 ± 18 grams after 12 weeks. No external signs of adverse reactions (*i.e.* swelling or redness) at the site of implant were observed in any of the rats during the course of the experiment. One animal, of the vital chondrogenic group, died prematurely, 7 weeks post-surgery. As the cause of death was unknown, the retrieved samples were excluded from the analysis. In addition, one devitalized chondrogenic femur sample was excluded from the microCT analysis due to scattering from an inappropriately placed titanium screw. Nevertheless, this sample was still suitable for histological analysis.

Neo-bone formation is induced by devitalized constructs when implanted subcutaneously

No difference in mineralized tissue volume was observed in the subcutaneous implants, with roughly 1-3 mm³ mineralized tissue volume present in all groups (Figure S6). In contrast, differences in new bone formation were observed based on histological evaluation (Figure 6). In more detail, small, localized areas of bone formation were observed in the vital

chondrogenic, vital hypertrophic and devital hypertrophic group ($0.48 \pm 0.68\%$, $0.23 \pm 0.33\%$ and $1.2 \pm 1.8\%$ of the total construct area, respectively). Nevertheless, a larger amount of neo-bone formation was observed in the devital chondrogenic group, with an average of $16.5 \pm 11\%$ of the total construct area. Although not statistically significant, on average larger areas of bone marrow were also observed in this group ($26 \pm 29\%$) compared to the vital chondrogenic ($0.12 \pm 0.27\%$), vital hypertrophic ($0.1 \pm 0.17\%$) and devital hypertrophic ($2.1 \pm 3.4\%$) ones. Finally, remnants of areas rich in GAGs were observed in all groups.

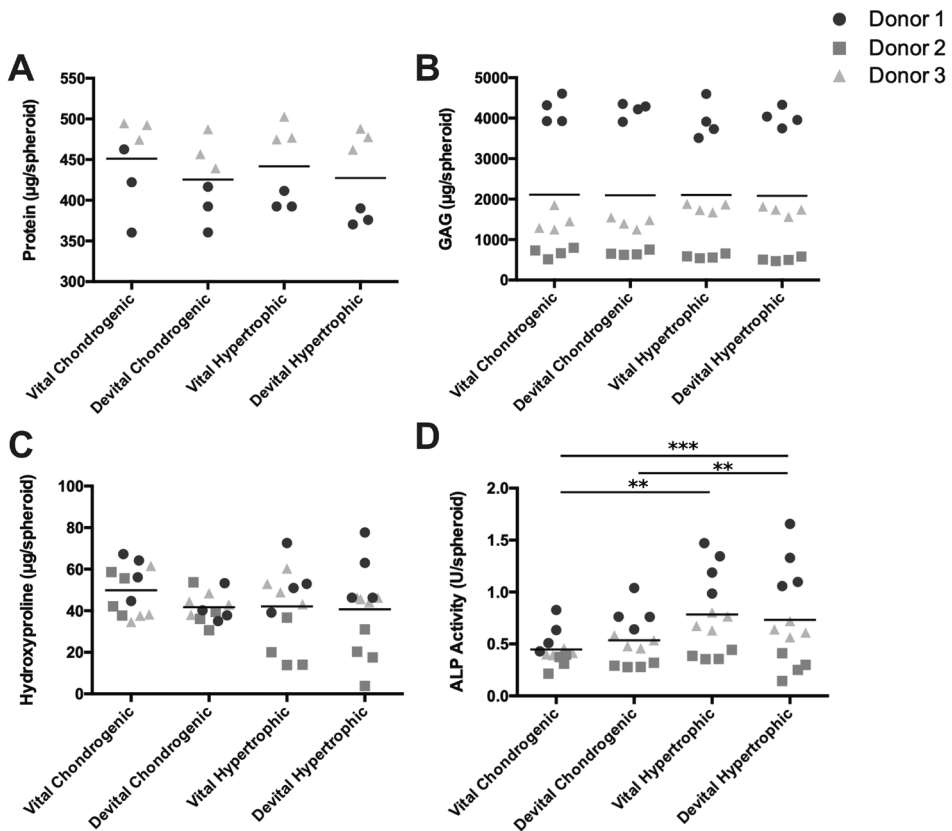


Figure 4. Protein content and activity is retained in the cartilage constructs after devitalization. Quantification of (A) total protein content, (B) GAGs, and (C) total hydroxyproline in the spheroids of the four groups before and after devitalization. (D) ALP activity was quantified as an indication of the retention of the bioactivity after devitalization. * $p < 0.05$, ** $p < 0.01$, *** $p < 0.001$.



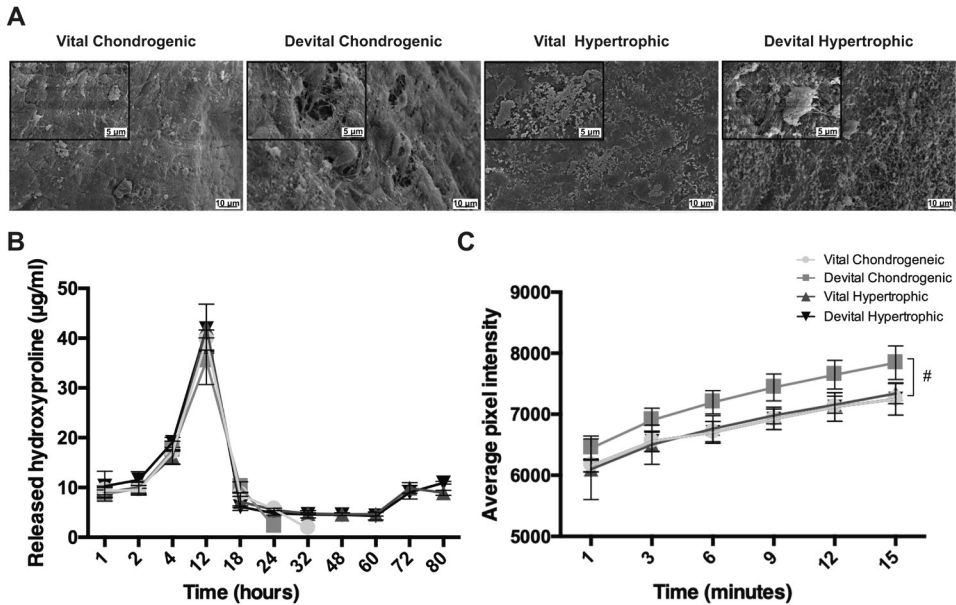


Figure 5. ECM porosity and degradation rate. **(A)** SEM pictures highlight the presence of a more porous surface in the devitalized chondrogenic group compared to the others. **(B)** 2/3 devitalized chondrogenic spheroids were already degraded after 18 hours, whereas the last one was degraded after 24 hours. The majority of the vital chondrogenic spheroids (2/3) was degraded by 24 hours, whereas 1/3 sample was degraded by 32 hours. A slower degradation rate was observed in the hypertrophic groups. **(C)** A higher average pixel intensity, which indicates higher amounts of iodixanol in the selected ROI, was observed in the devitalized chondrogenic group. #: significant compared to devital hypertrophic; * $p < 0.05$.

Devitalized cartilage constructs accelerate orthotopic bone formation

New mineralized bone formation was observed in all groups based on the microCT data and histological analysis (Figure 7, 8). The devitalized chondrogenic group outperformed all other groups, with a final mineralization volume of $97.4 \text{ mm}^3 \pm 11.2$ after 12 weeks. The mineralization volume of the devitalized hypertrophic group was $40.6 \text{ mm}^3 \pm 25.7$, $38 \text{ mm}^3 \pm 26.6$ for the vital chondrogenic group, and $28.2 \text{ mm}^3 \pm 23.9$ for the vital hypertrophic group (Figure 7A). In addition, a statistically significant increase in mineralization volume and complete mineralization of the defects already occurred after 4 weeks for the devitalized chondrogenic group (Figure 7A, 7C and Figure S7). Furthermore, after 12 weeks, full healing was observed in all 8 samples (100%) of the chondrogenic devital group. On the contrary, varying results were obtained in the other groups, with full bridging in 3/8 samples of the hypertrophic devital group (37.5%), in 1/3 samples of the chondrogenic vital control group (33%), and in none of the samples of the vital hypertrophic control group (0%) (Figure 7B).

H&E staining showed that in the chondrogenic devital group, the newly formed bone was remodeled and both the cortical and trabecular compartments of the femur were

restored after 12 weeks. In only 2/8 samples, small areas characterized by the presence of hypertrophic chondrocytes (3% of the ROI) were still observed after 12 weeks, indicating ongoing remodeling at the proximal edge of the defect (Figure 8). On the contrary, no cortical and trabecular compartments could be identified at the defect center of the other groups, not even in the fully bridged samples (Figure 7 C and 8 A and B). In addition, traces of the non-remodeled cartilaginous spheroids were found in the vital groups and the hypertrophic devital group (Figure 8).

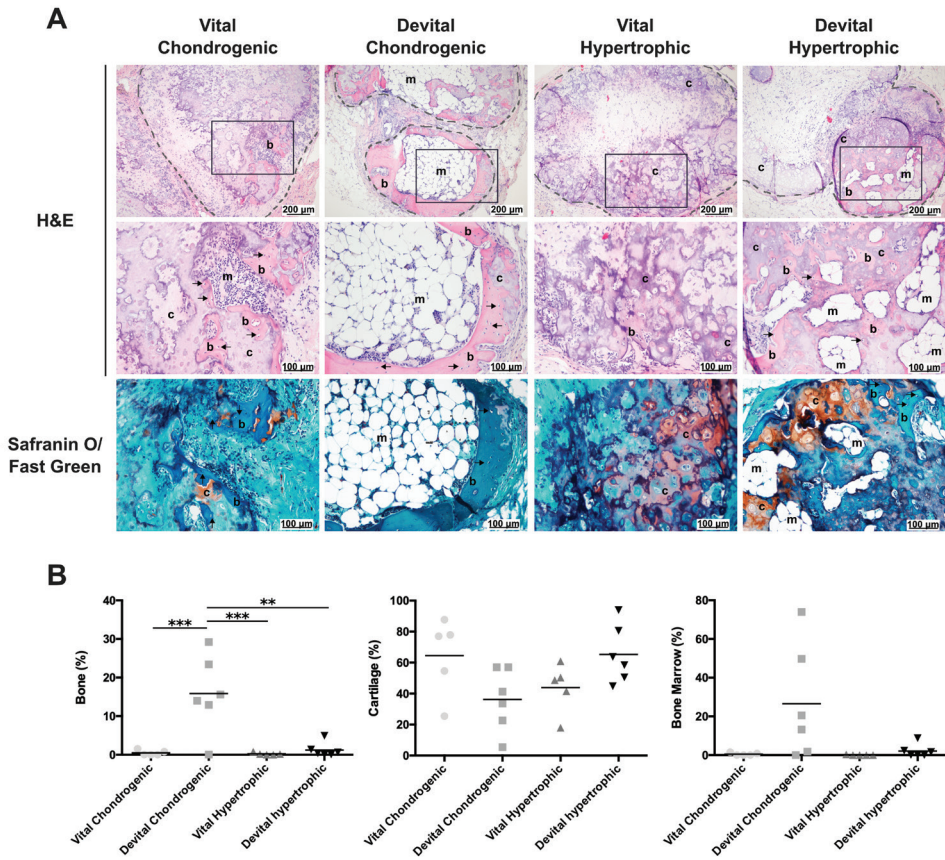


Figure 6. Subcutaneous endochondral bone formation 12 weeks post implantation. **(A)** Overview of the implanted constructs stained with H&E. The grey dotted lines indicate the edges of the constructs whereas the black boxes highlight the area depicted in the higher magnification pictures. New bone formation was observed in at least a few samples of all groups (bright pink in the H&E). Furthermore, bone marrow was observed, especially in both devitalized groups. Non-remodeled cartilage was evident in all groups (red staining in the Safranin O/fast green). b: bone; c: cartilage; m: bone marrow; arrows: osteocytes. **(B)** Results of the histomorphometric analysis performed 12 weeks post implantation display the highest bone formation for the devital chondrogenic group. * $p < 0.05$; ** $p < 0.01$; *** $p < 0.001$.

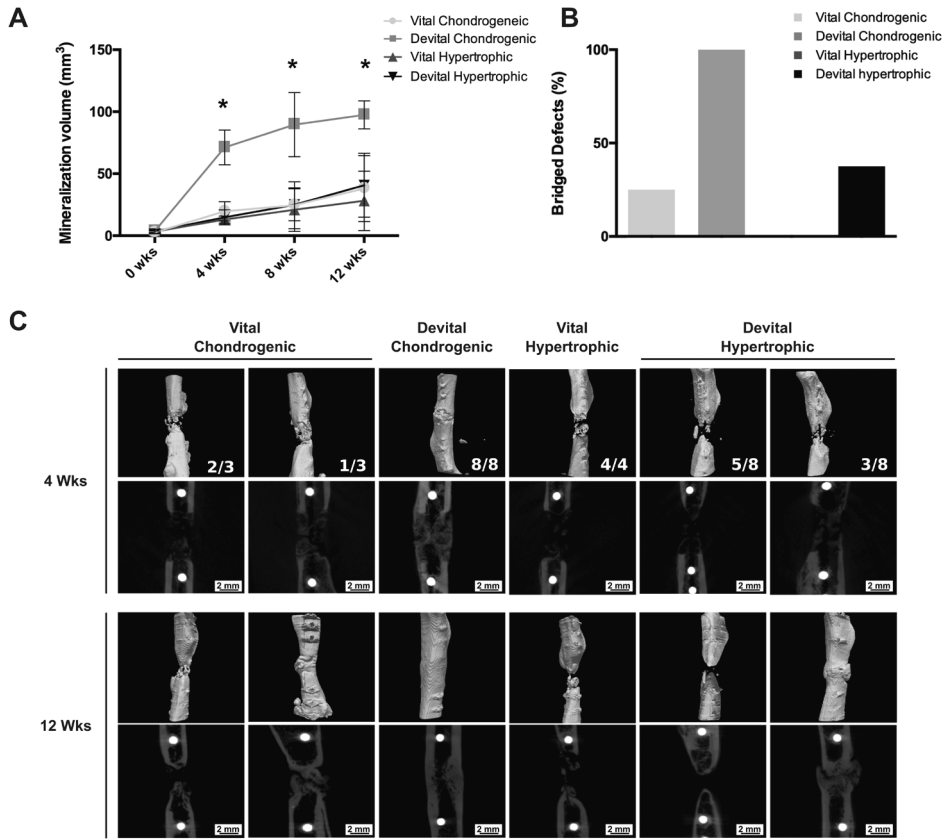


Figure 7. MicroCT-based evaluation of bone formation in the femur defects. **(A)** Quantification of mineralization over time for all groups. (* $p < 0.05$) **(B)** Different rate of defect bridging were observed between groups. Full defect healing was observed in 8/8 samples of the devital chondrogenic group (100%), 3/8 samples of the hypertrophic devital group (37.5%), 1/3 sample of the chondrogenic vital control group (33%) and in none of the vital hypertrophic control group. **(C)** 3D reconstructions and 2D images of the defects 4 and 12 weeks post-implantation. White circles: titanium screws.

DISCUSSION

We are the first to show accelerated bone formation by employing a devitalization strategy to engineer a soft-callus mimic that can be applied for bone regeneration purposes. Firstly, we demonstrated the suitability of this technique to obtain devitalized cartilaginous matrices that retained active biological cues. Secondly, we showed the effectiveness of using devitalized, allogeneic, chondrogenically differentiated MSCs to trigger EBR subcutaneously and to fully regenerate critical size defects *in vivo*. These unique and compelling findings mark a significant step forward in EBR-based strategies for bone tissue regeneration.

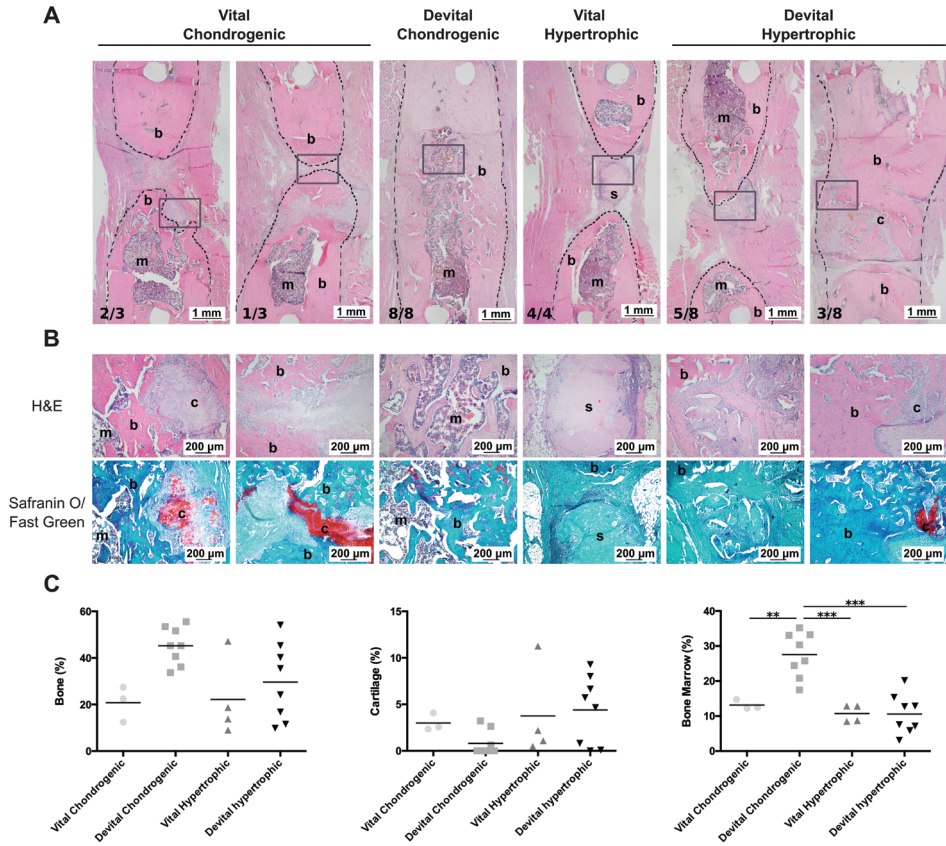


Figure 8. Endochondral bone formation in the femur defects 12 weeks post implantation. **(A)** Overview of the femur defects. The black dotted lines indicate the bone edges whereas the grey boxes highlight the magnified areas depicted in B. **(B)** Higher magnification images of H&E and Safranin O/fast green staining. New bone formation was observed at the defect edges for all groups. Remodeling and formation of a distinct cortical and cancellous compartment was observed in all samples of the devital chondrogenic group. Non-remodeled spheroids were still present in the center of the defect of a few samples belonging to both vital groups and the devital hypertrophic group. **(C)** The histomorphometric analysis presented a trend in bone formation comparable to the mineralization observed by microCT. * $p < 0.05$; ** $p < 0.01$; *** $p < 0.001$. b: bone; c: cartilage; s: spheroid; m: bone marrow.

So far, cartilaginous template devitalization never led to bone regeneration to the level achieved with living constructs [66, 104, 105]. Thus, to the best of our knowledge, this is the first time since the first report on endochondral bone regeneration that an acceleration of the devitalized constructs remodeling is presented [74], marking an important step in the light of clinical translation of this regenerative approach. The development of devitalized matrices that effectively trigger endochondral bone regeneration enables the production of “off-the-shelf” constructs that could be prepared in advance from allogeneic cell sources



and stored until needed [105, 164, 408]. The devital status brings an additional advantage to the table in the sense that it downscales product classification from an advanced therapy medicinal product (ATMP) to a medical device, to which less stringent regulations apply.

Our results show that devitalization does not affect the ECM composition of samples of either the chondrogenic or the hypertrophic group. While the retention of the collagenous and mineral component that we observed has been reported before using several decellularization or devitalization protocols [109, 111-113], the retainment of GAGs is in contrast to the more commonly observed reduction in GAGs [105, 109-113]. This decrease is often linked to the loss of bioactive proteins that are associated to the GAGs, such as growth factors and chemokines [412, 413]. This loss leads to reduced bone regenerative capacity of the devitalized cartilage-derived ECM compared to their respective vital counterparts *in vivo* [104, 105]. Even though a more in-depth characterization of the retainment of structure and presence of ECM components following devitalization could be done, our data confirms the preservation of collagens and GAGs and also suggests that enzyme activity is preserved.

Preserving biochemical integrity of a cell-derived ECM implies at the same time meager removal of cellular debris. It has been shown that the presence of foreign DNA, mitochondria, and cellular membranes skews macrophage populations towards a pro-inflammatory M1 phenotype, both *in vitro* and *in vivo* [107, 183]. This was reported to negatively affect tissue remodeling and the regenerative outcome in an abdominal wall defect in rats [107, 183]. Nevertheless, our recent work showed that EBR could be triggered by vital, allogeneic MSC-derived engineered cartilage, with limited evidence of immune rejection [414]. Thus, the presence of allogeneic cellular debris was not expected to negatively affect the bone regenerative process. Consistent with this hypothesis, in the present study, we showed that the conversion of allogeneic, devitalized spheroids into new bone tissue was not hampered by the presence of residual DNA. On the contrary, in the devital chondrogenic group, bridging of the femur osteotomy gap was observed in all animals already after 4 weeks and remodeling of the newly formed tissue into mature bone, with a cortical and trabecular compartment, was achieved within 12 weeks. In contrast, defect bridging was observed in only 33% of the vital chondrogenic group. A similar trend was observed for the hypertrophic group, where the devital group promoted a higher rate of defect bridging compared to the vital hypertrophic group. The reasons why the devital groups outperformed their respective living counterparts could be multiple. The changes in microarchitecture induced by the devitalization process [415-417] might have played a role. The increase in porosity and degradation rate of the samples could have favored a faster vessel ingrowth, growth factor exposure, host cell infiltration, and ultimately implant

remodeling into bone tissue. Nevertheless further studies should elucidate whether the presence of allogeneic living cells actively hampered bone formation. Specifically, a comparison between the immune response triggered by the vital and devitalized spheroids, especially in the early stages post-implantation, may lead to the identification of a specific branch of the immune response that accelerates or hinders endochondral bone regeneration.

Several studies have shown that active enhancement of the hypertrophic phenotype *in vitro* preceding the devitalization [66, 95, 105] or decellularization [104] improves the bone regenerative outcome *in vivo*. In the hypertrophically stimulated constructs, the secretion of pro-angiogenic and osteogenic growth factors, which enhance blood vessel invasion and osteogenesis *in vivo*, is promoted. Nevertheless, it has also been reported that ECM mineralization, as a result of the addition of β -glycerophosphate in the hypertrophic medium, could have an inhibitory effect on the release of VEGF and metalloproteinase [77]. This ultimately resulted in decreased pro-angiogenic and remodeling properties of the mineralized MSC pellets in an *in vitro* model [77] and in less bone formation *in vivo* [76]. In addition, it must not be neglected that, even upon induction of chondrogenic differentiation, MSCs present hallmarks of hypertrophy [74]. Thus, here we evaluated whether the use of hypertrophic medium and matrix mineralization before *in vivo* implantation was required in order to observe the conversion of the devitalized cartilage into new bone tissue. Our data suggests that chondrogenic differentiation of the samples -both, vital and devital- was sufficient to achieve new bone formation *in vivo* ectopically and orthotopically. In particular, the chondrogenically differentiated, devitalized samples displayed enhanced bone formation at both locations indicating that, in our system, active hypertrophy induction is not required. However, it should be noted that shorter or more prolonged hypertrophic stimulation periods could lead to other results.

All together, these results highlight the potential of a tissue engineered, allogeneic, devitalized MSC-based cartilaginous tissue as a powerful tool to increase the clinical translatability of endochondral bone regeneration. Our system presents several advantages. Firstly, it will facilitate potential upscaling of the engineered constructs without encountering the problem of the formation of a necrotic core during the chondrogenic differentiation stage. Specifically, the relatively small dimension of the cartilage spheroids allows the optimal differentiation of the MSCs without encountering problems associated with the oxygen and nutrients diffusion limits prior to devitalization [95]. The devital spheroids could then serve as building blocks to create larger constructs with different shapes and sizes to perfectly match the patient's defect. Nevertheless, additional studies need to be performed in order to confirm that upscaling to clinically relevant dimensions (from the mm^3 to the



cm³ range) still ensure uniform cell infiltration and tissue remodeling throughout the entire construct. Secondly, even if further analysis should be performed in order to confirm the absence of donor-derived cells in the neo-formed bone, in comparison to other systems [67, 95], here the regenerated tissue is theoretically of host origin. This will prevent the problem of long-term graft rejection. Lastly, the absence of living cells increases the clinical translatability of this approach, as it greatly simplifies logistical and regulatory aspects.

CONCLUSIONS

In this study we present for the first time an allogeneic, MSC-derived devitalized cartilage construct that goes beyond the state-of-the-art and outperforms its living equivalent, in terms of the speed of bone regeneration and the quality of the newly formed bone. The development of these constructs paves the way for a next generation of EBR-based strategies.

ACKNOWLEDGEMENTS

Project no. S-16-130G was supported by the AO Foundation. The antibody against collagen type II (II-II6B3), developed by T.F. Linsenmayer, was obtained from the DSHB developed under the auspices of the NICHD and maintained by The University of Iowa, Department of Biology, Iowa City, IA52242. Finally, the authors would like to thank Anja van der Sar for her gracious support during the animal experiments professor Harrie Weinans for the support with the microCT data acquisition and analysis.

SUPPLEMENTARY DATA

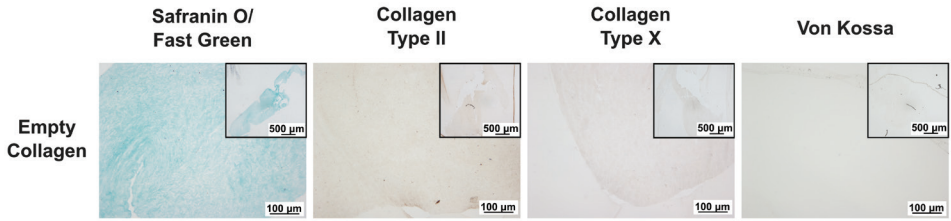


Figure S1. Histology of the empty collagen control samples after 31 days of culture. Representative images show no presence of GAGs, collagen type II or X, or mineralization. Inserts: sample overview.

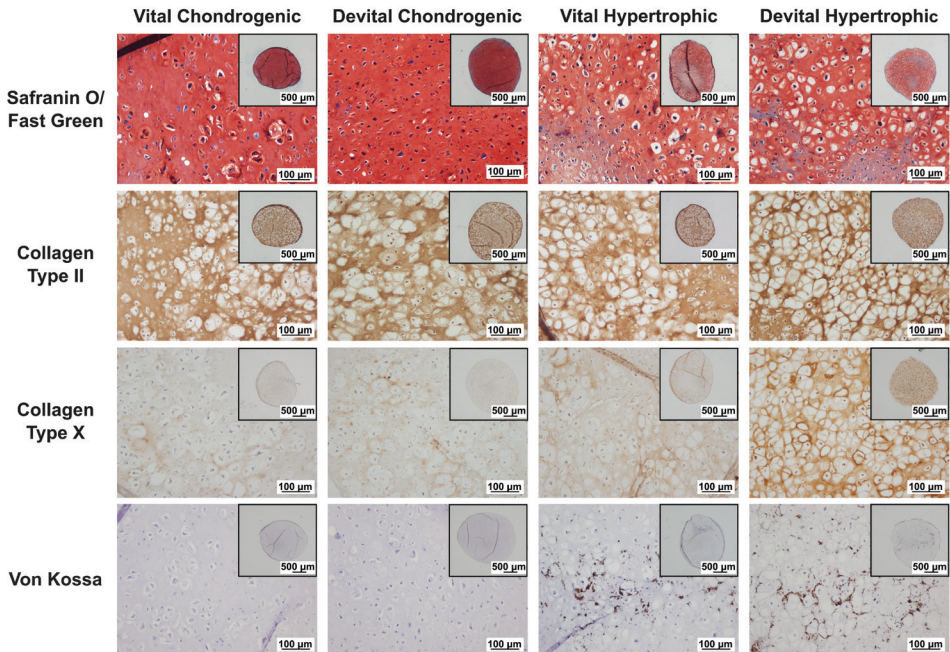


Figure S2. Characterization of the rat MSC spheroids before *in vivo* implantation. Chondrogenic differentiation was confirmed by the presence of GAGs (red staining) and collagen type II (brown staining) in all groups. Increased deposition of collagen type X and mineralization were observed in the vital and devital hypertrophic groups. No difference in ECM components could be detected after the devitalization procedure. Inserts: spheroid overview.



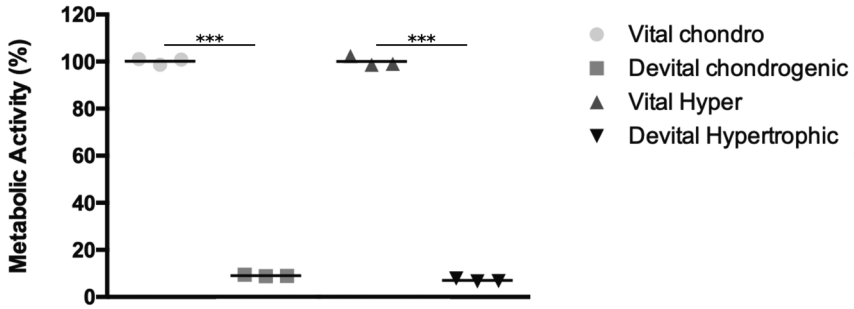


Figure S3. Metabolic activity of the rat MSC spheroids before *in vivo* implantation. Similar to the results obtained with the human MSCs, the metabolic activity of rat MSCs was reduced below the 10% for both devital groups. * $p < 0.05$; ** $p < 0.01$; *** $p < 0.001$.

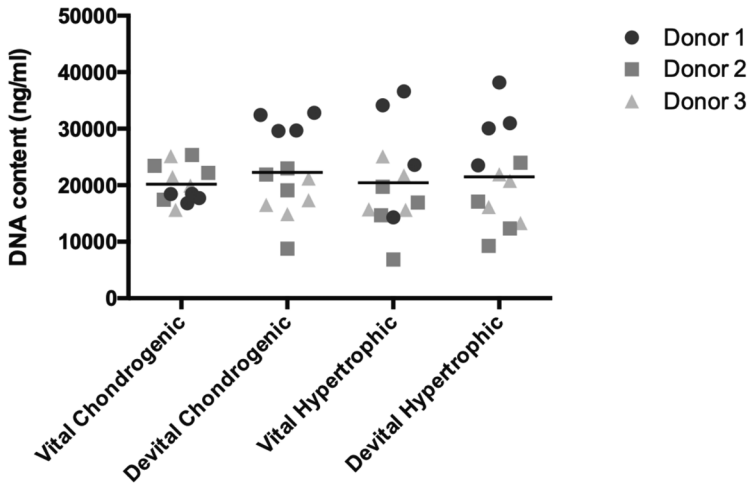


Figure S4. DNA content of the spheroids after 31 days of culture. DNA content was not significantly affected by the culture medium (chondrogenic or hypertrophic) or the devitalization procedure. * $p < 0.05$; ** $p < 0.01$; *** $p < 0.001$.

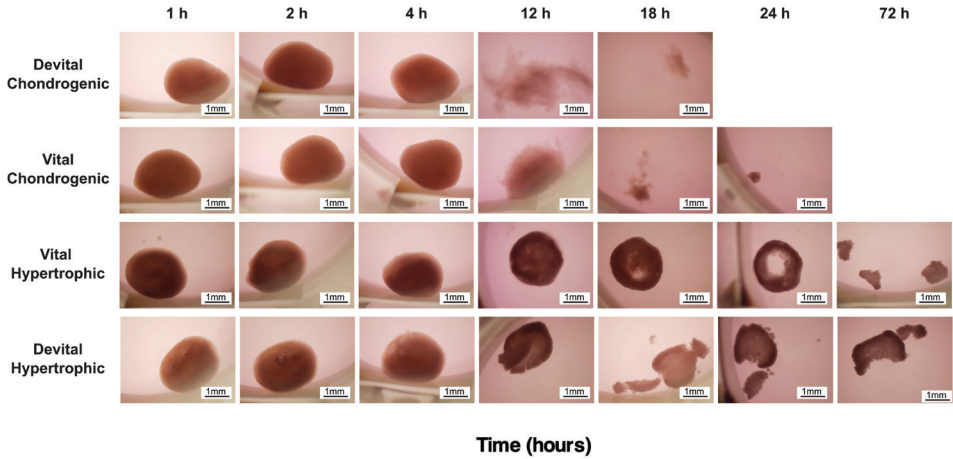


Figure S5. Overview of spheroid degradation over time for the four groups. Representative images of the spheroids appearance over time were taken to monitor degradation. All devital, chondrogenically differentiated spheroids were entirely degraded within 24 hours, while constructs belonging to the vital chondrogenic group were resolved 8 hours later. None of the spheroids from the hypertrophic groups were fully degraded after 80 hours.

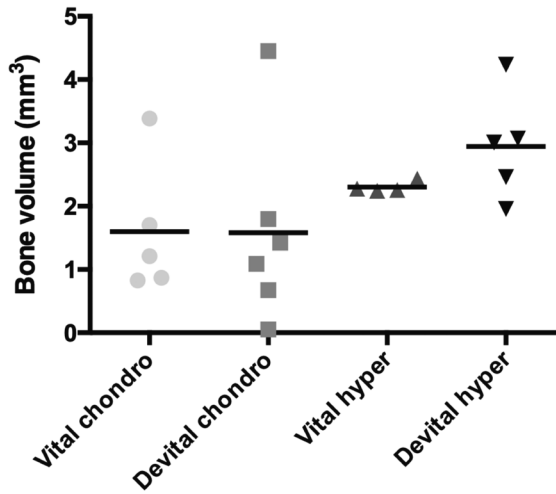


Figure S6. Mineralization of the subcutaneous implants from the four groups after 12 weeks. Statistical differences were evaluated with a one way ANOVA followed by Bonferroni multiple comparisons test (* $p < 0.05$).



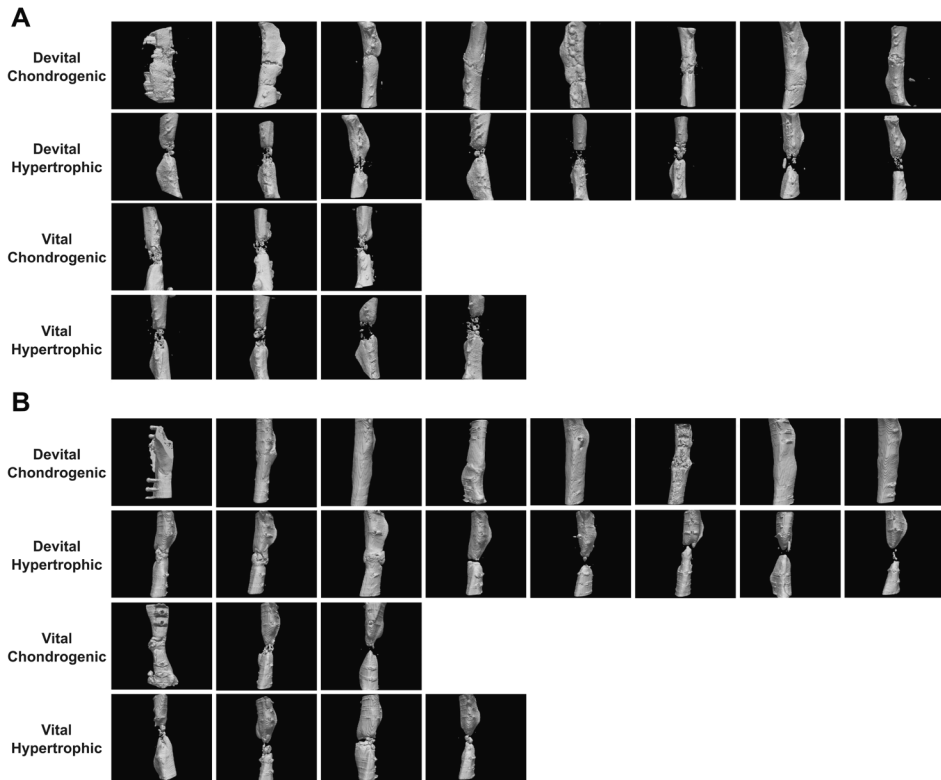


Figure S7. 3D reconstructions of the femur defects. **(A)** 3D reconstructions after 4 weeks and **(B)** 12 weeks.





Summary and general discussion

8



The aim of this thesis was to improve the clinical translation of endochondral bone regeneration (EBR)-based strategies to treat critical-sized bone defects. To achieve this goal, we first focused on identifying the factors that hinder the clinical implementation of EBR-based approaches. Some of these factors are described below.

A crucial requirement for a clinical treatment is to stimulate a predictable and reproducible regenerative response in the host. However, high variability in terms of bone regeneration have been observed between different studies or even within the same study [65, 69, 81, 261]. Not surprisingly, this heterogeneity in new bone formation appears to be largely associated with the heterogeneous level of chondrogenic differentiation that is achieved *in vitro* [61, 62, 81]. Variation in chondrogenesis of the mesenchymal stem cells (MSCs) is due to multiple factors, including the intrinsic inter-donor variability in chondrogenic potential, the length and type of stimuli provided during culture, and the differences in the chondro-supportive or chondro-inductive characteristics of the biomaterial used as cell carrier. Therefore, *in the first part of this thesis we developed cell-based and biomaterial-based strategies to overcome this challenge by engineering a cartilaginous template with more predictable and reproducible features in vitro.*

Another factor that delays the clinical implementation and marketing of tissue engineering (TE) products is the complex and constantly updating regulatory framework associated with the approval of cell-based therapeutics. As a consequence of these strict regulations, at the start of 2019, only 4 TE products had been authorized for commercialization in Europe [418]. Furthermore, logistical aspects that pertain to the storage of the engineered cartilage and the synchronization of the extensive laboratory work with the surgical schedule represent an additional challenge. Thus, *in the second part of this thesis, we improved the clinical translatability of EBR-based approaches by developing an allogeneic, off-the-shelf cartilaginous template.*

In the following sections, the main findings of our studies, their limitations, and their impact on the field of regenerative medicine are discussed. Finally, the additional translational challenges that still need to be addresses are outlined and discussed.

Dental pulp stem cells: a suitable cell source for fibrocartilage engineering

To overcome the challenges associated with the use of MSCs for EBR-application, the chondrogenic and hypertrophic potential of dental pulp stem cells (DPSCs) was thoroughly investigated. *In **chapter 2** we demonstrated that, under a different range of chondro-inductive stimuli, DPSCs produced a fibrocartilaginous matrix and did not acquire a hyaline chondrogenic or a hypertrophic chondrogenic phenotype. This led to conclude that under*



the current chondrogenic differentiation protocols, DPSCs were unsuitable as an alternative cell source for EBR.

As described in the introduction of this thesis, the use of bone marrow (BM)-derived MSCs for EBR-based approaches presents some limitations, including the unpredictability and donor-dependency of their chondrogenic potential [87-90]. In addition, the chondrogenic differentiation is severely reduced after a limited number of passages [91]. This could hinder the production of a sufficient number of cells to treat large bone defects (>10 cm³). To overcome these limitations, the chondrogenic potential of MSCs isolated from other tissues is currently under investigation [65, 67, 149]. In this thesis, DPSCs were initially selected as a promising candidate for EBR strategies, because of their higher proliferation rate compared to BM-MSCs, the high frequency of third molar extraction and the young age of the patients that require this surgical procedure (18-26 years old) [117, 119]. This last characteristic is particularly appealing as with age, a decrease in chondrogenic potential has been often observed for MSCs [88, 285, 419, 420]. In addition, the possibility of expanding DPSCs for 25 passages without losing osteogenic potential has been reported [115]. If this feature would also be valid for their chondrogenic potential, DPSCs could be used as an alternative cell source to overcome the decrease in chondrogenesis observed after BM-MSCs expansion. This would allow the possibility of obtaining clinically relevant cell numbers without sacrificing the quality of the cartilage template developed *in vitro*.

Our data indicates that DPSCs produce a more fibrocartilage-like ECM when exposed to a variety of chondro-inductive stimuli, as compared to the desired chondrogenic phenotype with hypertrophic features. In addition, even upon induction with specific hypertrophic stimuli, no collagen type X or mineralization was observed. Here, protocols exploiting concerted actions of growth factors, known to steer chondrogenic differentiation, were explored. As these did not provide useful results for EBR, the efficacy of alternative methods to enhance DPSC differentiation into the hyaline lineage could be tested in the future. For example, the exposure to hypoxic conditions during MSC and DPSC expansion could be beneficial [421-423]. In more detail, it has been shown that hypoxia plays an essential role in maintaining MSC and DPSC stem cell plasticity, promoting their proliferation and ultimately enhancing their differentiation towards specific lineages (*e.g.* osteogenic) [421-427]. Expansion under hypoxic conditions has proven to be effective for MSC chondrogenesis [421-423]. Nevertheless, whether this would also improve DPSC chondrogenesis and under which oxygen tension this effect would be achieved (*e.g.* 2-5%), has yet to be established.

In this thesis, we decided not to continue with further optimization of DPSC chondrogenic differentiation and instead use, in the next chapters, BM-MSCs. However, while the absence

of hyaline or hypertrophic markers renders DPSCs unsuitable for EBR applications, it could represent an advantage when aiming at the regeneration of fibrocartilaginous structures, like the disc in the temporomandibular joint [150] or the menisci in the knee [428]. In addition, the absence of hypertrophic features together with the fibrocartilaginous nature of the DPSC extracellular matrix could be advantageous for interface TE, where the goal is to develop a complex graft capable of restoring the transition between two tissues, such as ligament-to-bone or tendon-to-bone [429]. Here, the major challenge is to develop a TE product with two different tissues (*e.g.* fibrocartilage and bone) that maintain their individual characteristics but, at the same time, they fully integrate. Potentially, DPSCs and MSCs could be embedded in two different compartments of a bilayered scaffold and chondrogenically stimulated *in vitro*. This would result in the formation of a fibrocartilaginous layer on top of a hypertrophic chondrogenic layer. Upon *in vivo* implantation, the MSC layer would undergo EBR, potentially integrating with the existing bone, while the DPSC compartment would remain fibrocartilage. This approach could also be applied to regenerate, for example, the mandibular condyle. Specifically, it could be used to form the fibrocartilaginous layer that cover the condylar head and its interface with the underlying bone tissue [430].

Vitreous humor: an extracellular matrix-based biomaterial to guide MSC chondrogenesis

To enhance new bone formation following the endochondral pathway, a natural carrier biomaterial that highly resembles the cartilaginous matrix and optimally supports MSC chondrogenesis and their progression towards hypertrophy was identified. *In chapter 3 and 4, we demonstrated that the bioactive components in vitreous humor (VH) enhanced MSC chondrogenic differentiation compared to other 3D culture systems and ameliorate the inter-donor variability. Furthermore, VH supported MSC-derived chondrocyte hypertrophy in vitro and EBR in vivo.*

It has been suggested that the interaction between cells and their native extracellular matrix (ECM) triggers a variety of intra-cellular signals that promotes cell differentiation and new matrix deposition [431, 432]. Thus, it is logical to select ECM-based biomaterials to guide and enhance MSC chondrogenic differentiation. Currently, two different strategies that exploit the instructive features of the ECM-derived biomaterials can be identified [274]. Following a bottom-up approach, singular components of the ECM, such as collagen type II [433], hyaluronic acid [434] and chondroitin sulfate [435], are isolated and used to fabricate scaffolds [436] or to functionalize synthetic polymers [437]. Alternatively, using a top-down approach, native or engineered tissues are decellularized and the remaining ECM is employed as a bioactive 3D culture platform [432, 438]. Each of these



strategies presents some advantages and limitations. Specifically, the use of singular ECM components is ideal for a modular design, in which only proteins that trigger a specific cellular reaction are used to functionalize a 3D culture system [439]. However, this type of approach does not recapitulate the complexity of physical, biochemical and mechanical cues provided by the native microenvironment [274]. As a consequence, this could lead to unsatisfactory results in terms of support or induction of cell differentiation. On the other hand, using decellularized cartilage, cells are embedded in an environment that more closely resembles their native one. Nevertheless, the harsh, multistep procedures required to remove the chondrocyte debris from the dense cartilage tissue (*e.g.* DNA, cell membrane and organelles) often lead to the excessive removal of the bioactive molecules, causing heterogeneous results in terms of chondrogenic induction [105, 109-113].

The use of VH has allowed us to combine positive aspects of the bottom-up and top-down approaches, while overcoming their disadvantages. In particular, as VH possesses a biochemical composition similar to native cartilage, it provides a complex microenvironment richer in bioactive cues when compared to scaffolds composed by singular ECM components. In addition, as VH is already acellular, it does not require post-isolation processing to remove the undesired cellular component. This allows the complete retention of the biochemical cues of the ECM, including proteins, glycosaminoglycans and collagen. The use of VH as a 3D culture platform proved to be effective in consistently enhancing MSC chondrogenesis and supporting their progression towards hypertrophy. The reduced inter-donor variability observed in MSC-laden VH hydrogels suggests that specific characteristics of this biomaterial promoted a more homogeneous level of chondrogenic differentiation at the end of the *in vitro* culture period. To confirm this statement, future studies involving a higher number of MSC donors and VH batches are required. Also, it would be interesting to evaluate if VH has the potential to promote the chondrogenic differentiation of MSCs that are incapable to do so under current culture conditions. Thus, from a clinical translational perspective, VH could be used as a platform to produce a more reproducible cartilaginous template for autologous, cell-based EBR approaches. An interesting possibility would be to expand VH applications by increasing its mechanical properties and its shape stability by functionalizing it with methacrylate groups [440] or with other novel groups (*e.g.* norbornene-modified [441] or allylated [440]) that enable UV or visible light cross-linking. This would for example allow the development of a VH-based bioink that could be combined with state-of-the-art biofabrication techniques to engineer cartilaginous constructs of tailored geometries to reconstruct cartilage or bone defects with complex shapes.

Allogeneic MSCs: the delicate balance between new bone formation and immune response

To overcome the inter-donor variability issue, the use of pre-selected, allogeneic MSCs was proposed. *In chapter 6, we provided a proof of principle for the feasibility of triggering EBR with an allogeneic substrate, in the presence of a fully functional immune system. New bone formation was observed in all experimental animals, with full healing of the critical-size femur defect in 25% of the cases.*

Allogeneic transplantation of cartilage is currently used in the clinical practice. For instance, following an approach similar to the one proposed in this chapter, Zimmer Biomet DeNovo® NT Natural Tissue Graft, exploits allogeneic juvenile living cartilage with high regenerative potential to repair cartilage defects. Moreover, allogeneic, undifferentiated MSCs are under investigation in a number of clinical trials to treat Crohn's disease [352], graft-versus-host disease [351], myocardial infarction [442], and to promote cartilage regeneration [353, 443]. Considering these precedents, it is logical to envision the use of allogeneic MSCs also for other applications, including endochondral-based bone TE.

In this thesis, we demonstrated that it is possible to achieve new bone formation with allogeneic MSC-based cartilage tissue, even in immunocompetent animals. Though encouraging, the results achieved were suboptimal compared to those obtained by implanting the autologous, engineered cartilage. As a consequence, to propose the allogeneic cartilaginous template as a valid alternative to enhance the clinical translatability of EBR-based approaches, strategies to achieve a more homogeneous and predictable outcome need to be developed. Also, it is desirable to reach restoration of the critical-size bone defect, at least to an extent similar to the one achieved by the engineered autologous construct. Ideally, the approach would perform as good as the current clinical gold standard, autologous bone grafts.

In our work, we identified the activation of B lymphocytes as one possible explanation for the variable outcome in terms of bone regeneration by allogeneic, chondrogenic constructs. Thus, an interesting solution could be to combine the allogeneic cells with a carrier biomaterial, loaded with specific immunomodulatory [444] or immunosuppressive agents [379, 380]. This type of approach was recently proven to be effective in promoting the host acceptance of other types of non-autologous, engineered tissues [444]. For example, by exploiting a streptavidin-biotin-based system to conjugate FAS ligand (a pro-apoptotic agent that has an effect mainly on activated T cells) to the carrier biomaterial, the long-term survival of allogeneic pancreatic islets transplanted for the treatment of type 1 diabetes was ensured. Incorporating a similar system to locally and transiently deliver molecules that block the activation of specific immune players or induce a tolerogenic



environment could lead to enhanced and more reproducible bone formation. For instance, the use of monoclonal antibodies that specifically target B cells, such as rituximab or alemtuzumab, could be investigated [445]. Besides, such a temporary and local delivery of immunomodulatory molecules would be acceptable in the clinical practice, as their systemic, prolonged administration, which is associated with undesired morbidities, is avoided [446-448].

A final question we asked ourselves was: in case these immunomodulatory strategies would prove to be effective, could this allogeneic TE product be easily implemented in a clinical setting? While it would be advantageous to avoid the use of patient's own cells, a number of challenges still needs to be faced. For instance, as the presence of living cells makes the mid to long-term storage of the engineered construct impossible, a delay of 3-5 weeks has still to be taken into account in order to produce the living, engineered cartilage in the laboratory when needed. In addition, engineered tissues are classified by the European Medicines Agency as an advanced therapy medicinal product (ATMP) [418, 449]. Differently from the well-established regulatory framework for drugs, biologics, and medical devices, the one of ATMPs is complex and specific requirements may vary from product to product. This makes the clinical implementation of such therapeutic solutions particularly challenging [418].

Devitalized, allogeneic engineered cartilage: a bridge towards clinical translation

To increase the clinical relevance of EBR-based strategies, an off-the-shelf devitalized, allogeneic, cartilaginous construct was developed. *In chapter 7, we demonstrated that devitalized cartilaginous templates induced accelerated bone formation, consistently promoting the bridging of a critical-size femur defect as early as 4 weeks post-implantation.*

The numerous commercialization and logistical limitations associated with the use of cell-based regenerative strategies represent a major driving force in search for alternative therapeutic options. Here, an ideal solution is to decellularize or devitalize the engineered, cartilaginous tissue of allogeneic origin. The absence of living cells would greatly simplify the approval procedure, as the developed non-vital cartilage would no longer be classified as an ATMP [449]. In addition, the decellularized or devitalized engineered cartilage would be an off-the-shelf product that could be prepared in advance and readily used when needed. A number of decellularized cartilage products are currently used in the clinics, including Tutoplast® Cartilage or Chondrofix Allograft, which are derived from allogeneic cartilage. The fact that no clinically available product is intended for EBR applications is quite surprising, especially considering that the possibility of using non-vital cartilage to trigger bone formation is known since the first decades of the 20th century [409]. This is probably

due to the fact that the retention of certain bioactive cues is essential to trigger EBR in the absence of living cells. Thus, in the last part of this thesis we focused on engineering an off-the-shelf, devitalized, allogeneic cartilaginous template that retained its ECM components and bioactivity. This resulted in consistent induction of bone regeneration, with a percentage of defect healing comparable to the one achieved with living, cartilaginous constructs generated with autologous MSCs (100%). In addition, faster regeneration was observed in the devital allogeneic group, as complete bridging of the defect occurred as early as 4 weeks, whereas it took on average 8 weeks for the vital, autologous one.

This presents a promising start for bringing EBR-based approaches one step closer to the clinics. Nevertheless, a number of additional steps need to be taken before potentially evaluating the safety and efficacy of this devital TE product in a clinical trial. In the last part of this discussion, the road ahead is mapped. In particular, the challenges that need to be faced in each step are discussed.

The next translational challenge: construct upscaling

A major bottleneck in clinical translation of TE products is their upscaling to clinically relevant sizes. To give a concrete example, the efficacy of EBR-based strategies is often tested using cartilaginous constructs of relatively small dimensions in critical-size rat bone defects [63, 69, 82]. The largest cartilaginous template used to regenerate an orthotopic femur defect in rat had a volume of 135 mm³ [70] whereas the largest construct implanted subcutaneously presented a final volume of 0.95 cm³ [66]. However, in clinical practice, 1-2 cm³ represents the minimal volume of non-healing defects, but their range is mostly around 12 cm³ for maxillofacial defects. One of the main challenges in fabricating an engineered cartilage construct of such dimensions is the oxygen and nutrient diffusion limitation for a distance of > 150-200 μm from the culture medium [450]. As a consequence, a heterogeneous cell and ECM distribution develops, with a denser tissue layer at the construct periphery [67]. In particular, the hypoxic conditions in the center of the cm-scale engineered construct lead to the formation of a necrotic core, which could hamper new bone formation *in vivo* [67].

Similarly to other studies [66, 67, 95], in this thesis (**chapter 6 and 7**), the use of a multi-modular construct has been proposed to overcome this challenge. In more detail, instead of fabricating a monolithic cartilaginous construct of the required dimensions at once, the chondrogenic differentiation is performed in small modules. This ensures the optimal nutrient and oxygen exchange within them, allowing homogeneous cell differentiation and cartilaginous matrix deposition [67]. The single modules are then combined with a carrier material before *in vivo* implantation in order to create a multi-modular construct



of the desired shape and dimensions. In addition, the introduction of a devitalization step of the modules before their assembly prevents undesired changes in chondrocyte gene expression and protein secretion, which could occur upon implantation as a consequence of the different oxygen tension in the environment. In **chapter 7**, we demonstrated the effectiveness of this approach to regenerate a bone defect of 80 mm³. Therefore, future studies should focus on the validation of the efficacy of the here developed multi-modular devital allogeneic cartilage construct in a clinically relevant bone defect, in a large animal model.

Testing in a large animal model

One of the reasons why only a limited number of discoveries have been translated into clinical products is that the *in vitro* and *in vivo* preclinical models do not always adequately represent the human clinical situation. The advantages of using orthotopic or ectopic models in rats or mice for initial testing and proof-of-concept experiments are multiple, including their affordable price, the ease of their handling and the short breeding cycles [451]. Nevertheless, due to the dimensions of the animals, it is impossible to test constructs of clinically relevant size in an orthotopic location. Therefore, the next step towards the clinical translation of the engineered implants developed in **chapter 7** is to evaluate their efficacy in a large animal model. Small ruminants (goats and sheep) and pigs are the most indicated choice, because they present a bone composition, remodeling rate and micro and macro structure similar to the human one [452]. In addition, both small ruminants and pigs have a close physiological resemblance to humans, also from an immunological perspective [453-455]. However, as pigs are often difficult to handle and aggressive, a more amenable species might be preferred [452]. Therefore, in the next paragraph we will focus on goats.

The final goal of a future experiment in goats would be to define the potential applications of the devitalized implant and to evaluate its regenerative potential compared to the current clinical strategies for the treatment of bone defects. To define the clinical applications, it is crucial to determine whether the regenerative potential of the developed cartilaginous construct decreases as a consequence of an increase in bone defect size. For example, accelerated bone formation and complete healing could still be observed in mid-size bone defects (*e.g.* 2-5 cm³) whereas fibrotic infiltration could occur in the center of large defects (*e.g.* >10 cm³). Thus, defects of progressively increasing size should be included. In addition, it should be established whether the location (*e.g.* cranial area or long bones) affects the regeneration. This would help establishing whether this approach could be used to treat bone defects for both maxillofacial and orthopaedic applications. Therefore, in an

ideal experiment, the capability of the devitalized cartilage to induce new bone formation would be compared, for instance, in a maxillary sinus augmentation model (about 2 cm³) [456], combined with an *os ilium* defect, a non-load-bearing orthotopic model (about 3.5 cm³) [457], or a tibial segmental defect (up to 10 cm³) [458]. If the latter model is chosen, biofabrication techniques could be integrated to reinforce the hydrogel structure by adding, for example, a polycaprolactone cage [252, 459]. Finally, in these large bone defects, it is crucial to establish whether the bone regeneration induced by the devitalized constructs is comparable with autologous bone transplantation, the current clinical gold standard for bone regeneration. This would present the ultimate test for this EBR-based approach.

Production upscaling and automation

A first aspect that needs to be considered is that, although the pre-selection of allogeneic cells circumvents the inter-donor variability hurdle, it does not solve the challenge associated with the loss of chondrogenic differentiation over *in vitro* expansion. Thus, depending on the isolation yield, an adequate cell number to treat large bone defects (*e.g.* 1*10⁹ cells for a defect of 10 cm³) might not be reachable within a limited number of *in vitro* passages. To overcome this challenge, MSC expansion could be performed in a dedicated bioreactor system. One example is the microcarrier-based bioreactor developed by Scinus Cell Expansion where, on average, between 200 and 500 million MSCs can be obtained per donor, without compromising their differentiation properties [460]. In addition, single modules derived from multiple MSC donors could be combined to fabricate the cartilage template. However, whether the administration of more than one MSC donor at the same time could trigger a more pronounced immune response has to be determined.

Another important aspect to consider is that, so far, the single units have been produced manually, as only 8 constructs were required to fill an 80 mm³ defect in rats. However, if the same proportions were kept, around 1000 units would be required to treat one defect of 10 cm³. Thus, it is imperative to evaluate whether the production of the single modules and their culturing could be automated. For example, the use of fluidics-based micro-tissue singularization strategies could be an effective solution to produce high numbers of modules of predictable dimensions [252]. In addition, the use of bioreactor systems (*e.g.* spinner flasks [461]) during the differentiation phase would reduce the time and costs associated with the man-power required to manually refresh the medium of such a large number of constructs.



Good manufacturing practice regulations and economical considerations

In addition to the scientific and technical challenges described above, regulatory aspects also need to be considered. To reach the clinical trial stage, it is important that all the procedures and reagents used are at a good manufacturing practice (GMP) level. First of all, as cell debris is retained in the ECM, it is crucial to put systems in place to efficiently screen the MSC donors and exclude the ones that are affected by infectious diseases (*e.g.* HIV, Hepatitis B and C). Secondly, all the culturing procedures should be performed in closed, GMP-compliant systems, using culturing media with a defined chemical composition [460, 462, 463]. In addition, in this phase, it would also be important to establish markers to monitor, in real time, the differentiation of the constructs. For instance, medium sampling could be performed at regular intervals and MSC chondrogenesis could be evaluated with assays that reveal the presence of certain molecules (*e.g.* released GAGs). These quality controls provide a valuable internal control for the detection of any anomalies in the cellular differentiation process, which otherwise would be detected only at the end of differentiation. Finally, a clinically relevant biomaterial should be selected in order to assemble the multi-modular construct. For example, for non-load-bearing bone defects (*e.g.* cranial or alveolar ridge defects), medical grade fibrin glue could be used [50].

The last consideration regards the economic aspects related to the production of this devital TE product. Currently, the price of the authorized TE products on the market is high compared to other therapeutic options [418]. Nevertheless, different from the other commercially available TE-ATMP, the system developed in this thesis presents the advantage of not relying on autologous cells. As a personalized treatment for each patient is not required, the allogeneic single modules can be mass-produced, stored and used to treat multiple patients. This could decrease the overall cost of the procedure. However, to develop a competitive product, it is also essential, while designing the manufacturing process, to reduce the costs associated with cell expansion and differentiation to a minimum. This could ensure a positive outcome of a cost–benefit assessment, which is necessary to establish therapy reimbursement [464]. Besides, if the costs are contained, the engineered devital cartilage could be preferred over other types of commercially available biomaterials because, different from other types of synthetic grafts, it can be used as a stand-alone therapy and not only as an autograft extender.

CONCLUDING REMARKS

In the last two decades an exponential increase in research productivity in the field of tissue engineering was observed. Nevertheless, the number of TE-ATMP products implemented in the clinical practice can be counted on the fingers of one hand. Therefore, in this thesis we took a number of steps to overcome some of the challenges associated with the clinical translation of EBR-based strategies. In the first steps, we aimed at engineering a cartilaginous template with predictable and reproducible features. To achieve this goal we employed a cell-instructive biomaterial and allogeneic cells, pre-selected for their high chondrogenic potential. While evaluating the regenerative potential of the vital, allogeneic implants, we learnt that the development of a well-differentiated cartilaginous template is not the only requirement that needs to be satisfied in order to maximize new bone formation. In particular, the fine balance between bone regeneration and immune response triggered by the engineered cartilaginous implant should always be considered, as changing the physiological equilibrium existing between bone and immune cells could lead to poor regenerative outcomes. Thus, in search for a solution to tune host immune reaction while enhancing new bone formation, in the following step we developed a devitalized, engineered allogeneic cartilage construct that promoted consistent and accelerated new bone formation. These findings represent the first stepping stones in laying down a novel path towards the clinical translational of EBR-based strategies.





Summaries



NEDERLANDSE SAMENVATTING

Bot is een orgaan dat verantwoordelijk is voor de ondersteuning van zachte weefsels en voor de bescherming van vitale organen. Daarnaast draagt het bij aan de mobiliteit van het lichaam door te dienen als aanhechtingspunt en als hefboom voor de spieren. Bot heeft een groot vermogen zichzelf te herstellen na een breuk (grote regeneratieve capaciteit) waardoor het gros van de botbreuken volledig heelt zonder enige vorming van littekens. Echter, in 10% van alle defecten treedt er onvoldoende heling op, met name wanneer de defecten erg groot zijn. Bij defecten in het aangezicht en hoofd is dit vooral het geval in patiënten met een aangeboren afwijking (bijvoorbeeld een hazenlip of gespleten gehemelte), patiënten waarbij een tumor is verwijderd en/of die bestraling hebben ondergaan, na een ongeval of een infectie. Onvolledige heling komt niet alleen voor bij grote defecten van het hoofd, maar ook bij relatief kleine letsels zoals na het trekken van een tand. Hierdoor ontstaan defecten in het kaakbot, die met de tijd alleen maar groter worden door het ontbreken van een fysiologische belasting die normaal gesproken door de tand uitgeoefend wordt. De huidige therapieën richten zich voornamelijk op het vervangen van het missende stuk weefsel door middel van transplantatie van bot uit een ander deel van het lichaam naar het defect toe, bijvoorbeeld vanuit de ribben of het kuitbeen. Ondanks dat er goede resultaten worden behaald met deze procedures, kleven er toch vele nadelen aan, zoals complicaties door infecties, zenuwbeschadigingen en lokale ongemakken op de plaats waar het implantaat weggenomen is. Ook is er niet altijd genoeg bot aanwezig voor de transplantatie. Als alternatief kunnen er weefseltransplantaten van een donor gebruikt worden, hetgeen bekend staat als 'allogene transplantatie'. Met deze procedure worden echter minder goede resultaten behaald en daarnaast is er een kans op overdracht van ziektes tussen personen, en op afstoting van het donorweefsel.

Vanwege de bovengenoemde tekortkomingen van de huidige therapieën, wordt er veel onderzoek gedaan naar alternatieven voor deze behandelingen. Het veld van de regeneratieve geneeskunde richt zich onder andere op het onderzoek naar manieren om biologische weefselimplantaten te maken in het laboratorium met behulp van biomaterialen, cellen en biologische factoren. Wanneer deze biologische implantaten in een botdefect geïmplant worden, zullen deze het ontbrekende weefsel vervangen. Er zijn meerdere manieren waarop een dergelijk biologisch botimplantaat in het laboratorium gemaakt kan worden. In dit proefschrift hebben we de natuurlijke manier van botvorming van de pijpbeenderen en fractuurgenezing nagebootst: de endochondrale ossificatie. In dit proces vormt het bot op indirecte wijze op basis van een kraakbeen tussenstadium. Bloedvaten groeien dit kraakbeen binnen en voeren cellen aan die het kraakbeen omvormen naar nieuw botweefsel. In de afgelopen 15 jaar is het mogelijk gebleken om in het lab het

kraakbenig basisweefsel te genereren dat na implantatie in kleine diermodellen, zoals ratten en muizen, aanleiding geeft tot botvorming. De implantaten worden gemaakt met behulp van stamcellen uit het beenmerg. Ondanks deze vorderingen zijn er nog enkele problemen die opgelost moeten worden voordat deze wetenschappelijke resultaten vertaald kunnen worden naar een toepasbare therapie. Eén van de grootste knelpunten is de grote variatie in kraakbeenvorming vanuit stamcellen die uit het beenmerg van verschillende patiënten gehaald worden. Dit kan uiteenlopen van goede kraakbeenvorming door cellen van de ene patiënt tot helemaal geen kraakbeenvormende stamcellen voor een andere patiënt. Dit maakt het onmogelijk om een standaardtherapie te ontwikkelen die geschikt zou zijn voor iedere patiënt. Ook wordt de translatie naar de kliniek bemoeilijkt door logistieke en economische uitdagingen met betrekken tot het gebruik van levende (stam)cellen. Bij het gebruik van levende implantaten zit er een zekere tijdsdruk op het proces, gezien voltooid levende constructen direct geïmplantéerd moeten worden en niet opgeslagen kunnen worden tot aan hun gebruik. Daarnaast is het maken van een gepersonaliseerd implantaat voor elke patiënt een erg dure aangelegenheid, hetgeen de positie van de therapie op de commerciële markt niet ten goede komt.

Het doel van het werk in dit proefschrift was daarom om de strategieën voor endochondrale botregeneratie een stap dichterbij de kliniek te brengen. Derhalve is het eerste deel gericht op het creëren van een kraakbeenmodel met voorspelbare en betrouwbare karakteristieken. In **hoofdstuk 2** is geprobeerd om stamcellen uit een andere plek in het lichaam te halen in plaats van uit beenmerg. De cellen werden uit verstandskiezen geoogst en deze lieten kenmerken zien die horen bij regeneratie van fibreus kraakbeen (bv. zoals in de meniscus) en niet bij de regeneratie van bot via het kraakbeenstadium. Daarom is bestudeerd of de keuze voor een materiaal met specifieke eigenschappen de kraakbeenvorming van de beenmergstamcellen kon verbeteren. In het bijzonder is er in **hoofdstuk 3 en 4** gebruik gemaakt van het biomateriaal 'vitreous humor', een materiaal dat in het inwendige deel van het oog te vinden is. Er is specifiek voor het gebruik van dit biomateriaal gekozen vanwege zijn overeenkomsten met natuurlijk kraakbeen, qua compositie en biologische signalen. Ook al verbeterde dit materiaal de kraakbeenvorming van de stamcellen, dan nog zou deze aanpak het probleem van het gebruik van de patiënt-eigen cellen die mogelijk geen kraakbeen kunnen vormen niet verhelpen. Daarom is er in deel 2 van het proefschrift gekeken of stamcellen van een donor, en niet van de patiënt zelf, te gebruiken zijn voor de ontwikkeling van een kraakbeenconstruct. Het voordeel van deze strategie is dat vooraf al getest kan worden welke cellen goed kraakbeen kunnen vormen, en dat vervolgens alleen deze cellen voor een therapie ingezet worden. Desalniettemin is het mogelijk dat een afweerreactie van de patiënt een afstoting van het kraakbeen teweeg brengt, zoals ook

gebeurt bij orgaandonatie. Om hier in meer detail naar te kijken, is in de **hoofdstukken 5 en 6** gekeken naar de mogelijkheid om kraakbeenconstructen te gebruiken die gemaakt waren van niet-gerelateerde donorcellen (die immunologisch niet overeenkomen met die van de patiënt). Een interessante bevinding was dat kraakbeenimplantaten van donorcellen aanleiding gaven tot botvorming na implantatie, hoewel dit minder effectief was dan dat ellen van de patiënt zelf gebruikt werden. Tot slot is er in **hoofdstuk 7** gekeken naar een manier om de logistieke aspecten te vereenvoudigen. Dit is gedaan door een stuk kraakbeen te vormen op het lab, waarvan vóór de implantatie de cellen gedood werden. In dit hoofdstuk is gebleken dat er ook vanuit deze dode implantaten botvorming plaats kan vinden, en dat de bioactieve signalen van de cellen die in het construct behouden bleven, botregeneratie konden bewerkstelligen. Deze strategie zorgde zelfs voor een betere en snellere botregeneratie na implantatie in een rat dan wanneer levende constructen gebruikt werden. Het feit dat deze constructen dood waren, maakt opslag van het implantaat mogelijk. Dit zou betekenen dat een massaproductie van biologische implantaten mogelijk is, wat de kosten van een dergelijke therapie zou reduceren. Concluderend kunnen we stellen dat ondanks dat er nog uitdagingen zijn, de resultaten uit dit proefschrift een stap voorwaarts betekenen op weg naar een klinische therapie voor botdefecten op basis van endochondrale botregeneratie.

RIASSUNTO IN ITALIANO

L'osso rappresenta l'impalcatura del nostro corpo, dà supporto ai tessuti molli e protezione agli organi interni; funziona come punto di ancoraggio per i muscoli, rappresentando così un elemento fondamentale per garantire la mobilità al corpo umano. L'osso possiede una grande capacità rigenerativa, infatti, la maggior parte delle fratture guarisce completamente senza lasciare cicatrici. Nonostante questo, nel 10% dei difetti ossei viene riscontrata solamente una guarigione parziale, che spesso rende necessario un intervento chirurgico. Esempi di questi difetti ossei si riscontrano in pazienti che presentano malattie congenite come la palatoschisi, o a causa della rimozione di tumori ossei, o in seguito a gravi traumi o infezioni. In aggiunta a questa tipologia di difetti ossei estesi, si può riscontrare anche un'incompleta guarigione, ad esempio dopo l'estrazione di uno o più denti. In questo caso, oltre alla deficitaria guarigione, il riassorbimento del tessuto osseo continua progressivamente ad aumentare a causa della mancanza di carico fisiologico. Attualmente, la strategia terapeutica più utilizzata per il trattamento di queste condizioni cliniche consiste nel ripristino del tessuto mancante tramite trapianto autologo, ossia tramite l'utilizzo di un blocco osseo, che viene isolato dal paziente stesso, ma da un sito secondario (ad esempio dalle costole, dalla cresta iliaca o dal perone). Sebbene la percentuale di successo di questo tipo di trapianto sia molto elevata, questa procedura è associata a diverse complicazioni del sito donatore quali infezioni, danneggiamento di nervi e sensazione di dolore. Inoltre, la quantità di osso che può essere prelevata dal sito secondario non è sempre sufficiente per colmare completamente il difetto osseo o presenta una morfologia incongrua con il sito ricevente. Una delle possibili alternative al trapianto autologo è il trapianto allogenico, ovvero l'utilizzo di tessuto osseo isolato da un donatore. Tuttavia, la rigenerazione dell'osso indotta dal trapianto allogenico è inferiore rispetto a quello autologo. Inoltre, la possibilità di trasmissione di malattie e il rigetto del tessuto impiantato, a causa della risposta immunitaria del paziente, sono svantaggi aggiuntivi di questa procedura.

Date le limitazioni delle terapie attuali, la ricerca scientifica si sta focalizzando sullo sviluppo di terapie alternative. In particolare, il settore della medicina rigenerativa, si concentra sullo sviluppo di organi e tessuti in laboratorio tramite la combinazione di biomateriali, cellule staminali e fattori biologici. Lo scopo di queste nuove metodologie è sviluppare un tessuto osseo che, una volta impiantato, sostituisca la parte mancante, stimolando la completa guarigione del difetto. Al momento, si stanno esplorando diverse strategie che mirano a sviluppare impianti ossei in laboratorio. Questa tesi si è focalizzata sull'induzione della rigenerazione ossea mimando l'ossificazione endocondrale, processo che avviene fisiologicamente durante lo sviluppo delle ossa lunghe e la guarigione delle fratture. In queste situazioni, l'osso si forma indirettamente partendo da un "modello" costituito

da cartilagine. Durante la fase di ossificazione, questo modello o stampo di cartilagine è progressivamente invaso da vasi sanguigni, che garantiscono il sufficiente afflusso di cellule responsabili della conversione della cartilagine in nuovo tessuto osseo. Negli ultimi 15 anni è stato dimostrato che, partendo da cellule staminali isolate dal midollo osseo, è possibile generare in laboratorio lo stesso stampo cartilagineo presente fisiologicamente nel corpo umano durante la guarigione delle fratture. Dopo l'impianto in modelli animali piccoli come ratti e topi, questo tessuto cartilagineo ingegnerizzato è in grado di indurre la formazione nuovo osso ma, nonostante i notevoli risultati scientifici ottenuti, non è ancora possibile introdurre questo tipo di terapia nella realtà clinica. Il principale problema associato all'utilizzo di questa soluzione è l'estrema variabilità nella capacità delle cellule staminali isolate da diversi pazienti di generare in laboratorio la cartilagine da impiantare. In altre parole, questo vuol dire che le cellule staminali isolate dal midollo di alcuni pazienti sono in grado di produrre efficientemente l'impianto di cartilagine, mentre quelle isolate da altri pazienti risultano completamente incapaci di generare questo modello cartilagineo. Questo rende impossibile lo sviluppo di una terapia standardizzata, adatta a ogni paziente. Inoltre, l'utilizzo in clinica di impianti che sono costituiti da cellule staminali vive presenta diverse difficoltà logistiche ed economiche. In particolare, al fine di preservare le cellule vive all'interno dell'impianto, la cartilagine prodotta in laboratorio non può essere conservata e deve essere impiantata nel difetto osseo non appena è pronta. Infine, lo sviluppo in laboratorio di impianti di cartilagine personalizzati per ogni singolo paziente comporta spese insostenibili, che ostacolerebbero l'introduzione di una terapia basata su questa strategia nel mercato.

Lo scopo del lavoro presentato in questa tesi è quello di sviluppare metodologie per favorire l'implementazione clinica di strategie rigenerative che mimano il meccanismo di ossificazione endocondrale. Per raggiungere questo scopo, nella prima parte di questa tesi ci siamo focalizzati sullo sviluppo di uno stampo di cartilagine che presenti caratteristiche prevedibili e riproducibili. In particolare, nel **secondo capitolo** abbiamo valutato se le cellule staminali presenti nella polpa del dente del giudizio fossero in grado di creare uno stampo di cartilagine con caratteristiche migliori rispetto a quelle ottenute con le cellule staminali del midollo osseo. Purtroppo, le staminali della polpa dentaria si sono rivelate essere più utili per la rigenerazione della cartilagine fibrosa, presente ad esempio nei menischi, rispetto alla rigenerazione ossea tramite meccanismo endocondrale. Proseguendo nella nostra ricerca, nel **terzo e quarto capitolo** abbiamo cercato di sfruttare le caratteristiche specifiche dell'umor vitreo, un materiale di derivazione biologica, al fine di aumentare la capacità delle cellule isolate dal midollo osseo di creare il modello cartilagineo. L'umor vitreo, un componente dell'occhio, è stato selezionato perché presenta una composizione

chimica e segnali biologici simili a quelli presenti nella cartilagine, e può quindi influenzare positivamente il comportamento delle cellule staminali. La combinazione di questo biomateriale con le cellule staminali ha portato alla produzione di un modello di cartilagine che presenta caratteristiche migliori. Questo approccio però non può essere utilizzato se le cellule staminali del paziente sono completamente incapaci di produrre cartilagine. Dato questo limite, nella seconda parte della tesi, abbiamo esplorato la possibilità di usare cellule staminali derivate da donatore per creare l'impianto cartilagineo. Il vantaggio di questo approccio è la possibilità di verificare la capacità di generare il modello cartilagineo in laboratorio, prima del suo utilizzo clinico. In questo modo, solo le cellule staminali con il più alto potenziale di formare lo stampo di cartilagine saranno preservate e potranno essere utilizzate per creare una terapia standardizzata per tutti i pazienti. Nonostante questo vantaggio, il problema principale di questo approccio è la potenziale risposta del sistema immunitario del paziente, che potrebbe riconoscere le cellule del donatore come "estrane" e causare il rigetto del trapianto. Per questo motivo, nel **quinto e sesto capitolo** abbiamo caratterizzato l'intensità di questa risposta immunitaria e valutato la sua influenza sulla rigenerazione del difetto osseo indotta da cellule provenienti da un donatore. In questi capitoli, abbiamo descritto come la cartilagine ingegnerizzata a partire da cellule donatrici è in grado di indurre la formazione di nuovo tessuto osseo, anche se in modo meno efficiente rispetto alle cellule isolate dal midollo del paziente stesso. Infine, nel **settimo capitolo**, ci siamo focalizzati sullo sviluppo di strategie per semplificare le difficoltà logistiche associate con la preparazione e l'utilizzo di prodotti terapeutici composti da cellule staminali viventi. A tal fine, abbiamo sviluppato una strategia che potesse indurre la morte delle cellule staminali al termine della produzione dello stampo di cartilagine, ma allo stesso tempo consentisse di preservare i segnali biologici, presenti nella matrice attorno alle cellule, che sono necessari per la completa rigenerazione dell'osso. L'assenza di cellule vive permette una preparazione di questo prodotto su scala industriale e garantisce la possibilità di conservazione a medio-lungo termine, consentendo così la riduzione dei costi di produzione. In conclusione, anche se ci sono ancora delle sfide da affrontare, i risultati di questa tesi rappresentano un passo avanti verso l'implementazione in clinica di strategie rigenerative basate sul meccanismo di ossificazione endocondrale per il trattamento di difetti ossei.



References



1. Buck, D.W., 2nd and G.A. Dumanian, *Bone biology and physiology: Part I. The fundamentals*. *Plast Reconstr Surg*, 2012. **129**(6): p. 1314-20.
2. Buckwalter, J.A., et al., *Bone biology. I: Structure, blood supply, cells, matrix, and mineralization*. *Instr Course Lect*, 1996. **45**: p. 371-86.
3. Hadjidakis, D.J. and Androulakis, I., *Bone remodeling*. *Ann N Y Acad Sci*, 2006. **1092**: p. 385-96.
4. Frost, H.M., *Skeletal structural adaptations to mechanical usage (SATMU): 2. Redefining Wolff's law: the remodeling problem*. *Anat Rec*, 1990. **226**(4): p. 414-22.
5. Soysa, N.S. and N. Alles, *Osteoclast function and bone-resorbing activity: An overview*. *Biochem Biophys Res Commun*, 2016. **476**(3): p. 115-20.
6. Delgado-Calle, J., A.Y. Sato, and T. Bellido, *Role and mechanism of action of sclerostin in bone*. *Bone*, 2017. **96**: p. 29-37.
7. Uda, Y., et al., *Osteocyte Mechanobiology*. *Curr Osteoporos Rep*, 2017. **15**(4): p. 318-325.
8. Dimitriou, R., et al., *Bone regeneration: current concepts and future directions*. *BMC Med*, 2011. **9**: p. 66.
9. Claes, L., S. Recknagel, and A. Ignatius, *Fracture healing under healthy and inflammatory conditions*. *Nat Rev Rheumatol*, 2012. **8**(3): p. 133-43.
10. Schindeler, A., et al., *Bone remodeling during fracture repair: The cellular picture*. *Semin Cell Dev Biol*, 2008. **19**(5): p. 459-66.
11. Kolar, P., et al., *The early fracture hematoma and its potential role in fracture healing*. *Tissue Eng Part B Rev*, 2010. **16**(4): p. 427-34.
12. Kolar, P., et al., *Human early fracture hematoma is characterized by inflammation and hypoxia*. *Clin Orthop Relat Res*, 2011. **469**(11): p. 3118-26.
13. Einhorn, T.A. and L.C. Gerstenfeld, *Fracture healing: mechanisms and interventions*. *Nat Rev Rheumatol*, 2015. **11**(1): p. 45-54.
14. Hauser, C.J., et al., *The immune microenvironment of human fracture/soft-tissue hematomas and its relationship to systemic immunity*. *J Trauma*, 1997. **42**(5): p. 895-903; discussion 903-4.
15. Horst, K., et al., *Local inflammation in fracture hematoma: results from a combined trauma model in pigs*. *Mediators of inflammation*, 2015. **2015**: p. 126060-126060.
16. Schlundt, C., et al., *Macrophages in bone fracture healing: Their essential role in endochondral ossification*. *Bone*, 2015.
17. Schmidt-Bleek, K., et al., *Cellular composition of the initial fracture hematoma compared to a muscle hematoma: A study in sheep*. *Journal of Orthopaedic Research*, 2009. **27**(9): p. 1147-1151.
18. Gerstenfeld, L.C., et al., *Fracture healing as a post-natal developmental process: molecular, spatial, and temporal aspects of its regulation*. *J Cell Biochem*, 2003. **88**(5): p. 873-84.
19. Schmidt-Bleek, K., et al., *Inflammatory phase of bone healing initiates the regenerative healing cascade*. *Cell Tissue Res*, 2012. **347**(3): p. 567-73.
20. Lienau, J., et al., *Differential regulation of blood vessel formation between standard and delayed bone healing*. *J Orthop Res*, 2009. **27**(9): p. 1133-40.
21. Marsell, R. and T.A. Einhorn, *The biology of fracture healing*. *Injury*, 2011. **42**(6): p. 551-5.
22. Shapiro, F., *Bone development and its relation to fracture repair. The role of mesenchymal osteoblasts and surface osteoblasts*. *Eur Cell Mater*, 2008. **15**: p. 53-76.
23. Mackie, E.J., et al., *Endochondral ossification: how cartilage is converted into bone in the developing skeleton*. *Int J Biochem Cell Biol*, 2008. **40**(1): p. 46-62.

24. Gerstenfeld, L.C. and F.D. Shapiro, *Expression of bone-specific genes by hypertrophic chondrocytes: implication of the complex functions of the hypertrophic chondrocyte during endochondral bone development*. J Cell Biochem, 1996. **62**(1): p. 1-9.
25. Gawlitta, D., et al., *Modulating Endochondral Ossification of Multipotent Stromal Cells for Bone Regeneration*. Tissue Engineering Part B: Reviews, 2010. **16**(4): p. 385-395.
26. Nurminsky, D., et al., *Regulation of chondrocyte differentiation by actin-severing protein adseverin*. Dev Biol, 2007. **302**(2): p. 427-37.
27. Wilsman, N.J., et al., *Differential growth by growth plates as a function of multiple parameters of chondrocytic kinetics*. J Orthop Res, 1996. **14**(6): p. 927-36.
28. Schemitsch, E.H., *Size Matters: Defining Critical in Bone Defect Size!* J Orthop Trauma, 2017. **31 Suppl 5**: p. S20-s22.
29. Nauth, A., et al., *Managing bone defects*. J Orthop Trauma, 2011. **25**(8): p. 462-6.
30. Smith, B.T., et al., *Bone Tissue Engineering Challenges in Oral & Maxillofacial Surgery*. Adv Exp Med Biol, 2015. **881**: p. 57-78.
31. Giannoudis, P.V., H. Dinopoulos, and E. Tsiridis, *Bone substitutes: An update*. Injury, 2005. **36**(3, Supplement): p. S20-S27.
32. Van der Stok, J., et al., *Bone substitutes in the Netherlands - a systematic literature review*. Acta Biomater, 2011. **7**(2): p. 739-50.
33. Fernandez de Grado, G., et al., *Bone substitutes: a review of their characteristics, clinical use, and perspectives for large bone defects management*. J Tissue Eng, 2018. **9**: p. 2041731418776819.
34. Gómez-Barrena, E., et al., *Bone fracture healing: cell therapy in delayed unions and nonunions*. Bone, 2015. **70**: p. 93-101.
35. Gruskin, E., et al., *Deminerlized bone matrix in bone repair: History and use*. Advanced Drug Delivery Reviews, 2012. **64**(12): p. 1063-1077.
36. Albrektsson, T. and C. Johansson, *Osteoinduction, osteoconduction and osseointegration*. Eur Spine J, 2001. **10 Suppl 2**(Suppl 2): p. S96-101.
37. Markel, D.C., et al., *Characterization of the inflammatory response to four commercial bone graft substitutes using a murine biocompatibility model*. J Inflamm Res, 2012. **5**: p. 13-8.
38. Böstman, O. and H. Pihlajamäki, *Clinical biocompatibility of biodegradable orthopaedic implants for internal fixation: a review*. Biomaterials, 2000. **21**(24): p. 2615-2621.
39. van Dijk, L.A., et al., *MagnetOs, Vitoss, and Novabone in a Multi-endpoint Study of Posterolateral Fusion: A True Fusion or Not?* Clin Spine Surg, 2020.
40. van Dijk, L.A., et al., *Efficacy of a synthetic calcium phosphate with submicron surface topography as autograft extender in lapine posterolateral spinal fusion*. Journal of Biomedical Materials Research Part B: Applied Biomaterials, 2019. **107**(6): p. 2080-2090.
41. Orciani, M., et al., *Biofabrication and Bone Tissue Regeneration: Cell Source, Approaches, and Challenges*. Front Bioeng Biotechnol, 2017. **5**: p. 17.
42. Amini, A.R., C.T. Laurencin, and S.P. Nukavarapu, *Bone tissue engineering: recent advances and challenges*. Crit Rev Biomed Eng, 2012. **40**(5): p. 363-408.
43. Zhang, Y., et al., *An In Vitro Comparative Study of Multisource Derived Human Mesenchymal Stem Cells for Bone Tissue Engineering*. Stem Cells Dev, 2018. **27**(23): p. 1634-1645.
44. Paduano, F., et al., *Adipose Tissue as a Strategic Source of Mesenchymal Stem Cells in Bone Regeneration: A Topical Review on the Most Promising Craniomaxillofacial Applications*. International journal of molecular sciences, 2017. **18**(10): p. 2140.

45. Hattori, H., et al., *Bone formation using human adipose tissue-derived stromal cells and a biodegradable scaffold*. J Biomed Mater Res B Appl Biomater, 2006. **76**(1): p. 230-9.
46. Paino, F., et al., *Human DPSCs fabricate vascularized woven bone tissue: a new tool in bone tissue engineering*. Clin Sci (Lond), 2017. **131**(8): p. 699-713.
47. Wang, L., et al., *Musculoskeletal tissue engineering with human umbilical cord mesenchymal stromal cells*. Regen Med, 2011. **6**(1): p. 95-109.
48. Kim, S., et al., *In vivo bone formation from human embryonic stem cell-derived osteogenic cells in poly(d,l-lactic-co-glycolic acid)/hydroxyapatite composite scaffolds*. Biomaterials, 2008. **29**(8): p. 1043-53.
49. Bastami, F., et al., *Induced pluripotent stem cells as a new getaway for bone tissue engineering: A systematic review*. Cell Prolif, 2017. **50**(2).
50. Koolen, M., et al., *Complete regeneration of large bone defects in rats with commercially available fibrin loaded with BMP-2*. Eur Cell Mater, 2019. **38**: p. 94-105.
51. Mantripragada, V.P. and A.C. Jayasuriya, *Bone regeneration using injectable BMP-7 loaded chitosan microparticles in rat femoral defect*. Mater Sci Eng C Mater Biol Appl, 2016. **63**: p. 596-608.
52. García, J.R., A.Y. Clark, and A.J. García, *Integrin-specific hydrogels functionalized with VEGF for vascularization and bone regeneration of critical-size bone defects*. J Biomed Mater Res A, 2016. **104**(4): p. 889-900.
53. Mountziaris, P.M., et al., *Harnessing and modulating inflammation in strategies for bone regeneration*. Tissue Eng Part B Rev, 2011. **17**(6): p. 393-402.
54. Yuan, J., et al., *Repair of canine mandibular bone defects with bone marrow stromal cells and porous β -tricalcium phosphate*. Biomaterials, 2007. **28**(6): p. 1005-1013.
55. Ye, X., et al., *Ectopic Bone Regeneration by Human Bone Marrow Mononucleated Cells, Undifferentiated and Osteogenically Differentiated Bone Marrow Mesenchymal Stem Cells in Beta-Tricalcium Phosphate Scaffolds*. Tissue Engineering Part C: Methods, 2012. **18**(7): p. 545-556.
56. Thompson, E.M., et al., *Recapitulating endochondral ossification: a promising route to in vivo bone regeneration*. J Tissue Eng Regen Med, 2015. **9**(8): p. 889-902.
57. Nguyen, L.H., et al., *Vascularized bone tissue engineering: approaches for potential improvement*. Tissue Eng Part B Rev, 2012. **18**(5): p. 363-82.
58. Lyons, F.G., et al., *The healing of bony defects by cell-free collagen-based scaffolds compared to stem cell-seeded tissue engineered constructs*. Biomaterials, 2010. **31**(35): p. 9232-9243.
59. Klotz, B.J., et al., *Engineering of a complex bone tissue model with endothelialised channels and capillary-like networks*. Eur Cell Mater, 2018. **35**: p. 335-348.
60. Pennings, I., et al., *Effect of donor variation on osteogenesis and vasculogenesis in hydrogel cocultures*. Journal of tissue engineering and regenerative medicine, 2019. **13**(3): p. 433-445.
61. Thompson, E.M., et al., *An Endochondral Ossification-Based Approach to Bone Repair: Chondrogenically Primed Mesenchymal Stem Cell-Laden Scaffolds Support Greater Repair of Critical-Sized Cranial Defects Than Osteogenically Stimulated Constructs In Vivo*. Tissue Eng Part A, 2016. **22**(5-6): p. 556-67.
62. Scotti, C., et al., *Recapitulation of endochondral bone formation using human adult mesenchymal stem cells as a paradigm for developmental engineering*. Proc Natl Acad Sci U S A, 2010. **107**(16): p. 7251-6.
63. Jukes, J.M., et al., *Endochondral bone tissue engineering using embryonic stem cells*. Proc Natl Acad Sci U S A, 2008. **105**(19): p. 6840-5.

64. Doan, L., et al., *Engineered cartilage heals skull defects*. American journal of orthodontics and dentofacial orthopedics : official publication of the American Association of Orthodontists, its constituent societies, and the American Board of Orthodontics, 2010. **137**(2): p. 162.e1-163.
65. Osinga, R., et al., *Generation of a Bone Organ by Human Adipose-Derived Stromal Cells Through Endochondral Ossification*. Stem Cells Transl Med, 2016. **5**(8): p. 1090-7.
66. Epple, C., et al., *Prefabrication of a large pedicled bone graft by engineering the germ for de novo vascularization and osteoinduction*. Biomaterials, 2019. **192**: p. 118-127.
67. Nilsson Hall, G., et al., *Developmentally Engineered Callus Organoid Bioassemblies Exhibit Predictive In Vivo Long Bone Healing*. Advanced Science, 2020. **7**(2): p. 1902295.
68. Matsiko, A., et al., *An endochondral ossification approach to early stage bone repair: Use of tissue-engineered hypertrophic cartilage constructs as primordial templates for weight-bearing bone repair*. Journal of Tissue Engineering and Regenerative Medicine, 2018. **12**(4): p. e2147-e2150.
69. van der Stok, J., et al., *Chondrogenically differentiated mesenchymal stromal cell pellets stimulate endochondral bone regeneration in critical-sized bone defects*. Eur Cell Mater, 2014. **27**: p. 137-48; discussion 148.
70. Harada, N., et al., *Bone regeneration in a massive rat femur defect through endochondral ossification achieved with chondrogenically differentiated MSCs in a degradable scaffold*. Biomaterials, 2014. **35**(27): p. 7800-10.
71. Scotti, C., et al., *Engineering of a functional bone organ through endochondral ossification*. Proc Natl Acad Sci U S A, 2013. **110**(10): p. 3997-4002.
72. McDermott, A.M., et al., *Recapitulating bone development through engineered mesenchymal condensations and mechanical cues for tissue regeneration*. Science Translational Medicine, 2019. **11**(495): p. eaav7756.
73. Pittenger, M.F., et al., *Multilineage potential of adult human mesenchymal stem cells*. Science, 1999. **284**(5411): p. 143-7.
74. Pelttari, K., et al., *Premature induction of hypertrophy during in vitro chondrogenesis of human mesenchymal stem cells correlates with calcification and vascular invasion after ectopic transplantation in SCID mice*. Arthritis Rheum, 2006. **54**(10): p. 3254-66.
75. Coyle, C.H., N.J. Izzo, and C.R. Chu, *Sustained hypoxia enhances chondrocyte matrix synthesis*. J Orthop Res, 2009. **27**(6): p. 793-9.
76. Farrell, E., et al., *In-vivo generation of bone via endochondral ossification by in-vitro chondrogenic priming of adult human and rat mesenchymal stem cells*. BMC Musculoskelet Disord, 2011. **12**: p. 31.
77. Farrell, E., et al., *Chondrogenic priming of human bone marrow stromal cells: a better route to bone repair?* Tissue Eng Part C Methods, 2009. **15**(2): p. 285-95.
78. Dennis, S.C., et al., *Endochondral ossification for enhancing bone regeneration: converging native extracellular matrix biomaterials and developmental engineering in vivo*. Tissue engineering. Part B, Reviews, 2015. **21**(3): p. 247-266.
79. Bernhard, J., et al., *Tissue-engineered hypertrophic chondrocyte grafts enhanced long bone repair*. Biomaterials, 2017. **139**: p. 202-212.
80. Visser, J., et al., *Endochondral bone formation in gelatin methacrylamide hydrogel with embedded cartilage-derived matrix particles*. Biomaterials, 2015. **37**: p. 174-82.
81. Knuth, C.A., et al., *Mesenchymal stem cell-mediated endochondral ossification utilising micropellets and brief chondrogenic priming*. Eur Cell Mater, 2017. **34**: p. 142-161.

82. Daly, A.C., et al., *3D printed microchannel networks to direct vascularisation during endochondral bone repair*. *Biomaterials*, 2018. **162**: p. 34-46.
83. Freeman, F.E. and L.M. McNamara, *Endochondral Priming: A Developmental Engineering Strategy for Bone Tissue Regeneration*. *Tissue Eng Part B Rev*, 2017. **23**(2): p. 128-141.
84. Yang, W., et al., *Effects of in vitro chondrogenic priming time of bone-marrow-derived mesenchymal stromal cells on in vivo endochondral bone formation*. *Acta Biomater*, 2015. **13**: p. 254-65.
85. Sheehy, E.J., D.J. Kelly, and F.J. O'Brien, *Biomaterial-based endochondral bone regeneration: a shift from traditional tissue engineering paradigms to developmentally inspired strategies*. *Materials Today Bio*, 2019. **3**: p. 100009.
86. Sheehy, E.J., et al., *Engineering cartilage or endochondral bone: a comparison of different naturally derived hydrogels*. *Acta Biomater*, 2015. **13**: p. 245-53.
87. Sivasubramanian, K., et al., *Bone Marrow-Harvesting Technique Influences Functional Heterogeneity of Mesenchymal Stem/Stromal Cells and Cartilage Regeneration*. *Am J Sports Med*, 2018. **46**(14): p. 3521-3531.
88. Payne, K.A., D.M. Didiano, and C.R. Chu, *Donor sex and age influence the chondrogenic potential of human femoral bone marrow stem cells*. *Osteoarthritis Cartilage*, 2010. **18**(5): p. 705-13.
89. Gawlitta, D., et al., *Hypoxia impedes hypertrophic chondrogenesis of human multipotent stromal cells*. *Tissue Eng Part A*, 2012. **18**(19-20): p. 1957-66.
90. Kim, M., et al., *Donor Variation and Optimization of Human Mesenchymal Stem Cell Chondrogenesis in Hyaluronic Acid*. *Tissue Eng Part A*, 2018. **24**(21-22): p. 1693-1703.
91. Narcisi, R., et al., *Long-term expansion, enhanced chondrogenic potential, and suppression of endochondral ossification of adult human MSCs via WNT signaling modulation*. *Stem Cell Reports*, 2015. **4**(3): p. 459-72.
92. Solchaga, L.A., et al., *Fibroblast Growth Factor-2 Enhances Proliferation and Delays Loss of Chondrogenic Potential in Human Adult Bone-Marrow-Derived Mesenchymal Stem Cells*. *Tissue Engineering Part A*, 2009. **16**(3): p. 1009-1019.
93. Kiernan, C.H., et al., *The immune response to allogeneic differentiated mesenchymal stem cells in the context of bone tissue engineering*. *Tissue Eng Part B Rev*, 2017.
94. Kiernan, C.H., et al., *Allogeneic chondrogenically differentiated human mesenchymal stromal cells do not induce immunogenic responses from T lymphocytes in vitro*. *Cytotherapy*, 2016. **18**(8): p. 957-69.
95. Todorov, A., et al., *Fat-Derived Stromal Vascular Fraction Cells Enhance the Bone-Forming Capacity of Devitalized Engineered Hypertrophic Cartilage Matrix*. *Stem Cells Transl Med*, 2016. **5**(12): p. 1684-1694.
96. Chatterjea, A., et al., *Suppression of the immune system as a critical step for bone formation from allogeneic osteoprogenitors implanted in rats*. *J Cell Mol Med*, 2014. **18**(1): p. 134-42.
97. Lohan, P., et al., *Changes in immunological profile of allogeneic mesenchymal stem cells after differentiation: should we be concerned?* *Stem Cell Res Ther*, 2014. **5**(4): p. 99.
98. Ryan, A.E., et al., *Chondrogenic differentiation increases antidonor immune response to allogeneic mesenchymal stem cell transplantation*. *Mol Ther*, 2014. **22**(3): p. 655-67.
99. English, K., *Mechanisms of mesenchymal stromal cell immunomodulation*. *Immunol Cell Biol*, 2013. **91**(1): p. 19-26.
100. Faiella, W. and R. Atoui, *Immunotolerant Properties of Mesenchymal Stem Cells: Updated Review*. *Stem Cells International*, 2016. **2016**: p. 7.

101. Ankrum, J.A., J.F. Ong, and J.M. Karp, *Mesenchymal stem cells: immune evasive, not immune privileged*. *Nat Biotechnol*, 2014. **32**(3): p. 252-60.
102. Le Blanc, K., et al., *HLA expression and immunologic properties of differentiated and undifferentiated mesenchymal stem cells*. *Exp Hematol*, 2003. **31**(10): p. 890-6.
103. Gawlitta, D., et al., *Decellularized cartilage-derived matrix as substrate for endochondral bone regeneration*. *Tissue Eng Part A*, 2015. **21**(3-4): p. 694-703.
104. Cunniffe, G.M., et al., *Porous decellularized tissue engineered hypertrophic cartilage as a scaffold for large bone defect healing*. *Acta Biomaterialia*, 2015. **23**: p. 82-90.
105. Bourguine, P.E., et al., *Osteoinductivity of engineered cartilaginous templates devitalized by inducible apoptosis*. *Proceedings of the National Academy of Sciences of the United States of America*, 2014. **111**(49): p. 17426-17431.
106. Sutherland, A.J., et al., *The bioactivity of cartilage extracellular matrix in articular cartilage regeneration*. *Advanced healthcare materials*, 2015. **4**(1): p. 29-39.
107. Londono, R., et al., *The effect of cell debris within biologic scaffolds upon the macrophage response*. *Journal of biomedical materials research. Part A*, 2017. **105**(8): p. 2109-2118.
108. Keane, T.J. and S.F. Badylak, *The host response to allogeneic and xenogeneic biological scaffold materials*. *Journal of tissue engineering and regenerative medicine*, 2015. **9**(5): p. 504-511.
109. Quang Le, B., C. Van Blitterswijk, and J. De Boer, *An Approach to In Vitro Manufacturing of Hypertrophic Cartilage Matrix for Bone Repair*. *Bioengineering (Basel, Switzerland)*, 2017. **4**(2): p. 35.
110. Beck, E.C., et al., *Chondroinduction from Naturally Derived Cartilage Matrix: A Comparison Between Devitalized and Decellularized Cartilage Encapsulated in Hydrogel Pastes*. *Tissue engineering. Part A*, 2016. **22**(7-8): p. 665-679.
111. Utomo, L., et al., *Preparation and characterization of a decellularized cartilage scaffold for ear cartilage reconstruction*. *Biomedical materials (Bristol, England)*, 2015. **10**(1): p. 015010-015010.
112. Sutherland, A.J., et al., *Decellularized cartilage may be a chondroinductive material for osteochondral tissue engineering*. *PLoS one*, 2015. **10**(5): p. e0121966-e0121966.
113. Vas, W.J., et al., *Decellularized Cartilage Directs Chondrogenic Differentiation: Creation of a Fracture Callus Mimetic*. *Tissue Engineering Part A*, 2018. **24**(17-18): p. 1364-1376.
114. Perry, J.M., et al., *Matrix Reloaded: Devitalized Cartilage as a Functional Extracellular Niche to Promote Osteogenesis and Angiogenesis*. *The FASEB Journal*, 2016. **30**(1_supplement): p. 9.2-9.2.
115. Zhang, W., et al., *Multilineage differentiation potential of stem cells derived from human dental pulp after cryopreservation*. *Tissue Eng*, 2006. **12**(10): p. 2813-23.
116. Hilkens, P., et al., *Effect of isolation methodology on stem cell properties and multilineage differentiation potential of human dental pulp stem cells*. *Cell Tissue Res*, 2013. **353**(1): p. 65-78.
117. Gronthos, S., et al., *Postnatal human dental pulp stem cells (DPSCs) in vitro and in vivo*. *Proc Natl Acad Sci U S A*, 2000. **97**(25): p. 13625-30.
118. Anitua, E., M. Troya, and M. Zaldueño, *Progress in the use of dental pulp stem cells in regenerative medicine*. *Cytotherapy*, 2018. **20**(4): p. 479-498.
119. Graziano, A., et al., *Dental pulp stem cells: a promising tool for bone regeneration*. *Stem Cell Rev*, 2008. **4**(1): p. 21-6.

120. Kruijt Spanjer, E.C., et al., *Taking the endochondral route to craniomaxillofacial bone regeneration: A logical approach?* J Craniomaxillofac Surg, 2017. **45**(7): p. 1099-1106.
121. Tirino, V., et al., *Identification, isolation, characterization, and banking of human dental pulp stem cells.* Methods Mol Biol, 2012. **879**: p. 443-63.
122. Tamaki, Y., et al., *In vitro analysis of mesenchymal stem cells derived from human teeth and bone marrow.* Odontology, 2013. **101**(2): p. 121-32.
123. Ponnaiyan, D. and V. Jegadeesan, *Comparison of phenotype and differentiation marker gene expression profiles in human dental pulp and bone marrow mesenchymal stem cells.* Eur J Dent, 2014. **8**(3): p. 307-13.
124. Alge, D.L., et al., *Donor-matched comparison of dental pulp stem cells and bone marrow-derived mesenchymal stem cells in a rat model.* J Tissue Eng Regen Med, 2010. **4**(1): p. 73-81.
125. Takebe, Y., et al., *Cryopreservation Method for the Effective Collection of Dental Pulp Stem Cells.* Tissue Eng Part C Methods, 2017. **23**(5): p. 251-261.
126. Nuti, N., et al., *Multipotent Differentiation of Human Dental Pulp Stem Cells: a Literature Review.* Stem Cell Reviews and Reports, 2016. **12**(5): p. 511-523.
127. Morad, G., L. Kheiri, and A. Khojasteh, *Dental pulp stem cells for in vivo bone regeneration: a systematic review of literature.* Arch Oral Biol, 2013. **58**(12): p. 1818-27.
128. La Noce, M., et al., *Cytoplasmic Interactions between the Glucocorticoid Receptor and HDAC2 Regulate Osteocalcin Expression in VPA-Treated MSCs.* Cells, 2019. **8**(3): p. 217.
129. Koyama, N., et al., *Evaluation of pluripotency in human dental pulp cells.* J Oral Maxillofac Surg, 2009. **67**(3): p. 501-6.
130. Mokry, J., et al., *Telomere attrition occurs during ex vivo expansion of human dental pulp stem cells.* J Biomed Biotechnol, 2010. **2010**: p. 673513.
131. Grottkau, B.E., P.P. Purudappa, and Y.F. Lin, *Multilineage differentiation of dental pulp stem cells from green fluorescent protein transgenic mice.* Int J Oral Sci, 2010. **2**(1): p. 21-7.
132. Iohara, K., et al., *Side population cells isolated from porcine dental pulp tissue with self-renewal and multipotency for dentinogenesis, chondrogenesis, adipogenesis, and neurogenesis.* Stem Cells, 2006. **24**(11): p. 2493-503.
133. Chai, Y., et al., *Fate of the mammalian cranial neural crest during tooth and mandibular morphogenesis.* Development, 2000. **127**(8): p. 1671-9.
134. Sophia Fox, A.J., A. Bedi, and S.A. Rodeo, *The basic science of articular cartilage: structure, composition, and function.* Sports Health, 2009. **1**(6): p. 461-8.
135. Allen, K.D. and K.A. Athanasiou, *Tissue Engineering of the TMJ disc: a review.* Tissue Eng, 2006. **12**(5): p. 1183-96.
136. Pierdomenico, L., et al., *Multipotent Mesenchymal Stem Cells with Immunosuppressive Activity Can Be Easily Isolated from Dental Pulp.* Transplantation, 2005. **80**(6): p. 836-842.
137. Sternberg, H., et al., *A human embryonic stem cell-derived clonal progenitor cell line with chondrogenic potential and markers of craniofacial mesenchyme.* Regen Med, 2012. **7**(4): p. 481-501.
138. Spath, L., et al., *Explant-derived human dental pulp stem cells enhance differentiation and proliferation potentials.* J Cell Mol Med, 2010. **14**(6b): p. 1635-44.
139. Nemeth, C.L., et al., *Enhanced chondrogenic differentiation of dental pulp stem cells using nanopatterned PEG-GelMA-HA hydrogels.* Tissue Eng Part A, 2014. **20**(21-22): p. 2817-29.
140. Pereira, L.O., et al., *Comparison of stem cell properties of cells isolated from normal and inflamed dental pulps.* Int Endod J, 2012. **45**(12): p. 1080-90.

141. Alvarez, R., et al., *Single CD271 marker isolates mesenchymal stem cells from human dental pulp*. *Int J Oral Sci*, 2015. **7**(4): p. 205-12.
142. Yoo, J.U., et al., *The chondrogenic potential of human bone-marrow-derived mesenchymal progenitor cells*. *J Bone Joint Surg Am*, 1998. **80**(12): p. 1745-57.
143. Caron, M.M., et al., *Redifferentiation of dedifferentiated human articular chondrocytes: comparison of 2D and 3D cultures*. *Osteoarthritis Cartilage*, 2012. **20**(10): p. 1170-8.
144. Puetzer, J.L., J.N. Petite, and E.G. Lobo, *Comparative review of growth factors for induction of three-dimensional in vitro chondrogenesis in human mesenchymal stem cells isolated from bone marrow and adipose tissue*. *Tissue Eng Part B Rev*, 2010. **16**(4): p. 435-44.
145. Collignon, A.M., et al., *Mouse Wnt1-CRE-Rosa(Tomato) Dental Pulp Stem Cells Directly Contribute to the Calvarial Bone Regeneration Process*. *Stem Cells*, 2019. **37**(5): p. 701-711.
146. Farndale, R.W., D.J. Buttle, and A.J. Barrett, *Improved quantitation and discrimination of sulphated glycosaminoglycans by use of dimethylmethylene blue*. *Biochim Biophys Acta*, 1986. **883**(2): p. 173-7.
147. Liu, Y., A. Beyer, and R. Aebersold, *On the Dependency of Cellular Protein Levels on mRNA Abundance*. *Cell*, 2016. **165**(3): p. 535-50.
148. Vogel, C. and E.M. Marcotte, *Insights into the regulation of protein abundance from proteomic and transcriptomic analyses*. *Nature reviews. Genetics*, 2012. **13**(4): p. 227-232.
149. Isobe, Y., et al., *Comparison of human mesenchymal stem cells derived from bone marrow, synovial fluid, adult dental pulp, and exfoliated deciduous tooth pulp*. *Int J Oral Maxillofac Surg*, 2016. **45**(1): p. 124-31.
150. Bousnaki, M., et al., *Fibro/chondrogenic differentiation of dental stem cells into chitosan/alginate scaffolds towards temporomandibular joint disc regeneration*. *J Mater Sci Mater Med*, 2018. **29**(7): p. 97.
151. Mata, M., et al., *In Vivo Articular Cartilage Regeneration Using Human Dental Pulp Stem Cells Cultured in an Alginate Scaffold: A Preliminary Study*. *Stem Cells Int*, 2017. **2017**: p. 8309256.
152. Rizk, A. and A.B. Rabie, *Human dental pulp stem cells expressing transforming growth factor beta3 transgene for cartilage-like tissue engineering*. *Cytotherapy*, 2013. **15**(6): p. 712-25.
153. Dai, J., et al., *The effect of co-culturing costal chondrocytes and dental pulp stem cells combined with exogenous FGF9 protein on chondrogenesis and ossification in engineered cartilage*. *Biomaterials*, 2012. **33**(31): p. 7699-711.
154. Vater, C., P. Kasten, and M. Stiehler, *Culture media for the differentiation of mesenchymal stromal cells*. *Acta Biomater*, 2011. **7**(2): p. 463-77.
155. Wang, Y., et al., *Enhanced BMP signaling prevents degeneration and leads to endochondral ossification of Meckel's cartilage in mice*. *Dev Biol*, 2013. **381**(2): p. 301-11.
156. Stocum, D.L. and W.E. Roberts, *Part I: Development and Physiology of the Temporomandibular Joint*. *Curr Osteoporos Rep*, 2018. **16**(4): p. 360-368.
157. Indrawattana, N., et al., *Growth factor combination for chondrogenic induction from human mesenchymal stem cell*. *Biochem Biophys Res Commun*, 2004. **320**(3): p. 914-9.
158. Shen, B., et al., *BMP-2 enhances TGF-beta3-mediated chondrogenic differentiation of human bone marrow multipotent mesenchymal stromal cells in alginate bead culture*. *Tissue Eng Part A*, 2009. **15**(6): p. 1311-20.
159. Shen, B., et al., *The role of BMP-7 in chondrogenic and osteogenic differentiation of human bone marrow multipotent mesenchymal stromal cells in vitro*. *J Cell Biochem*, 2010. **109**(2): p. 406-16.

160. Sivasubramaniyan, K., et al., *Cell-surface markers identify tissue resident multipotential stem/stromal cell subsets in synovial intimal and sub-intimal compartments with distinct chondrogenic properties*. Osteoarthritis and Cartilage, 2019.
161. Falguni, P., et al., *Printing three-dimensional tissue analogues with decellularized extracellular matrix bioink*. Nature Communications, 2014. **5**.
162. Badylak, S.F., D.O. Freytes, and T.W. Gilbert, *Extracellular matrix as a biological scaffold material: Structure and function*. Acta Biomater, 2009. **5**(1): p. 1-13.
163. Brown, B.N., et al., *Comparison of three methods for the derivation of a biologic scaffold composed of adipose tissue extracellular matrix*. Tissue Eng Part C Methods, 2011. **17**(4): p. 411-21.
164. Cheng, C.W., L.D. Solorio, and E. Alsberg, *Decellularized tissue and cell-derived extracellular matrices as scaffolds for orthopaedic tissue engineering*. Biotechnology advances, 2014. **32**(2): p. 462-484.
165. Fitzpatrick, L.E. and T.C. McDevitt, *Cell-derived matrices for tissue engineering and regenerative medicine applications(1)*. Biomaterials science, 2015. **3**(1): p. 12-24.
166. Benders, K.E.M., et al., *Extracellular matrix scaffolds for cartilage and bone regeneration*. Trends in Biotechnology, 2013. **31**(3): p. 169-176.
167. Crapo, P.M., T.W. Gilbert, and S.F. Badylak, *An overview of tissue and whole organ decellularization processes*. Biomaterials, 2011. **32**(12): p. 3233-3243.
168. Schwarz, S., et al., *Decellularized Cartilage Matrix as a Novel Biomatrix for Cartilage Tissue-Engineering Applications*. Tissue Engineering Part A, 2012. **18**(21-22): p. 2195-2209.
169. Stapleton, T.W., et al., *Development and characterization of an acellular porcine medial meniscus for use in tissue engineering*. Tissue Eng Part A, 2008. **14**(4): p. 505-18.
170. Visser, J., et al., *Crosslinkable Hydrogels Derived from Cartilage, Meniscus, and Tendon Tissue*. Tissue Engineering Part A, 2015. **21**(7-8): p. 1195-1206.
171. Garreta, E., et al., *Tissue engineering by decellularization and 3D bioprinting*. Materials Today, 2017. **20**(4): p. 166-178.
172. Ghanavi, P., M. Kabiri, and M.R. Doran, *The rationale for using microscopic units of a donor matrix in cartilage defect repair*. Cell Tissue Res, 2012. **347**(3): p. 643-8.
173. Sutherland, A.J., et al., *Decellularized Cartilage May Be a Chondroinductive Material for Osteochondral Tissue Engineering*. PLoS ONE, 2015. **10**(5): p. e0121966.
174. Sutherland, A.J., et al., *The bioactivity of cartilage extracellular matrix in articular cartilage regeneration*. Adv Healthc Mater, 2015. **4**(1): p. 29-39.
175. Elder, B.D., D.H. Kim, and K.A. Athanasiou, *Developing an articular cartilage decellularization process toward facet joint cartilage replacement*. Neurosurgery, 2010. **66**(4): p. 722-7; discussion 727.
176. Pearle, A.D., R.F. Warren, and S.A. Rodeo, *Basic science of articular cartilage and osteoarthritis*. Clinics in Sports Medicine, 2005. **24**(1): p. 1-12.
177. Vega, S.L., M.Y. Kwon, and J.A. Burdick, *Recent advances in hydrogels for cartilage tissue engineering*. Eur Cell Mater, 2017. **33**: p. 59-75.
178. Elder, B.D., S.V. Eleswarapu, and K.A. Athanasiou, *Extraction techniques for the decellularization of tissue engineered articular cartilage constructs*. Biomaterials, 2009. **30**(22): p. 3749-56.
179. Stocco, E., et al., *Tailored PVA/ECM scaffolds for cartilage regeneration*. Biomed Res Int, 2014. **2014**: p. 762189.

180. Levorson, E.J., et al., *Cell-derived polymer/extracellular matrix composite scaffolds for cartilage regeneration, Part 2: construct devitalization and determination of chondroinductive capacity*. Tissue Eng Part C Methods, 2014. **20**(4): p. 358-72.
181. Stone, K.R., et al., *Porcine and bovine cartilage transplants in cynomolgus monkey: I. A model for chronic xenograft rejection*. Transplantation, 1997. **63**(5): p. 640-5.
182. Revell, C.M. and K.A. Athanasiou, *Success rates and immunologic responses of autogenic, allogenic, and xenogenic treatments to repair articular cartilage defects*. Tissue Eng Part B Rev, 2009. **15**(1): p. 1-15.
183. Keane, T.J., et al., *Consequences of ineffective decellularization of biologic scaffolds on the host response*. Biomaterials, 2012. **33**(6): p. 1771-1781.
184. Brown, B.N., et al., *Macrophage phenotype and remodeling outcomes in response to biologic scaffolds with and without a cellular component*. Biomaterials, 2009. **30**(8): p. 1482-91.
185. Sophia Fox, A.J., A. Bedi, and S.A. Rodeo, *The Basic Science of Articular Cartilage: Structure, Composition, and Function*. Sports Health, 2009. **1**(6): p. 461-468.
186. Bishop, P., *The biochemical structure of mammalian vitreous*. Eye (Lond), 1996. **10 (Pt 6)**: p. 664-70.
187. Le Goff, M.M. and P.N. Bishop, *Adult vitreous structure and postnatal changes*. Eye (Lond), 2008. **22**(10): p. 1214-22.
188. Bishop, P.N., *Structural macromolecules and supramolecular organisation of the vitreous gel*. Prog Retin Eye Res, 2000. **19**(3): p. 323-44.
189. Donati, S., et al., *Vitreous Substitutes: The Present and the Future*. BioMed Research International, 2014. **2014**: p. 12.
190. Bishop, P.N., et al., *Extraction and characterization of the tissue forms of collagen types II and IX from bovine vitreous*. Biochem J, 1994. **299 (Pt 2)**: p. 497-505.
191. Goel, M., et al., *Aqueous humor dynamics: a review*. Open Ophthalmol J, 2010. **4**: p. 52-9.
192. Ulrich, J.N., et al., *Components of the fibrinolytic system in the vitreous body in patients with vitreoretinal disorders*. Clinical & Experimental Ophthalmology, 2008. **36**(5): p. 431-436.
193. Meyer, K. and J.W. Palmer, *The Polysaccharide Of The Vitreous Humor*. Journal of Biological Chemistry, 1934. **107**(3): p. 629-634.
194. Murthy, K.R., et al., *Proteomic analysis of human vitreous humor*. Clin Proteomics, 2014. **11**(1): p. 29.
195. Burdick, J.A. and G.D. Prestwich, *Hyaluronic Acid Hydrogels for Biomedical Applications*. Advanced materials (Deerfield Beach, Fla.), 2011. **23**(12): p. H41-H56.
196. Kim, I.L., R.L. Mauck, and J.A. Burdick, *Hydrogel design for cartilage tissue engineering: a case study with hyaluronic acid*. Biomaterials, 2011. **32**(34): p. 8771-82.
197. Sze, J.H., J.C. Brownlie, and C.A. Love, *Biotechnological production of hyaluronic acid: a mini review*. 3 Biotech, 2016. **6**(1): p. 67.
198. Egger, S.F., et al., *Bacterial Growth in Human Vitreous Humor*. Experimental Eye Research, 1997. **65**(6): p. 791-795.
199. Davey, P., M. Barza, and C. Peckman, *Spontaneous inhibition of bacterial growth in experimental gram-negative endophthalmitis*. Invest Ophthalmol Vis Sci, 1987. **28**(5): p. 867-73.
200. Hanashima, C. and H. Namiki, *Reduced viability of vascular endothelial cells by high concentration of ascorbic acid in vitreous humor*. Cell Biol Int, 1999. **23**(4): p. 287-98.
201. Yang, J., et al., *Vitreous humor and albumin augment the proliferation of cultured retinal precursor cells*. J Neurosci Res, 2009. **87**(2): p. 495-502.

202. Luty, G.A., et al., *Regulation of cell growth by vitreous humour*. J Cell Sci, 1985. **76**: p. 53-65.
203. Varshochian, R., et al., *Albuminated PLGA nanoparticles containing bevacizumab intended for ocular neovascularization treatment*. J Biomed Mater Res A, 2015. **103**(10): p. 3148-56.
204. Mohammadpour, M., et al., *Penetration of silicate nanoparticles into the corneal stroma and intraocular fluids*. Cornea, 2014. **33**(7): p. 738-43.
205. Abdallah, W., et al., *Vitreous oxygenation in retinal ischemia reperfusion*. Invest Ophthalmol Vis Sci, 2011. **52**(2): p. 1035-42.
206. Uesugi, K., et al., *A Self-Assembling Peptide Gel as a Vitreous Substitute: A Rabbit Study*. Invest Ophthalmol Vis Sci, 2017. **58**(10): p. 4068-4075.
207. Nishikawa, Y., et al., *A comparison of sex steroid concentration levels in the vitreous and serum of patients with vitreoretinal diseases*. PLoS One, 2017. **12**(7): p. e0180933.
208. Tracy, C.J., et al., *Intravitreal Implantation of Genetically Modified Autologous Bone Marrow-Derived Stem Cells for Treating Retinal Disorders*. Adv Exp Med Biol, 2016. **854**: p. 571-7.
209. Becker, S., et al., *Allogeneic Transplantation of Muller-Derived Retinal Ganglion Cells Improves Retinal Function in a Feline Model of Ganglion Cell Depletion*. Stem Cells Transl Med, 2016. **5**(2): p. 192-205.
210. Mesentier-Louro, L.A., et al., *Distribution of mesenchymal stem cells and effects on neuronal survival and axon regeneration after optic nerve crush and cell therapy*. PLoS One, 2014. **9**(10): p. e110722.
211. Balaiya, S., et al., *Growth factors/chemokines in diabetic vitreous and aqueous alter the function of bone marrow-derived progenitor (CD34+) cells in humans*. Am J Physiol Endocrinol Metab, 2014. **307**(8): p. E695-702.
212. Liu, Z., G. Fu, and A. Liu, *The relationship between inflammatory mediator expression in the aqueous humor and secondary glaucoma incidence after silicone oil tamponade*. Exp Ther Med, 2017. **14**(6): p. 5833-5836.
213. Dick, J., et al., *Postoperative Tropheryma whipplei endophthalmitis - a case report highlighting the additive value of molecular testing*. JMM Case Rep, 2017. **4**(10): p. e005124.
214. Boss, J.D., et al., *Assessment of Neurotrophins and Inflammatory Mediators in Vitreous of Patients With Diabetic Retinopathy*. Invest Ophthalmol Vis Sci, 2017. **58**(12): p. 5594-5603.
215. Foster, W.J., *Vitreous Substitutes*. Expert review of ophthalmology, 2008. **3**(2): p. 211-218.
216. Schon, B., et al., *Validation of a high-throughput microtissue fabrication process for 3D assembly of tissue engineered cartilage constructs*. Cell and Tissue Research, 2012. **347**(3): p. 629-642.
217. Brown, G.C.J., et al., *Covalent Incorporation of Heparin Improves Chondrogenesis in Photocurable Gelatin-Methacryloyl Hydrogels*. Macromolecular Bioscience: p. 1700158.
218. Abbadessa, A., et al., *A Synthetic Thermosensitive Hydrogel for Cartilage Bioprinting and Its Biofunctionalization with Polysaccharides*. Biomacromolecules, 2016. **17**(6): p. 2137-47.
219. Matheson, L.A., R.S. Labow, and J.P. Santerre, *Biodegradation of polycarbonate-based polyurethanes by the human monocytes-derived macrophage and U937 cell systems*. J Biomed Mater Res, 2002. **61**(4): p. 505-13.
220. Passmore, J.S., P.T. Lukey, and S.R. Ress, *The human macrophage cell line U937 as an in vitro model for selective evaluation of mycobacterial antigen-specific cytotoxic T-cell function*. Immunology, 2001. **102**(2): p. 146-56.
221. Dini, L., et al., *In vitro study of the interaction of polyalkilimide and polyvinyl alcohol hydrogels with cells*. Tissue Cell, 2005. **37**(6): p. 479-87.

222. Wang, C.X., et al., *High-speed compression of single alginate microspheres*. Chemical Engineering Science, 2005. **60**(23): p. 6649-6657.
223. Hertz, H., *Ueber die Berührung fester elastischer Körper*. Journal für die Reine und Angewandte Mathematik, 1882. **1882**(92): p. 156-171.
224. Jin, H. and J.L. Lewis, *Determination of Poisson's ratio of articular cartilage by indentation using different-sized indenters*. J Biomech Eng, 2004. **126**(2): p. 138-45.
225. Woodfield, T.B., et al., *Scaffolds for tissue engineering of cartilage*. Crit Rev Eukaryot Gene Expr, 2002. **12**(3): p. 209-36.
226. Beck, E.C., et al., *Chondroinduction from Naturally Derived Cartilage Matrix: A Comparison Between Devitalized and Decellularized Cartilage Encapsulated in Hydrogel Pastes*. Tissue Eng Part A, 2016. **22**(7-8): p. 665-79.
227. Bruyneel, A.A.N. and C.A. Carr, *Ambiguity in the Presentation of Decellularized Tissue Composition: The Need for Standardized Approaches*. Artificial Organs, 2016.
228. Morgan, C.R., F. Magnotta, and A.D. Ketley, *Thiol/ene photocurable polymers*. Journal of Polymer Science: Polymer Chemistry Edition, 1977. **15**(3): p. 627-645.
229. Bruyneel, A.A.N. and C.A. Carr, *Ambiguity in the Presentation of Decellularized Tissue Composition: The Need for Standardized Approaches*. Artificial Organs, 2017. **41**(8): p. 778-784.
230. Swann, D.A., *Chemistry and biology of the vitreous body*. Int Rev Exp Pathol, 1980. **22**: p. 1-64.
231. Snowden, J.M., D.R. Eyre, and D.A. Swann, *Vitreous structure. VI. Age-related changes in the thermal stability and crosslinks of vitreous, articular cartilage and tendon collagens*. Biochim Biophys Acta, 1982. **706**(2): p. 153-7.
232. Bos, K.J., et al., *Axial structure of the heterotypic collagen fibrils of vitreous humour and cartilage*. Journal of Molecular Biology, 2001. **306**(5): p. 1011-1022.
233. Brewton, R.G., D.W. Wright, and R. Mayne, *Structural and functional comparison of type IX collagen-proteoglycan from chicken cartilage and vitreous humor*. J Biol Chem, 1991. **266**(8): p. 4752-7.
234. Braga-Vilela, A.S., et al., *Extracellular matrix of porcine pericardium: biochemistry and collagen architecture*. J Membr Biol, 2008. **221**(1): p. 15-25.
235. Poole, A.R., et al., *Composition and structure of articular cartilage: a template for tissue repair*. Clinical Orthopaedics & Related Research, 2001(391 Suppl): p. S26-33.
236. Kwack K, W.S., Cha YY, Park SJ, Kim HJ, Lee SK, Kang HJ, *Effects of gelatin on proliferation of cord blood derived mesenchymal stem cells*. The FASEB Journal, 2008. **22**(819.6).
237. Lee, C.R., A.J. Grodzinsky, and M. Spector, *Modulation of the contractile and biosynthetic activity of chondrocytes seeded in collagen-glycosaminoglycan matrices*. Tissue Eng, 2003. **9**(1): p. 27-36.
238. Zaleskas, J.M., et al., *Contractile forces generated by articular chondrocytes in collagen-glycosaminoglycan matrices*. Biomaterials, 2004. **25**(7-8): p. 1299-308.
239. Ohsawa, S., N. Yasui, and K. Ono, *Contraction of collagen gel by the dedifferentiated chondrocytes*. Cell Biol Int Rep, 1982. **6**(8): p. 767-74.
240. Spector, M., *Musculoskeletal connective tissue cells with muscle: expression of muscle actin in and contraction of fibroblasts, chondrocytes, and osteoblasts*. Wound Repair Regen, 2001. **9**(1): p. 11-8.
241. Kinner, B. and M. Spector, *Smooth muscle actin expression by human articular chondrocytes and their contraction of a collagen-glycosaminoglycan matrix in vitro*. J Orthop Res, 2001. **19**(2): p. 233-41.

242. Caron, M.M.J., et al., *Redifferentiation of dedifferentiated human articular chondrocytes: comparison of 2D and 3D cultures*. *Osteoarthritis and Cartilage*, 2012. **20**(10): p. 1170-1178.
243. Schrobback, K., T.J. Klein, and T.B. Woodfield, *The importance of connexin hemichannels during chondroprogenitor cell differentiation in hydrogel versus microtissue culture models*. *Tissue Eng Part A*, 2015. **21**(11-12): p. 1785-94.
244. Derycke, L.D. and M.E. Bracke, *N-cadherin in the spotlight of cell-cell adhesion, differentiation, embryogenesis, invasion and signalling*. *Int J Dev Biol*, 2004. **48**(5-6): p. 463-76.
245. O'Driscoll, S.W., C.N. Commisso, and J.S. Fitzsimmons, *Type II collagen quantification in experimental chondrogenesis*. *Osteoarthritis Cartilage*, 1995. **3**(3): p. 197-203.
246. Woodfield, T.B., et al., *The regulation of expanded human nasal chondrocyte re-differentiation capacity by substrate composition and gas plasma surface modification*. *Biomaterials*, 2006. **27**(7): p. 1043-1053.
247. Miot, S., et al., *Effects of scaffold composition and architecture on human nasal chondrocyte redifferentiation and cartilaginous matrix deposition*. *Biomaterials*, 2005. **26**(15): p. 2479-2489.
248. Marlovits, S., et al., *Changes in the ratio of type-I and type-II collagen expression during monolayer culture of human chondrocytes*. *J Bone Joint Surg Br*, 2004. **86**(2): p. 286-95.
249. Peysselon, F. and S. Ricard-Blum, *Heparin-protein interactions: from affinity and kinetics to biological roles. Application to an interaction network regulating angiogenesis*. *Matrix Biol*, 2014. **35**: p. 73-81.
250. Nissi, M.J., et al., *Estimation of mechanical properties of articular cartilage with MRI – dGEMRIC, T2 and T1 imaging in different species with variable stages of maturation*. *Osteoarthritis and Cartilage*, 2007. **15**(10): p. 1141-1148.
251. Woodfield, T.B.F., et al., *Design of porous scaffolds for cartilage tissue engineering using a three-dimensional fiber-deposition technique*. *Biomaterials*, 2004. **25**(18): p. 4149-4161.
252. Mekhileri, N.V., et al., *Automated 3D bioassembly of micro-tissues for biofabrication of hybrid tissue engineered constructs*. *Biofabrication*, 2018. **10**(2): p. 024103.
253. Rimmer, S., *Biomedical Hydrogels: Biochemistry, Manufacture and Medical Applications*. 2011, Cambridge: Woodhead Publishing Limited.
254. Nickerson, C.S., *Engineering the mechanical properties of ocular tissues*. 2005, California institute of technology.
255. Lim, K.S., et al., *New Visible-Light Photoinitiating System for Improved Print Fidelity in Gelatin-Based Bioinks*. *ACS Biomaterials Science & Engineering*, 2016. **2**(10): p. 1752-1762.
256. Bertlein, S., et al., *Thiol-ene clickable gelatin as a flexible platform bioink for biofabrication via 3D bioprinting and digital light processing*. *Advanced Materials*, 2017.
257. Di Luca, A., et al., *Toward mimicking the bone structure: design of novel hierarchical scaffolds with a tailored radial porosity gradient*. *Biofabrication*, 2016. **8**(4): p. 045007.
258. Schuurman, W., et al., *Cartilage regeneration using zonal chondrocyte subpopulations: a promising approach or an overcomplicated strategy?* *J Tissue Eng Regen Med*, 2015. **9**(6): p. 669-78.
259. Lenas, P., M. Moos, and F.P. Luyten, *Developmental engineering: a new paradigm for the design and manufacturing of cell-based products. Part I: from three-dimensional cell growth to biomimetics of in vivo development*. *Tissue Eng Part B Rev*, 2009. **15**(4): p. 381-94.
260. Gawlitta, D., et al., *Modulating endochondral ossification of multipotent stromal cells for bone regeneration*. *Tissue Eng Part B Rev*, 2010. **16**(4): p. 385-95.

261. Freeman, F.E., et al., *A Developmental Engineering-Based Approach to Bone Repair: Endochondral Priming Enhances Vascularization and New Bone Formation in a Critical Size Defect*. *Front Bioeng Biotechnol*, 2020. **8**: p. 230.
262. Knuth, C.A., et al., *Collagen type X is essential for successful mesenchymal stem cell-mediated cartilage formation and subsequent endochondral ossification*. *Eur Cell Mater*, 2019. **38**: p. 106-122.
263. Dickhut, A., et al., *Calcification or dedifferentiation: requirement to lock mesenchymal stem cells in a desired differentiation stage*. *J Cell Physiol*, 2009. **219**(1): p. 219-26.
264. Dickhut, A., et al., *Chondrogenesis of mesenchymal stem cells in gel-like biomaterials in vitro and in vivo*. *Front Biosci*, 2008. **13**: p. 4517-28.
265. Benders, K.E., et al., *Multipotent Stromal Cells Outperform Chondrocytes on Cartilage-Derived Matrix Scaffolds*. *Cartilage*, 2014. **5**(4): p. 221-30.
266. Almeida, H.V., et al., *Porous Scaffolds Derived from Devitalized Tissue Engineered Cartilaginous Matrix Support Chondrogenesis of Adult Stem Cells*. *ACS Biomaterials Science & Engineering*, 2017. **3**(6): p. 1075-1082.
267. Schneider, C., et al., *Systematic Comparison of Protocols for the Preparation of Human Articular Cartilage for Use as Scaffold Material in Cartilage Tissue Engineering*. *Tissue Engineering Part C: Methods*, 2016. **22**(12): p. 1095-1107.
268. Huang, Z., O. Godkin, and G. Schulze-Tanzil, *The Challenge in Using Mesenchymal Stromal Cells for Recellularization of Decellularized Cartilage*. *Stem Cell Reviews and Reports*, 2017. **13**(1): p. 50-67.
269. Lindberg, G.C.J., et al., *Intact vitreous humor as a potential extracellular matrix hydrogel for cartilage tissue engineering applications*. *Acta Biomater*, 2019. **85**: p. 117-130.
270. Hanashima, C. and H. Namiki, *Reduced Viability Of Vascular Endothelial Cells By High Concentration Of Ascorbic Acid In Vitreous Humor*. *Cell Biology International*, 1999. **23**(4): p. 287-298.
271. Sheibani, N., et al., *Thrombospondin-1, a natural inhibitor of angiogenesis, is present in vitreous and aqueous humor and is modulated by hyperglycemia*. *Biochem Biophys Res Commun*, 2000. **267**(1): p. 257-61.
272. Kilkenny, C., et al., *Improving Bioscience Research Reporting: The ARRIVE Guidelines for Reporting Animal Research*. *PLOS Biology*, 2010. **8**(6): p. e1000412.
273. Doube, M., et al., *BoneJ: Free and extensible bone image analysis in ImageJ*. *Bone*, 2010. **47**(6): p. 1076-9.
274. Renth, A.N. and M.S. Detamore, *Leveraging "raw materials" as building blocks and bioactive signals in regenerative medicine*. *Tissue Eng Part B Rev*, 2012. **18**(5): p. 341-62.
275. Matsiko, A., et al., *Addition of hyaluronic acid improves cellular infiltration and promotes early-stage chondrogenesis in a collagen-based scaffold for cartilage tissue engineering*. *Journal of the Mechanical Behavior of Biomedical Materials*, 2012. **11**: p. 41-52.
276. Varghese, S., et al., *Chondroitin sulfate based niches for chondrogenic differentiation of mesenchymal stem cells*. *Matrix Biology*, 2008. **27**(1): p. 12-21.
277. Hildebrand, A., et al., *Interaction of the small interstitial proteoglycans biglycan, decorin and fibromodulin with transforming growth factor beta*. *Biochem J*, 1994. **302 (Pt 2)**(Pt 2): p. 527-34.
278. Takeuchi, Y., Y. Kodama, and T. Matsumoto, *Bone matrix decorin binds transforming growth factor-beta and enhances its bioactivity*. *J Biol Chem*, 1994. **269**(51): p. 32634-8.

279. Naveiras, O., et al., *Bone-marrow adipocytes as negative regulators of the haematopoietic microenvironment*. *Nature*, 2009. **460**(7252): p. 259-263.
280. Belaid-Choucair, Z., et al., *Human Bone Marrow Adipocytes Block Granulopoiesis Through Neuropilin-1-Induced Granulocyte Colony-Stimulating Factor Inhibition*. *STEM CELLS*, 2008. **26**(6): p. 1556-1564.
281. Tuljapurkar, S.R., et al., *Changes in human bone marrow fat content associated with changes in hematopoietic stem cell numbers and cytokine levels with aging*. *Journal of Anatomy*, 2011. **219**(5): p. 574-581.
282. Siddappa, R., et al., *Donor variation and loss of multipotency during in vitro expansion of human mesenchymal stem cells for bone tissue engineering*. *J Orthop Res*, 2007. **25**(8): p. 1029-41.
283. Evans, C.H., *Barriers to the clinical translation of orthopedic tissue engineering*. *Tissue Eng Part B Rev*, 2011. **17**(6): p. 437-41.
284. Strom, T.B., L.J. Field, and M. Ruediger, *Allogeneic stem cells, clinical transplantation and the origins of regenerative medicine*. *Curr Opin Immunol*, 2002. **14**(5): p. 601-5.
285. Kanawa, M., et al., *Age-dependent decrease in the chondrogenic potential of human bone marrow mesenchymal stromal cells expanded with fibroblast growth factor-2*. *Cytherapy*, 2013. **15**(9): p. 1062-72.
286. Thaanat, O., et al., *Immunopathology of rejection: do the rules of solid organ apply to vascularized composite allotransplantation?* *Curr Opin Organ Transplant*, 2015. **20**(6): p. 596-601.
287. Walsh, M.C., et al., *Osteoimmunology: interplay between the immune system and bone metabolism*. *Annu Rev Immunol*, 2006. **24**: p. 33-63.
288. Croes, M., et al., *Local induction of inflammation affects bone formation*. *Eur Cell Mater*, 2017. **33**: p. 211-226.
289. Glass, G.E., et al., *TNF-alpha promotes fracture repair by augmenting the recruitment and differentiation of muscle-derived stromal cells*. *Proc Natl Acad Sci U S A*, 2011. **108**(4): p. 1585-90.
290. Chan, J.K., et al., *Low-dose TNF augments fracture healing in normal and osteoporotic bone by up-regulating the innate immune response*. *EMBO Mol Med*, 2015. **7**(5): p. 547-61.
291. Croes, M., et al., *Inflammation-Induced Osteogenesis in a Rabbit Tibia Model*. *Tissue Eng Part C Methods*, 2017. **23**(11): p. 673-685.
292. Guo, S.Q., et al., *Immunological study of allogeneic mesenchymal stem cells during bone formation*. *J Int Med Res*, 2009. **37**(6): p. 1750-9.
293. Berner, A., et al., *Autologous vs. allogeneic mesenchymal progenitor cells for the reconstruction of critical sized segmental tibial bone defects in aged sheep*. *Acta Biomater*, 2013. **9**(8): p. 7874-84.
294. Niemeyer, P., et al., *Transplantation of human mesenchymal stem cells in a non-autogenous setting for bone regeneration in a rabbit critical-size defect model*. *Acta Biomater*, 2010. **6**(3): p. 900-8.
295. Niemeyer, P., et al., *Xenogenic transplantation of human mesenchymal stem cells in a critical size defect of the sheep tibia for bone regeneration*. *Tissue Eng Part A*, 2010. **16**(1): p. 33-43.
296. Couto, D.L., et al., *Tissue engineering of rat bladder using marrow-derived mesenchymal stem cells and bladder acellular matrix*. *PLoS One*, 2014. **9**(12): p. e111966.

297. Grinnemo, K.H., et al., *Xenoreactivity and engraftment of human mesenchymal stem cells transplanted into infarcted rat myocardium*. J Thorac Cardiovasc Surg, 2004. **127**(5): p. 1293-300.
298. Noonan, K.J., et al., *Changes in cell, matrix compartment, and fibrillar collagen volumes between growth-plate zones*. J Orthop Res, 1998. **16**(4): p. 500-8.
299. Bahney, C.S., et al., *Stem cell-derived endochondral cartilage stimulates bone healing by tissue transformation*. J Bone Miner Res, 2014. **29**(5): p. 1269-82.
300. Chung, R., et al., *Roles of neutrophil-mediated inflammatory response in the bony repair of injured growth plate cartilage in young rats*. J Leukoc Biol, 2006. **80**(6): p. 1272-80.
301. Reinke, S., et al., *Terminally differentiated CD8(+) T cells negatively affect bone regeneration in humans*. Sci Transl Med, 2013. **5**(177): p. 177ra36.
302. Schlundt, C., et al., *Immune modulation as a therapeutic strategy in bone regeneration*. J Exp Orthop, 2015. **2**(1): p. 1.
303. Toben, D., et al., *Fracture healing is accelerated in the absence of the adaptive immune system*. J Bone Miner Res, 2011. **26**(1): p. 113-24.
304. Schlundt, C., et al. *Targeting the Adaptive Immune System to Enhance Bone Healing—Possible Strategies*. in *Orthopaedic Research Society*. 2016. Orlando, FL, USA.
305. Wu, A.C., et al., *Unraveling macrophage contributions to bone repair*. Bonekey Rep, 2013. **2**: p. 373.
306. Kovach, T.K., et al., *Interactions between MSCs and immune cells: implications for bone healing*. J Immunol Res, 2015. **2015**: p. 752510.
307. Pacifici, R., *Osteoimmunology and its implications for transplantation*. Am J Transplant, 2013. **13**(9): p. 2245-54.
308. Caetano-Lopes, J., H. Canhao, and J.E. Fonseca, *Osteoimmunology—the hidden immune regulation of bone*. Autoimmun Rev, 2009. **8**(3): p. 250-5.
309. Walsh, M.C. and Y. Choi, *Biology of the TRANCE axis*. Cytokine Growth Factor Rev, 2003. **14**(3-4): p. 251-63.
310. Sato, K., et al., *Th17 functions as an osteoclastogenic helper T cell subset that links T cell activation and bone destruction*. J Exp Med, 2006. **203**(12): p. 2673-82.
311. Mori, G., et al., *The Interplay between the bone and the immune system*. Clin Dev Immunol, 2013. **2013**: p. 720504.
312. Li, Y., et al., *B cells and T cells are critical for the preservation of bone homeostasis and attainment of peak bone mass in vivo*. Blood, 2007. **109**(9): p. 3839-48.
313. Walsh, M.C. and Y. Choi, *Biology of the RANKL-RANK-OPG System in Immunity, Bone, and Beyond*. Front Immunol, 2014. **5**: p. 511.
314. Salgado, A.J., O.P. Coutinho, and R.L. Reis, *Bone tissue engineering: state of the art and future trends*. Macromol Biosci, 2004. **4**(8): p. 743-65.
315. Boehler, R.M., J.G. Graham, and L.D. Shea, *Tissue engineering tools for modulation of the immune response*. Biotechniques, 2011. **51**(4): p. 239-40, 242, 244 passim.
316. Franz, S., et al., *Immune responses to implants - a review of the implications for the design of immunomodulatory biomaterials*. Biomaterials, 2011. **32**(28): p. 6692-709.
317. Zhuo, R., C.A. Siedlecki, and E.A. Vogler, *Autoactivation of blood factor XII at hydrophilic and hydrophobic surfaces*. Biomaterials, 2006. **27**(24): p. 4325-32.
318. Sperling, C., et al., *Blood coagulation on biomaterials requires the combination of distinct activation processes*. Biomaterials, 2009. **30**(27): p. 4447-56.

319. Nilsson, B., et al., *The role of complement in biomaterial-induced inflammation*. Mol Immunol, 2007. **44**(1-3): p. 82-94.
320. Hu, W.J., et al., *Molecular basis of biomaterial-mediated foreign body reactions*. Blood, 2001. **98**(4): p. 1231-8.
321. McFarland, C.D., et al., *Protein adsorption and cell attachment to patterned surfaces*. J Biomed Mater Res, 2000. **49**(2): p. 200-10.
322. Jenney, C.R. and J.M. Anderson, *Adsorbed serum proteins responsible for surface dependent human macrophage behavior*. J Biomed Mater Res, 2000. **49**(4): p. 435-47.
323. Anderson, J.M., A. Rodriguez, and D.T. Chang, *Foreign body reaction to biomaterials*. Semin Immunol, 2008. **20**(2): p. 86-100.
324. Nimeri, G., et al., *Oxygen radical production in neutrophils interacting with platelets and surface-immobilized plasma proteins: role of tyrosine phosphorylation*. J Biomed Mater Res A, 2003. **67**(2): p. 439-47.
325. Ekdahl, K.N., et al., *Innate immunity activation on biomaterial surfaces: A mechanistic model and coping strategies*. Adv Drug Deliv Rev, 2011. **63**(12): p. 1042-50.
326. Labow, R.S., E. Meek, and J.P. Santerre, *Neutrophil-mediated biodegradation of medical implant materials*. J Cell Physiol, 2001. **186**(1): p. 95-103.
327. Anderson, J.M. and A.K. McNally, *Biocompatibility of implants: lymphocyte/macrophage interactions*. Semin Immunopathol, 2011. **33**(3): p. 221-33.
328. Mosser, D.M. and J.P. Edwards, *Exploring the full spectrum of macrophage activation*. Nat Rev Immunol, 2008. **8**(12): p. 958-69.
329. Anderson, J.M., *Multinucleated giant cells*. Curr Opin Hematol, 2000. **7**(1): p. 40-7.
330. Williams, D.F., *On the mechanisms of biocompatibility*. Biomaterials, 2008. **29**(20): p. 2941-53.
331. Kou, P.M. and J.E. Babensee, *Macrophage and dendritic cell phenotypic diversity in the context of biomaterials*. J Biomed Mater Res A, 2011. **96**(1): p. 239-60.
332. Galili, U., *Avoiding detrimental human immune response against mammalian extracellular matrix implants*. Tissue Eng Part B Rev, 2015. **21**(2): p. 231-41.
333. Le Moine, A., M. Goldman, and D. Abramowicz, *Multiple pathways to allograft rejection*. Transplantation, 2002. **73**(9): p. 1373-81.
334. Charles A Janeway, J., Paul Travers, Mark Walport, and Mark J Shlomchik, in *Immunobiology: The Immune System in Health and Disease*. 2001, Garland Science: New York.
335. Rudolph, M.G., R.L. Stanfield, and I.A. Wilson, *How TCRs bind MHCs, peptides, and coreceptors*. Annu Rev Immunol, 2006. **24**: p. 419-66.
336. Joffre, O.P., et al., *Cross-presentation by dendritic cells*. Nat Rev Immunol, 2012. **12**(8): p. 557-69.
337. Sherman, L.A. and S. Chattopadhyay, *The molecular basis of allorecognition*. Annu Rev Immunol, 1993. **11**: p. 385-402.
338. Brown, K., S.H. Sacks, and W. Wong, *Coexpression of donor peptide/recipient MHC complex and intact donor MHC: evidence for a link between the direct and indirect pathways*. Am J Transplant, 2011. **11**(4): p. 826-31.
339. Afzali, B., G. Lombardi, and R.I. Lechler, *Pathways of major histocompatibility complex allorecognition*. Curr Opin Organ Transplant, 2008. **13**(4): p. 438-44.
340. Brown, K., M. Fidanboyulu, and W. Wong, *Intercellular exchange of surface molecules and its physiological relevance*. Arch Immunol Ther Exp (Warsz), 2010. **58**(4): p. 263-72.
341. Mahdi, B.M., *A glow of HLA typing in organ transplantation*. Clin Transl Med, 2013. **2**(1): p. 6.

342. Marino, J., J. Paster, and G. Benichou, *Allorecognition by T Lymphocytes and Allograft Rejection*. *Front Immunol*, 2016. **7**: p. 582.
343. Karahan, G.E., F.H. Claas, and S. Heidt, *B Cell Immunity in Solid Organ Transplantation*. *Front Immunol*, 2016. **7**: p. 686.
344. Spahn, J.H., W. Li, and D. Kreisel, *Innate immune cells in transplantation*. *Curr Opin Organ Transplant*, 2014. **19**(1): p. 14-9.
345. Meisel, R., et al., *Human bone marrow stromal cells inhibit allogeneic T-cell responses by indoleamine 2,3-dioxygenase-mediated tryptophan degradation*. *Blood*, 2004. **103**(12): p. 4619-21.
346. Wood, K.J., A. Bushell, and J. Hester, *Regulatory immune cells in transplantation*. *Nat Rev Immunol*, 2012. **12**(6): p. 417-30.
347. English, K., et al., *Cell contact, prostaglandin E2 and transforming growth factor beta 1 play non-redundant roles in human mesenchymal stem cell induction of CD4+CD25Highforkhead box P3+ regulatory T cells*. *Clinical & Experimental Immunology*, 2009. **156**(1): p. 149-160.
348. Spaggiari, G.M., et al., *MSCs inhibit monocyte-derived DC maturation and function by selectively interfering with the generation of immature DCs: central role of MSC-derived prostaglandin E2*. *Blood*, 2009. **113**(26): p. 6576-83.
349. Djouad, F., et al., *Mesenchymal stem cells inhibit the differentiation of dendritic cells through an interleukin-6-dependent mechanism*. *Stem Cells*, 2007. **25**(8): p. 2025-32.
350. Schepers, K. and W.E. Fibbe, *Unraveling mechanisms of mesenchymal stromal cell-mediated immunomodulation through patient monitoring and product characterization*. *Ann N Y Acad Sci*, 2016. **1370**(1): p. 15-23.
351. Munneke, J.M., et al., *The Potential of Mesenchymal Stromal Cells as Treatment for Severe Steroid-Refractory Acute Graft-Versus-Host Disease: A Critical Review of the Literature*. *Transplantation*, 2016. **100**(11): p. 2309-2314.
352. Panes, J., et al., *Expanded allogeneic adipose-derived mesenchymal stem cells (Cx601) for complex perianal fistulas in Crohn's disease: a phase 3 randomised, double-blind controlled trial*. *Lancet*, 2016. **388**(10051): p. 1281-90.
353. Wang, L.T., et al., *Human mesenchymal stem cells (MSCs) for treatment towards immune- and inflammation-mediated diseases: review of current clinical trials*. *J Biomed Sci*, 2016. **23**(1): p. 76.
354. Chen, X., et al., *Chondrogenic differentiation alters the immunosuppressive property of bone marrow-derived mesenchymal stem cells, and the effect is partially due to the upregulated expression of B7 molecules*. *Stem Cells*, 2007. **25**(2): p. 364-70.
355. Zheng, Z.H., et al., *Allogeneic mesenchymal stem cell and mesenchymal stem cell-differentiated chondrocyte suppress the responses of type II collagen-reactive T cells in rheumatoid arthritis*. *Rheumatology (Oxford)*, 2008. **47**(1): p. 22-30.
356. Du, W.J., et al., *Mesenchymal Stem Cells Derived from Human Bone Marrow and Adipose Tissue Maintain Their Immunosuppressive Properties After Chondrogenic Differentiation: Role of HLA-G*. *Stem Cells Dev*, 2016. **25**(19): p. 1454-69.
357. Mukonoweshuro, B., et al., *Immunogenicity of undifferentiated and differentiated allogeneic mouse mesenchymal stem cells*. *J Tissue Eng*, 2014. **5**: p. 2041731414534255.
358. Nauta, A.J., et al., *Mesenchymal stem cells inhibit generation and function of both CD34+-derived and monocyte-derived dendritic cells*. *J Immunol*, 2006. **177**(4): p. 2080-7.

359. Kiernan, C.H.K., A.; Peeters, M.; Wolvius, E.B.; Brama, P.A.J.; Farrell, E., *Allogeneic chondrogenically differentiated human bone marrow stromal cells do not induce complete dendritic cell maturation in vitro*, in *25th conference of the Netherlands society for Biomaterials and Tissue Engineering (NBTE)*, <http://nbte.nl/wp-content/uploads/2016/11/20161126-Program-NBTE-25th-Annual-Meeting-2016-abstracts.pdf>, Editor. 2016: Lunteren, 2016. p. 64.
360. Butnariu-Ephrat, M., et al., *Resurfacing of goat articular cartilage by chondrocytes derived from bone marrow*. Clin Orthop Relat Res, 1996(330): p. 234-43.
361. Li, Y. and F. Lin, *Mesenchymal stem cells are injured by complement after their contact with serum*. Blood, 2012. **120**(17): p. 3436-43.
362. Technau, A., et al., *Adipose tissue-derived stem cells show both immunogenic and immunosuppressive properties after chondrogenic differentiation*. Cytotherapy, 2011. **13**(3): p. 310-7.
363. Kawabe, N. and M. Yoshinai, *The repair of full-thickness articular cartilage defects. Immune responses to reparative tissue formed by allogeneic growth plate chondrocyte implants*. Clin Orthop Relat Res, 1991(268): p. 279-93.
364. Romaniuk, A., et al., *Rejection of cartilage formed by transplanted allogeneic chondrocytes: evaluation with monoclonal antibodies*. Transpl Immunol, 1995. **3**(3): p. 251-7.
365. Masuoka, K., et al., *Tissue engineering of articular cartilage using an allograft of cultured chondrocytes in a membrane-sealed atelocollagen honeycomb-shaped scaffold (ACHMS scaffold)*. J Biomed Mater Res B Appl Biomater, 2005. **75**(1): p. 177-84.
366. Rahfoth, B., et al., *Transplantation of allograft chondrocytes embedded in agarose gel into cartilage defects of rabbits*. Osteoarthritis Cartilage, 1998. **6**(1): p. 50-65.
367. Shangkai, C., et al., *Transplantation of allogeneic chondrocytes cultured in fibroin sponge and stirring chamber to promote cartilage regeneration*. Tissue Eng, 2007. **13**(3): p. 483-92.
368. Gross, A.E., N. Shasha, and P. Aubin, *Long-term followup of the use of fresh osteochondral allografts for posttraumatic knee defects*. Clin Orthop Relat Res, 2005(435): p. 79-87.
369. Adkisson, H.D., et al., *Immune evasion by neocartilage-derived chondrocytes: Implications for biologic repair of joint articular cartilage*. Stem Cell Res, 2010. **4**(1): p. 57-68.
370. Wang, Y., et al., *Microarray analysis of proliferative and hypertrophic growth plate zones identifies differentiation markers and signal pathways*. Bone, 2004. **35**(6): p. 1273-93.
371. Bahney, C.S., et al., *The multifaceted role of the vasculature in endochondral fracture repair*. Front Endocrinol (Lausanne), 2015. **6**: p. 4.
372. Oshima, Y., et al., *Pivotal role of Bcl-2 family proteins in the regulation of chondrocyte apoptosis*. J Biol Chem, 2008. **283**(39): p. 26499-508.
373. Shapiro, I.M., et al., *Fate of the hypertrophic chondrocyte: microenvironmental perspectives on apoptosis and survival in the epiphyseal growth plate*. Birth Defects Res C Embryo Today, 2005. **75**(4): p. 330-9.
374. Yang, L., et al., *Hypertrophic chondrocytes can become osteoblasts and osteocytes in endochondral bone formation*. Proc Natl Acad Sci U S A, 2014. **111**(33): p. 12097-102.
375. Zhou, X., et al., *Chondrocytes transdifferentiate into osteoblasts in endochondral bone during development, postnatal growth and fracture healing in mice*. PLoS Genet, 2014. **10**(12): p. e1004820.
376. Liu, H., et al., *The immunogenicity and immunomodulatory function of osteogenic cells differentiated from mesenchymal stem cells*. J Immunol, 2006. **176**(5): p. 2864-71.

377. TrabANELLI, S., et al., *The Human Mesenchymal Stromal Cell-Derived Osteocyte Capacity to Modulate Dendritic Cell Functions Is Strictly Dependent on the Culture System*. J Immunol Res, 2015. **2015**: p. 526195.
378. Niemeyer, P., et al., *Comparison of immunological properties of bone marrow stromal cells and adipose tissue-derived stem cells before and after osteogenic differentiation in vitro*. Tissue Eng, 2007. **13**(1): p. 111-21.
379. Song, Y., et al., *Feasibility of localized immunosuppression: 3. Preliminary evaluation of organosilicone constructs designed for sustained drug release in a cell transplant environment using dexamethasone*. Pharmazie, 2012. **67**(5): p. 394-9.
380. Frei, A.W., et al., *Local delivery of fingolimod from three-dimensional scaffolds impacts islet graft efficacy and microenvironment in a murine diabetic model*. J Tissue Eng Regen Med, 2017. **12**(2): p. 393-404.
381. van Rood, J.J., *Double role of HLA in organ transplantation*. World J Surg, 2000. **24**(7): p. 823-7.
382. Ayala Garcia, M.A., et al., *The major histocompatibility complex in transplantation*. J Transplant, 2012. **2012**: p. 842141.
383. Evans, C.H., et al., *Facilitated endogenous repair: making tissue engineering simple, practical, and economical*. Tissue Eng, 2007. **13**(8): p. 1987-93.
384. Evans, C.H., *Advances in regenerative orthopedics*. Mayo Clin Proc, 2013. **88**(11): p. 1323-39.
385. Longoni, A., et al., *The impact of immune response on endochondral bone regeneration*. npj Regenerative Medicine, 2018. **3**(1): p. 22.
386. Kiernan, C.H., et al., *Allogeneic chondrogenically differentiated human bone marrow stromal cells do not induce dendritic cell maturation*. J Tissue Eng Regen Med, 2018.
387. Mathieux, E., et al., *IgG Response to Intracerebral Xenotransplantation: Specificity and Role in the Rejection of Porcine Neurons*. American Journal of Transplantation, 2014. **14**(5): p. 1109-1119.
388. Niemietz, T., et al., *Xenogeneic transplantation of articular chondrocytes into full-thickness articular cartilage defects in minipigs: fate of cells and the role of macrophages*. Cell Tissue Res, 2014. **358**(3): p. 749-61.
389. Navarro-Alvarez, N. and Y.G. Yang, *Lack of CD47 on donor hepatocytes promotes innate immune cell activation and graft loss: a potential barrier to hepatocyte xenotransplantation*. Cell Transplant, 2014. **23**(3): p. 345-54.
390. Ide, K., et al., *Role for CD47-SIRPalpha signaling in xenograft rejection by macrophages*. Proc Natl Acad Sci U S A, 2007. **104**(12): p. 5062-6.
391. Moreau, A., et al., *Effector mechanisms of rejection*. Cold Spring Harb Perspect Med, 2013. **3**(11).
392. Schlundt, C., et al., *Individual Effector/Regulator T Cell Ratios Impact Bone Regeneration*. Front Immunol, 2019. **10**: p. 1954.
393. Vadori, M. and E. Cozzi, *The immunological barriers to xenotransplantation*. Tissue Antigens, 2015. **86**(4): p. 239-53.
394. Lohan, P., et al., *Anti-Donor Immune Responses Elicited by Allogeneic Mesenchymal Stem Cells and Their Extracellular Vesicles: Are We Still Learning?* Front Immunol, 2017. **8**: p. 1626.
395. Colvin, R.B. and R.N. Smith, *Antibody-mediated organ-allograft rejection*. Nat Rev Immunol, 2005. **5**(10): p. 807-17.
396. Su, J.A., et al., *The clinical impact of donor-specific antibodies on antibody-mediated rejection and long-term prognosis after heart transplantation*. Curr Opin Organ Transplant, 2019.

397. Huber-Lang, M., A. Kovtun, and A. Ignatius, *The role of complement in trauma and fracture healing*. *Seminars in Immunology*, 2013. **25**(1): p. 73-78.
398. Mödinger, Y., et al., *Complement involvement in bone homeostasis and bone disorders*. *Seminars in Immunology*, 2018. **37**: p. 53-65.
399. Bergdolt, S., et al., *Osteoblast-specific overexpression of complement receptor C5aR1 impairs fracture healing*. *PLoS One*, 2017. **12**(6): p. e0179512.
400. Gill, T.J., 3rd, et al., *The major histocompatibility complex of the rat*. *Transplantation*, 1987. **43**(6): p. 773-85.
401. Spees, J.L., R.H. Lee, and C.A. Gregory, *Mechanisms of mesenchymal stem/stromal cell function*. *Stem Cell Res Ther*, 2016. **7**(1): p. 125.
402. Hoshiba, T., et al., *Decellularized matrices for tissue engineering*. *Expert opinion on biological therapy*, 2010. **10**(12): p. 1717-1728.
403. Lu, H., et al., *Cultured cell-derived extracellular matrix scaffolds for tissue engineering*. *Biomaterials*, 2011. **32**(36): p. 9658-9666.
404. Chen, X.-D., et al., *Extracellular matrix made by bone marrow cells facilitates expansion of marrow-derived mesenchymal progenitor cells and prevents their differentiation into osteoblasts*. *Journal of bone and mineral research : the official journal of the American Society for Bone and Mineral Research*, 2007. **22**(12): p. 1943-1956.
405. Lin, H., et al., *Influence of decellularized matrix derived from human mesenchymal stem cells on their proliferation, migration and multi-lineage differentiation potential*. *Biomaterials*, 2012. **33**(18): p. 4480-4489.
406. Cunniffe, G.M., et al., *Tissue-specific extracellular matrix scaffolds for the regeneration of spatially complex musculoskeletal tissues*. *Biomaterials*, 2019. **188**: p. 63-73.
407. Song, J.J. and H.C. Ott, *Organ engineering based on decellularized matrix scaffolds*. *Trends in Molecular Medicine*, 2011. **17**(8): p. 424-432.
408. Webber, M.J., et al., *A perspective on the clinical translation of scaffolds for tissue engineering*. *Annals of biomedical engineering*, 2015. **43**(3): p. 641-656.
409. Asami, G. and W. Dock, *EXPERIMENTAL STUDIES ON HETEROPLASTIC BONE FORMATION*. *The Journal of experimental medicine*, 1920. **32**(6): p. 745-766.
410. Cunniffe, G.M., et al., *Growth plate extracellular matrix-derived scaffolds for large bone defect healing*. *European cells & materials*, 2017. **33**: p. 130-142.
411. Creemers, L.B., et al., *Microassay for the assessment of low levels of hydroxyproline*. *BioTechniques*, 1997. **22**(4): p. 656-658.
412. Schönherr, E. and H.J. Hausser, *Extracellular matrix and cytokines: a functional unit*. *Developmental immunology*, 2000. **7**(2-4): p. 89-101.
413. Kim, Y.S., et al., *Applications of decellularized extracellular matrix in bone and cartilage tissue engineering*. *Bioengineering & Translational Medicine*, 2019. **4**(1): p. 83-95.
414. Longoni, A., et al., *Endochondral Bone Regeneration by Non-Autologous Mesenchymal Stem Cells*. *Frontiers in bioengineering and biotechnology*, 2020.
415. Madhally, S.V. and H.W. Matthew, *Porous chitosan scaffolds for tissue engineering*. *Biomaterials*, 1999. **20**(12): p. 1133-1142.
416. Jiankang, H., et al., *Fabrication and characterization of chitosan/gelatin porous scaffolds with predefined internal microstructures*. *Polymer*, 2007. **48**(15): p. 4578-4588.
417. Freytes, D.O., et al., *Hydrated versus lyophilized forms of porcine extracellular matrix derived from the urinary bladder*. *Journal of biomedical materials research. Part A*, 2008. **87**(4): p. 862-872.

418. Seoane-Vazquez, E., V. Shukla, and R. Rodriguez-Monguio, *Innovation and competition in advanced therapy medicinal products*. EMBO Molecular Medicine, 2019. **11**(3): p. e9992.
419. O'Driscoll, S.W.M., et al., *The chondrogenic potential of periosteum decreases with age*. Journal of Orthopaedic Research, 2001. **19**(1): p. 95-103.
420. Choudhery, M.S., et al., *Donor age negatively impacts adipose tissue-derived mesenchymal stem cell expansion and differentiation*. Journal of Translational Medicine, 2014. **12**(1): p. 8.
421. Meretoja, V.V., et al., *The effect of hypoxia on the chondrogenic differentiation of co-cultured articular chondrocytes and mesenchymal stem cells in scaffolds*. Biomaterials, 2013. **34**(17): p. 4266-4273.
422. Müller, J., et al., *Hypoxic conditions during expansion culture prime human mesenchymal stromal precursor cells for chondrogenic differentiation in three-dimensional cultures*. Cell Transplant, 2011. **20**(10): p. 1589-602.
423. Xu, Y., et al., *In Vitro Expansion of Adipose-Derived Adult Stromal Cells in Hypoxia Enhances Early Chondrogenesis*. Tissue Engineering, 2007. **13**(12): p. 2981-2993.
424. Ahmed, N.E.-M.B., et al., *The effects of hypoxia on the stemness properties of human dental pulp stem cells (DPSCs)*. Scientific reports, 2016. **6**: p. 35476-35476.
425. Iida, K., et al., *Hypoxia enhances colony formation and proliferation but inhibits differentiation of human dental pulp cells*. Arch Oral Biol, 2010. **55**(9): p. 648-54.
426. Sakdee, J.B., et al., *Hypoxia-amplified proliferation of human dental pulp cells*. J Endod, 2009. **35**(6): p. 818-23.
427. Kwon, S.Y., et al., *Hypoxia Enhances Cell Properties of Human Mesenchymal Stem Cells*. Tissue Eng Regen Med, 2017. **14**(5): p. 595-604.
428. Sweigart, M.A. and K.A. Athanasiou, *Toward tissue engineering of the knee meniscus*. Tissue Eng, 2001. **7**(2): p. 111-29.
429. Seidi, A., et al., *Gradient biomaterials for soft-to-hard interface tissue engineering*. Acta Biomaterialia, 2011. **7**(4): p. 1441-1451.
430. Kuroda, S., et al., *Biomechanical and biochemical characteristics of the mandibular condylar cartilage*. Osteoarthritis and Cartilage, 2009. **17**(11): p. 1408-1415.
431. Rosso, F., et al., *From Cell-ECM interactions to tissue engineering*. Journal of Cellular Physiology, 2004. **199**(2): p. 174-180.
432. Cai, R., et al., *Influence of stepwise chondrogenesis-mimicking 3D extracellular matrix on chondrogenic differentiation of mesenchymal stem cells*. Biomaterials, 2015. **52**: p. 199-207.
433. Berendsen, A.D., et al., *Contraction-induced Mmp13 and -14 expression by goat articular chondrocytes in collagen type I but not type II gels*. J Tissue Eng Regen Med, 2012. **6**(9): p. 721-30.
434. Park, S.H., et al., *Chondrogenesis of rabbit mesenchymal stem cells in fibrin/hyaluronan composite scaffold in vitro*. Tissue Eng Part A, 2011. **17**(9-10): p. 1277-86.
435. Wang, T. and F. Yang, *A comparative study of chondroitin sulfate and heparan sulfate for directing three-dimensional chondrogenesis of mesenchymal stem cells*. Stem Cell Res Ther, 2017. **8**(1): p. 284.
436. Francioli, S.E., et al., *Effect of three-dimensional expansion and cell seeding density on the cartilage-forming capacity of human articular chondrocytes in type II collagen sponges*. J Biomed Mater Res A, 2010. **95**(3): p. 924-31.
437. Chang, K.Y., et al., *The application of type II collagen and chondroitin sulfate grafted PCL porous scaffold in cartilage tissue engineering*. J Biomed Mater Res A, 2010. **92**(2): p. 712-23.

438. Rowland, C.R., et al., *The effects of crosslinking of scaffolds engineered from cartilage ECM on the chondrogenic differentiation of MSCs*. *Biomaterials*, 2013. **34**(23): p. 5802-5812.
439. Klotz, B.J., et al., *A Versatile Biosynthetic Hydrogel Platform for Engineering of Tissue Analogues*. 2019. **8**(19): p. e1900979.
440. Rothrauff, B.B., et al., *Efficacy of thermoresponsive, photocrosslinkable hydrogels derived from decellularized tendon and cartilage extracellular matrix for cartilage tissue engineering*. *J Tissue Eng Regen Med*, 2018. **12**(1): p. e159-e170.
441. Muñoz, Z., H. Shih, and C.-C. Lin, *Gelatin hydrogels formed by orthogonal thiol–norbornene photochemistry for cell encapsulation*. *Biomaterials Science*, 2014. **2**(8): p. 1063-1072.
442. Hare, J.M., et al., *A randomized, double-blind, placebo-controlled, dose-escalation study of intravenous adult human mesenchymal stem cells (prochymal) after acute myocardial infarction*. *J Am Coll Cardiol*, 2009. **54**(24): p. 2277-86.
443. de Windt, T.S., et al., *Allogeneic Mesenchymal Stem Cells Stimulate Cartilage Regeneration and Are Safe for Single-Stage Cartilage Repair in Humans upon Mixture with Recycled Autologous Chondrons*. *Stem cells (Dayton, Ohio)*, 2017. **35**(1): p. 256-264.
444. Headen, D.M., et al., *Local immunomodulation Fas ligand-engineered biomaterials achieves allogeneic islet graft acceptance*. *Nature materials*, 2018. **17**(8): p. 732-739.
445. Hartono, C., T. Muthukumar, and M. Suthanthiran, *Immunosuppressive drug therapy*. *Cold Spring Harbor perspectives in medicine*, 2013. **3**(9): p. a015487-a015487.
446. Fireman, M., et al., *Immunosuppressants*. *Psychosomatics*, 2004. **45**(4): p. 354-360.
447. Cvetkovic, M., et al., *The deleterious effects of long-term cyclosporine A, cyclosporine G, and FK506 on bone mineral metabolism in vivo*. *Transplantation*, 1994. **57**(8): p. 1231-7.
448. Gottschalk, S., et al., *Age and sex differences in the effects of the immunosuppressants cyclosporine, sirolimus and everolimus on rat brain metabolism*. *NeuroToxicology*, 2011. **32**(1): p. 50-57.
449. *Regulation (EC) No 1394/2007 of the European Parliament and of the Council of 13 November 2007 on advanced therapy medicinal products and amending Directive 2001/83/EC and Regulation (EC) No 726/2004 E.P.a.o.t.* Council, Editor. 2007: Official Journal of the European Union.
450. Lovett, M., et al., *Vascularization Strategies for Tissue Engineering*. *Tissue Engineering Part B: Reviews*, 2009. **15**(3): p. 353-370.
451. O'Loughlin, P.F., et al., *Selection and development of preclinical models in fracture-healing research*. *J Bone Joint Surg Am*, 2008. **90 Suppl 1**: p. 79-84.
452. Pearce, A.I., et al., *Animal models for implant biomaterial research in bone: a review*. *Eur Cell Mater*, 2007. **13**: p. 1-10.
453. Scheerlinck, J.-P.Y., *The Immune System of Sheep and Goats*, in *Encyclopedia of Immunobiology*, M.J.H. Ratcliffe, Editor. 2016, Academic Press: Oxford. p. 526-531.
454. Bailey, M., Z. Christoforidou, and M.C. Lewis, *The evolutionary basis for differences between the immune systems of man, mouse, pig and ruminants*. *Veterinary Immunology and Immunopathology*, 2013. **152**(1): p. 13-19.
455. Rothkötter, H.-J., *Anatomical particularities of the porcine immune system—A physician's view*. *Developmental & Comparative Immunology*, 2009. **33**(3): p. 267-272.
456. Klijn, R.J., et al., *Maxillary sinus augmentation with microstructured tricalcium phosphate ceramic in sheep*. *Clinical Oral Implants Research*, 2012. **23**(3): p. 274-280.
457. Kruyt, M.C., et al., *Bone tissue engineering and spinal fusion: the potential of hybrid constructs by combining osteoprogenitor cells and scaffolds*. *Biomaterials*, 2004. **25**(9): p. 1463-73.

458. Sparks, D.S., et al., *A preclinical large-animal model for the assessment of critical-size load-bearing bone defect reconstruction*. *Nature Protocols*, 2020. **15**(3): p. 877-924.
459. Visser, J., et al., *Reinforcement of hydrogels using three-dimensionally printed microfibres*. *Nat Commun*, 2015. **6**: p. 6933.
460. Das, R., et al., *Preparing for cell culture scale-out: establishing parity of bioreactor- and flask-expanded mesenchymal stromal cell cultures*. *Journal of Translational Medicine*, 2019. **17**(1): p. 241.
461. Janjanin, S., et al., *Mold-Shaped, Nanofiber Scaffold-Based Cartilage Engineering Using Human Mesenchymal Stem Cells and Bioreactor*. *Journal of Surgical Research*, 2008. **149**(1): p. 47-56.
462. Nold, P., et al., *Good manufacturing practice-compliant animal-free expansion of human bone marrow derived mesenchymal stroma cells in a closed hollow-fiber-based bioreactor*. *Biochemical and Biophysical Research Communications*, 2013. **430**(1): p. 325-330.
463. Rojewski, M.T., et al., *GMP-Compliant Isolation and Expansion of Bone Marrow-Derived MSCs in the Closed, Automated Device Quantum Cell Expansion System*. *Cell Transplantation*, 2013. **22**(11): p. 1981-2000.
464. Bubela, T., et al., *Bringing regenerative medicines to the clinic: the future for regulation and reimbursement*. *Regenerative Medicine*, 2015. **10**(7): p. 897-911.



Acknowledgements



... And we have finally reached the section of the thesis that everyone is going to read first. Let's be honest, we all love science, otherwise we would have not chosen this crazy job. However, you have heard me presenting so many times at the group meetings that I would not expect anyone to be eager to dive into my chapters ☺ ... So let's start with the acknowledgments!

I would like to start by thanking my promotion team. **Prof. dr. Rosenberg, dr. ir. Gawlitta**, you have been with me every step of the way for the past 5 years. Dear Toine, I will always be grateful to you for giving me the opportunity to do my PhD in your department. You have always given me a different perspective on my work, always trying to keep the group focused on the clinical application of our research. I really enjoyed our meetings and the enthusiasm you have showed for my results, even the smallest ones, was really contagious and truly encouraging. Besides the scientific aspect, I really appreciate that you have always been interested in my personal life, always asking me about my family and checking if I was doing ok. Dear Debby, there are so many things I would like to say, and it's so difficult to summarize them in a few lines! On the one hand you are a serious, thorough scientist, always asking the right questions and noticing the details that everybody else overlooked. On the other hand, you are this cheerful, easy-going person who got me drunk the first time we went for dinner together and played pranks on me on April's fool. What I loved the most about working together is that I could always speak my mind and you were always interested in hearing my opinion and ideas. I believe that doing my PhD under your supervision helped me to grow as a scientist and as a person. Finally **dr. Utomo**, the last addition to my promotion team. Lizette, even if you only joined us in the last few months of my PhD, I appreciate all of our scientific discussions and your (almost ☺) tireless effort to improve my English. I wish you the best in all your future endeavors.

My dear paranimfen, **Jorgos** and **Irina**, I owe you a big thank. Jorgos, you have always been there for me when I needed, never tired of listening to the same things over and over again. It's impressive that you were not fed up with me when frankly I was fed up with myself ☺. The past four years would have not been the same without you. I really enjoyed all the time we spent together, climbing (or better, you watching me falling down in a not really graceful way...), playing videogames, talking about life or simply hanging out. Irina, you were the first person I met during my interview at the UMC. I will never forget how you pretended to know the Italian university I graduated from just to give me a head start to get the position ☺. You and the entire Mancini's family (yes, all of you, even Bru...) always made me feel at home. I can never say thank you enough for all the delicious warm dinners you and **Fred** cooked for me when I was finishing late, our afternoon coffees and the board game nights trying to defend the Wall from the White Walkers.

It goes without saying that the past years would have been a lot less fun without my colleagues from the **Kaak group**. Honestly, it has been a long time since I last considered you as just my colleagues because over the years you have all become very good friends of mine. **Barbi**, we have met for the first time so long ago, during our master internship in Enschede! I am so glad that I had the chance to know you better over the years. I loved our bouldering session on Sundays and our talks about life in front of a tea afterwards. You are really a genuine person and I have always admired your positive attitude, always trying to find the silver lining even when things were not going the way you wanted. **Iris**, what can I say? We are the strangest duo that ever tried to work together. You like to make lists, plan ahead and organize every details whereas... Well, let's just say that I am more of a person that likes to play it by ear ☺. I like to think that we learned a bit from each other: you realized that things can always take a wrong turn, no matter how perfect the plan was and I learned that organizing a bit my mess is not such a bad idea after all (even though my lab bench seems to always find its own way towards chaos...). One of the few things you never managed to teach me is how to dance salsa ☺. Honestly it was a lost cause since the beginning, but I was always looking forward to hearing all about your stories on Monday morning. Barbi, Iris, not having you sitting right across of my desk in our "flex" office felt a bit like the end of an era. It's hard to think that the three of us started this journey together 5 years ago and now we are all (almost) done. Thank you for everything, I could have never wished for someone better to share this time with. **Luuk**, the only guy in our group! No wonder you were hiding at Kuros most of the time ☺... It was really nice to have you around at the RMCU a bit more in the past year, especially because I could always count on you for a coffee break or for a last minute borrel - even if you don't know how to drink limoncello the correct way. **Leanne**, the new addition to our group. Although we have not known each other for long, I consider you one of my closest friends. I will always be grateful to you for reminding me that the working place can also be a fun environment. I think we really bonded when we discovered that we are both foodies: from that moment on, the desks in our office have always been covered with snacks. I really enjoyed hanging out with you, especially because we often ended up having the most absurd evenings. I promise I will do my best to train my tolerance to spicy food for our reunion on the Sydney Harbor Bridge ☺. Finally, I would like to thank the members of the **Kaak department**. I appreciate the enthusiasm with which you were attending and giving feedbacks at the beer and pizza meetings and the RM-child meetings. They really helped me to better understand the challenges and problems you face every day in the clinical practice.

A special thank goes also to **Ana, Inge, Lisa, Valentine, Lea, Sophie** and **Abbie**, the students that were involved in the projects and helped me build the chapters of this thesis. Thanks to all of you I discovered that I really enjoy teaching and mentoring students.

Khoonono, of course you deserve a special place in this section! I am so glad that I became a proud member of your brunch club and that over the years we became such good friends. I really see you as a mentor and I know I can always rely on your good advices. I guess dying your hair gray did make you wiser ☺. I have always looked forward to your visits in the Netherlands, to chat about life, host dinners, watch anime and TV series. Carrying you around on my bike, trying not to fall while you were screaming “Panda!” still remains one of my favorite memories from my first year. I am really excited to start my next big working adventure with you in New Zealand.

Dear **Mattie**, sometimes I felt like the entire lab would fall into complete chaos without you there, always helping everybody! Since the beginning of my PhD you have been my TomTom around the lab and you have always been my go-to person when I had doubts. I have learnt so much from you, including how to change the toner of a printer ☺. Plus, chatting together while cutting at the microtome or over a coffee made my long days much more enjoyable.

Riccardo, you also helped me so much during these years. Although your schedule progressively became busier and busier, you have always found the time to sit down with me to talk about scientific or personal problems. You are one of the kindest and more knowledgeable people I have ever met. I really admire you as a scientist and I wish you all the best for your future career.

Dear colleagues from the **orthopedics department**, I can never thank you enough for welcoming me in your lab when we were still at the UMC. Even if we were from different departments, it has never felt like it, as we always helped each other. Thanks also for all the fun times outside the office hours, at borrels, lab dinners, conferences and at the climbing gym (...Mylene I guess this last one mainly applies to you ☺). I would also like to thank **Marta** from the Laboratory of Translation Immunology of the UMC and **Gabby** from the CReaTE group in New Zealand. It was a pleasure to collaborate with both of you and I am really happy with the results we achieved together. Finally, all the people that worked with me at the GDL deserve a big thank you. **Anja**, I am not sure how I would have managed without you. I was a bit lost and afraid of messing up everything when I first started my experiments there. I had soooo many questions at the beginning! ☺ Thanks for guiding me and for teaching me how to address my rats properly: “lieffie!”

A great thanks goes to my friends, without whom the past years would have been a lot less fun. **Imke**, I never thought I would have ever met someone as talented as me at singing! The world is simply not ready for our amazing karaoke performances ☺. Thanks for keeping me well fed with the incredible amount of Polish chocolate you were always stocking in your

“flex” office and I really miss having coffee breaks at Genmab with you! **Vivian**, who would have ever thought that such an organized German and a messy Italian could get along so well? I really enjoyed partying with you (...back in your partying days ☺) and I was always looking forward to hearing your amazing stories! Climbing together has been one of my favorite ways to relax during the PhD, even though we always ended up chatting on the crash mat rather than actually climbing ☺. You are a great confidant and I wish you all the best with finishing your PhD! **Soraya**, I am so glad we shared the ups and downs of having to write the thesis, it made it a lot easier... and I am quite relieved that motivating each other to write worked out better than the time we tried to subscribe to the gym together! Together with **Stefano, Paolo and Pess** (...and Jorgos of course!) we shared quite some unforgettable evenings, playing cards, making barbecues or simply having drinks and discussing about everything that popped into our mind. Thanks to you guys I have never felt alone and I knew I could always rely on you. **Miriam**, I like to think that my adventures here in the Netherlands started with you in Enschede. You have always been there encouraging me and showing more enthusiasm towards what I was doing than anybody else. Thanks for everything, the weekends when you were visiting were always the best ones. **Anna**, thanks for listening to all my rants during the first years of my PhD and for pushing me to climb more! Thanks to you I really developed a passion for this sport, although it's not the same without you rolling with me on the crash mat ☺. **Deji**, you were one of the first friends I made in the Netherlands. With you I shared some interesting adventures, including our trip to IKEA in the first weeks with your wobbly bike and trying to paint your first apartment. **Tullis**, who would have ever thought that we were going to meet again years after high school in the Netherlands? Thanks for patiently listening to all my stories and for throwing a sarcastic comment every now and then. I really enjoyed our dinner at Sumo. **Mimmo**, it was so much fun having you around in the lab! I must say, when you were at the RMCU my coffee breaks were lasting forever because you always had the most incredible stories about your PhD in Israel! I really enjoyed spending time with you and I wish you all the best with your new job in the US. **Preet**, the newest addition to this list. Thanks for always trying to keep me active. You had such a difficult task, because after 9.30 p.m. laying on my sofa wearing pajama becomes such an attractive option... Thanks for giving me a lot of support while making constantly fun of me at the same time: it is a really weird technique but it actually worked out quite well ...And last, but not least, thanks to **Michele**. We had a bit of a rocky start because we are both super stubborn and overly confident in our opinions. However, you became one of my dearest friends and I could always call you whenever I needed to talk. You have this incredible ability of making every evening more fun and make people around you laugh and enjoy themselves. Our dinners (...for some reason always on a Tuesday), my visits in Rotterdam and the conference in Greece are some of the happiest memories of my PhD.

... L'ultimo ringraziamento è per la mia **famiglia**. Mamma, papà so che per voi non è stato facile non avermi sempre a portata di mano ma nonostante questo mi avete sempre supportato e spinto a fare ciò che volevo. Grazie per aver ascoltato tutte le mie (infinite) lamentele, essere sempre stati in grado di darmi ottimi consigli e soprattutto per avermi aiutato con ben due traslochi 😊. Tutta la determinazione e impegno che ho messo nel portare a termine questo lavoro l'ho imparata da voi. Marti, grazie per esserci sempre stata quando avevo bisogno (...ore e ore di telefonate 😊) e soprattutto grazie per essermi sempre venuta a trovare! I week-end che abbiamo passato assieme sono sempre stati molto interessanti, a partire dal mio primo King's Day in Olanda 😊. Un grazie di cuore è doveroso anche ai miei nonni, gli zii e i miei cugini, che si sono sempre interessati alle mie disavventure in Olanda e hanno sempre trasformato ogni volta che tornavo a casa in un'occasione speciale.



List of publications
Curriculum vitae



LIST OF PUBLICATIONS

1. [A. Longoni](#), I. Pennings, G.C.J. Lindberg, T.B.F Woodfield, A.J.W.P. Rosenberg, K.S Lim, D. Gawlitta. *Vitreous humor as instructive biomaterial to support mesenchymal stem cell hypertrophy and endochondral ossification*. In preparation
2. I. Pennings, [A. Longoni](#), Q. Vallmajo-Martin, C. Cheng, M. Ehrbar, A.J.W.P Rosenberg, D. Gawlitta. *Pre-differentiation period of pre-vascularized bone constructs containing calcium phosphates favours and accelerates in vivo bone formation*. Submitted
3. [A. Longoni](#), I. Pennings, M. Cuenca Lopera, M.H.P. van Rijn, V. Peperzak, A.J.W.P. Rosenberg, R. Levato, D. Gawlitta. *Endochondral bone regeneration by non-autologous mesenchymal stem cells*. *Frontiers in bioengineering and biotechnology*, 2020
4. [A. Longoni](#), L. Utomo, I.E.M. van Hooijdonk, G.K.P. Bittermann, V.C. Vetter, E.C. Kruijt Spanjer, J. Ross, A.J.W.P. Rosenberg, D. Gawlitta. *The chondrogenic differentiation potential of dental pulp stem cells*. *European Cells and Materials*, 2020. 39:121-135
5. J. P. Garcia, [A. Longoni](#), D. Gawlitta, A.J.W.P. Rosenberg, M.W. Grinstaff, J. Töyräs, H. Weinans, L. Creemers, B. Pouran. *Contrast enhanced computed tomography for real-time quantification of glycosaminoglycans in cartilage tissue engineered constructs*. *Acta Biomaterialia*, 2019. 100:202-212
6. G.C.J. Lindberg, [A. Longoni](#), K.S Lim, A.J.W.P. Rosenberg, G.J Hooper, D. Gawlitta, T.B.F Woodfield. *Intact vitreous humor as a potential extracellular matrix hydrogel for cartilage tissue engineering applications*. *Acta Biomaterialia*, 2019. 85:117-130.
7. M. Koolen, [A. Longoni](#), J. van der Stok, O. Van der Jagt, D. Gawlitta, H. Weinans. *Complete regeneration of large bone defects in rats with commercially available fibrin loaded with BMP-2*. *European Cells and Materials*, 2019. 17;38:94-105.
8. [A. Longoni](#), L Knežević, K Schepers, H Weinans, A.J.W.P. Rosenberg, D. Gawlitta. *The impact of immune response on endochondral bone regeneration*. *npj Regenerative Medicine*, 2018. 29;3:22
9. G. Criscenti, C. De Maria, [A. Longoni](#), C.A. van Blitterswijk, H.A.M. Fernandes, G. Vozzi, L. Moroni. *Soft-molecular imprinted electrospun scaffolds to mimic specific biological tissues*. *Biofabrication*, 2018. (4):045005
10. G. Criscenti, A. Vasilevich, [A. Longoni](#), C. De Maria, C.A. van Blitterswijk, R. Truckenmuller, G. Vozzi, J. De Boer, L. Moroni. *3D screening device for the evaluation of cell response to different electrospun microtopographies*. *Acta Biomaterialia*, 2017. 55:310-322

11. [A. Longoni](#), A. Di Luca, G. Criscenti, C. Mota, C.A. van Blitterswijk, L. Moroni. *Toward mimicking the bone structure: design of novel hierarchical scaffolds with a tailored radial porosity gradient*. *Biofabrication*, 2016. 8(4):045007.
12. S.C. Neves, C. Mota, [A. Longoni](#), C.C. Barrias, P.L. Granja, L. Moroni. *Additive manufactured polymeric 3D scaffolds with tailored surface topography influence mesenchymal stromal cells activity*. *Biofabrication*, 2016. 8(2):025012.
13. Di Luca, [A. Longoni](#), G. Criscenti, I. Lorenzo-Moldero, M. Klein-Gunnewiek, J. Vancso, C.A. van Blitterswijk, C. Mota, L. Moroni. *Surface energy and stiffness discrete gradients in additive manufactured scaffolds for osteochondral regeneration*. *Biofabrication*, 2016. 8(1):015014
14. G. Criscenti, [A. Longoni](#), A. Di Luca, C. De Maria, C.A. van Blitterswijk, G. Vozzi, L. Moroni. *Triphasic scaffolds for the regeneration of the bone–ligament interface*. *Biofabrication*, 2015. 8(1):015009.

CURRICULUM VITAE

Alessia Longoni was born on 9th December 1990 in Como, Italy. In 2009, she graduated from the local high school, the Collegio Arcivescovile Castelli. Afterwards, she studied “Biomedical and Pharmaceutical Biotechnology” at Università Vita-Salute San Raffaele. She obtained a BSc in 2012 with a final thesis entitled “Bone biology and architecture decoding for medical device encoding”. This thesis represented her first interaction with the field of Tissue Engineering. The same year, she started her master in Cellular and Molecular Biotechnology at Università Vita-Salute San Raffaele, where she graduated *cum laude* in 2014. During this period, Alessia carried out her research project at MIRA Institute, University of Twente, under the supervision of Prof. dr. Lorenzo Moroni. Here, she expanded her interest in bone regeneration, writing a dissertation entitled “Toward mimicking the bone structure: design of scaffolds with tailored porosity gradient”. In the spring of 2015 she started a PhD at the department of Maxillofacial Surgery and Special Dental Care in the Regenerative Medicine program of the University Medical Center Utrecht, under the supervision of Prof. dr. A.J.W.P Rosenberg and dr. ir. D. Gawlitta. As a part of her PhD she continued working on bone regeneration, with a focus on translational aspects of regenerative approaches that mimics endochondral ossification. The results of this PhD research are presented in this thesis.

